

GREAT AUSTRALIAN BIGHT RESEARCH PROGRAM

RESEARCH REPORT SERIES

Delineation and characterisation of cold hydrocarbon seeps

Final Report GABRP Project 5.1

Andrew Ross, Christine Trefry, Lurnet Langhi, Julian Strand, Charlotte Stalvies, Manzur Ahmed, Stephane Armand, David Fuentes, Se Gong, Steven Sesatak, Emma Crooke, Xiubin Qi, Mike Gresham, Asrar Talukder and Stacey Maslin

GABRP Research Report Series Number 17

August 2017



DISCLAIMER

The partners of the Great Australian Bight Research Program advises that the information contained in this publication comprises general statements based on scientific research. The reader is advised that no reliance or actions should be made on the information provided in this report without seeking prior expert professional, scientific and technical advice. To the extent permitted by law, the partners of the Great Australian Bight Research Program (including its employees and consultants excludes all liability to any person for any consequences, including but not limited to all losses, damages, costs, expenses and any other compensation, arising directly or indirectly from using this publication (in part or in whole and any information or material contained in it.

The GABRP Research Report Series is an Administrative Report Series which has not been reviewed outside the Great Australian Bight Research Program and is not considered peer-reviewed literature. Material presented may later be published in formal peer-reviewed scientific literature.

COPYRIGHT

©2017

THIS PUBLICATION MAY BE CITED AS:

Ross, A., Trefry, C., Langhi, L., Strand, J., Stalvies, C., Ahmed, M., Armand, S., Fuentes, D., Gong, S., Sestak, S., Crooke, E., Qi, X., Gresham, M., Talukder, A. and Maslin, S. (2017). Delineation and characterisation of cold hydrocarbon seeps. Final Report GABRP Project 5.1. Great Australian Bight Research Program, GABRP Research Report Series Number 17, 144pp.

CONTACT

Dr Andrew Ross
CSIRO
e: Andrew.Ross@csiro.au

FOR FURTHER INFORMATION

www.misa.net.au/GAB

GREAT AUSTRALIAN BIGHT RESEARCH PROGRAM

The Great Australian Bight Research Program is a collaboration between BP, CSIRO, the South Australian Research and Development Institute (SARDI), the University of Adelaide, and Flinders University. The Program aims to provide a whole-of-system understanding of the environmental, economic and social values of the region; providing an information source for all to use.

Contents

LIST OF FIGURES.....	i
LIST OF TABLES.....	vi
ACKNOWLEDGEMENTS.....	vii
EXECUTIVE SUMMARY	1
1. INTRODUCTION	4
Overview	4
Background and Need.....	4
Objectives.....	5
Project tasks and methods used	6
Task 1: Structural assessment	6
Task 2: Satellite-based remote sensing	7
Task 3: Voyage planning	8
Task 4:.....	8
Task 5: Sample analysis, data interpretation and development of understanding of potential leakage and active petroleum systems in the GAB.....	9
2. STRUCTURAL ASSESMENT AND CONTROL ON POTENTIAL HYDROCARBON LEAKAGE	10
Ceduna Sub-basin overview.....	10
Rapid structural screening for marine survey target delineation.....	15
Leakage indicator screening outcomes	20
Introduction to structural assessment.....	21
Seismic data used	21
Seismic data quality	23
Seismic Interpretation.....	24
2D line & Geoscience Australia Interpretation.....	24
Trim 3D interpretation.....	24
Fault selection for further modelling.....	30
Depth conversion	31
Stratigraphic Forward Model.....	32
Modelling parameters	34
Trim Geomodel.....	37
Fault Seal – Potential impacts on across fault flow	41
Shale Gouge Ratio.....	41
Trim across fault seal modelling results	41
Summary.....	46
Fault Seal – Upfault flow indicators	47
Biogenic mound complexes in the Bight Basin.....	47
Early Tertiary geobodies in the Ceduna Sub-basin.....	48

Origin of mound complexes in the central Ceduna Sub-basin	52
Structural assessment and control on potential hydrocarbon leakage conclusions	54
3. SATELLITE BASED REMOTE SENSING FOR SEA SURFACE SLICKS.....	55
Historical synthetic aperture radar data holdings	55
Geoscience Australia SAR data	56
AMSA SAR data	57
Synthetic aperture radar SAR area of interest and acquisition program definition.....	59
Synthetic aperture radar capture program results and discussion	61
4. VOYAGE PLANNING AND PROJECT 5.1 OUTCOMES FOR THE GAB SS2013_CO2 AND IN2015_CO2 VOYAGES.....	65
Reconnaissance survey through R/V Southern Surveyor research charter (SS2013_CO2)	65
Seep target prioritisation process	65
Baseline sampling areas	69
R/V Southern Surveyor research charter (SS2013_CO2) voyage equipment.....	69
IN2015_CO2 planning	71
SS2013_CO1 Geological interpretation	71
IN2015_CO2 Geological data interpretation	78
Evidence of seepage from GABRP voyages.....	82
5. SAMPLE ANALYSIS, DATA INTERPRETATION AND DEVELOPMENT OF UNDERSTANDING OF POTENTIAL LEAKAGE AND ACTIVE PETROLEUM SYSTEMS IN THE GAB	83
Introduction	83
Samples	85
Sampling planning	85
Sample collection and handling.....	85
Samples selected for analysis	87
Geochemical Experimental procedures	98
Extraction of organic matter from water	98
Quantitative analysis of PAH in the solvent extract of water.....	98
Extraction of GO net	98
Preparation of sediment samples.....	98
Extraction of organic matter from sediment sample	99
GC-MS analyses of extractable organic matter	99
Molecular composition of headspace gases	99
Isotopic composition of headspace gases	100
Geochemical Results	100
Geochemistry of organic matter in water and related samples.....	100
Quantitative analysis of PAHs in top and niskin waters	101
Qualitative investigation of extractable organic matter in top and niskin waters.....	101
Extractable organic matter of Go net and Go net blank samples	111

	Extractable organic matter of other samples.....	117
	Geochemistry of organic matter in seabed sediments	117
	Geochemistry of headspace gases	121
	Geochemical analysis conclusions	123
6.	CONCLUSION	124
7.	REFERENCES.....	125
	APPENDIX 1: DATA MANAGEMENT	134
	Raw Datasets Created:.....	134
	Survey Database	134
	Data Processing and Derived Datasets:	139
	Geochemistry data sets created:.....	139
	Data Curation and Archive:.....	141
	Data Access, Use Agreements and Licensing:.....	141
	Publication of Datasets:	141
	APPENDIX 2: STUDENT PROJECTS	141
	APPENDIX 3: PROJECT PUBLICATIONS	141
	Reports.....	141
	Presentations and Conference abstracts.....	142
	Papers	142
	Patents: None	142
	Media Releases: None	142
	APPENDIX 4: INTELLECTUAL PROPERTY	142
	Unique discoveries: None	142
	Action plan: Not applicable.....	142
	APPENDIX 5: TASK 2 SAR DATA.....	143

LIST OF FIGURES

Figure 1 Cross-section through the eastern Madura Shelf and Ceduna Sub-basin. From Bradshaw et al., 2003.	12
Figure 2 Cross-section through the eastern Madura Shelf, Ceduna Sub-basin and eastern Recherche Sub-basin. From Bradshaw et al., 2003.	12
Figure 3 Cross-section through the eastern Madura Shelf, Ceduna Sub-basin and eastern Recherche Sub-basin. From Bradshaw et al., 2003.	13
Figure 4 Bight Basin stratigraphic correlation chart showing basin phases and predicted source rock intervals (modified from Blevin et al., 2000 and Totterdell et al., 2000). The sea level curve (Haq et al., 1988) is modified to the time scale of Gradstein et al. (2004).....	14
Figure 5 Map of the Ceduna Basin overlain by the exploration block outlines and the Flinders Deepwater 2D seismic lines. The picked anomalies and their ranking groupings are also shown. The location of Figure 6 and Figure 7 are also shown on the figure.	17
Figure 6 An excerpt of the dwgab 08 Flinders Deepwater 2D seismic line (area 1) showing highlighted features of interest. The image shows bright seismic amplitudes in several locations up the sequence toward the seafloor (blue circles) as well as a loss of seismic signal close to the fault plane which could be interpreted as the result of the formation of a gas chimney (green arrow). In addition there is evidence of recent reactivation of the fault due shown by seabed displacement.....	18
Figure 7 An excerpt of the dwgab 03 Flinders Deepwater 2D seismic line (area 8) showing highlighted features of interest. The image shows bright seismic amplitudes in the sequence (blue circle) as well as a loss of seismic signal close to the fault plane which could be interpreted as the result of fluid migration close to the fault plane (green arrow). In addition there is evidence shallow gas in the section as evidenced by the bright shallow amplitude (purple circle) and a fractured/disrupted sea floor which could be due to fluid escape (green circle).	19
Figure 8 Location of the ‘Ceduna Delta’, the up to 17 km thick sedimentary fill of the Ceduna Sub-basin in the Bight Basin on the southern Australian margin (after Teasdale, 2004).	22
Figure 9 Ceduna Sub-basin with location of seismic data. After Somerville, 2001.	22
Figure 10 Santonian Top Tiger Supersequence horizon interpreted on the Trim 3D survey on every 40 th inline (1200 m) and 100 th crossline (1250 m). The Trim 3D survey is ~60 km x ~20 km.	25
Figure 11 Attribute fault cube. A) Crossline of original Trim 3D seismic. B) Fault enhancement filter applied to same crossline of original Trim 3D seismic. C) Similarity attribute on original Trim 3D seismic. D) Similarity attribute on filtered Trim 3D seismic.	26
Figure 12 Time slice through attribute fault cube in the lower Hammerhead Supersequence. The Trim 3D survey is ~60 km x ~20 km.	27
Figure 13 Fault interpretation on the Trim 3D survey on every 100 th crossline (1250 m) and on time slices every 500 ms TWT between 2600 ms TWT and 4100 ms TWT. The horizon is the Santonian top Tiger. The Trim 3D survey is ~60 km x ~20 km.	28
Figure 14 Structural pattern for the Trim 3D survey showing the main northwest oriented compartments. The Trim 3D survey is ~60 km x ~20 km.	29
Figure 15 Trim 3D crosslines with attribute fault cube overlying seismic data. Location on Figure 12 with a) and b) to the northwest and the southeast, respectively. Light blue=Top White Pointer (Cenomanian); green=intra Tiger (Coniacian); orange=Top Tiger (Santonian); pink= intra	

Hammerhead (Early Campanian); purple=intra Hammerhead (Campanian); red=Top Hammerhead (Paleocene).	29
Figure 16 Close up of the upper Hammerhead structural pattern showing relay patterns.	30
Figure 17 Faults subset for geological modelling and fault seal analysis. The Trim 3D survey is ~60km x ~20km.	31
Figure 18 Stratigraphic Forward Modelling has a four step iterative workflow. The simulation workflow is repeated while modifying the conceptual model and input parameters until appropriate convergence with available data is achieved.	33
Figure 19 The 100 x 600 km Sedsim stratigraphic forward modelling area with source points located with red dots superimposed over the divisions of the Bight Basin (after Totterdell & Bradshaw, 2004).	35
Figure 20 Visualisation of the whole Ceduna Sub-basin Sedsim model. Colour relates to siliclastic grain proportion. Vertical exaggeration is ~x10. Fences are spaced at 160 km.	36
Figure 21 0.5 km resolution Sedsim output. The model illustrates a transition from marine (dark brown) Tiger Supersequence at the base through shoreline (yellow) and finally fluvio-deltaic facies (green) of the Hammerhead Supersequence. The corners of the Trim 3D survey are marked (T1-4). Fences are spaced at 4 km.	37
Figure 22 Bottom five surfaces in the RMS structural model illustrating fault polygons for the largest faults interpreted in the Trim 3D survey. View from SW, colours represent depth on a surface basis.	38
Figure 23 140 layer Geocellular shale content volume for the sandiest case, V_{shale} is ~0.1.	39
Figure 24 Intermediate case 140 layer Geocellular, V_{shale} is ~0.14.	39
Figure 25 Intermediate case 140 layer Geocellular, V_{shale} is ~0.19.	40
Figure 26 140 layer Geocellular shale content volume for the shaliest case, V_{shale} is ~0.30.	40
Figure 27 SGR derived for the sandiest case (~0.1 V_{shale}). Green is 'go' for across fault leakage, red is where leakage is 'stopped'. The colour scheme is based on standard SGR publications (e.g. Yielding, 2002). In this case faults are dominantly leaky, but yellow areas indicate the presence of areas with some potential for fault seal and red, >0.3 SGR indicates probable sealing in even this the sandiest case. Again viewed from the SW in all cases.	42
Figure 28 SGR derived for the ~0.14 V_{shale} case. Most of the faults display at least some potential for sealing (yellow to orange, 0.1 to 0.25 SGR) where they cut the Hammerhead Supersequence in this case. Grosser scale banding in the Tiger and Lowest Hammerhead Supersequence indicate transitions between offshore marine (red) and shoreface (green) facies in this case.	43
Figure 29 SGR derived from the ~0.19 V_{shale} case. Occurrence of 0.25 to 0.3 SGR values in this model indicates increasing potential for sealing in the Hammerhead Supersequence.	44
Figure 30 SGR derived from the ~0.3 V_{shale} case. Unsurprisingly in the shaliest case the faults are predicted to be almost entirely sealing, with only bands of thick shoreface sands at the transition between the supersequences displaying obvious potential for leakage.	45
Figure 31 Combined two-way travel time thicknesses of the siliclastic delta sequence (grayscale) and overlying bryozoan reef mound complexes (B1 in red, B2 in blue) in the northern Ceduna Sub-basin. J1—Jerboa-1; P1—Potoroo-1. From Sharples et al, 2014.	47
Figure 32 Volcanic cone at the top of the Wobbecong Supersequence in the central Ceduna Sub-basin (Flinders 2D line 64) with wash-out effect and velocity pull-up. The section is 13km long. Location on Figure 33.	49

Figure 33 Mound complexes in the central Ceduna Sub-basin. Locations of Figure 36 and Figure 37 are shown near the acoustic contact and the Trim 3D survey, respectively.	50
Figure 34 Interpreted mound complex in the central Ceduna Sub-basin on Flinders 2D line 53, ~3 km to the southeast of an acoustic contact and sub-bottom profile anomaly. The section is 9500 m long. Location on Figure 33.....	50
Figure 35 Interpreted mound complex in the central Ceduna Sub-basin on Flinders 2D line 48. The section is 9500 m long. Location on Figure 33.....	51
Figure 36 3D view of the interpreted mound complex ~3 km to the southeast of an acoustic contact and sub-bottom profile anomaly. The thickest part of the mound is on the lower hanging-wall compartment. Location on Figure 33.....	51
Figure 37 Interpreted mound complex on the Trim 3D seismic survey. A) 3D geometry of the mound complex. B) Thickness data showing the main parts of the mound complex develop on the hanging-wall compartment. Location on Figure 33.....	52
Figure 38 Synthetic Aperture Radar sea surface anomalies for the Great Australian Bight for the historical data.	58
Figure 39 Area of interest used for planning of SAR capture program showing area of interest inset and historical SAR anomalies.	59
Figure 40 SAR scenes (4) having part of the scene coverage within the area of interest for the period April 6th to 15th 2013 from the various SAR satellite platforms.	60
Figure 41 Predominant wind field across the 4 SAR scenes obtained during the study.	61
Figure 42 Cosmo-skymed 1 synthetic aperture radar scene for April 6th 2013 report for area of interest with slicks identified in the middle top of the scene (one slick) and the bottom right (cluster of slicks).	63
Figure 43 Combined historical and capture program (CSTARS Slick Features) sea surface synthetic aperture radar anomalies for the Great Australian Bight.....	64
Figure 44 Showing target areas 1-3 interpreted as having indications of potential seepage. The labelled lines are the available public 2D seismic holdings. Black or light blue dots are seismic anomalies. The ringed seismic anomaly sites are shown below in Figure 45 and Figure 46. The purple outlined areas are slick extents from the GA/NPA 199/2000 SAR study whereas the red areas are potential slick extents from the CSTARS data collected during this study.	66
Figure 45 2D seismic line woofdw0065 seismic anomalies showing the seafloor scarp to the north east and fractured/disrupted seafloor with small/shallow faults and fractures. In the shallow subsurface bright spots and possible associated gas chimneys.	67
Figure 46 2D seismic line dwgab 27-m seismic anomaly showing a sharp fractured/disrupted sea floor incised furrow related to a deeper and chaotic faulting interpreted as a possible fluid conduit with occasional bright spots present.....	68
Figure 47 SS2013_C01 multibeam bathymetry data collected over voyage track and potential seep target areas.	72
Figure 48. SS2013_C01 multibeam bathymetry data collected over potential seep target areas..	73
Figure 49. SS2013_C01 multibeam bathymetry of potential seepage Area 1.....	74
Figure 50. SS2013_C01 multibeam bathymetry of the eastern section of potential seepage Area 2.	75

Figure 51. SS2013_C01 multibeam bathymetry of the eastern section of potential seepage Area 3.	76
Figure 52. SS2013_C01 Acoustic contacts recorded during the voyage.....	77
Figure 53. SS2013_C01 low rank TR_SC_102 acoustic water column anomaly (Inset A). With associated subbottom profiler data collected across the area (inset B). Inset C was previously erroneously associated with the .TR_SC_102 location.....	78
Figure 54. Mulibeam bathymetry collected across the Ceduna and Duntroon sub basins of the Great Australian Bight during the IN2015_C02 voyage.....	79
Figure 55. Normalised mulibeam backscatter collected across the Ceduna and Duntroon sub basins of the Great Australian Bight during the IN2015_C02 voyage. The data was normalised to 65dB. Soft sediments are represented as dark grey whilst harder sediments are represented as light grey.	80
Figure 56. Location of beam trawl 141 (BEAMT_141) displayed on bathymetric map, showing historical seismic lines across the area.	81
Figure 57. DWGAB/22B 2D seismic cross section scaled to the extent of Figure 56, with the location of beam trawl 141 marked.....	82
Figure 58 Map of the central and eastern GAB regions showing the 25 sampling stations (blue circles) on five transects (T1-5). Mapped features are: the former GAB Marine Park (blue outline, now part of the larger Great Australian Bight Commonwealth Marine Reserve); other Commonwealth Marine Reserves (grey outlines); BP lease areas in which exploratory activities will occur (green outlines). Isobaths: 200 m (green), 1000m (red), 2000m (blue) 3000 m (brown).	84
Figure 59 Photographs of sample types analysed as part of this report. Moving clockwise from far left: Multicore liner containing sediment core exhibiting colour variations throughout sediments, which are overlain by seawater; decanting water from the sediment-water interface into 1 L amber glass bottle (top water samples); sectioning extruded sediment; sediment section wrapped in clean aluminium foil and sealed into IsoPak bag for headspace gas analysis; sediment section before being wrapped in clean aluminium foil.	86
Figure 60 Map showing the distribution of samples selected for analysis from the CSIRO and BP-Fugro GAB marine surveys, 2013. Coloured dots overlying one another represent multiple samples collected from one location during the R/V Southern Surveyor cruise; stars overlying each other represent headspace gas and sediment sample collected during the M/V Southern Supporter marine survey.	90
Figure 61 Total ion chromatogram showing the overall hydrocarbon distributions in the extractable organic matter of a Niskin water sample.....	105
Figure 62 Total ion chromatograms showing the overall hydrocarbon distributions in the extractable organic matter of top and Niskin Water samples.....	106
Figure 63 Histograms showing the distributions of n-alkanes and regular isoprenoids in the extractable organic matter of Top and Niskin water samples.....	107
Figure 64 Distribution of alkylbenzenes, naphthalene, phenanthrene, biphenyl, dibenzothiophene and alkylated homologues in the extractable organic matter of top and Niskin water samples. Values calculated from the responses in the <i>m/z</i> 106, 120, 134, 128, 142, 156, 170, 184, 198, 178, 192, 206, 220, 154, 168, 182, 184, 198 and 212 mass chromatograms.	108
Figure 65 Total ion chromatograms showing overall hydrocarbon distributions in extractable organic matter of the GO net and GO net blank samples.	112

Figure 66 Histograms showing the distributions of n-alkanes and regular isoprenoids in the extractable organic matter of the GO net and GO net blank samples.	115
Figure 67 Distribution of alkylbenzenes, naphthalene, phenanthrene, biphenyl, dibenzothiophene and alkylated homologues in the GO net and GO net blank samples scaled to show all hydrocarbons. Values calculated from the responses in the <i>m/z</i> 106, 120, 134, 128, 142, 156, 170, 184, 198, 178, 192, 206, 220, 154, 168, 182, 184, 198 and 212 mass chromatograms.	116
Figure 68 Stages of sediment sample preparation for solvent extraction of organic matter: (a) A rectangular shaped core was cut out and then placed onto clean glass Petri dishes, (b) core was cut into smaller pieces on a piece of clean aluminium foil, (c) air dried core was crushed into powder and preserved in Pyrex glass bottles and (d) solvent extracts ready for GC-MSD analyses.....	119
Figure 69 Total ion chromatograms of (a) extractable organic matter of a sediment sample collected during Southern Surveyor cruise and (b) associated Accelerated Solvent Extractor system blank showing overall hydrocarbon distributions.	120

LIST OF TABLES

Table 1 Seismic and interpreted geological feature classification criteria used in the rapid assessment of the potential for conduits for hydrocarbon seepage from the sub-surface.	15
Table 2 Nominal horizons interpreted for the Trim 3D survey.	24
Table 3 Satellite Synthetic Aperture Radar platforms and modes used during the study.	60
Table 4 SAR acquisitions for the four scenes.	60
Table 5 Predominant wind field across SAR scene obtained during the study.	61
Table 6 Descriptions of sample types collected during the CSIRO and BP-Fugro marine surveys of the Great Australian Bight, 2013.	85
Table 7 Selection criteria for sediment and water samples collected during the R/V Southern Surveyor cruise.	87
Table 8 Selection criteria for sediment samples collected during the M/V Southern Supporter cruise.	89
Table 9 Water samples selected for analysis.	91
Table 10 Sediment samples selected for analysis.	94
Table 11 Headspace gas samples selected for analysis.	95
Table 12 Amount of hydrocarbons (μg compound/L water) detected in the top and Niskin water samples collected during Southern Surveyor Cruise 2013.	102
Table 13 Amount of hydrocarbons (μg compound/L water) detected in the top and Niskin water samples collected during Southern Surveyor Cruise 2013.	103
Table 14 Aliphatic hydrocarbon parameters of extractable organic matter isolated from the top and Niskin water samples collected during Southern Surveyor Cruise 2013.	109
Table 15 Aromatic hydrocarbon parameters of extractable organic matter isolated from the top and Niskin water samples collected during Southern Surveyor Cruise 2013.	110
Table 16 Aliphatic hydrocarbon parameters of GO net and GO net blank samples.	113
Table 17 Aromatic hydrocarbon parameters of GO net and GO net blank samples.	114
Table 18 Extraction yields of selected sediment samples.	118
Table 19 Molecular composition of selected headspace gases expressed in normalized percent (based on air free calculation)	122
Table 20 Stable carbon isotopic composition of selected headspace gases.	122

ACKNOWLEDGEMENTS

The Great Australian Bight Research Program is a collaboration between BP, CSIRO, the South Australian Research and Development Institute (SARDI), the University of Adelaide, and Flinders University. The Program aims to provide a whole-of-system understanding of the environmental, economic and social values of the region; providing an information source for all to use.

The voyage data and samples used in the delivery of this project would not be possible if not for the dedication of the voyage participants on the SS2013_C02 and IN2015_C02 Marine National Facility (MNF). In particular the voyage chief scientists are thanked (Alan Williams, SS2013_C02 and Rudy Kloser, IN2015_C02) as well as both the scientific, MNF teams and crew of the vessels.

CSIRO is thanked for the permission to use internal research outcomes from sedimentary forward models to enhance the outcomes of this project.

Selected images in this report © Commonwealth of Australia (Geoscience Australia) 2016. These products are released under the Creative Commons Attribution 4.0 International Licence. <http://creativecommons.org/licenses/by/4.0/legalcode>

EXECUTIVE SUMMARY

Project 5.1 (Delineation and characterization of cold hydrocarbon seeps) forms a component in Theme 5 (petroleum systems) of the Great Australian Bight Research Program.

The overall intent of the project was to address the perceived risk of hydrocarbon generation in the Bight Basin, and the Ceduna Sub-basin through investigation of potential hydrocarbon seepage mechanisms and occurrence, and provide valuable pre-drill understandings of baseline hydrocarbon concentrations at preselected reference sites.

To identify potential sites of hydrocarbon seepage a multidisciplinary approach was taken which incorporated; the interpretation of seismic data, determination of fault leakage risk through a structural and geomechanical evaluation, identification of seabed features and morphologies indicative of seepage, delineation of water column acoustic contacts indicative of fluid and gas escape from the seabed, classification of sea surface slick anomalies and sampling of the seafloor in areas of possible seepage and far field locations to understand the distribution of hydrocarbons in sediments.

Of the 81 areas of interest identified from the rapid screening of 2D seismic data for leakage indicators no one area displayed unequivocal evidence of fluid leakage through the subsurface to the seafloor. This does not preclude seepage being present within the GAB and ranking of the features determined that features with the highest potential for leakage were strongly biased towards the outboard deep water slope of the Ceduna basin.

Static geomodels populated by V_{shale} have been derived for the Trim 3D volume using seismic interpretation, basic well petrophysics and stratigraphic forward modelling outputs. These model outputs have enabled the faulted models to be tested for a possible range of SGR related sealing scenarios. The most likely V_{shale} scenarios indicate that the Hammerhead Supersequence in the vicinity of the Trim survey is distributed right at the most sensitive range of values with respect to across fault seal (i.e. 0.1 to 0.25 SGR).

Biogenic mound complexes interpreted at the Middle Eocene hiatus are potentially indicate hydrocarbon paleo-seeps and perhaps more specifically paleo-leakage up faults. Such an interpretation would support the presence of an active hydrocarbon system at the time of Middle Eocene extension, fault movement and reactivation, however this requires further research to eliminate other controls on their formation.

Structural and geomechanical assessment modelling data do not conclusively predict sealing or leaking with respect to across fault flow, with the geomodel predicting intermediate across fault flow behaviors in the most likely probable scenarios with (~ 0.14 and ~ 0.19 V_{shale}). These model iterations however demonstrate the high sensitivity to the modelled lithologies to across fault flow sealing.

Sea surface slick studies included the acquisition of 4 additional synthetic aperture radar scenes which augmented the 231 publically available scenes. The 23 sea surface anomalies were identified within the four additional scene captures which clustered in proximity to anomalies identified in prior scene captures. These data were used in conjunction with the areas of interest identified for 2D seismic data screening to determine the areas for subsequent reconnaissance on the SS2013_C02 voyage.

Planning for the SS2013_C02 voyage identified three seafloor areas that reconnaissance for potential seepage could be undertaken within the very limited time window of the voyage. From the data collected during this SS2013_C02 voyage and the subsequent IN2015_C02 voyage there is only weak evidence for possible seepage from the data collected, in part due to the very limited time spent on these activities as part of the voyages. This outcome is not a definitive indication of the absence of seepage in the basin, as the basin comprises a very large area and there continues to be a paucity of data collected to specifically identify areas of seepage.

84 samples were collected from areas not anticipated to be areas of seepage on the SS2013_C02 voyage and by a 2013 BP chartered M/V Fugro Southern Supporter voyage. These headspace gas, water, sediment and surface slick samples were subjected to geochemical analysis dependent on their type.

The quantitative analysis of solvent extracts isolated from seawater samples indicate that polycyclic aromatic hydrocarbons (PAHs) are largely absent in/around the BP permits in the Great Australian Bight, Australia. Smaller amount of naphthalene, a highly volatile bicyclic aromatic hydrocarbon, detected in majority of the samples is probably a contaminant cumulatively inherited from solvents, glassware and/or unknown source(s).

The qualitative organic geochemical analyses of extractable organic matter isolated from seawater, seabed sediment, and GO net samples, and headspace gases extracted from multicore/piston core samples collected from the Great Australian Bight region indicate that petroleum hydrocarbons are either absent or below the limits of detection pointing to an absence of active hydrocarbon seepage in and around the sampling region. Two water and one GO net sample samples containing trace amounts of thermogenic hydrocarbons are likely to be inherited from a contaminant oil of an unknown source.

The seabed sediment samples contain variable amounts of extractable organic matter ranging from 0 to 3200 mg EOM/kg of sediment which do not comprise any detectable quantities of petroleum hydrocarbons.

The headspace gas samples analysed in this report do not contain any detectable amounts of petroleum hydrocarbons (i.e., methane, ethane, etc.). CO₂ gas detected in these samples ranged from low to very high amounts (\approx 1-50 %), and had highly variable $\delta^{13}\text{C}$ CO₂ values. The isotopic data indicate an origin of Southern Surveyor CO₂ sample gas originates from

magmatic sources and Southern Supporter CO₂ gas originates from mixed magmatic and recent organic matter sources.

1. INTRODUCTION

Overview

The Great Australian Bight, and particularly the Ceduna Sub-basin, is considered as one of the most prospective deep water frontier basins in offshore Australia (Totterdell et al 2008). It contains up to 15 km of mid to Late Cretaceous deltaic and marine sediments within the Tiger and Hammerhead Super Sequences that provide potential reservoirs, seals and oil-prone source rocks at several stratigraphic levels (Blevin et al. 2000; Totterdell et al. 2000; Struckmeyer et al. 2001).

Whilst the Great Australian Bight is a prospective basin for hydrocarbons very few samples have been analysed to establish if the sediments have measurable concentrations of naturally occurring hydrocarbons in waters and sediments.

Background and Need

Currently, no liquid hydrocarbons have been recovered from the Great Australian Bight (GAB) therefore, an active petroleum system has yet to be proven. This is despite evidence that hydrocarbons are leaking naturally into the GAB (i.e. asphaltite strandings, McKirdy et al., 1986, 1994; Currie et al., 1992; Padley et al., 1993; Padley, 1995, Hall et al., 2012) and identification of from fluid inclusion studies of possible hydrocarbon migration routes and accumulation zones within the exploration wells drilled in the basin (Lisk et al 2001, Ruble et al., 2001, Kempton et al., 2016, Bourdet et al., 2016).

Generally, there is low spatial coverage of data from all data sources, from swath bathymetry to well samples. The recent addition of the Ceduna 3D seismic survey conducted by PGS on behalf of BP has significantly augmented existing 2D and 3D seismic data coverage in the basin.

On initiation of this project seven known prior marine surveys had been undertaken by Geoscience Australia and CSIRO studying aspects of the geology of the Great Australian Bight between 1989 and 2007. However only one of these surveys attempted to delineate hydrocarbon seepage (SS01/2007; Totterdell and Mitchell 2009). Whilst the number of marine surveys performed in the GAB appears to be numerous, only recent advances in marine survey technologies, the collection of new seismic data and remote sensing data sets have permitted a more detailed understanding of the GAB geology and permit more precise survey planning to occur.

One approach used to gain an understanding of petroleum systems within sedimentary basins is the study of hydrocarbon seeps. Hydrocarbon seeps are the seafloor expression of the geological migration pathways from active source rocks to the surface. The migration of hydrocarbon fluids to the seabed is mediated by faults and carrier beds which act as migration and leakage conduits to the surface and the processes of their occurrence is well documented (Talukder, 2012). Seeps have been used to confirm the presence of active

petroleum systems in many sedimentary basins worldwide (Angola, Brazil, Caspian Sea, Gulf of Mexico, Browse basin), and permit geochemical characterisation of the generated hydrocarbons in these basins prior to drilling.

Understanding the distribution and occurrence of hydrocarbon seeps in areas of oil and gas exploration and development activities is also an important consideration in the determination of likely baseline environmental conditions. In particular, the measurement of naturally occurring hydrocarbon loadings within an ecosystem are an important consideration when considering community function and structure.

Integrated studies which consider the complete leakage and seepage system from deep geological horizons to ocean surface are used to identify (if present), characterise and sample hydrocarbon seeps. This approach includes:

- interpretation of seismic data
- determination of fault leakage risk through a structural and geomechanical evaluation
- identification of seabed features and morphologies indicative of seepage
- delineation of water column acoustic contacts indicative of fluid and gas escape from the seabed
- classification of sea surface slick anomalies
- Sampling of the seafloor in areas of possible seepage and far field locations to understand the distribution of hydrocarbons in sediments

Objectives

The overall intent of the project was to enhance the prospectivity of the basin by providing proof of an active petroleum system and provide valuable pre-drill understandings of baseline hydrocarbon concentrations at preselected reference sites (in conjunction with the benthic theme project 3.1).

This multidisciplinary study aimed to develop an understanding of the potential mechanisms for hydrocarbon migration and hydrocarbon seepage in the GAB, with a reconnaissance survey to be undertaken to acoustically characterise areas potential seepage. Secondly the reconnaissance survey also aimed to sample and geochemically analyse water and sediment samples for hydrocarbons from preselected reference sites (away from areas of potential natural seepage) to understand pre-drill baseline conditions.

Through structural assessment the main subsurface structural elements potentially acting as pathways for hydrocarbons and leading to seepage at the seabed were to be defined. This was combined natural seepage reconnaissance mapping, to develop potential targets (both seeps and habitats) for further benthic study.

Through the use of satellite-based remote sensing additional complimentary data was collected to develop potential seep target locations. This was based on newly acquired or archival synthetic aperture radar (SAR) data for the GAB and integrated the SAR observations with oceanographic data and the underlying interpreted geology to further delineate possible seepage zones. These zones, if detected, were likely to be areas of key deepwater benthic biodiversity and thus this activity was performed in collaboration with the participants from the Benthic Biodiversity team in project 3.1.

The samples taken during the baseline-reconnaissance survey were also to be subjected to various geochemical analyses with subsequent data interpretation of the hydrocarbon baseline conditions that exist GAB.

Project tasks and methods used

Task 1: Structural assessment

Through structural assessment the main subsurface structural elements potentially acting as pathways for hydrocarbons and leading to seepage at the seabed were defined. This was combined natural seepage reconnaissance mapping, to develop potential targets (both seeps and habitats) for further benthic study.

a. Structural screening for marine surveys

The first phase of the structural assessment was aimed at providing an initial screening of potential targets for the 2013 marine reconnaissance survey.

In the first instance, a preliminary structural reconnaissance of the publicly available seismic survey data sets identified deep-rooted faults that intercept the seabed forming potential migration pathways for hydrocarbons (Talukder, 2012). This activity identified the most promising potential sites for surveying in early 2013. The screening considered:

- Fault displacement
- Fault geometry and distribution
- Fault linkage
- Petroleum system elements
- Seismic leakage indicators

The structural screening with the natural seepage mapping (Task 2) and any evidence of subsurface migration pathways was correlated against indications of seepage at the seabed and in the water column (where data was available). Furthermore, localized subsurface structural interpretation was carried out where morphological features at the seabed or acoustic data in the water column suggested fluid seepage.

The initial structural screening was updated based on the outcome of the marine reconnaissance survey. This resulted in the definition of an initial model for the plumbing

system and the leakage mechanism(s) in the Ceduna Sub-basin. Due to the limited regional interpretations, regional stratigraphic and structural interpretations and basin modelling the structural screening was limited to existing public domain data sets.

The output from this aspect of the study is summarised in section 2.

b. Structural control on hydrocarbon leakage

The second phase of Task 1 aimed to investigate the structural control(s) on hydrocarbon leakage. The overall objective was to define the mechanism(s) of hydrocarbon leakage associated with faults, to predict the key risk factors and define a relative risk model for fault-related leakage.

The initial structural screening and the outcomes of the marine survey were used to assess the first order risk factor(s) and define specific area(s) where further analysis is required in order to predict the impact of structures on fluid flow and define a regional risk pattern. The specific work plan for the second phase of Task 1 was defined following the structural screening and marine surveys, various investigative techniques were considered including:

- Local mapping of seismic leakage indicators to calibrate the assessment of leakage pathways (e.g. Ligtenberg, 2005; Langhi et al., 2010).
- Investigation of fault rock composition and membrane seal capacity that together represent a key control on leakage from reservoirs to thief zones or the seabed (Giger et al., 2010; Ciftci et al., 2012b).
- Investigation of the 3D distribution of faults as a control on leakage mechanism(s) (Zhang et al., 2009).

The investigative techniques used during the second phase of Task 1 improved the understanding of structural control(s) on potential hydrocarbon leakage. Furthermore, these individual outcomes were integrated into a relative risk model (Ciftci et al., 2012a) in order to define the key specific geological risk factors and their influence on fault leakage in the Ceduna Sub-basin.

The output from this aspect of the study is summarised in section 2.

Task 2: Satellite-based remote sensing

The aims of this task were to undertake a limited study to define the location of potential hydrocarbon seeps using the Nigel Press and Associates (NPA) global synthetic aperture radar (SAR) sea surface slick database (provided by BP) for the GAB. Particular attention was paid to temporally consistent features and a limited number of SAR image captures were collected over areas of high interest.

The SAR data was integrated with oceanographic data to define potential areas of seafloor origin. These areas, in combination with underlying geological interpretations, were used to

restrict candidate seafloor seepage locations and provide targets for further ship based investigation.

The output from this aspect of the study is described within section 3.

Task 3: Voyage planning

This task was focussed on the development of a detailed reconnaissance survey plan based on the outcomes of the prior tasks as they become available with areas possible seepage ranked and prioritised. As the reconnaissance survey was a joint voyage between Themes 5 and 3, planning conducted in collaboration with the Theme 3 leaders. The survey design detailed survey aims, areas of interest and sampling approaches.

The output from this aspect of the study is described within the voyage plan (voyage plan on MNF website <http://www.mnf.csiro.au/~media/Files/Voyage-plans-and-summaries/Southern-Surveyor/Voyage%20plans-summaries/2013/VOYAGE%20PLAN%20c02-13.ashx>) and within section 4.

Task 4:

a. Reconnaissance survey through R/V Southern Surveyor research charter

This survey, occurring between the 3rd to the 22nd April 2013 collected various data types from the sea surface to the shallow sub-seafloor. Potential seep sites were mapped using the acoustic systems including, water column single beam echo sounder, bathymetry and backscatter multibeam and sub-bottom profiler.

Sampling at preselected reference sites (away from areas of potential natural seepage) to understand pre-drill baseline conditions was also undertaken and included water column water sampling, and sediment sampling (in conjunction with Benthic Biodiversity Theme 3), to establish baseline geochemical hydrocarbon conditions.

Water and sediment sample were be obtained using conventional CTD and grab/core systems as well as utilising CSIRO-developed platforms such as the benthic observation and grab system (BOAGS) that integrated visual (HD video and stereo cameras), acoustic (echo sounder and acoustic Doppler current profiler, ADCP), hydrocarbon and other sensor data. Sediments were sampled using a multi-corer fitted to the BOAGS.

The interpreted data from this aspect of the study is described within section 4 and the voyage summary can be found on the <http://www.mnf.csiro.au/~media/Files/Voyage-plans-and-summaries/Southern-Surveyor/Voyage%20plans-summaries/2013/VOYAGE%20SUMMARY%20c02-13.ashx>.

b. Geological interpretation of IN2015_C02 acoustic data

As an additional subtask the 5.1 project team reviewed the water column and seafloor bathymetry data collected from the IN2015_C02 GABRP voyage. The purpose of the review of this data was to identify any geological features which could be indicative of fluid escape from subsurface. This this aspect of the study is described within section 4.

Task 5: Sample analysis, data interpretation and development of understanding of potential leakage and active petroleum systems in the GAB.

Water samples and sediment cores were examined using a variety of techniques including: headspace gas analysis (bulk and isotopic); conventional extraction, isolation and GC-MS of higher-molecular-weight (C12+) hydrocarbons. The data was interpreted in context of the baseline conditions that are expected within the GAB. These results are detailed within section 5.

2. STRUCTURAL ASSESMENT AND CONTROL ON POTENTIAL HYDROCARBON LEAKAGE

Ceduna Sub-basin overview

The Ceduna Sub-basin is the dominant depocentre of the Mesozoic to Cenozoic Bight Basin that developed along Australia's southern margin during a period of extension and passive margin evolution that commenced in the Middle–Late Jurassic (Figure 8; Teasdale, 2004). The Ceduna Sub-basin contains in excess of 15km of syn- and post-rift Mesozoic sediments (Figure 1, Figure 2 and Figure 3). It occurs in water depth ranging from 200 m to over 4000 m and has an area of approximately 90,000 km² (Figure 9; Sommerville, 2001). The northern margin is characterised by a series of fault-bound half grabens that contain Middle Jurassic to Early Cretaceous syn-rift fill (Figure 3). The southwestern boundary is interpreted at the basinward edge of an associated toe-thrust zone. The sub-basin is characterised by five main phases of evolution (King & Mee, 2004; Totterdell & Bradshaw, 2004; Blevin & Cathro, 2008):

A Late Jurassic Early Cretaceous mechanical subsidence phase due to a phase of intracontinental extension. Extensional deformation in the Ceduna Sub-basin appears to have been focused along a pre-existing NW–SE-trending margin of the Gawler Craton resulted in simple half graben along the eastern margin of the sub-basin. The rift fill comprises the Callovian–Kimmeridgian Sea Lion Supersequence and the Tithonian–early Berriasian Minke Supersequence (Figure 4).

- An Early Cretaceous phase of slow thermal subsidence represented by the largely non-marine Berriasian Southern Right Supersequence and the Valanginian to mid-Albian Bronze Whaler Supersequence (Figure 4). The onlapping, sag-fill geometry of the succession suggests that accommodation was created largely by thermal subsidence and compaction, with deposition concentrated over the earlier half graben.
- A second period of active extension during the Early–Late Cretaceous causing rapid subsidence in the sub-basin. The high subsidence rates recorded from the mid-Albian are possibly controlled by an interplay between thermal subsidence, mechanical extension and gravity-driven growth faulting (Mulgara Fault Family) in the White Pointer delta. This period of accelerated subsidence continued until the commencement of sea-floor spreading between Australia and Antarctica in the Late Santonian, and coincided with a period of rising global sea level. This resulted in a major marine flooding event, and widespread deposition of the marine Blue Whale Supersequence, followed by deposition of the White Pointer and Tiger supersequences (Figure 4). Gravity-driven, detached extensional and contractional faults formed during the Cenomanian as a result of deltaic progradation. The

deposition of the Tiger Supersequence coincides with a period of upper crustal extension resulting in the formation of large displacement, almost west–east-striking faults and the reactivation of many Cenomanian growth faults.

- The Late Cretaceous break-up associated with the first true oceanic crust at ~83 Ma (anomaly 33, Sayers et al., 2001). This coincides with the base of the Hammerhead Supersequence (Figure 4). This boundary can be strongly erosional and characterised by significant incisions believed to be the result of uplift related to the commencement of sea-floor spreading.
- A post break-up thermal subsidence phase that coincided with the second, large progradational delta development resulting from a massive influx of sediments giving rise to the characteristic, prograding shelf-margin geometries of the Ceduna Delta succession with the deposition of the Hammerhead Supersequence (Figure 4). A localised region of gravity-driven structures and simple, planar normal faulting developed with the latter reactivating older faults. Faulting appears to be latest Maastrichtian–Early Paleocene in age. Totterdell and Bradshaw (2004) suggest that the faulting was probably related to flexure of the margin caused by sediment loading during the Late Cretaceous.

Half-spreading rates were extremely slow from the Campanian (~83 Ma) until the Middle Eocene (~43 Ma), reaching a maximum of around 10 mm/year, although spreading rates were generally much less. From around 43 Ma, half-spreading rates rapidly increased to about 20 mm/year in a N-S orientation (Tikku & Cande, 1999). In the post Eocene period, deposition of marine carbonates reflects deepening water and the end of the effect of regional tectonics on the development of the Bight Basin (Fraser & Tilbury, 1979).

Late Cretaceous and Tertiary igneous rocks have been interpreted on seismic data (Totterdell et al., 2000) and Tertiary volcanic rocks have been dredged from the Bight Basin (Davies et al., 1989; Clarke & Alley, 1993). Schofield & Totterdell (2008) detailed the distribution of the volcanic and intrusive bodies in the Ceduna Sub-basin and related them to the acceleration in seafloor spreading during the Middle Eocene.

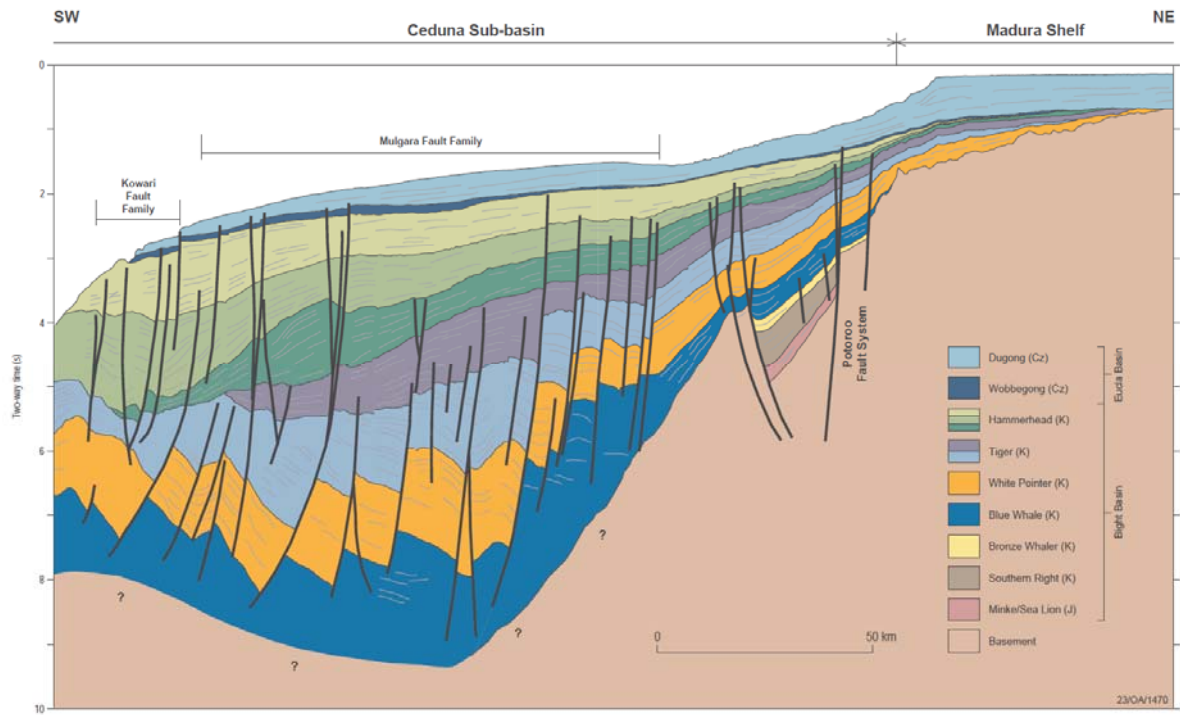


Figure 1 Cross-section through the eastern Madura Shelf and Ceduna Sub-basin. From Bradshaw et al., 2003.

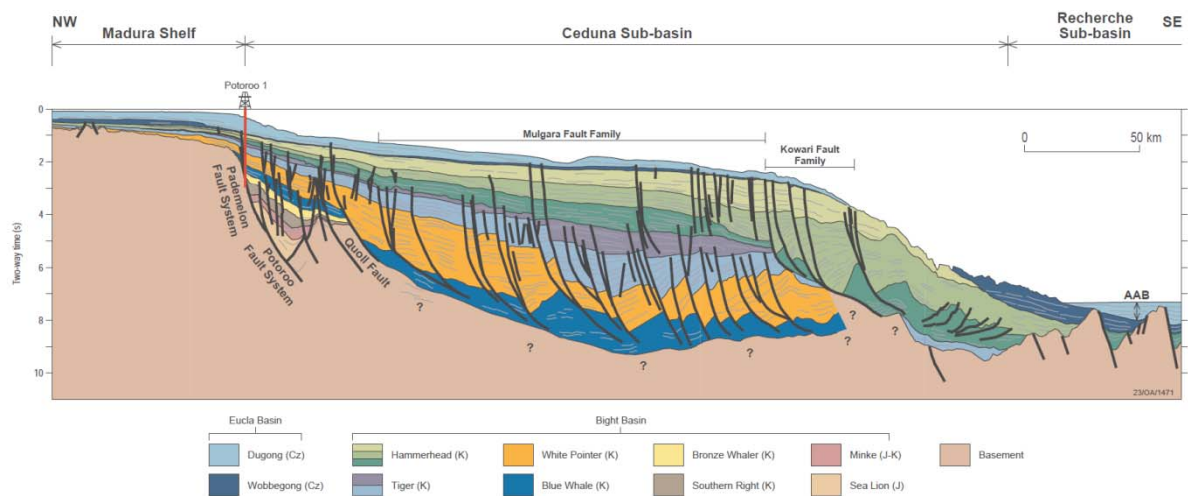


Figure 2 Cross-section through the eastern Madura Shelf, Ceduna Sub-basin and eastern Recherche Sub-basin. From Bradshaw et al., 2003.

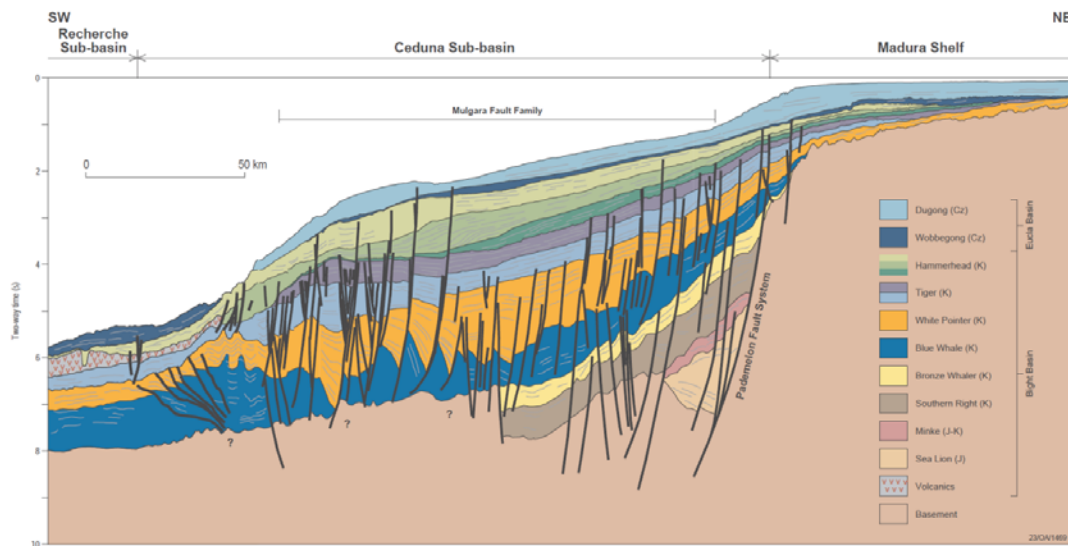


Figure 3 Cross-section through the eastern Madura Shelf, Ceduna Sub-basin and eastern Recherche Sub-basin. From Bradshaw et al., 2003.

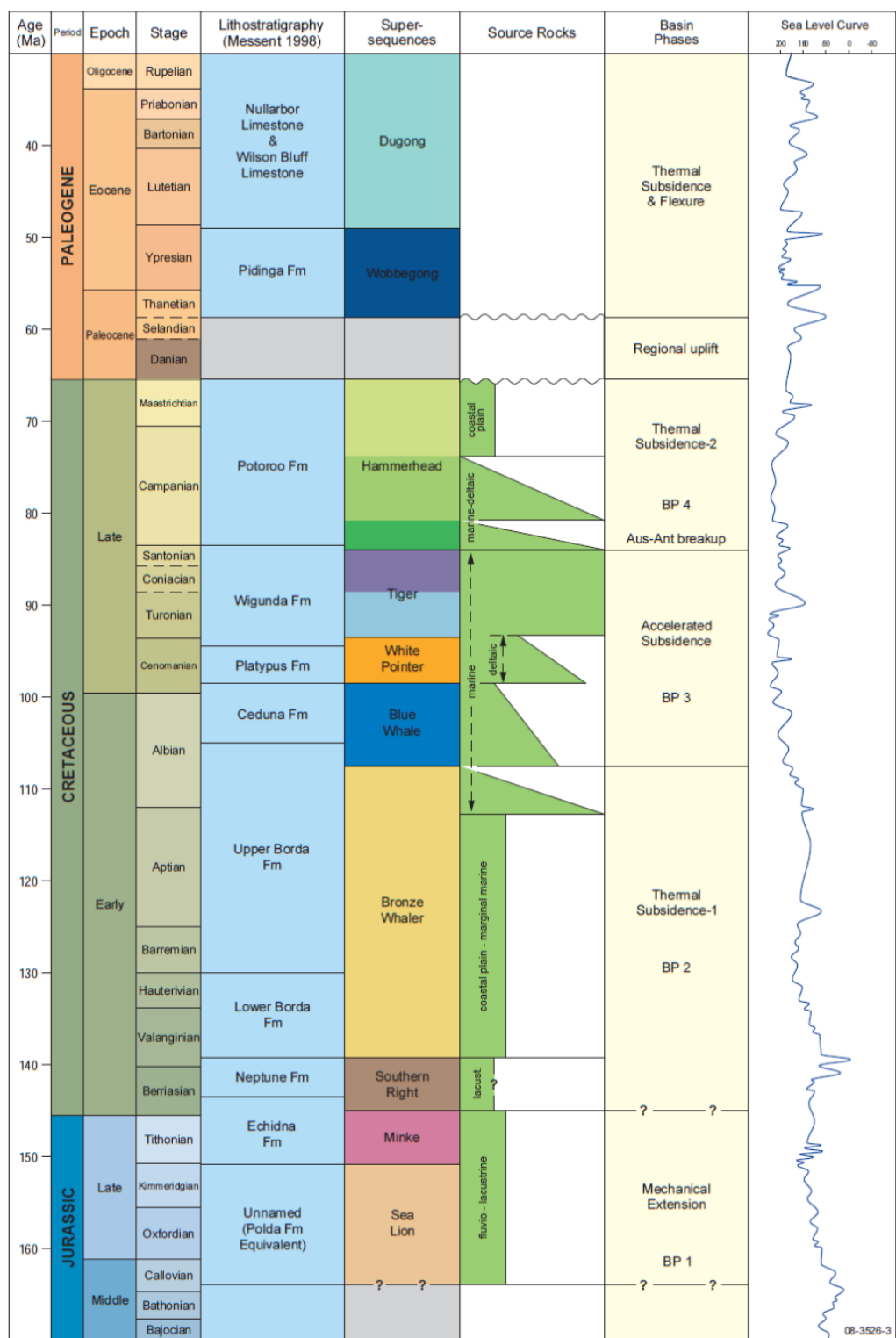


Figure 4 Bight Basin stratigraphic correlation chart showing basin phases and predicted source rock intervals (modified from Blevin et al., 2000 and Totterdell et al., 2000). The sea level curve (Haq et al., 1988) is modified to the time scale of Gradstein et al. (2004).

Rapid structural screening for marine survey target delineation

The initial phase of the structural assessment activities of the project was to delineate structural features that can be associated with potential leakage. This rapid screening was performed in advance of the 2013 Southern Surveyor (SS2013_C02) reconnaissance survey to develop and understanding of the structural styles and anomalies that could possibly be attributed to leakage.

To perform this activity the open file Flinders Deepwater 2D (2000) seismic survey data provided by Geoscience Australia in an IHS Kingdom seismic project format was used for the assessment. The data was used 'as received' with no further processing applied. All of the Flinders 2D seismic survey lines were assessed using a series of classification criteria based on previously published seismic attribute examples indicative of potential seepage (Talukder 2012, Obrien & Woods 1995) and fall under the general categories of:

- Fault displacement
- Fault geometry and distribution
- Fault linkage
- Petroleum system elements
- Seismic leakage indicators

The full list of classification schema are shown in Table 1 below. On screening of the 2D seismic lines the picks based on the classifications shown in Table 1 were ranked in order of priority. These seismic picks and their grouped rankings are shown in Figure 5 examples of the types of features identified are shown in Figure 6 and Figure 7.

Table 1 Seismic and interpreted geological feature classification criteria used in the rapid assessment of the potential for conduits for hydrocarbon seepage from the sub-surface.

ABBREVIATION	DESCRIPTION
SB	Fractured/Disrupted Sea floor
BS	Bright Spots
TFBI	Tilted Fault Block-large
TFBs	Tilted Fault Block-small
F	Faults-Conduit to Fluid Flow
FF	Small/shallow faults and fractures
BU	Carbonate Build Ups
Ch	Chimneys
LF	Listric Fault-Conduit to flow?
PG	Progrades allowing fluid to flow updip through permeable strata
CW	Canyon Wall-fluid conduit?
FLST	Fractured Limestone-shallow reservoirs?

HG	Half Graben with associated BS passing up wall
SGP	Shallow Gas Pockets
HAShRes	High amplitude Shale Reservoir?
TB	Tilted (shallow) Basement
FluidEsc	Fluid Escape
N	Noise
GR	Graben
CH	Channel incision with BS's
IF	Injection feature (most likely seismic artefact)
M	Potential Migration pathways
SF	Surface Fault
FS	Flower Structure

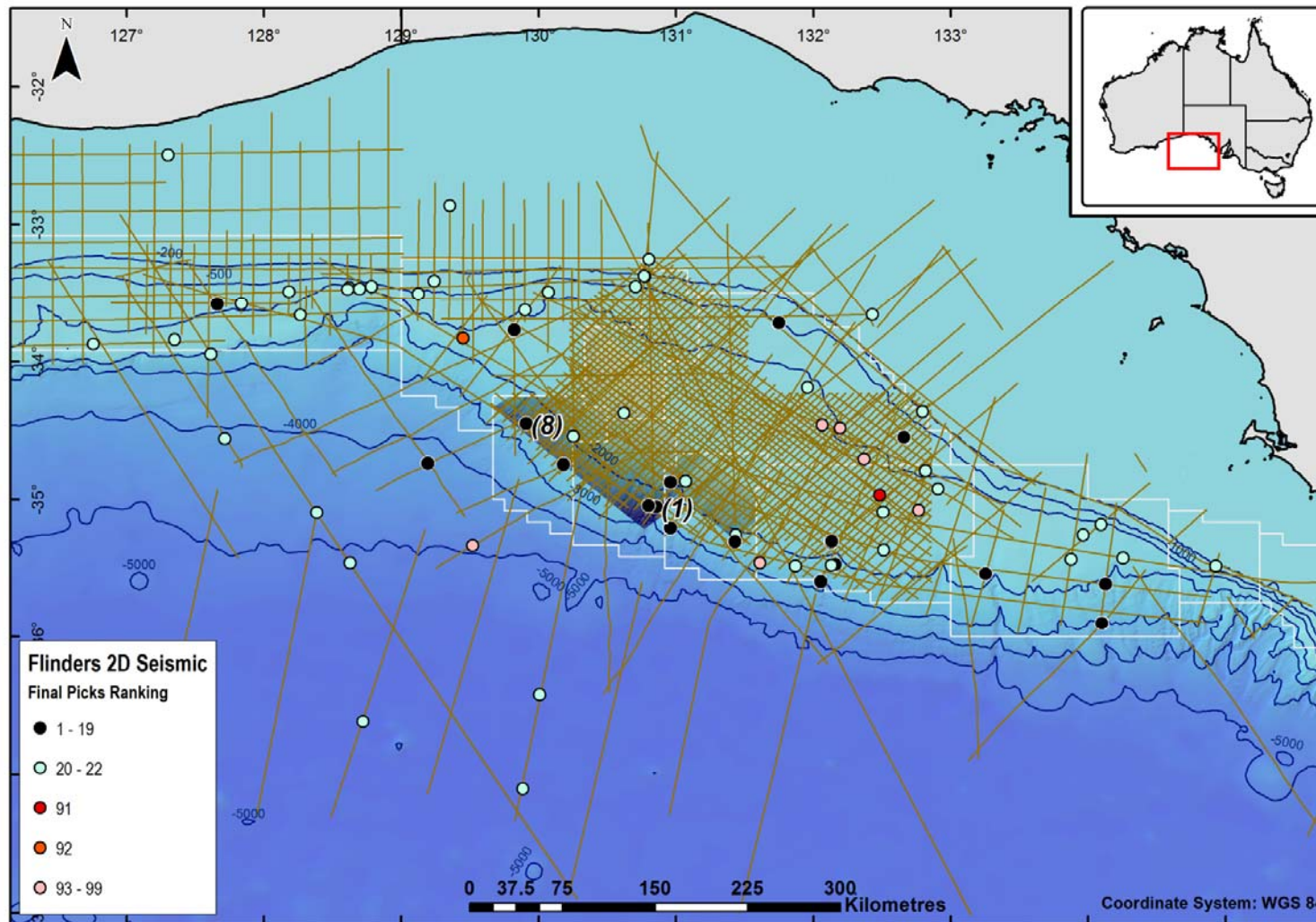


Figure 5 Map of the Ceduna Basin overlain by the exploration block outlines and the Flinders Deepwater 2D seismic lines. The picked anomalies and their ranking groupings are also shown. The location of Figure 6 and Figure 7 are also shown on the figure.

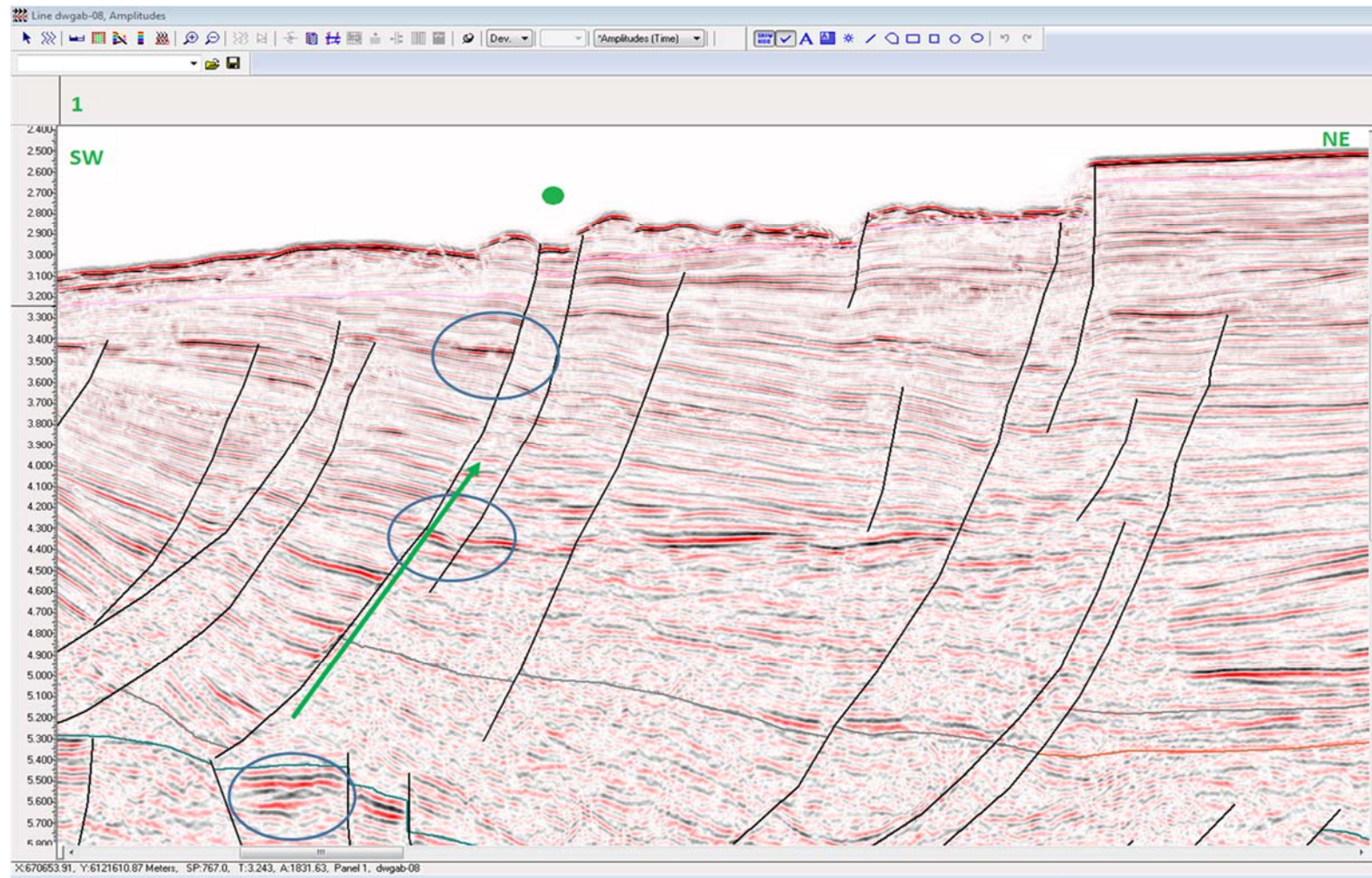


Figure 6 An excerpt of the dwgab 08 Flinders Deepwater 2D seismic line (area 1) showing highlighted features of interest. The image shows bright seismic amplitudes in several locations up the sequence toward the seafloor (blue circles) as well as a loss of seismic signal close to the fault plane which could be interpreted as the result of the formation of a gas chimney (green arrow). In addition there is evidence of recent reactivation of the fault due shown by seabed displacement.

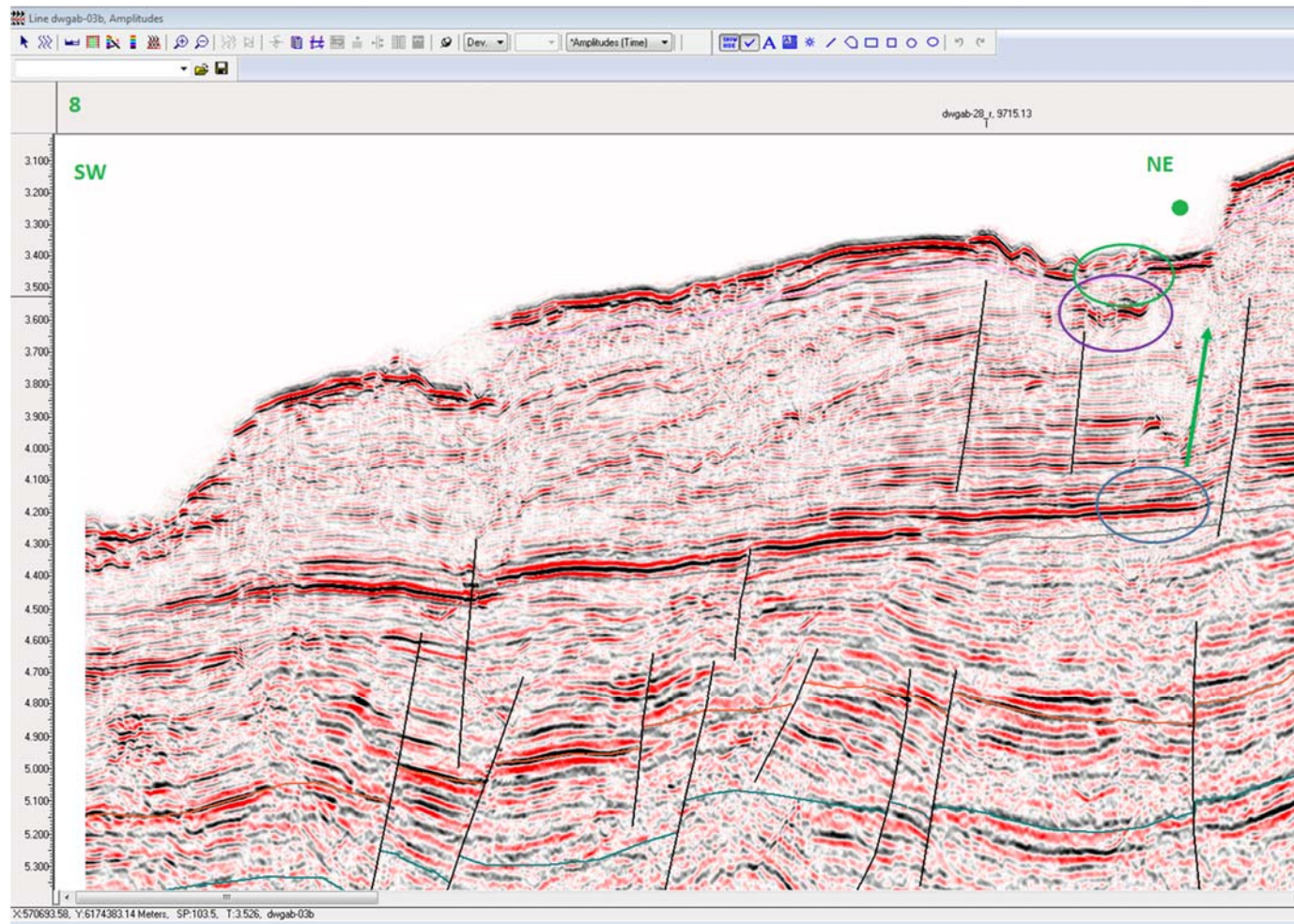


Figure 7 An excerpt of the dwgab 03 Flinders Deepwater 2D seismic line (area 8) showing highlighted features of interest. The image shows bright seismic amplitudes in the sequence (blue circle) as well as a loss of seismic signal close to the fault plane which could be interpreted as the result of fluid migration close to the fault plane (green arrow). In addition there is evidence shallow gas in the section as evidenced by the bright shallow amplitude (purple circle) and a fractured/disrupted sea floor which could be due to fluid escape (green circle).

Leakage indicator screening outcomes

The process identified 81 areas of interest. Whilst many features of interest were identified, no one area displayed unequivocal evidence of fluid leakage through the subsurface to the seafloor. This is not unexpected as the Geoscience Australia review of the same dataset also did not identify clear evidence of leakage. This does not preclude seepage being present within the GAB. Each basin where leakage occurs displays different seismic signatures. The leakage features are also often highly localised and thus may not be captured within the 2D seismic grids or be below seismic resolution.

The ranking of the features determined by the CSIRO team with the highest potential for leakage were strongly biased towards the outboard deep water slope of the Ceduna basin. Typically in areas where the interpreted overlying Dugong and Wobbecong sequences have been lost through slope failure to reveal Top Hammerhead sequence deposits.

Some of these features correlated spatially with historical Synthetic Aperture Radar anomalies and thus helped prioritise the limit additional numbers of captures to be collected discussed in the subsequent Synthetic Aperture Radar section.

Introduction to structural assessment

The second phase of Task 1 in the project agreement aimed to investigate the structural control(s) on hydrocarbon leakage and migration in the Ceduna Sub-basin (Figure 8 and Figure 9). The overall objective is to define the mechanism(s) of any hydrocarbon leakage, trapping and migration potentially associated with faults and to predict the key risk factors. The initial planning proposed a variety of research directions and investigation techniques. Based on data availability and the suitability of techniques to address issues of structural control(s) on hydrocarbon leakage within the Ceduna Sub-basin geological framework some of these research directions were not pursued while emphasis was put on others.

Initial mapping of fault linkage was performed during the structural interpretation of the Trim 3D survey and 2D datasets and displacement and timing of faulting were investigated. The distribution of clay material, required to investigate fault rock composition and membrane seal capacity was derived from sets of sub-basin scale forward stratigraphic models that were integrated into a 3D geological model of the Trim area. Investigation of the number, distribution and interaction of faults was carried out using the Trim 3D survey and regional 2D surveys. A thorough structural interpretation of the Trim 3D survey is used to investigate the fault rock composition and membrane seal capacity and their impact on hydrocarbon preservation.

The investigation of fault rock composition and membrane seal capacity was carried out as this likely represents the primary control on the preservation of hydrocarbon and compartmentalization of reservoir in stacked reservoirs-seal couplets. In addition mapping of seismic leakage indicators to calibrate the assessment of leakage pathways was partly undertaken. Investigation of geobodies at the Middle Eocene transition between the siliciclastic and carbonate deposition highlights features interpreted as biogenic mound complexes and potentially related to fluids paleo-leakage up faults and/or hydrocarbon paleo-seeps.

Seismic data used

The investigation of the structural control(s) on hydrocarbon leakage relies on:

- Open-file 2D seismic data acquired from Geoscience Australia (Figure 9) and mostly the Flinders Deepwater 2D seismic dataset (~16,000 km) covering the central Ceduna Sub-basin and the Deepwater GAB seismic dataset (~5000 km).
- Open-file Trim 3D seismic survey acquired from Geoscience Australia (Figure 9).
- Gnarlyknots-1A Well Completion Report and wireline data.

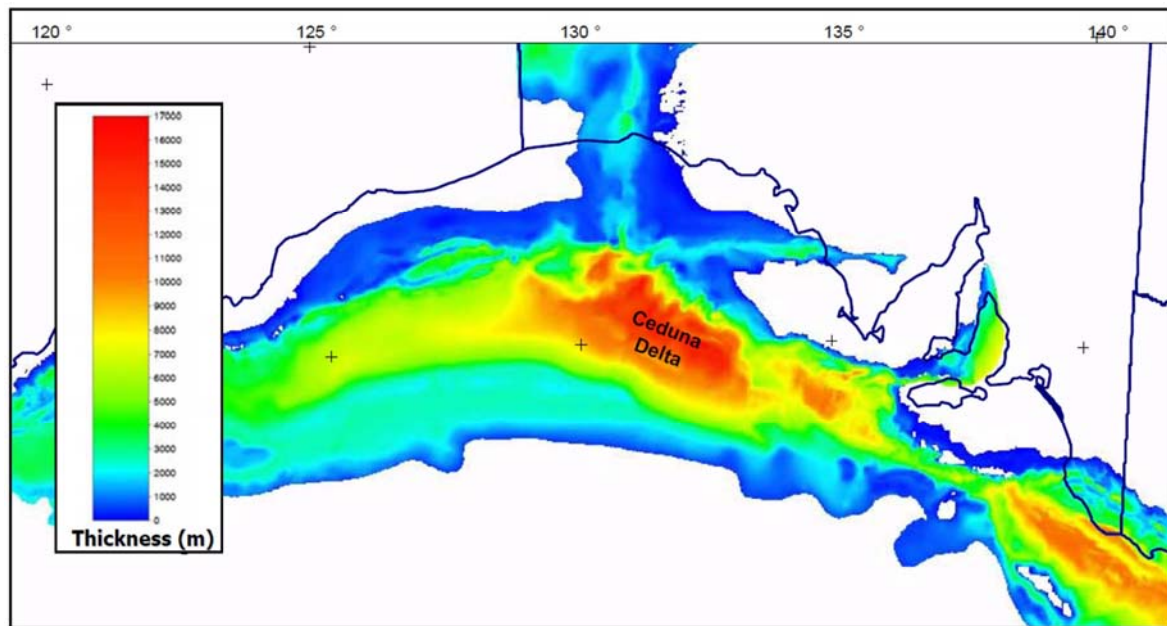


Figure 8 Location of the 'Ceduna Delta', the up to 17 km thick sedimentary fill of the Ceduna Sub-basin in the Bight Basin on the southern Australian margin (after Teasdale, 2004).

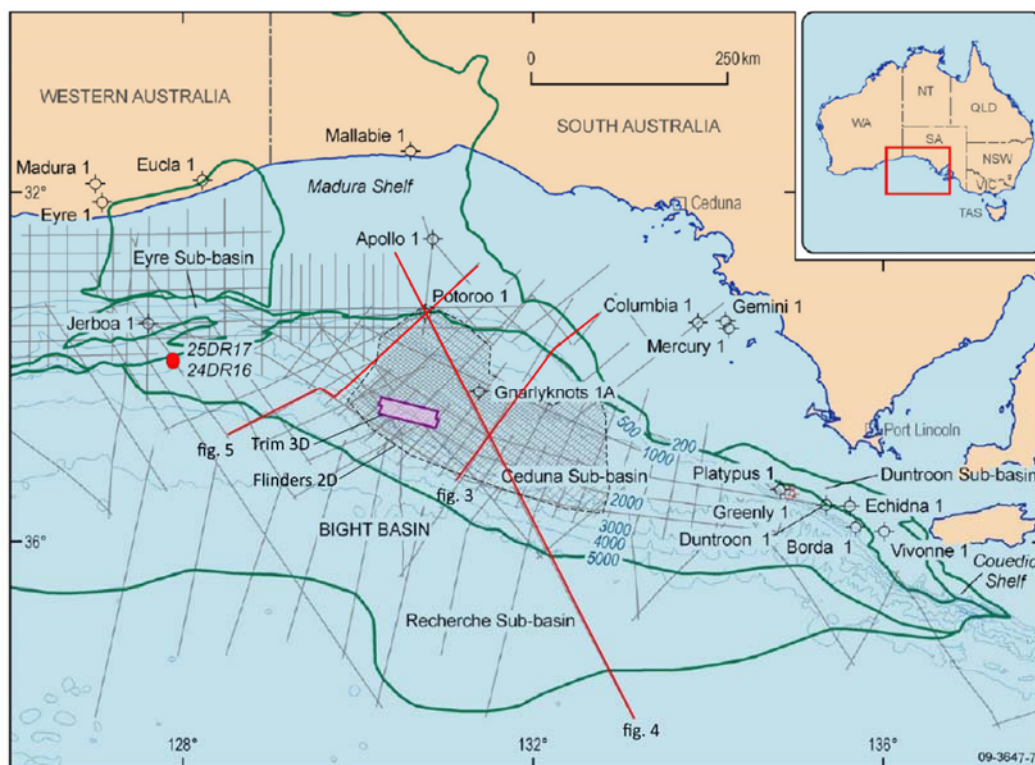


Figure 9 Ceduna Sub-basin with location of seismic data. After Somerville, 2001.

Seismic data quality

The quality of 2D seismic data ranges from adequate to good. The higher density of lines covers the central Ceduna Sub-basin with classic line spacings between 4km and 8km (Flinders 2D) in the southeast and northeast direction, respectively. Additional 2D lines cover the western and eastern part of the Ceduna Sub-basin with line spacing between 7km and 25 km. Some reflectors are interpretable in the 2D lines at 10 sec TWT.

The quality of the Trim 3D survey is adequate for the purposes of a reasonably stringent interpretation, but not particularly good; the dataset covers an area of 1200 km², ~60 km long in the inline direction (WNW) and ~20 km long in the crossline direction (NNE). The spacing is 30m and 12.5m between inlines and crosslines, respectively. The version in the Geoscience Australia distribution was geometrically distorted: the seismic volume had been flattened at the sea-floor; therefore the water column had to be restored. Reflections in the northwest half of the survey are not as pronounced as the southeast, especially at depth, which might indicate an issue with data acquisition, lithology or most likely processing as there is quite an abrupt change in quality between the two halves of the survey. Triangles of poorly resolved data occur in the shadow of the significant faults.

Seismic Interpretation

2D line & Geoscience Australia Interpretation

Geoscience Australia provided an initial interpretation of the main supersequence boundaries (Figure 4) with the Deepwater GAB 2D survey.

Additional regional interpretation was undertaken to provide initial screening for potential targets for the 2013 marine survey and to refine the regional stratigraphic and structural frameworks. The mapping of the main faults and the supersequence boundaries was extended on the Flinders and Deepwater GAB 2D surveys (Figure 9) and tied to well data where possible.

Trim 3D interpretation

The Trim 3D survey was interpreted to produce the underpinning for a static geological model focused on the Tiger and Hammerhead supersequences.

The dataset covers the top of the Ceduna delta system where gravity-driven extension is responsible for the development of a system of normal faults during the Cretaceous (Backé et al., 2012). The survey is located approximately 300 km from the coast, 130 km south of Potoroo-1 and 80 km WSW of Garnlyknots-1A (Figure 9).

Six horizons were interpreted from the Cenomanian to the Paleocene for the Tiger and Hammerhead supersequences (Figure 4; Table 2). The top White Pointer (Cenomanian), top Tiger (Santonian) and top Hammerhead (Paleocene) are tied to the Geoscience Australia interpretations (e.g. Krassay & Totterdell, 2003; Totterdell & Krassay, 2003; Totterdell & Bradshaw, 2004; Schofield & Totterdell, 2008); the intraformational horizons are tied to data and interpretations from Gnarlyknots-1 well (e.g. Woodside, 2004; King & Mee, 2004; Tapley et al, 2005). The horizons were picked on every 40th inline (1200 m) and 100th crossline (1250 m).

Table 2 Nominal horizons interpreted for the Trim 3D survey.

Horizon	Supersequence
Paleocene	Top Hammerhead
Campanian	Intra Hammerhead
Early Campanian	Intra Hammerhead
Santonian	Top Tiger
Coniacian	Intra Tiger
Cenomanian	Top White Pointer

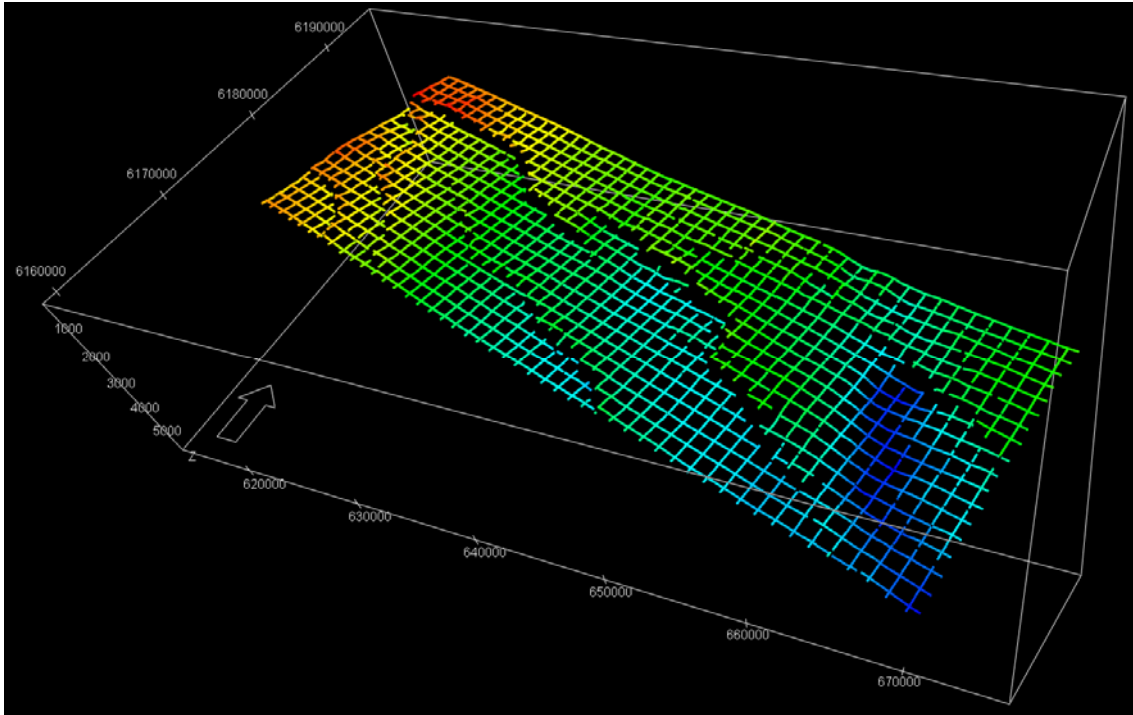


Figure 10 Santonian Top Tiger Supersequence horizon interpreted on the Trim 3D survey on every 40th inline (1200 m) and 100th crossline (1250 m). The Trim 3D survey is ~60 km x ~20 km.

The Trim 3D dataset was filtered to improve detection of faults using a workflow modified from dGB Earth Science (Friso Brouwer, pers. comm.). A fault enhancement filter that sharpens the faults and smooths non-fault discontinuities was designed by integrating dip attributes, similarity attributes, median filter and diffusion filter (dGB, 2012).

Coherency attributes were applied to the filtered seismic data to derive an attribute fault cube (Figure 11) that was used to highlight discontinuities and refine the structural interpretation (Figure 12). The faults are picked on every 100th crossline (1250 m) and on time slices every 500 ms TWT between 2600 ms TWT and 4100 ms TWT (Figure 13).

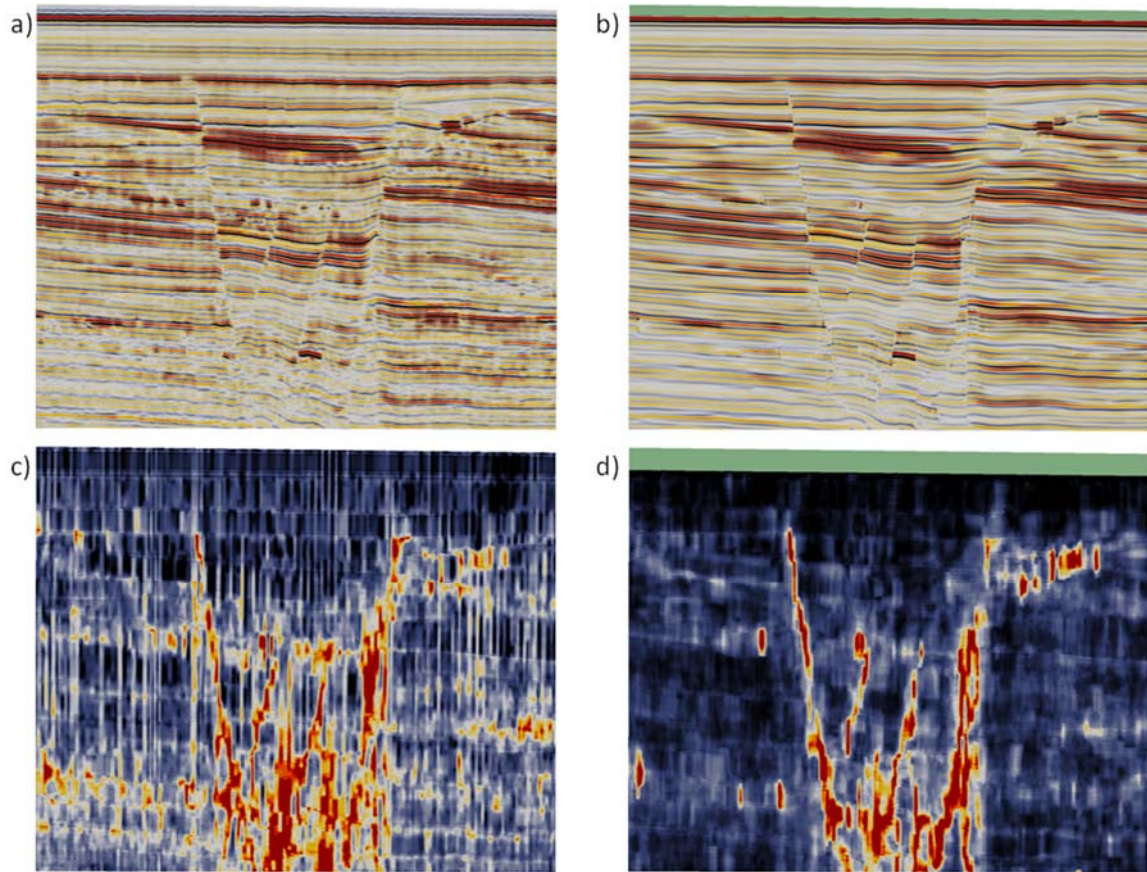


Figure 11 Attribute fault cube. A) Crossline of original Trim 3D seismic. B) Fault enhancement filter applied to same crossline of original Trim 3D seismic. C) Similarity attribute on original Trim 3D seismic. D) Similarity attribute on filtered Trim 3D seismic.

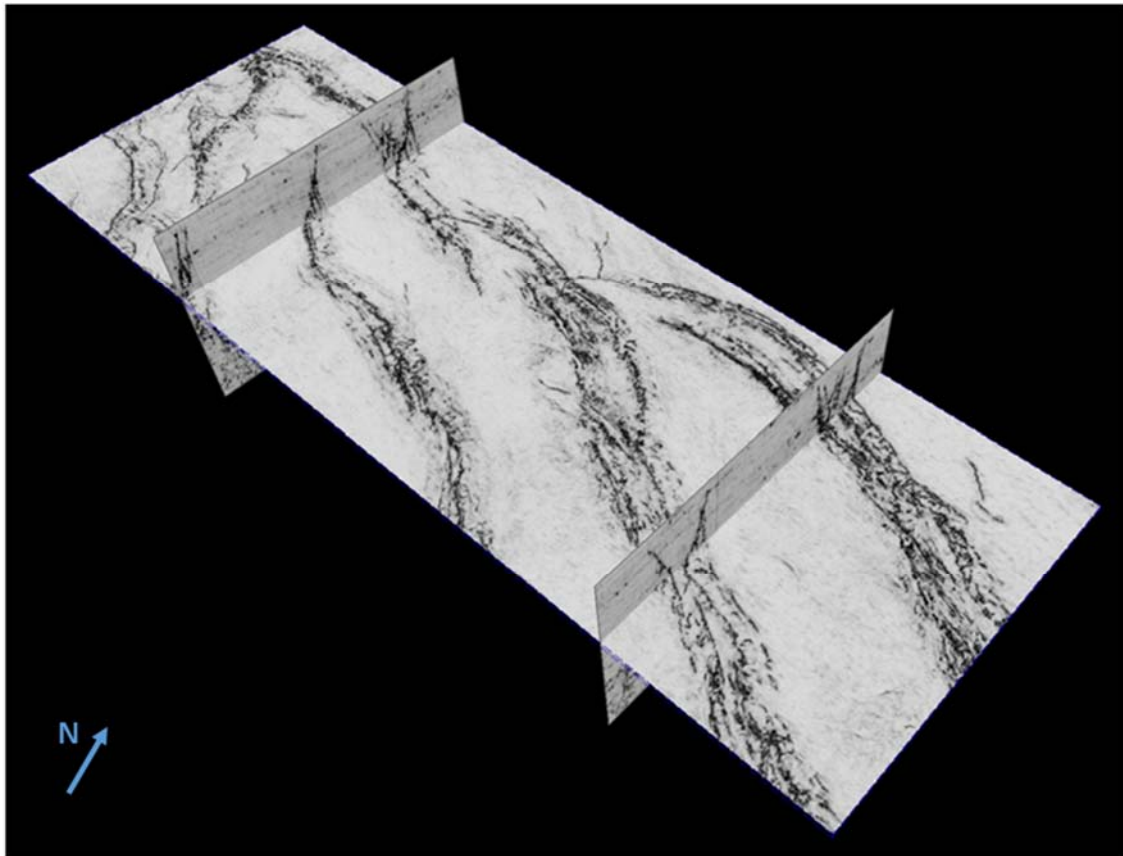


Figure 12 Time slice through attribute fault cube in the lower Hammerhead Supersequence. The Trim 3D survey is ~60 km x ~20 km.

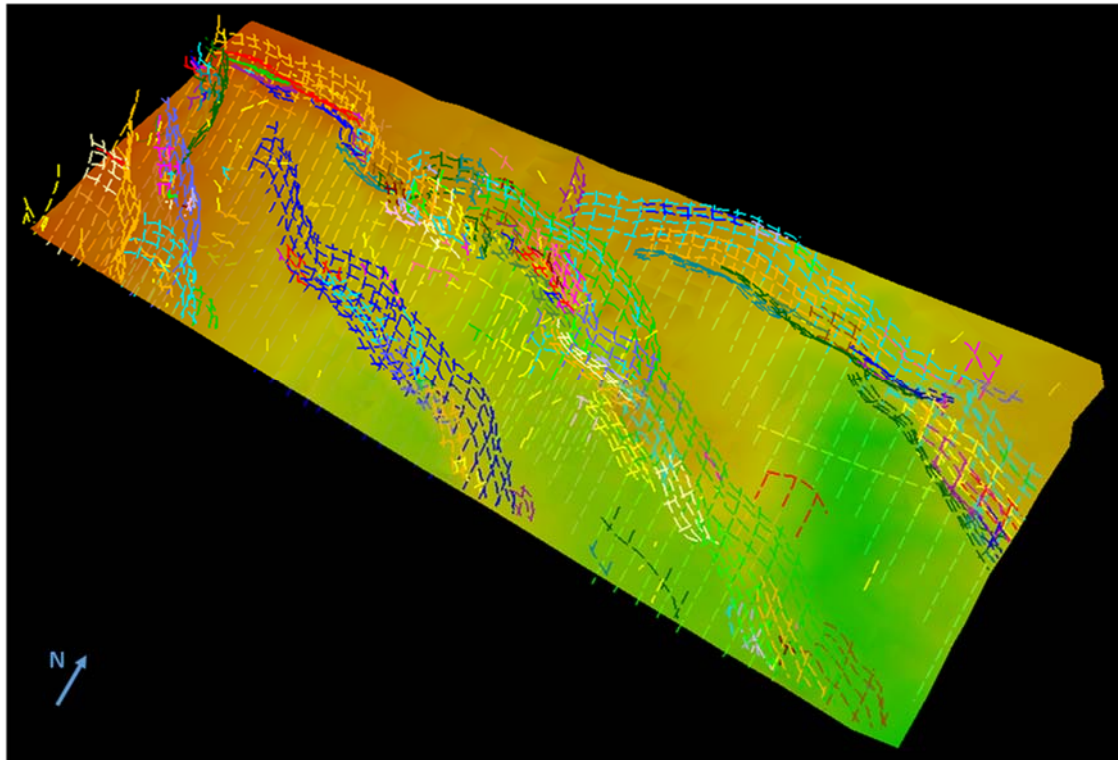


Figure 13 Fault interpretation on the Trim 3D survey on every 100th crossline (1250 m) and on time slices every 500 ms TWT between 2600 ms TWT and 4100 ms TWT. The horizon is the Santonian top Tiger. The Trim 3D survey is ~60 km x ~20 km.

175 faults were initially interpreted with a general northwest orientation (Figure 14). The trace lengths range from ~500 m to ~45,000 m and the maximum throws range from ~15m to ~1100m. The dip is generally toward the southwest for the largest faults (10,000-45,000 m long), however they can be curvilinear with tips and bends oriented to the west or the north-northwest; the smaller faults can be either synthetic or antithetic to the main faults (Figure 14 and Figure 15).

For the Late Cretaceous Tiger and Hammerhead supersequences, over the Trim 3D survey, the structure is characterised by a series of northwest oriented blocks (Figure 14) delimited by main southwest dipping faults (length: ~10,000-45,000 m, throw: ~300-1100 m). The secondary faults (length: ~500-10,000 m, throw: ~15-1100 m) are mostly restricted to the Hammerhead Supersequence (Figure 15). The main and secondary fault overlap forming complex connectivity between blocks through series of relays (Figure 16). Although the use of time slices through the attribute fault cube ensures a good control on the lateral extent of faults, disconnection of main and secondary structural features is expected at lower resolution with the occurrence of more relays.

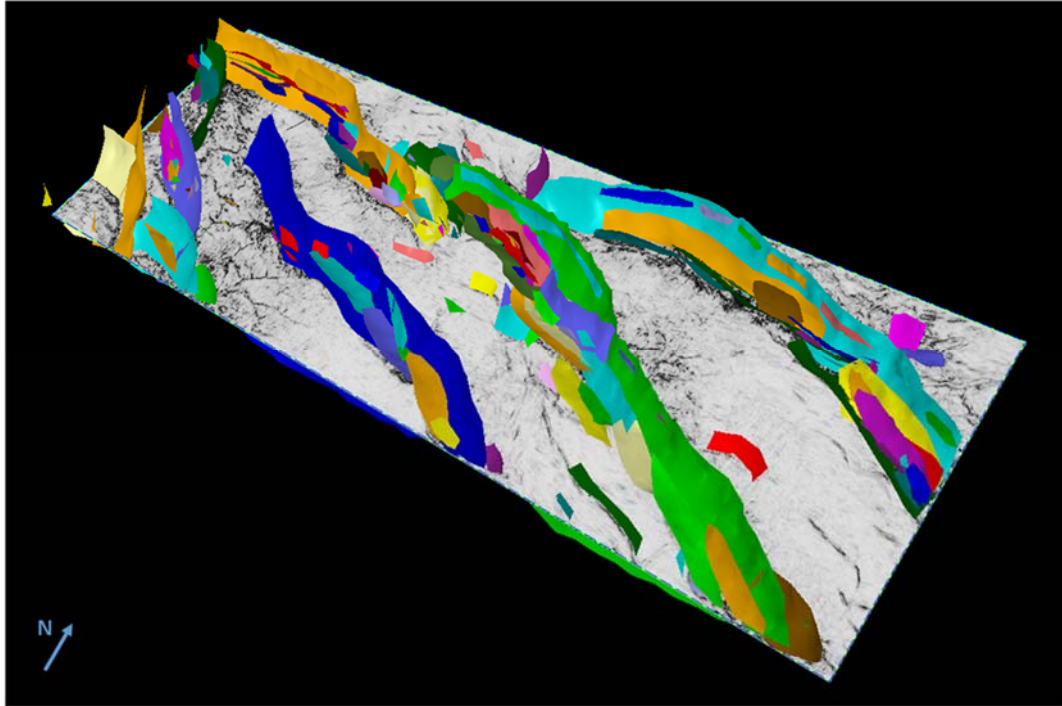


Figure 14 Structural pattern for the Trim 3D survey showing the main northwest oriented compartments. The Trim 3D survey is ~60 km x ~20 km.

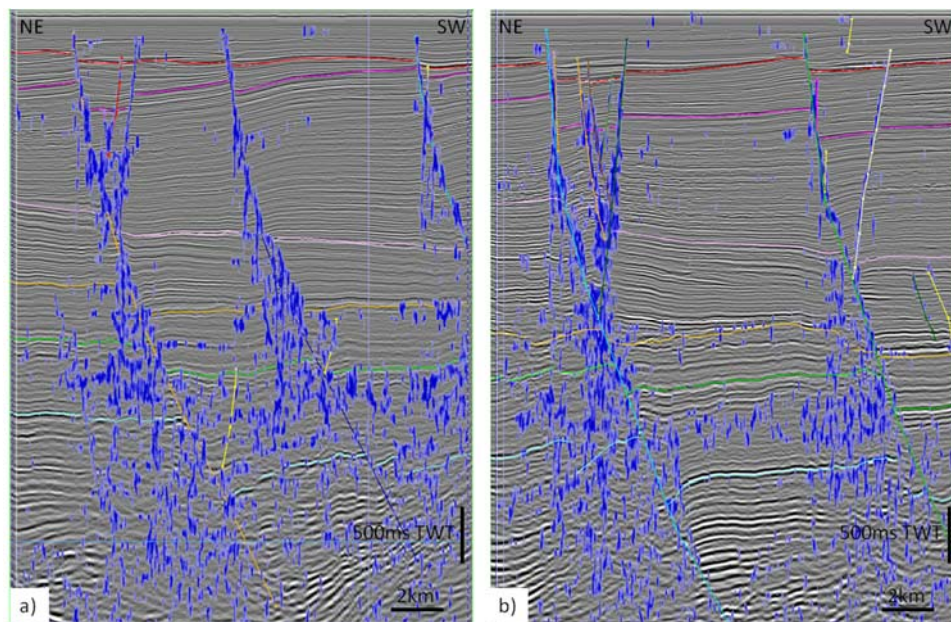


Figure 15 Trim 3D crosslines with attribute fault cube overlying seismic data. Location on Figure 12 with a) and b) to the northwest and the southeast, respectively. Light blue=Top White Pointer (Cenomanian); green=intra Tiger (Coniacian); orange=Top Tiger (Santonian); pink= intra Hammerhead (Early Campanian); purple=intra Hammerhead (Campanian); red=Top Hammerhead (Paleocene).

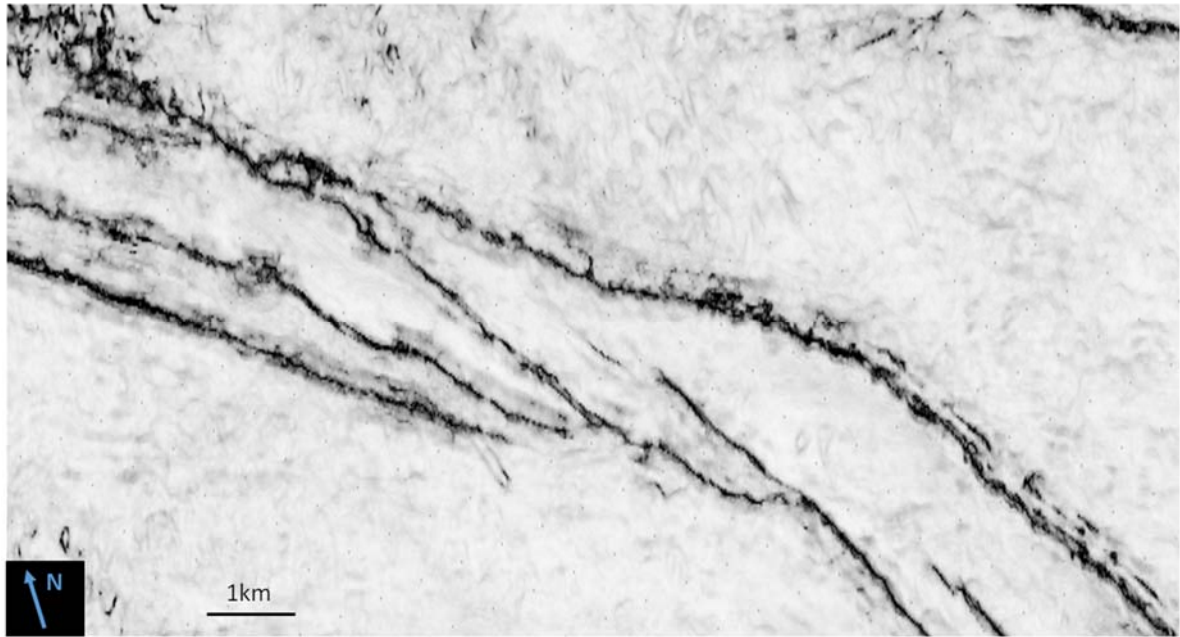


Figure 16 Close up of the upper Hammerhead structural pattern showing relay patterns.

Fault selection for further modelling

A subset of 32 faults was selected for further geological modelling and fault seal analysis (Figure 17); it comprises the main block bounding faults and the largest secondary faults. All faults dip toward the southwest as these comprise all the major structures. The common dip enables a geocellular model to be constructed for a much more significant thickness, which would be compromised if antithetic faults were included.

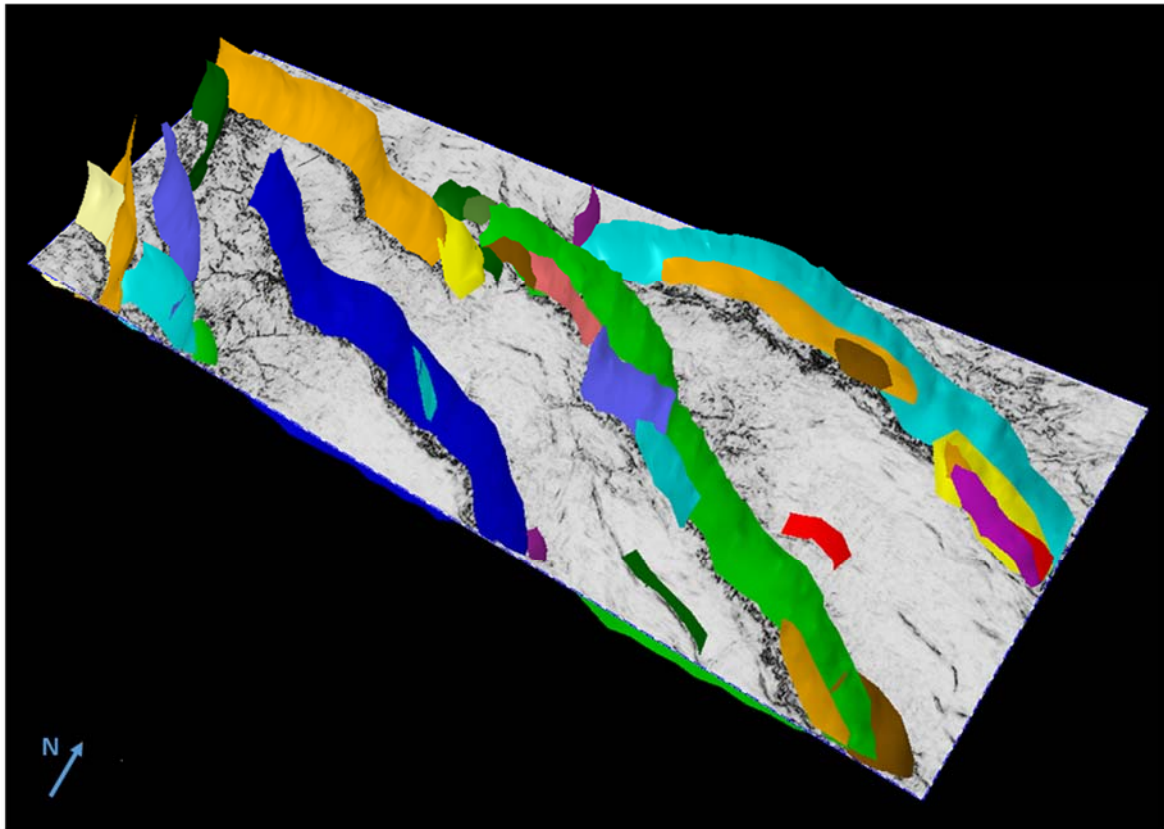


Figure 17 Faults subset for geological modelling and fault seal analysis. The Trim 3D survey is ~60km x ~20km.

Depth conversion

The Geoscience Australia release Trim 3D seismic survey distribution contained interval velocities for the dataset. The picked surfaces and the faults were converted using this data. The biggest issue was that the released Trim 3D volume is flattened to the seafloor which in fact varies in excess of 800 m across the survey area. The depth conversion of the data is therefore potentially the source of some error within the interpretation, though this might potentially be an issue at the scale of an individual hydrocarbon accumulation it should not significantly impact the across fault seal findings of this study as the outcomes for the several kilometre thick Hammerhead and Tiger supersequences are independent of depth at the scale of the potential errors.

Stratigraphic Forward Model

As part of an internal CSIRO, wider scale investigation a stratigraphic forward (SedSim) model of the Ceduna Sub-basin has been created. The goal of this model has been to predict potential sedimentary composition of the sub-basin, in particular to model potential constituents of the fringes of the Ceduna Delta, which are up to several hundreds of kilometres from the nearest well control.

Stratigraphic Forward Modelling is a sedimentary process simulation that recreates the way that stratigraphic successions develop and are preserved. It reproduces numerically the physical processes that eroded, transported, deposited and modified the sediments over varying time periods. In a forward modelling approach, data are not used as the anchor points for facies interpolation or extrapolation, but to test and validate the results of the simulation.

Stratigraphic forward modelling is an iterative approach, where input parameters have to be modified until the results are validated by actual data. SedSim workflow is illustrated in Figure 18. Stratigraphic Forward Modelling enables the prediction of facies in areas where data are sparse, unevenly distributed, or at inappropriate resolution.

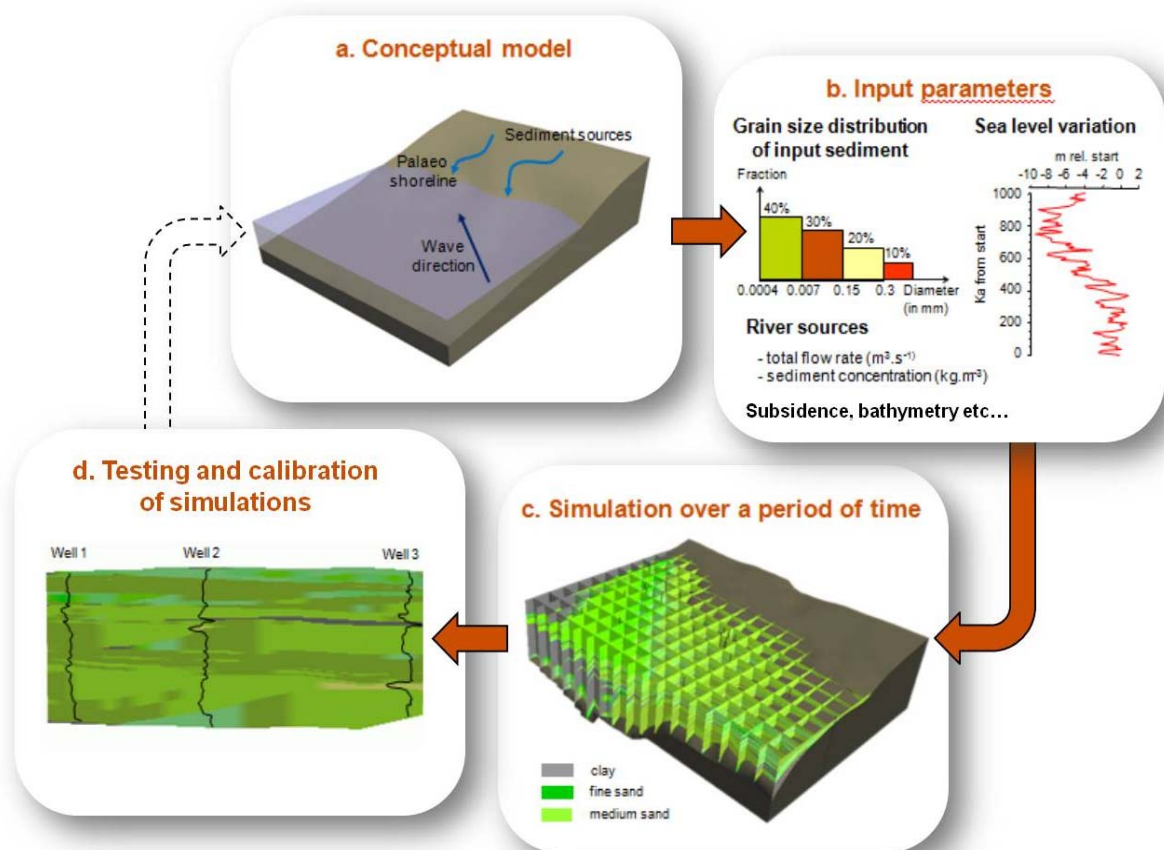


Figure 18 Stratigraphic Forward Modelling has a four step iterative workflow. The simulation workflow is repeated while modifying the conceptual model and input parameters until appropriate convergence with available data is achieved.

For this study the Sedsim three-dimensional stratigraphic forward modelling package that was developed originally at Stanford University by D. Tetzlaff and J. Wendebourg under the supervision of Prof. J. Harbaugh was used. It has since been modified and extended at the University of Adelaide and CSIRO by C. Dyt, F. Li and T. Salles (Griffiths & al., 2001). Sedsim models sediment erosion, transport and deposition, and predicts clastic and carbonate sediment distribution on a given bathymetric surface. In Sedsim the Navier-Stokes equations and the continuity equation are simplified and solved by using a marker-in-cell technique in two horizontal dimensions (Tetzlaff & Harbaugh, 1989). Flow velocity, water depth and sediment load are represented at points that move with the fluid. At each time step the position and velocity of each fluid element are recalculated, and the sediment transfer between the surface and the fluid element is calculated at the grid points. Past studies that have demonstrated the value of using Sedsim modelling include those by Griffiths et al. (2001), Li et al. (2005), Griffiths & Dyt (2001), Griffiths & Paraschivoiu (1998), Koltermann & Gorelick (1992), Martinez & Harbaugh (1993), Meyer et al. (2011), Salles et al. (2009, 2011a, 2011b).

SedSim is restricted to four user specified siliciclastic grain sizes. Additionally there is the option to include growth of two types of carbonates (for example coral and forams) and two types of organic material (for example algae and vegetation), and their resultant clastic grains after erosion. The options to include the effects of tectonic subsidence and compaction have been utilised in this project. Additionally SedSim has the ability to model a wider range of factors influencing deposition than have been used in this study, i.e. wave effects, aeolian processes, loading / isostasy, slope failures and turbidites / gravity flows. For more detailed consideration of the algorithms used by SedSim the reader is referred to Tetzlaff & Harbaugh (1989).

SedSim output is composed of a sedimentary thickness for each grain class in meters for each given time increment. For example there might be 20 m thickness of clay grains within a 100 m thick time interval. If this clay content is distributed evenly throughout the unit then its potential for constituting a top-seal is limited. If however the clay grains are concentrated in a single 10 m layer within the time interval it may well have far more significant implications for the direction of flow, in particular vertical flow through the model. As such this aspect of SedSim output has to be kept in consideration and the data needs to be analysed with a certain degree of thought.

Modelling parameters

One of the primary goals of the stratigraphic forward modelling was to keep as many of the variables as possible as uniform as possible. The idea being to use the scientifically established variables, i.e. the sea-level curve (Haq et al., 1987; 1988) and the evolving tectonic subsidence of the Australian southern margin as summarised above (Totterdell & Bradshaw, 2004; Blevin & Cathro, 2008; Lane et al., 2012) as the primary driving forces for model complexity. Source locations (Figure 19) and sedimentary concentration remain constant through the model run. Sedimentary input is varied through the history of the large scale Ceduna Sub-basin model, though this variation is kept to a minimum. During Hammerhead deposition the discharge at the main source reaches its maximum at 3500 m³/s which is not an exceptional figure (Gupta, 2007). Observations in the 2D and 3D seismic surveys (and earlier studies, e.g. Krassay & Totterdell, 2003) suggest that the main entry point for Hammerhead Supersequence material is near to or slightly to the west of the Potoroo-1 well, having been transported across the Madura Shelf. The further field source for the sediment is suggested by fission track thermotectonic studies of the crystalline terranes of southwestern and south Australia which suggest that >4 km of material was removed from these terranes during the late Permian and Mesozoic (Killick, 1998; Kohn et al., 2000; Kohn et al., 2002)

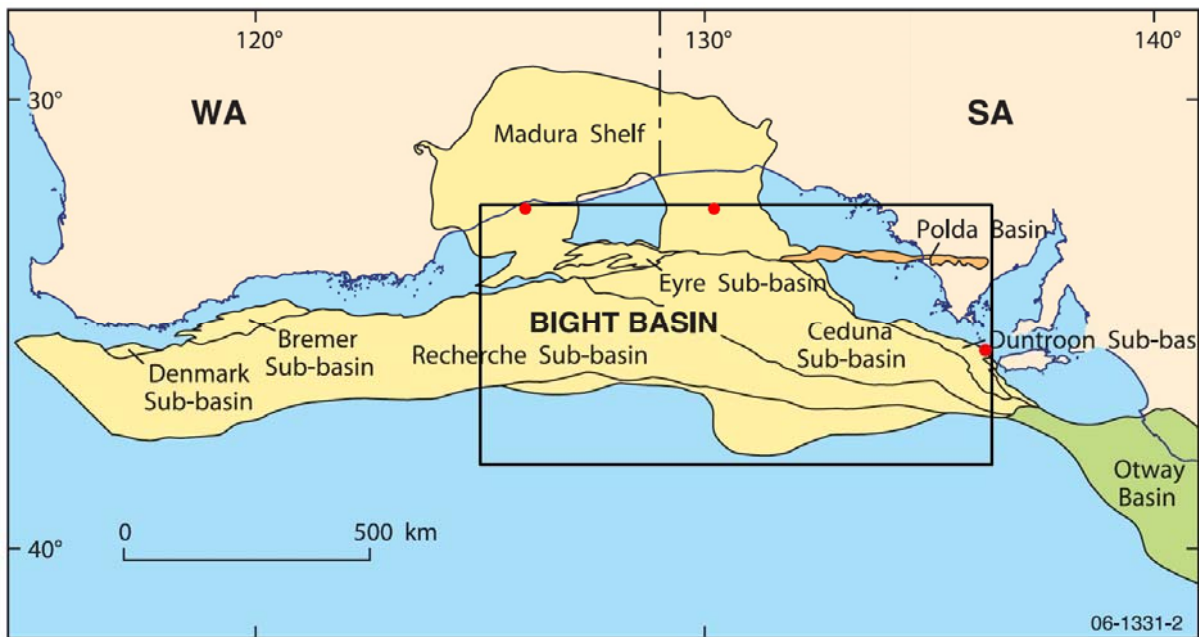


Figure 19 The 100 x 600 km Sedsim stratigraphic forward modelling area with source points located with red dots superimposed over the divisions of the Bight Basin (after Totterdell & Bradshaw, 2004).

The large scale Sedsim forward model was run over an area of 1100 x 600 km, with coarse 20 km node spacing (Figure 19). The initial Ceduna Sub-basin models were run from 163 to 65 Ma with a 1 Ma interval. Figure 20 illustrates example Sedsim output for the whole Ceduna Sub-basin model.

While the 20 km grid limits the model realisation s to large scale basin scale features therefore sedimentary features at the scale of an oilfield or for the Trim survey area are not resolved. Sedsim however enables this problem to be overcome by providing the functionality of nesting a finer scale grid within the larger coarse scale grid. For Trim area an 80 x 60 km sub-grid was modelled at 0.5 km resolution. As the focus of interest of this study is the Hammerhead and Tiger super-sequences, the model run was initiated at 95 Ma and the temporal resolution of the models was increased so that each layer represented 200 ka. The resultant fine-scale sub-grid was used for fault seal analysis.

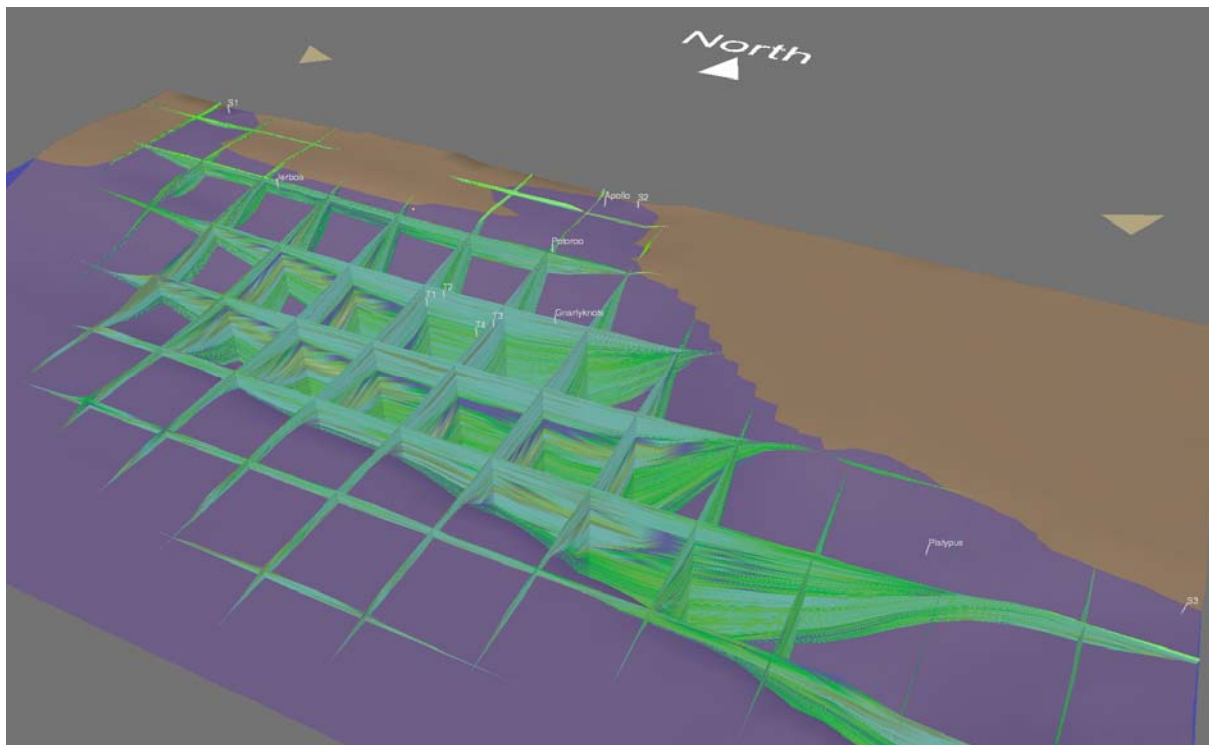


Figure 20 Visualisation of the whole Ceduna Sub-basin Sedsim model. Colour relates to siliclastic grain proportion. Vertical exaggeration is $\sim \times 10$. Fences are spaced at 160 km.

The basis for modelling the sedimentology is underpinned by data from the Gnarlyknobs-1 well. There are publically obtainable LAS data and a well completion report (Woodside, 2004). Unfortunately the WCR appears to some extent contain some inaccuracies, the gamma ray log (GR) to V_{shale} derivation described in the text is over-simplified and the curve which would result from it does not match the curve which is presented in the subsequent figure within the WCR. When the described derivation is repeated the resulting mean V_{shale} for the sequence would be ~ 0.6 , which does not match the description of the lithology in the WCR. Attempting to match the curve illustrated in the WCR can be achieved using a simple linear transformation which results in $\sim 0.4 V_{\text{shale}}$. This outcome still seems fairly high. In light of the questionable gamma interpretation presented in the released WCR log interpretation fundamentals were revisited and a generic workflow was implemented to derive V_{shale} from the raw gamma data (Larionov, 1969; Asquith & Krygowski, 2004). Raw GR data generally occurs in the range of about 20 to 200 GR API units and in practice is clipped to get rid of anomalous values before any transformation is applied. Woodside report that they clipped to 90 % of the largest value in their presented interval and treated this as representing 100 % shale, which is questionable. If we take the clipping (31-75 GR API) which could have been used to reproduce the published Woodside V_{shale} curve but additionally apply an text book standard, non-linear transform to the data then $\sim 0.3 V_{\text{shale}}$ is achieved. As such a methodology is based on the highest GR value present not the highest possible (generally in the range 150 to 200) and as such will probably over represent the shale content, as such this is the point which the shaliest sequence modelled will be

matched. The upper cut value was incrementally increased by 20 GR API units (95, 115, 135 GR API) to give ~ 0.19 , ~ 0.15 and ~ 0.1 V_{shale} , these values were targeted to form the output of the forward modelled sequence. It should be noted that 200 GR API which is probably the upper feasible limit to clip at results in ~ 0.05 V_{shale} , potentially not too far off the mark given the sandy description of the sequence.

The only parameters varied between the Sedsim models including the Trim survey area, fine-scale runs, are the proportions of the four siliclastic grains. All other variables remain constant over the run. The four siliclastic grains used in the model are the same as for the series of while Ceduna Sub-basin models and comprise medium sand, fine sand, medium silt and clay. In the four nested models the respective percentages of each are 10, 15, 15, 60; 15, 25, 25, 30; 25, 25, 25, 25 and 35, 30, 20, 15. Figure 21 illustrates the 0.5 km resolution nested model.

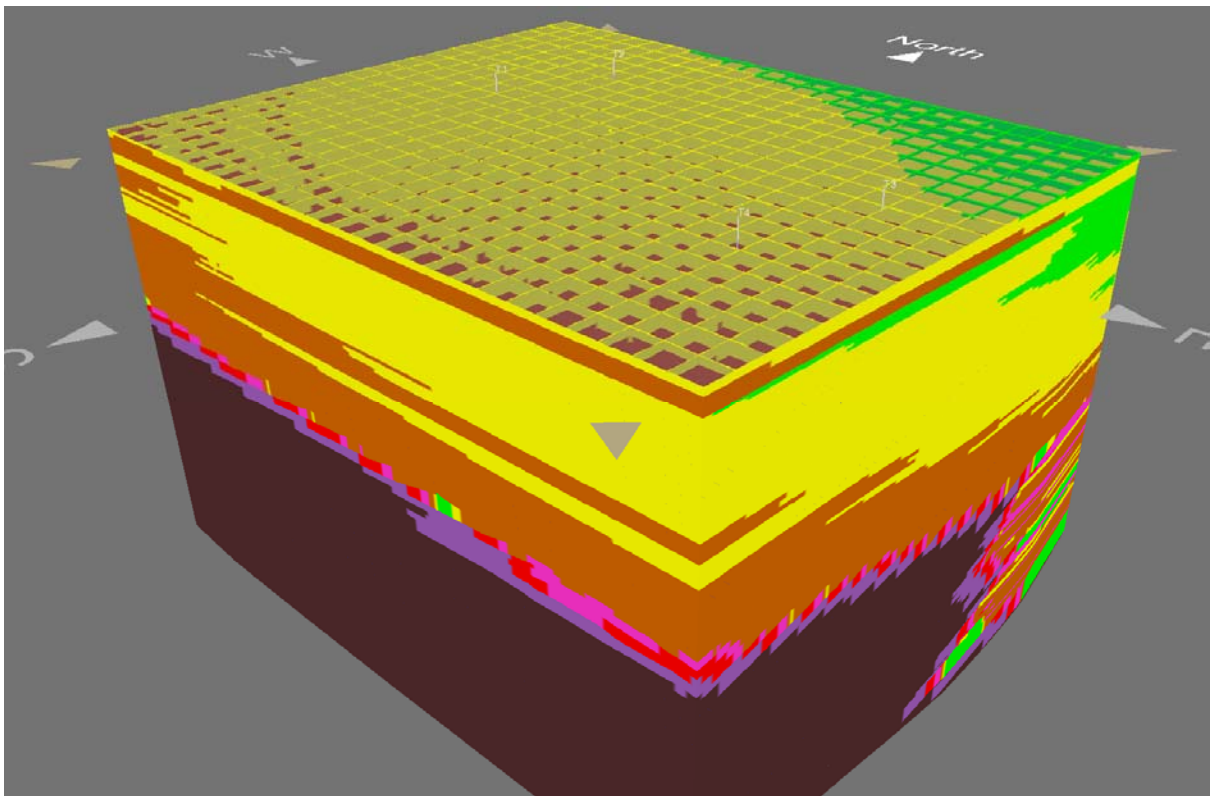


Figure 21 0.5 km resolution Sedsim output. The model illustrates a transition from marine (dark brown) Tiger Supersequence at the base through shoreline (yellow) and finally fluvio-deltaic facies (green) of the Hammerhead Supersequence. The corners of the Trim 3D survey are marked (T1-4). Fences are spaced at 4 km.

Trim Geomodel

The depth converted layers and fault surfaces interpreted from seismic have been combined into a five layer structural framework using the structural modelling module in RMS (Figure 22). The 140 layer Sedsim output is tied to the ages of the picked horizons in the model and

this framework is used to divide up the Sedsim output to populate the model based on the coarser layer framework of the structural model. It should be noted at this point that the Sedsim data is based on age consistent horizons whereas the interpreted stratigraphic horizons of the structural models are based on the physical responses of the lithology to seismic and are not necessarily age related, this is a potential source of error though with the accumulated assumptions in the modelling at this stage the discrepancy is not expected to unduly affect the fault sealing results. Geocellular V_{shale} volumes increasing in shale content are illustrated in Figure 23 through Figure 26. The four cases are all thought to be possible models; however the intermediate cases are thought to be the more likely real world scenarios.

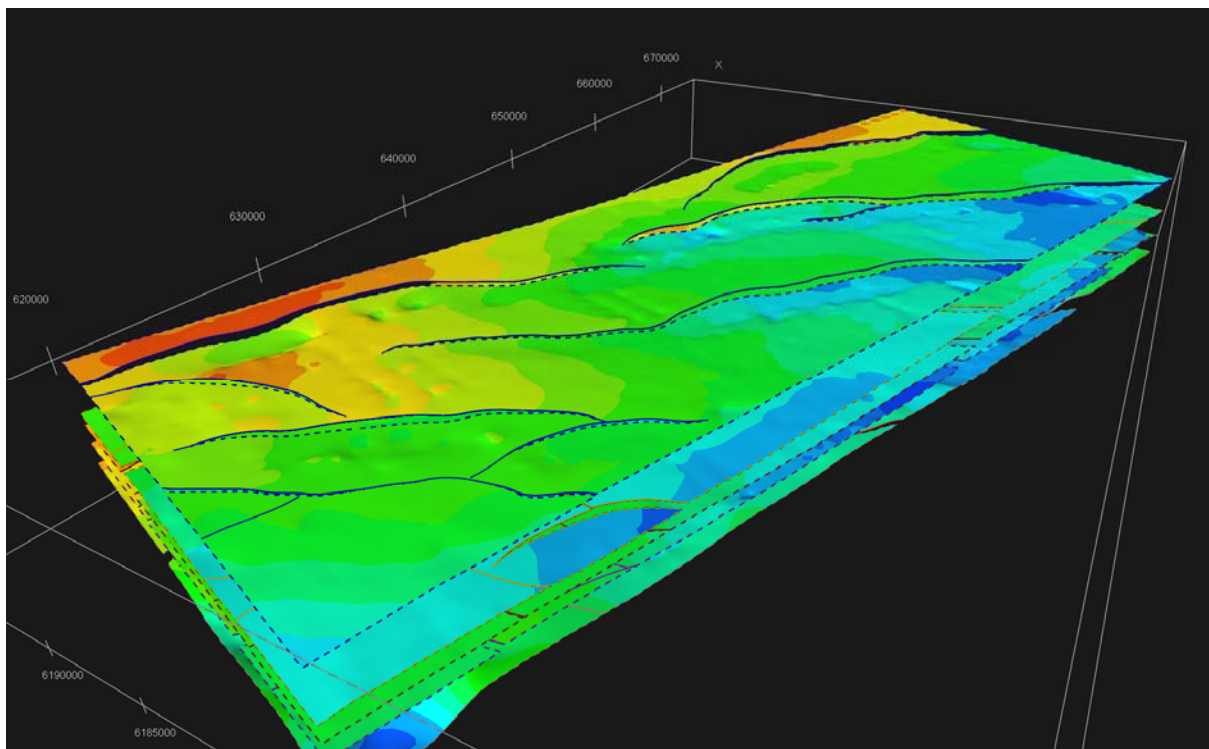


Figure 22 Bottom five surfaces in the RMS structural model illustrating fault polygons for the largest faults interpreted in the Trim 3D survey. View from SW, colours represent depth on a surface basis.

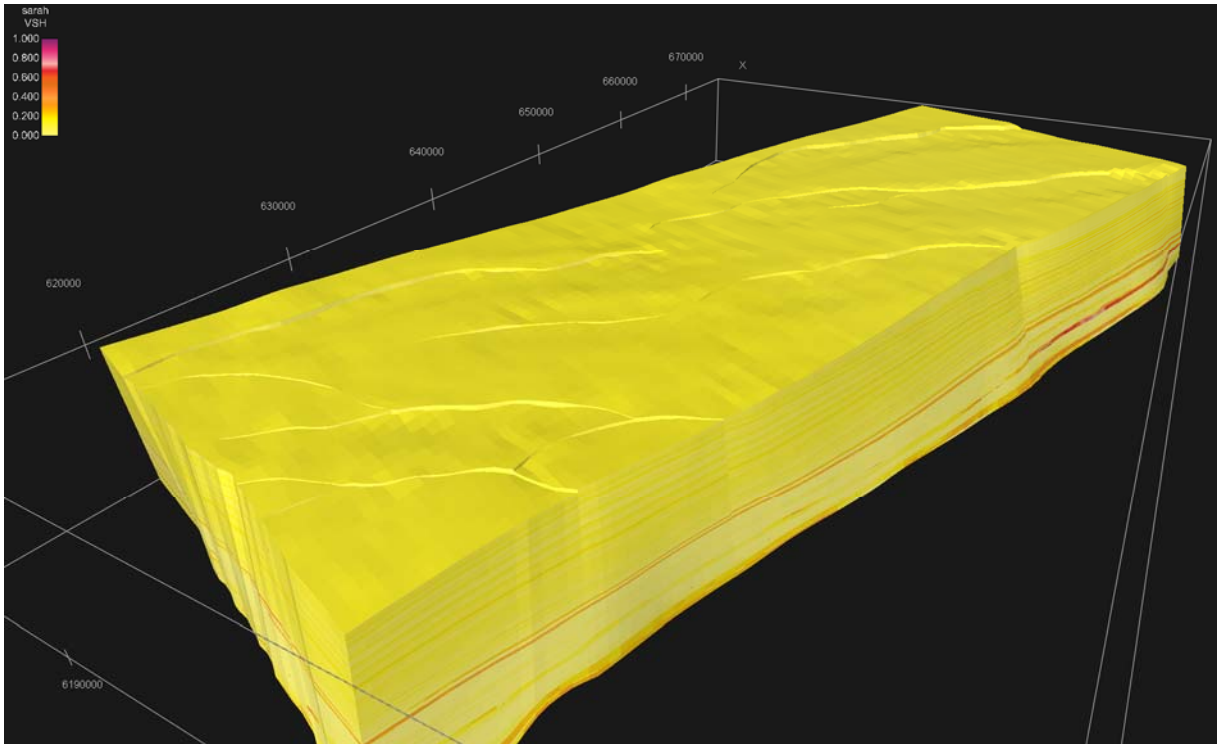


Figure 23 140 layer Geocellular shale content volume for the sandiest case, V_{shale} is ~ 0.1 .

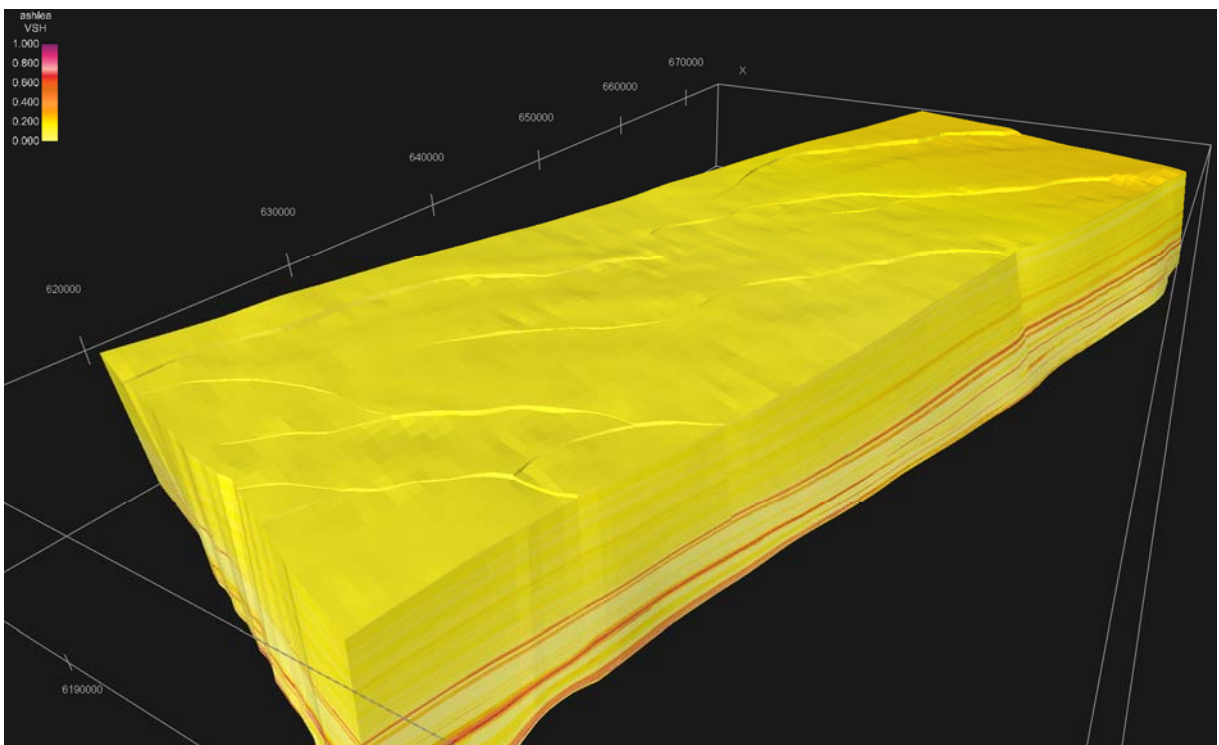


Figure 24 Intermediate case 140 layer Geocellular, V_{shale} is ~ 0.14 .

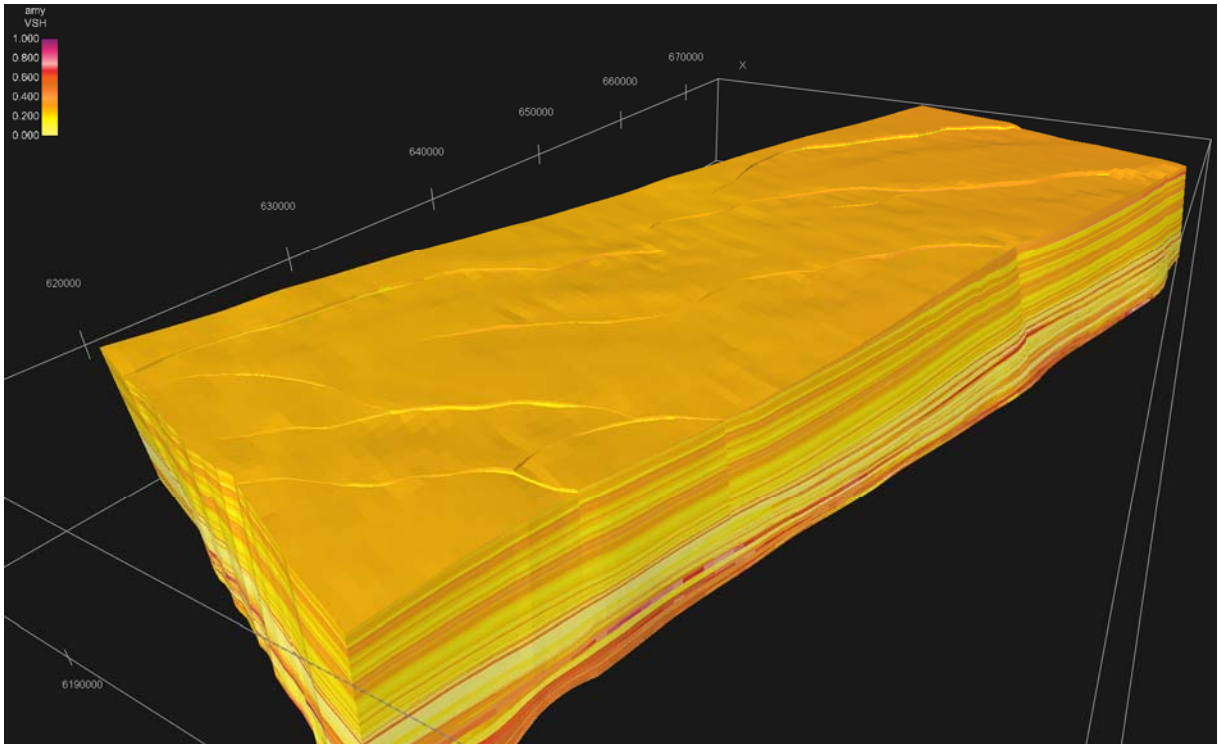


Figure 25 Intermediate case 140 layer Geocellular, V_{shale} is ~ 0.19 .

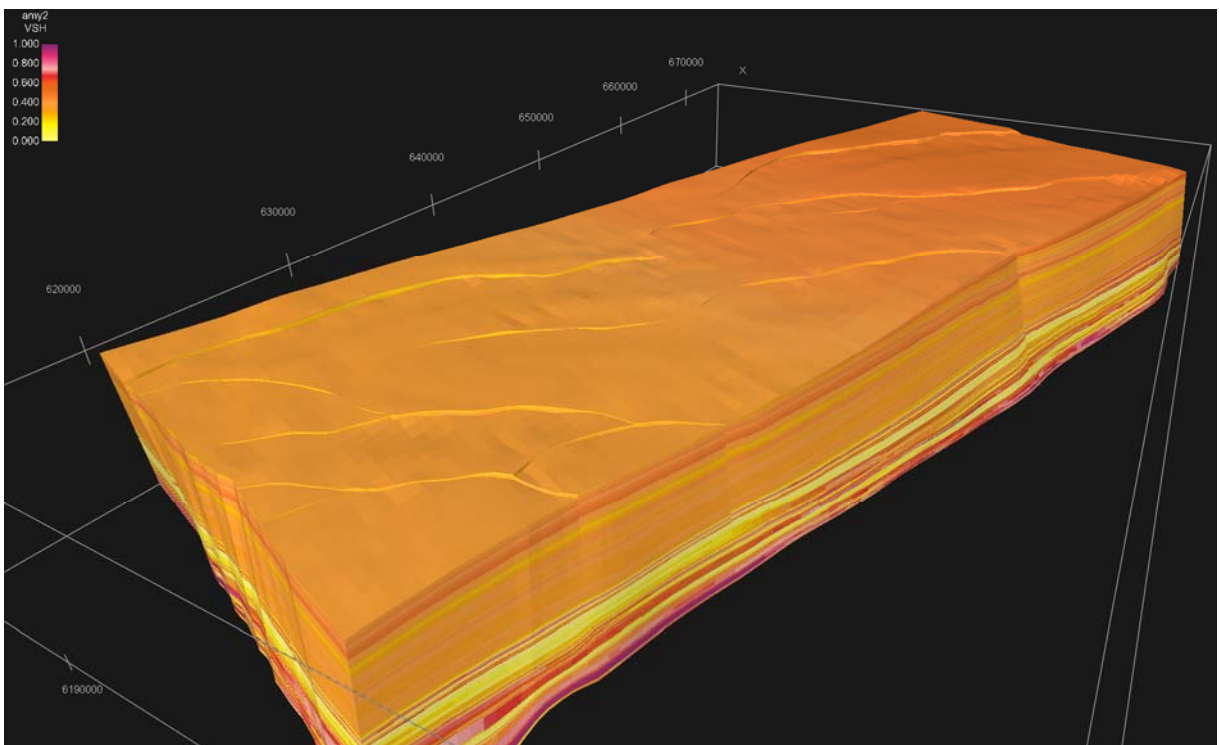


Figure 26 140 layer Geocellular shale content volume for the shaliest case, V_{shale} is ~ 0.30 .

Fault Seal – Potential impacts on across fault flow

The southward dipping sediments of the Hammerhead Delta are cut by approximately perpendicular faults. It is important to assess the across-fault sealing properties of these faults as they are optimally placed to impact migration through the Hammerhead Delta, potentially disrupting flow, but also creating possibilities for suitable hydrocarbon traps.

Shale Gouge Ratio

To assess the sealing capacity of sand on sand faulted juxtapositions, a number of different fault-seal algorithms may be utilised. Shale Gouge Ratio (SGR), defined in publications by Fristad et al. (1997), Yielding et al. (1997) and Freeman et al. (1998), is an attempt to predict the proportion of shale incorporated into a fault zone. At each point on the fault, the algorithm calculates the net content of shale / clay in the volume of rock that has slipped past that point on the fault. The implicit assumption in this algorithm is that material is incorporated into the fault gouge in the same proportions as it occurs in the wall rocks in the slipped interval. If this assumption is true, then SGR can provide a direct estimate of the up-scaled composition of the fault zone as a result of the mechanical processes of faulting. A high SGR value corresponds to more phyllosilicate in the fault zone and therefore to higher capillary threshold pressure and lower permeability. Case studies (e.g. Yielding 2002; Sperrevik et al. 2002; Dockrill and Shipton 2010; Bretan et al. 2011; Manzocchi et al. 2010) have shown that there is a general correlation between the measured clay content of a fault zone and the calculated SGR value, higher SGR values being derived for fault zones containing a higher observed clay content. In many basins in particular the Brent Province (Yielding, 2002), it is observed that $SGR > 0.15$ corresponds to faults that are sealing to hydrocarbons.

Trim across fault seal modelling results

Across-fault sealing results are illustrated in Figure 27 to Figure 30.

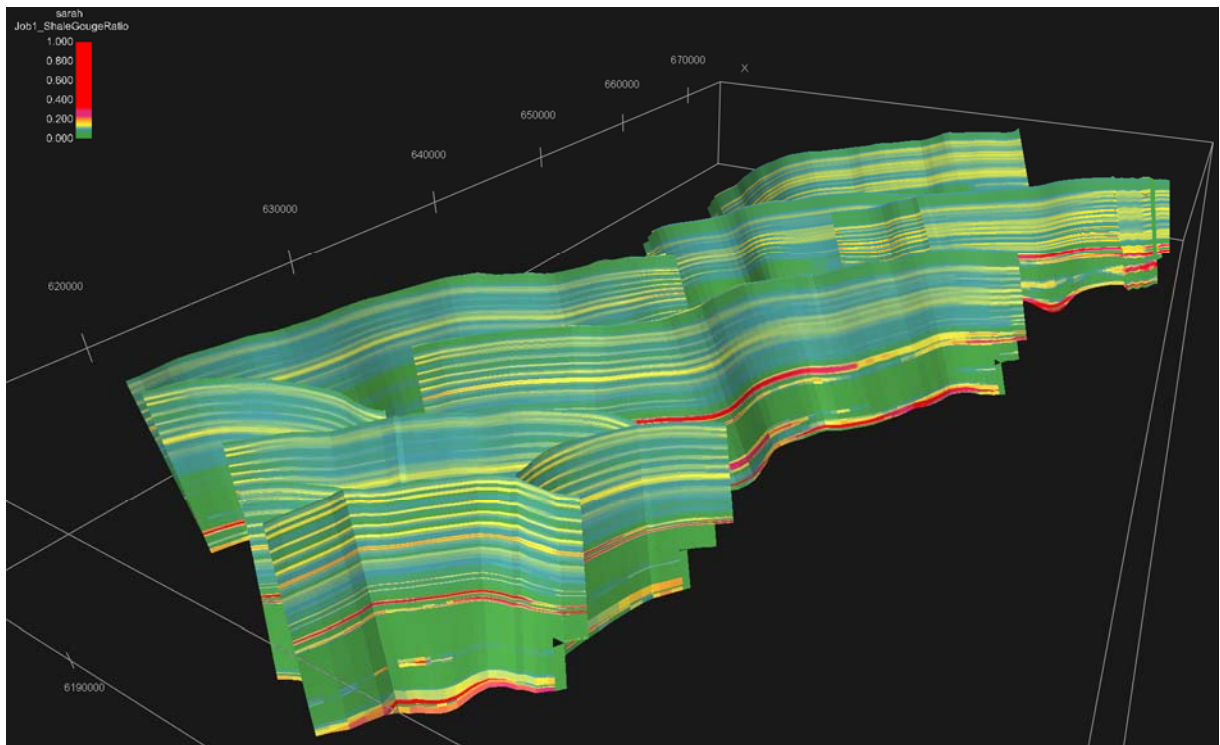


Figure 27 SGR derived for the sandiest case ($\sim 0.1 V_{\text{shale}}$). Green is 'go' for across fault leakage, red is where leakage is 'stopped'. The colour scheme is based on standard SGR publications (e.g. Yielding, 2002). In this case faults are dominantly leaky, but yellow areas indicate the presence of areas with some potential for fault seal and red, >0.3 SGR indicates probable sealing in even this the sandiest case. Again viewed from the SW in all cases.

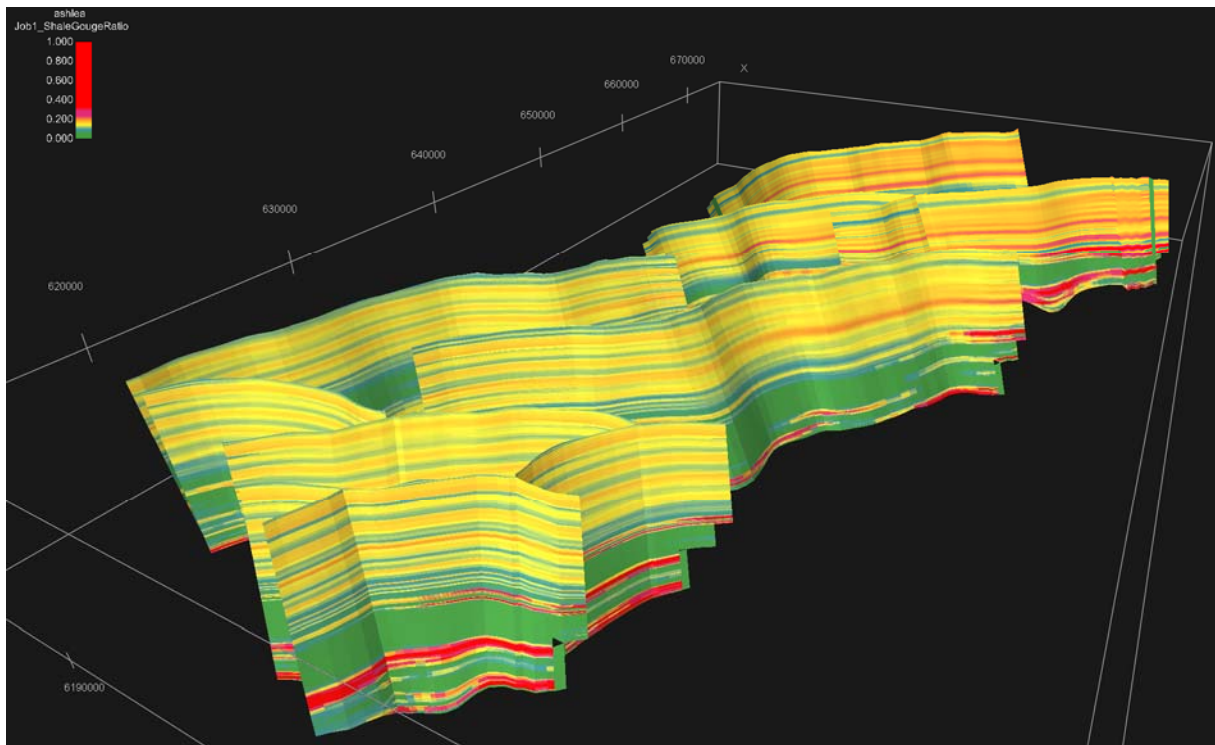


Figure 28 SGR derived for the $\sim 0.14 V_{\text{shale}}$ case. Most of the faults display at least some potential for sealing (yellow to orange, 0.1 to 0.25 SGR) where they cut the Hammerhead Supersequence in this case. Grosser scale banding in the Tiger and Lowest Hammerhead Supersequence indicate transitions between offshore marine (red) and shoreface (green) facies in this case.

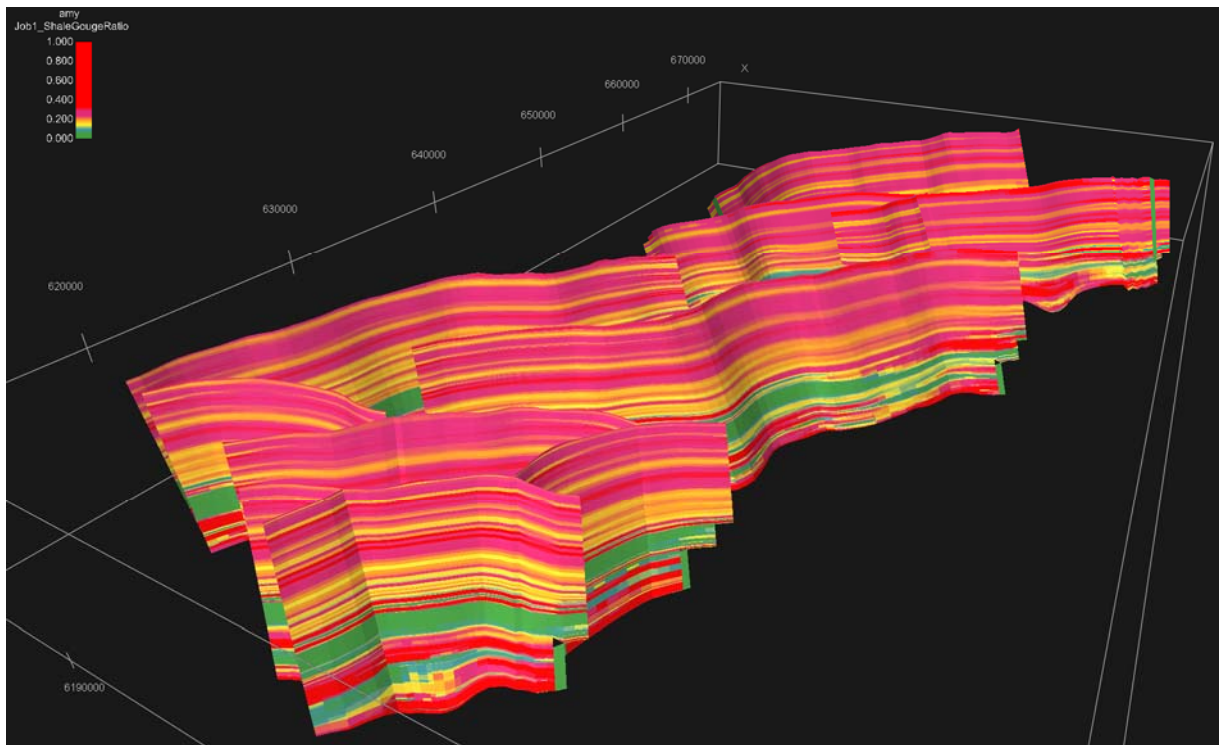


Figure 29 SGR derived from the $\sim 0.19 V_{\text{shale}}$ case. Occurrence of 0.25 to 0.3 SGR values in this model indicates increasing potential for sealing in the Hammerhead Supersequence.

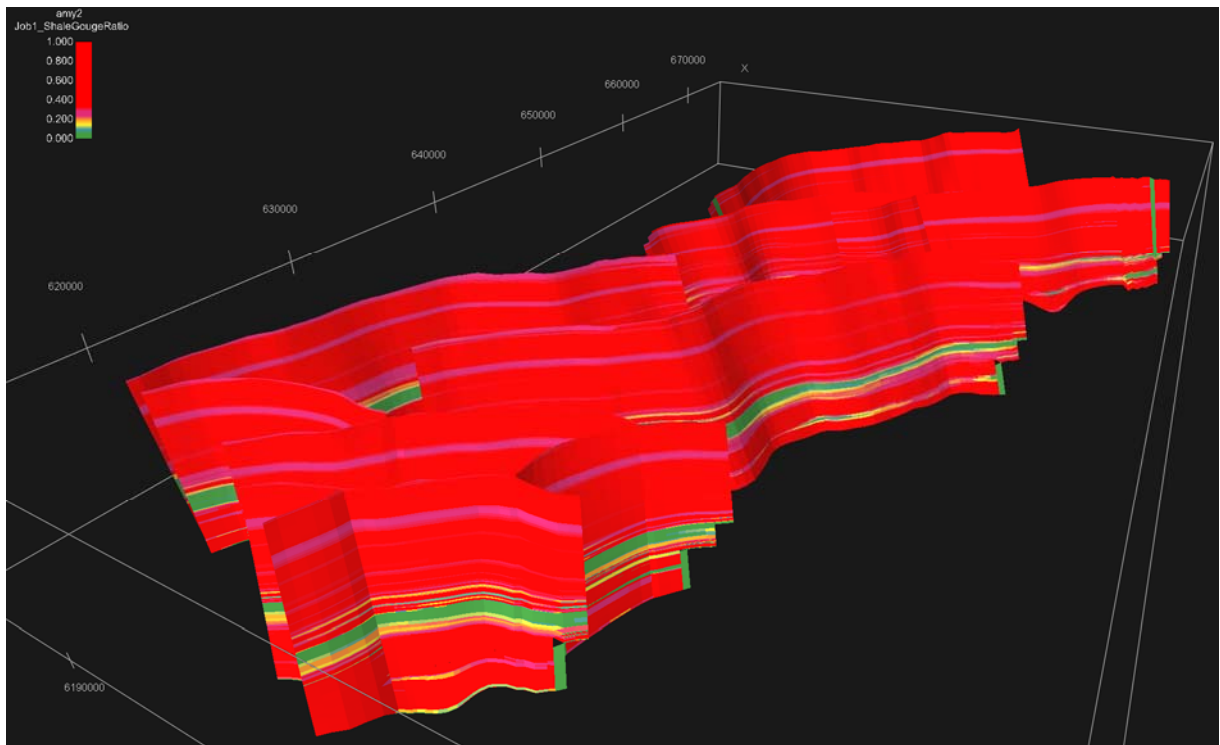


Figure 30 SGR derived from the $\sim 0.3 V_{\text{shale}}$ case. Unsurprisingly in the shaliest case the faults are predicted to be almost entirely sealing, with only bands of thick shoreface sands at the transition between the supersequences displaying obvious potential for leakage.

Summary

The results of the modelling do not conclusively predict sealing or leaking with respect to across fault flow. In fact the four cases modelled lie directly across the field of phyllosilicate framework fault rocks which are associated with the sealing to leaking transition in fault zone membrane sealing potential, between 0.15 and 0.3 SGR (Fisher & Knipe, 1998; Yielding, 2002; Underschultz, 2007). The sandiest case predicts very little sealing to across fault flow, while the shaliest case predicts mostly sealing. The probable scenario is thought to be one of the in between cases (~ 0.14 and $\sim 0.19 V_{\text{shale}}$) at which stage across fault flow sealing exhibits a high sensitivity to the modelled lithologies.

The GR to V_{shale} conversion is vital to the results of the across fault seal modelling; potential cases have been tested and it is felt that the likely range of scenarios have been covered.

Fault Seal – Upfault flow indicators

Based on Synthetic Aperture Radar data and Airborne Laser Fluorosensor data Struckmeyer et al. (2001) suggested that restricted liquid hydrocarbon present-day seepage is occurring along the outer margin of the Ceduna Sub-basin. Indirect evidence of possible shallow gas was provided by the sub-bottom profiler data collected in the northern central Ceduna Sub-basin, and on the north-eastern flank (Totterdell and Mitchell, 2009). Data collected in these areas included enhanced reflections that can be interpreted as indicating the presence of shallow gas.

Biogenic mound complexes in the Bight Basin

Feary and James (1995, 1998) reported Eocene to Pleistocene cold water biogenic mounds in the Eyre Sub-basin and Madura Shelf with stacked architecture and constructed primarily by bryozoans (Feary et al., 2000; James et al., 2004). In the northern Ceduna Sub-basin, Sharples et al. (2014) reported large Early Tertiary bryozoans mound complexes (Potoroo-1 exploration well, Taylor, 1975) interpreted along the paleobathymetric threshold provided by the paleo-shelf edge of the Paleocene to mid-Eocene post-rift Wobbecong delta (Figure 31). Bryozoan biogenic mounds are a recurring worldwide phenomenon throughout the Phanerozoic, and their origin is one of the most controversial topics in carbonate sedimentology (James et al, 2004). Their growth usually relies on low energy environments and an increased nutrient supply (e.g. Hageman et al, 2003; Sharples et al, 2014). Jollivet et al (1990) reported high density of bryozoan in deep faunal assemblage observed near cold seeps in the Barbados accretionary prism. Kennicutt et al (1985) and Brook et al (1987) reported dense (other) biological communities associated with regions of oil and gas seepage.

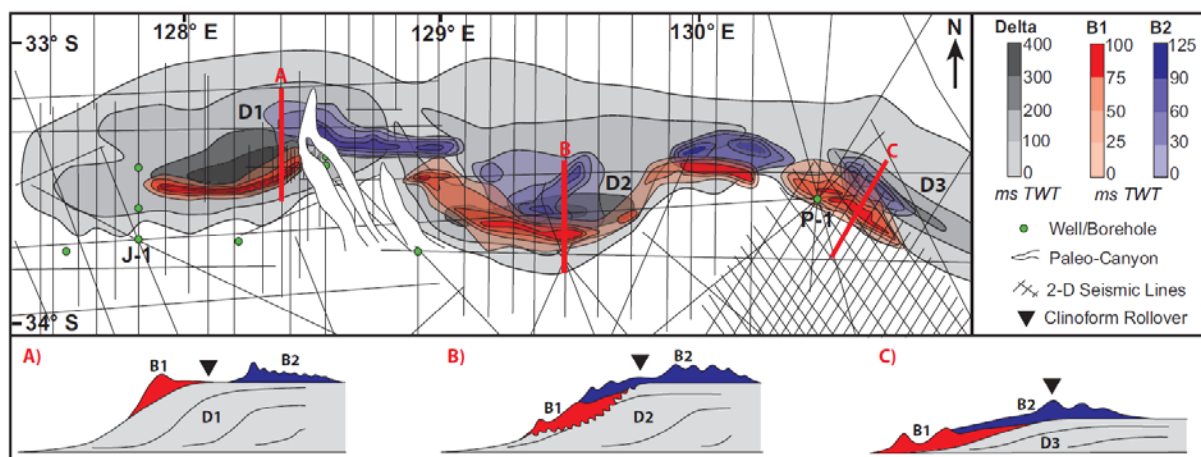


Figure 31 Combined two-way travel time thicknesses of the siliciclastic delta sequence (grayscale) and overlying bryozoan reef mound complexes (B1 in red, B2 in blue) in the northern Ceduna Sub-basin. J1—Jerboa-1; P1—Potoroo-1. From Sharples et al, 2014.

2D and 3D open-file seismic data in the Ceduna Sub-basin (Figure 9) have been investigated to re-evaluate the occurrence of fault-related paleo leakage indicators in the geological record. Additional geobodies with similar characteristics than the documented biogenic mound complexes are present in the central and southern Ceduna Sub-basin at the transition between siliciclastic and carbonate deposition (i.e. Early Tertiary, Wobbecong Supersequence). The distribution of these mounds appears to be (partly?) controlled by faults, however unlike the bryozoan mounds of the Madura Shelf and Eyre and northern Ceduna Sub-basins they do not appear to be directly associated with topographic highs such as fault scarps or prograding wedges but develop over both hanging-wall and footwall compartments, potentially indicating a link to fault related fluid seepage through the paleo seabed.

Early Tertiary geobodies in the Ceduna Sub-basin

In the Ceduna Sub-basin the Paleocene and Eocene are a transitional period with end of the thick deltaic Hammerhead and more localised Wobbecong supersequences and the initiation of the Dugong cold water carbonates (Figure 4). Although the continental break-up initiated during the Late Cretaceous (Sayers et al., 2001), half-spreading rates were extremely slow until the Eocene. The Early Tertiary was a period of active tectonism with fault reactivation and new fault initiation, and volcanism.

In the central Ceduna Sub-basin, the Early Tertiary transition between siliciclastic and carbonate deposition is characterised by two main categories of geobody: igneous bodies and mound complexes interpreted as biogenic reef complexes.

Eocene igneous bodies mostly located in the central/eastern part of the sub-basin and the southern Madura Shelf. Extrusive igneous bodies include volcanic cone and lava flow. The volcanic cones (Figure 32) display typical broad conical shapes and an internal seismic character that varies from chaotic to more continuous with occurrence of internal stacked cones. Their seismic facies is characterised by high amplitude reflectors caused by large impedance contrasts with the surrounding sediments and characteristic wash-out effect (i.e. transparent reflectors) and potential velocity pull-up below the bodies. Lava flows occur mostly in association with volcanic cones, they typically form subparallel and very high amplitude reflectors with discontinuous internal pattern. Extrusive igneous bodies are often underlain by intrusive igneous bodies (sills and dykes). The high seismic amplitude of these bodies is also caused by large impedance contrasts with the surrounding sediments and wash-out effects are locally present below (Schofield & Totterdell, 2008).

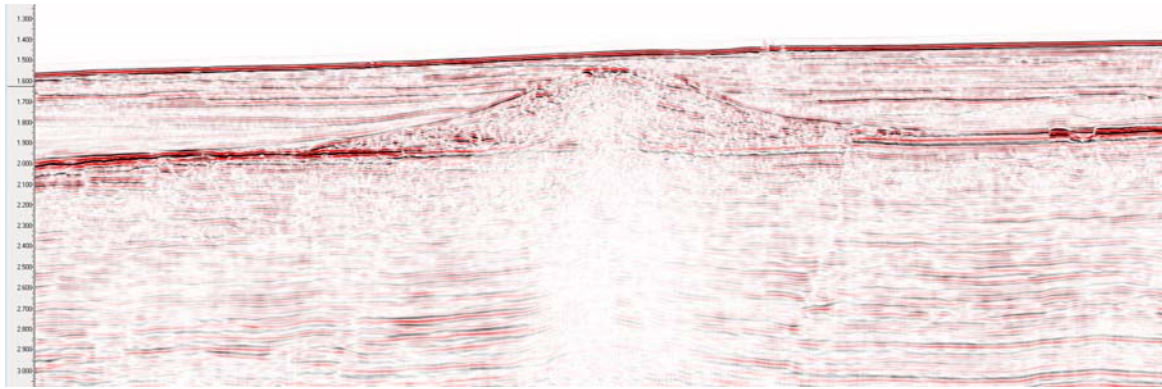


Figure 32 Volcanic cone at the top of the Wobbecong Supersequence in the central Ceduna Sub-basin (Flinders 2D line 64) with wash-out effect and velocity pull-up. The section is 13km long. Location on Figure 33.

In the central Ceduna Sub-basin several mound complexes are interpreted from 2D seismic surveys and the Trim 3D seismic survey (Figure 33). Some of those mounds were previously interpreted as extrusive volcanics (Schofield & Totterdell, 2008). They are mainly located in the central Ceduna Sub-basin in an approximately 80 km wide north-south region east of Trim 3D. To the east, biogenic mound complexes are absent and the Base Tertiary transition between siliciclastic and carbonate deposition is mainly characterised by extrusive volcanics (Schofield & Totterdell, 2008). As reported in the Eyre and northern Ceduna Sub-basins (Sharples et al., 2014), the mound complexes interpreted in the central Ceduna Sub-basin postdate the top Hammerhead unconformity. Their bases are usually found within or near the top of the thin Paleocene-Eocene Wobbecong Supersequence. The mound complexes' height are between 40 ms TWT and 180 ms TWT or 50 m and 200 m. The mound tops and the internal reflections within the mounds are average to high amplitude suggesting moderate to high impedance contrast with the surrounding sediments. The seismic amplitude can vary laterally within the mounds and the reflectors can become locally discontinuous (Figure 34 and Figure 35). The mound complexes differentiate from potential mass transports (e.g. debris flows, slides, and slump) by generally higher amplitude, lower amplitude variation and more internal continuity (e.g. Moscardelli et al., 2006; Wu et al., 2011) and differentiate from turbidites by the absence of observed canyon or submarine feeder conduit, nearby associated/stacked lobes and channels above lobes (e.g. Shanmugam and Moiola, 1988; Gervais et al, 2006), by the morphology of the bodies with turbidite lobes classically forming sheet-like deposits (e.g. Shanmugam and Moiola, 1991) and showing greater length than width (e.g. Reading, 1996; Deptuck et al, 2008), by the seismic facies with turbidites commonly exhibiting chaotic and discontinuous reflectors (sand) or flat parallel reflectors (mud) (Shanmugam and Moiola, 1988) different from constructed internal architecture observed in the central Ceduna Subbasin.

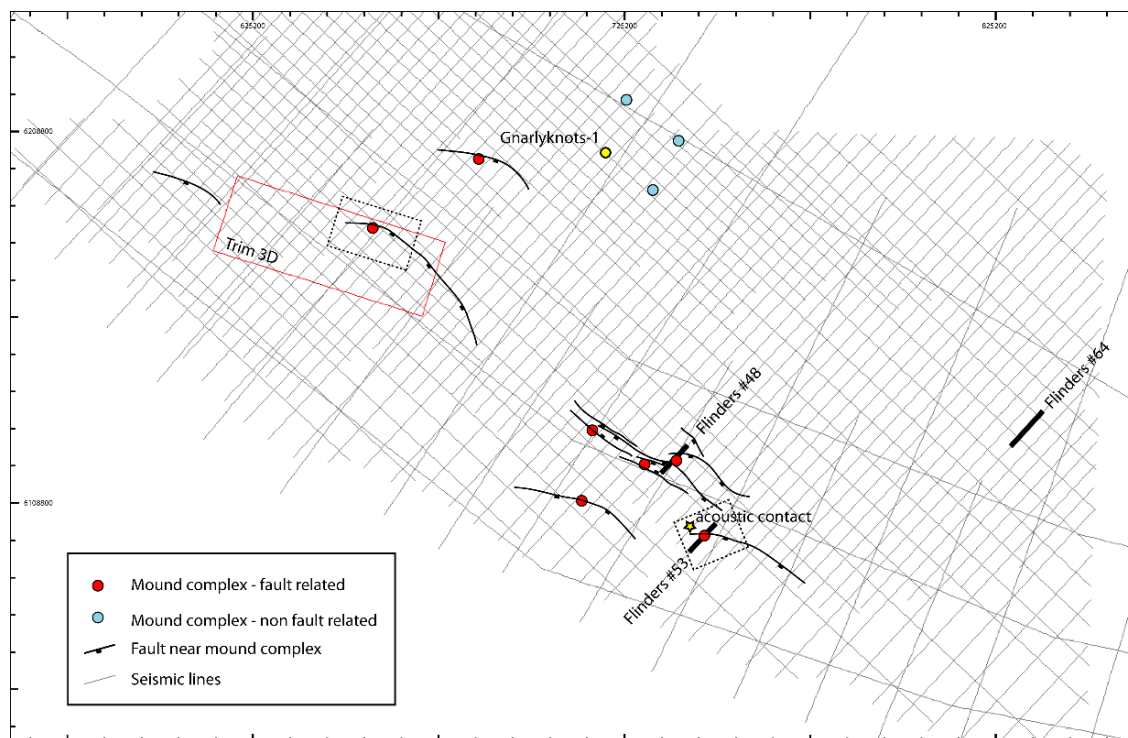


Figure 33 Mound complexes in the central Ceduna Sub-basin. Locations of Figure 36 and Figure 37 are shown near the acoustic contact and the Trim 3D survey, respectively.

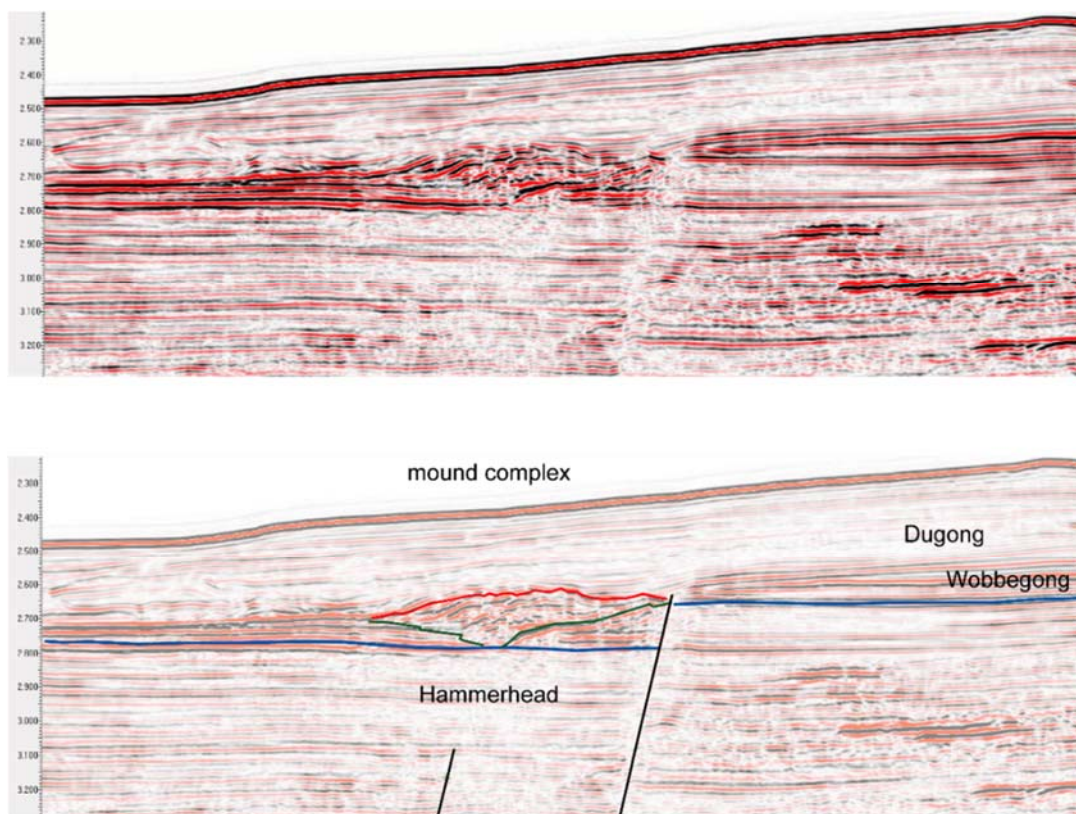


Figure 34 Interpreted mound complex in the central Ceduna Sub-basin on Flinders 2D line 53, ~3 km to the southeast of an acoustic contact and sub-bottom profile anomaly. The section is 9500 m long. Location on Figure 33.

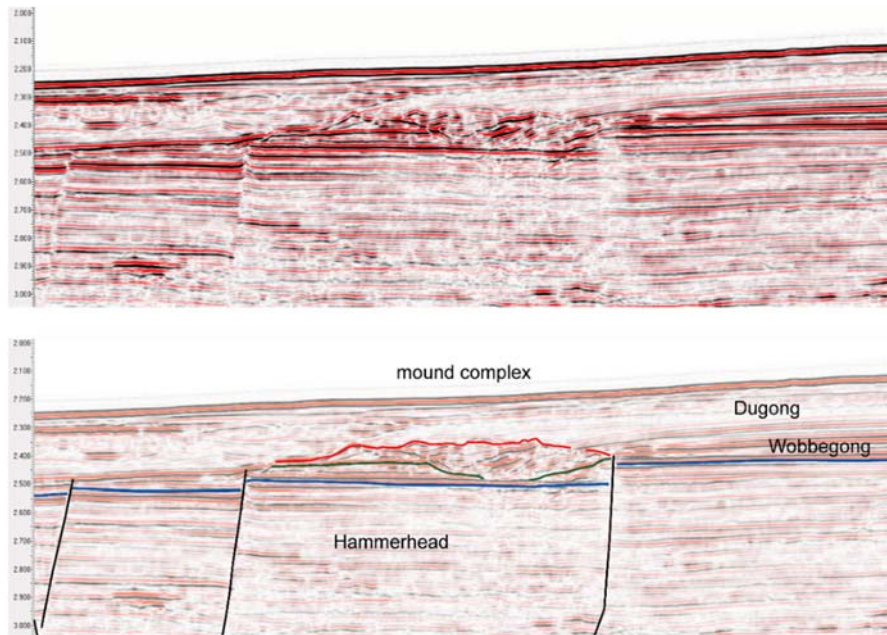


Figure 35 Interpreted mound complex in the central Ceduna Sub-basin on Flinders 2D line 48. The section is 9500 m long. Location on Figure 33.

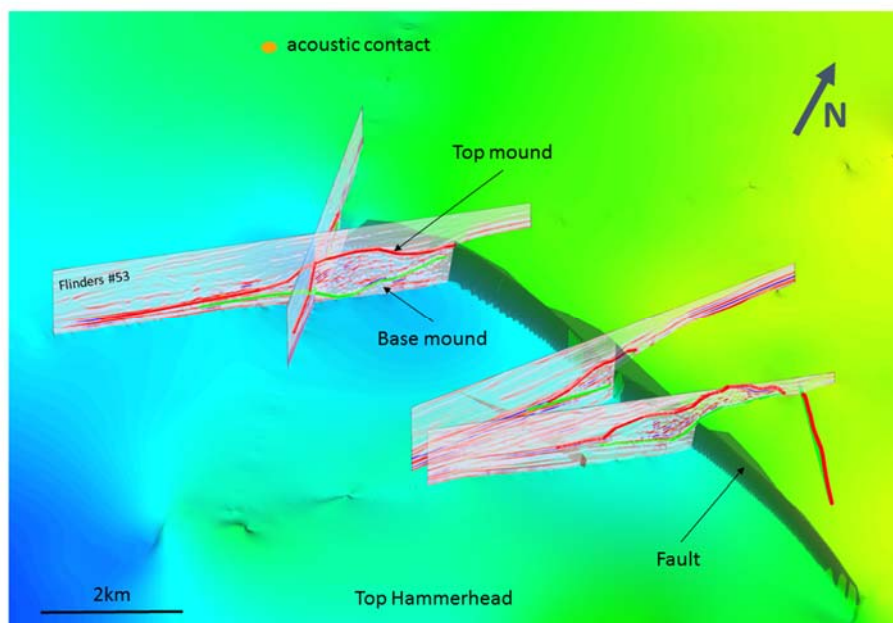


Figure 36 3D view of the interpreted mound complex ~3 km to the southeast of an acoustic contact and sub-bottom profile anomaly. The thickest part of the mound is on the lower hanging-wall compartment. Location on Figure 33.

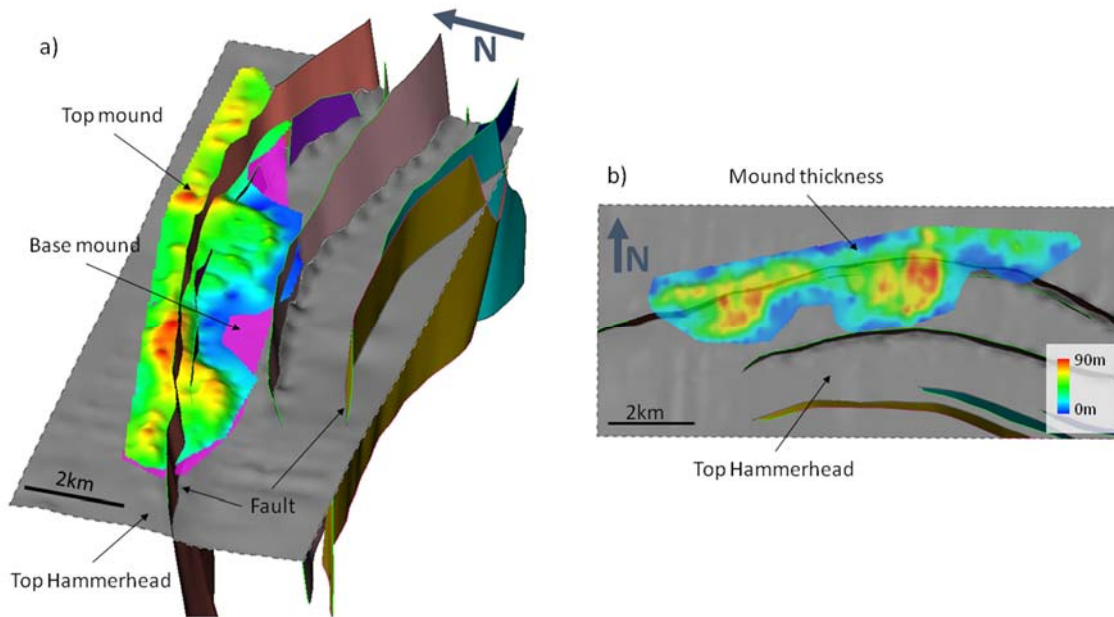


Figure 37 Interpreted mound complex on the Trim 3D seismic survey. A) 3D geometry of the mound complex. B) Thickness data showing the main parts of the mound complex develop on the hanging-wall compartment. Location on Figure 33.

The newly interpreted mound complexes interpreted on 2D and 3D seismic data show a general E-W to WNW-ESE orientation and are usually relate to underlying Late Cretaceous to Paleocene faults (Figure 34, Figure 35, Figure 36 and Figure 37).

The mound complexes display geometries and internal configurations typical of biogenic build ups with progradational, aggradational and mounded patterns and average to high seismic amplitude (Feary & James, 1995; 1998; James et al., 2004; Sharples et al., 2014).

Origin of mound complexes in the central Ceduna Sub-basin

The development of cold water bryozoans reef complexes reported from the Eyre Sub-basin, Madura Shelf and northern Ceduna Sub-basins has been related to the interaction between regional tectonic and local and global paleo-oceanographic processes (Feary & James, 1995; 1998; Feary et al., 2000; James et al., 2004; Sharples et al., 2014). Tectonic and sea level fluctuation controlled the Eocene Wobbeong progradational siliciclastic wedge, in the proximal part of the Ceduna Delta, which provided a paleobathymetric threshold (i.e. topographic high) where the biogenic mounds preferentially developed.

Jollivet et al. (1990) introduced an alternative model for the development of carbonate reefs and bioherms where reef growth is related to hydrocarbon seepage rather than controlled by climatic and bathymetric elements. There are indications of links between benthic chemosynthetic communities and authigenic carbonates and petroleum seeps in petroleum basins (i.e. Gulf of Mexico, e.g. Roberts & Aharon, 1994; Roberts et al., 2006; Cordes et al.,

2008; Becker et al., 2009; Atlantic, e.g. Hovland et al., 1998; Henriot et al., 2001; Hovland & Risk, 2003; Pierre & Fouquet, 2007). Similar observations have been made on the Australian North West Shelf (e.g. O'Brien & Woods, 1995; Lavering & Jones, 2001; O'Brien et al., 2002; Langhi et al., 2010; Logan et al., 2010) where Hovland et al. (1994) suggested a link between the formation of Late Tertiary carbonate buildups and focussed hydrocarbon seepage up fault conduits and localised venting of gas at the seafloor in the Vulcan Sub-basin.

While Sharples et al. (2014) suggested that the positions of the mound complexes in the northern Ceduna Sub-basins were controlled by the bathymetric relief, a majority of the newly interpreted mound complexes in the central Ceduna Sub-basin are clearly associated with an underlying faults (Figure 33). Seismic interpretation suggests that most of these fault-related mound complexes are associated with WNW-ESE oriented segments (Figure 36 and Figure 37). These segments represent parts of main NW-oriented curvilinear Late Cretaceous to Paleocene faults.

To the south of the central Ceduna Sub-basin a sub-bottom profile anomaly has been recorded during the Great Australian Bight 2013 seep survey on the R/V Southern Surveyor (742477 m E 6101850 m S, UTM 52 S; Figure 34 and Figure 36); it shows a wipe out zone with uplifted horizons that could be interpreted as surface disturbed zone. The sub-bottom profile anomaly is directly overlaid by a vertical water column acoustic contact with morphology similar to hydro-acoustic flares observed in other hydrocarbon seep studies (e.g. Talukder et al., 2013; Langhi et al., 2014). A ~12 km long E-W oriented mound complex with a maximum thickness of ~170 m is interpreted ~3 km to the southeast of the contact (Figure 36). The mound overlies the western tip of a ~35 km long fault with a local offset around 160 m at the top Hammerhead Supersequence (Figure 36). The mound develops over both the footwall and hanging-wall compartment of the fault with its thickest part located in the lower block.

Although the development and growth of the Early Cenozoic mound complexes in the central Ceduna Sub-basin could be controlled by oceanographic processes, their distributions do not support a purely bathymetric control.

Additional research primarily based on 3D seismic mapping is required to confirm the biogenic nature of the interpreted mound complexes, the relationship to the underlying structures and to confirm the link to fault-related hydrocarbon leakage. If confirmed this relationship would provide a tool for determining paleo-leakage and constrain petroleum system and hydrocarbon migration.

Structural assessment and control on potential hydrocarbon leakage conclusions

Of the 81 areas of interest identified from the rapid screening of 2D seismic data for leakage indicators no one area displayed unequivocal evidence of fluid leakage through the subsurface to the seafloor. This does not preclude seepage being present within the GAB and ranking of the features determined that features with the highest potential for leakage were strongly biased towards the outboard deep water slope of the Ceduna basin.

Static geomodels populated by V_{shale} have been derived for the Trim 3D volume using seismic interpretation, basic well petrophysics and stratigraphic forward modelling outputs. These model outputs have enabled the faulted models to be tested for a possible range of SGR related sealing scenarios. The most likely V_{shale} scenarios indicate that the Hammerhead Supersequence in the vicinity of the Trim survey is distributed right at the most sensitive range of values with respect to across fault seal (i.e. 0.1 to 0.25 SGR).

Biogenic mound complexes interpreted at the Middle Eocene hiatus are potentially indicate hydrocarbon paleo-seeps and perhaps more specifically paleo-leakage up faults. Such an interpretation would support the presence of an active hydrocarbon system at the time of Middle Eocene extension, fault movement and reactivation, however this requires further research to eliminate other controls on their formation.

3. SATELLITE BASED REMOTE SENSING FOR SEA SURFACE SLICKS

In order to gain a more detailed understanding of the potential for liquid hydrocarbon seepage into the marine environment within the Great Australian Bight a limited Synthetic Aperture Radar (SAR) study was undertaken in combination with a review of historical Synthetic Aperture Radar data holdings and reports across the region.

The SAR technique is a frequently used technique to identify sea surface slicks, the sea surface expression of seafloor hydrocarbon seeps, during exploration in frontier basins. The technique is only able to detect slicks on the sea surface and therefore gas dominated hydrocarbon seeps are not detected by the technique. The SAR technique measures radar back scatter from the sea surface which caused by millimetre scale surface ripples. Dampening of these ripples due to differences between the surface tension of water and oil leads to an absence of radar backscatter response in areas where slicks are present. It is important to note that the data produced using the technique is subject to prevailing weather conditions and other natural phenomena (e.g. algal blooms, bathymetric effects; see Jones et al 2005, and references therein) and anthropogenic causes can give rise to similar features to those produced by oil slicks produced by seeps. Therefore careful and considered interpretation of the data is required.

This task, was focussed on first the review of existing data sets to help identify potential areas of seepage. Secondly to collect limited SAR data coincident with the SS2013_C02 survey to identify occurrence and location of SAR anomalies at the time of the survey in order to support the on-board research team in modifying their survey route during the SS2013_c02 voyage. If features were identified within the captures they were to be used to inform possible sampling locations of previously unidentified natural seeps.

SAR data reviewed and collected during this task of the project was collected using various satellite platforms with various effective resolutions. Collection of the limited number of additional SAR captures task is performed in collaboration with a third party SAR data supplier, CSTARS.

Historical synthetic aperture radar data holdings

There are several sources of historical SAR data which are known and these data are shown in **Error! Reference source not found..** These data have been collected using various satellite platforms and with different resolutions between 1999 and 2014. The SAR anomalies have been identified across much of the geographic extent of the GAB.

The data sets available to this project include 211 scenes captured by Geoscience Australia (formally AGSO; 56 scenes in 1999 and 155 scenes in 2005/2006) and 20 scenes captured by the Australian Maritime Safety Authority (AMSA) in 2013 (Pers. comm. AMSA, 2015) over the area of interest. In addition the Nigel Press & Associates (NPA) global SAR database for the GAB was also provided by BP for inclusion in this part of the study. The comparison of

this data set with the publically available data showed little difference between data holdings. As this data is confidential it has not been incorporated further in this report.

Geoscience Australia SAR data

In 1999 the Australian Geological Survey Organisation (AGSO, now GA) in collaboration with Nigel Press & Associates (NPA), AUSLIG (the Australian Centre for Remote Sensing) and RadarSAT International undertook a major study of the basins in the Great Australian Bight with the primary focus to evaluate hydrocarbon migration and seepage collecting 56 scene captures (Stuckmeyer, 2000). The study was built around a combination of RadarSat and ERS SAR data – this SAR data was integrated with regional geological information and other hydrocarbon indicators such as seismic direct hydrocarbon indicators and legacy Airborne Laser Fluorosensor (ALF) data to provide an assessment of the likely charge characteristics of the region. The results of the study suggested that there was active liquid seepage with the Great Australian Bight basin system however it was restricted.

The results of the SAR investigation are tabulated below:

A total of 107 slicks were mapped (Figure 38). These include:

- 4 rank 2 slicks (high to moderate confidence)
- 36 rank 3 slicks (moderate to low confidence)
- 6 interpreted remnant pollution slicks
- 61 individual natural film slicks (INFS). These are interpreted to be generally unrelated to hydrocarbon seepage, although in some cases, a hydrocarbon-related origin cannot be excluded.

Direct correlation of the individual seeps with geological features was not possible as none of the reported seep locations coincided with subsurface fluid escape features from the limited seismic data availability in the basin.

The study highlighted the fact that there appears to be more of an abundance of slicks in the NW Shelf compared to the GAB – this may be due to a number of reasons.

- Differences in water depth, swell height and water temperature – an example being consistently high swells that may account for the small size and scattered nature of slicks
- High seal and trap integrity in the greater part of the GAB basin system
- Low number of seeps could reflect a low density of hydrocarbon accumulations
- Hydrocarbon leakage is episodic

In 2005 and 2006 as part of their precompetitive data collection for the Australian Government's New Petroleum Program (2003-2007) GA collected 155 SAR captures over the Great Australian Bight using the European Space Agency's Remote Sensing SAR Satellite (ERS-2). The captures we collected over three months between December 2005 and February 2006 and analysis of the scenes identified 15 second rank potential slicks and 61 third rank potential slicks. A high proportion of the SAR anomalies identified were located to the west of the Ceduna Basin in EPP 43 and the distribution of anomalies was distinctly different from those encountered in the 1999 acquisition program data. In part these data were used in the planning of the R/V Southern Surveyor Survey SS01/2007 (Totterdell and Mitchel 2009).

AMSA SAR data

The 20 AMSA scene captures were collected and interpreted by KSAT. None of the captures interpreted by KSAT were interpreted to include potential slicks.

On reinterpretation of the SAR images by CSIRO, 10 low rank/confidence anomalies were identified within 6 of the SAR scenes (Figure 38). One particular feature identified fell within a prior anomaly cluster identified in the previous GA studies in the very deep water to the south of the Ceduna basin. Other AMSA data CSIRO interpreted anomalies appear singularly.

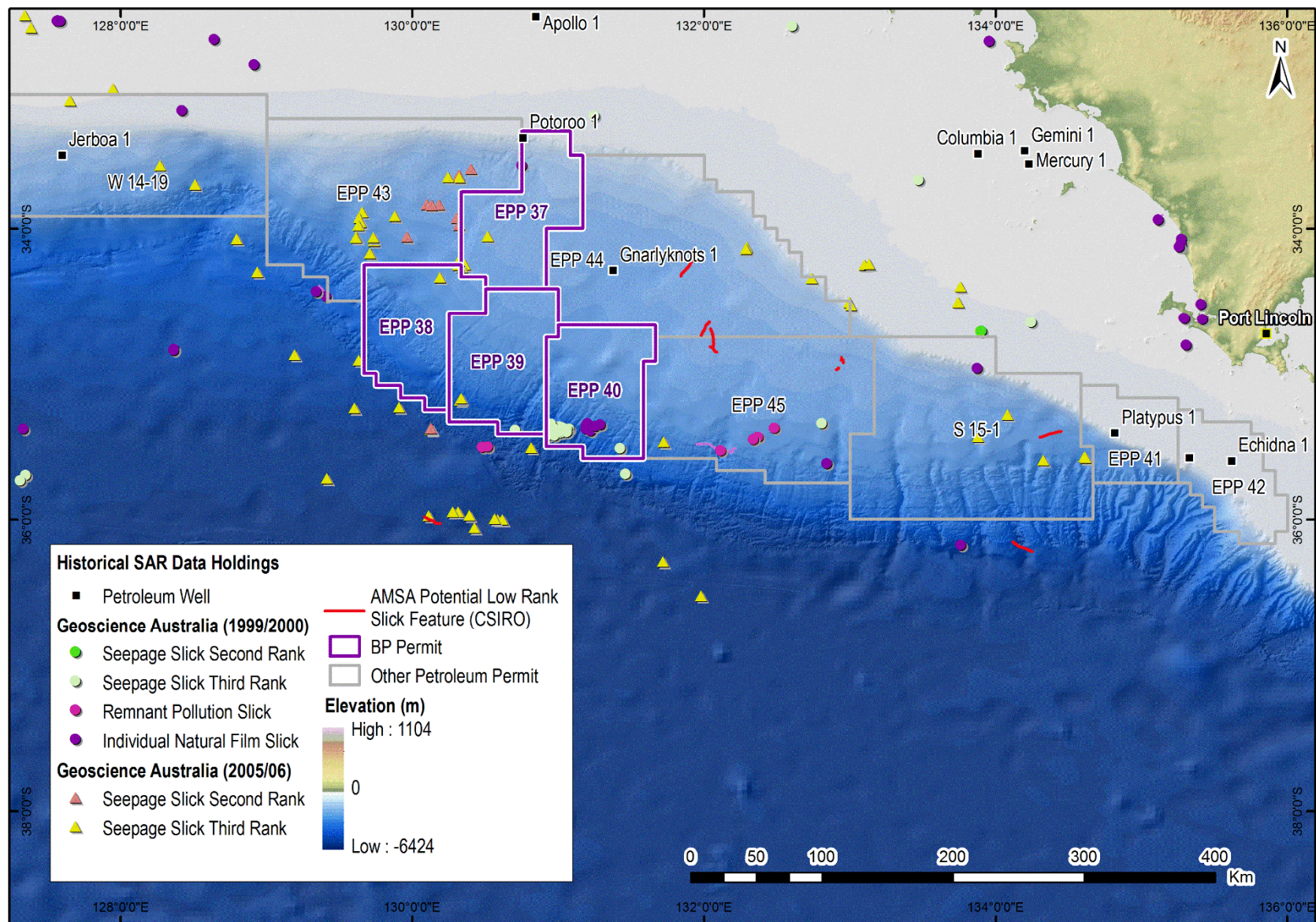


Figure 38 Synthetic Aperture Radar sea surface anomalies for the Great Australian Bight for the historical data.

Synthetic aperture radar SAR area of interest and acquisition program definition

To assist in SAR scene capture planning, an area of interest was selected which was based on historical SAR data holdings as well as the geographical extent of the Ceduna sub-basin (Figure 39). An area of interest of the four SAR scene captures was created over the location of several of the highly ranked potential leakage indicators defined through the structural screening for marine survey target delineation task. This area of interest was used for scene capture planning with the various satellite data providers providing high frequency coverage over the GAB. The criteria for any potential scene capture were that they had to have some overlap within the area of interest (see example scenes in Figure 40).

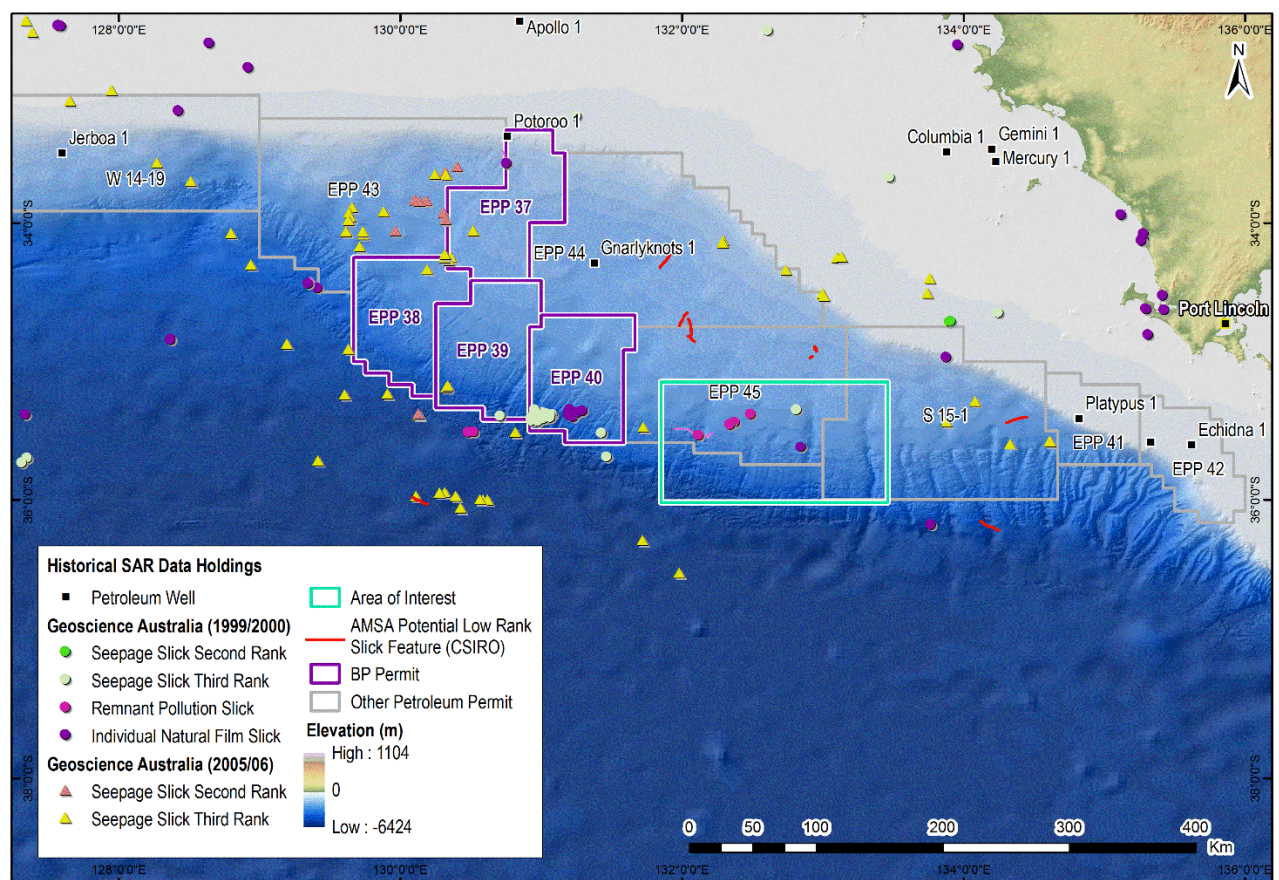


Figure 39 Area of interest used for planning of SAR capture program showing area of interest inset and historical SAR anomalies.

Table 3 Satellite Synthetic Aperture Radar platforms and modes used during the study.

SATELLITE:	RISAT-1	TERRASAR-X	RADARSAT-2	COSMO-SKYMED
Mode	All modes	Wide ScanSAR	Wide	Wide Region
Resolution	25m	40m	30m	30m
Scene size	115km width	270km x 200km	150km width	100km x 100km
Regime	Sun-synchronous	Low earth	Sun-synchronous	Sun-synchronous

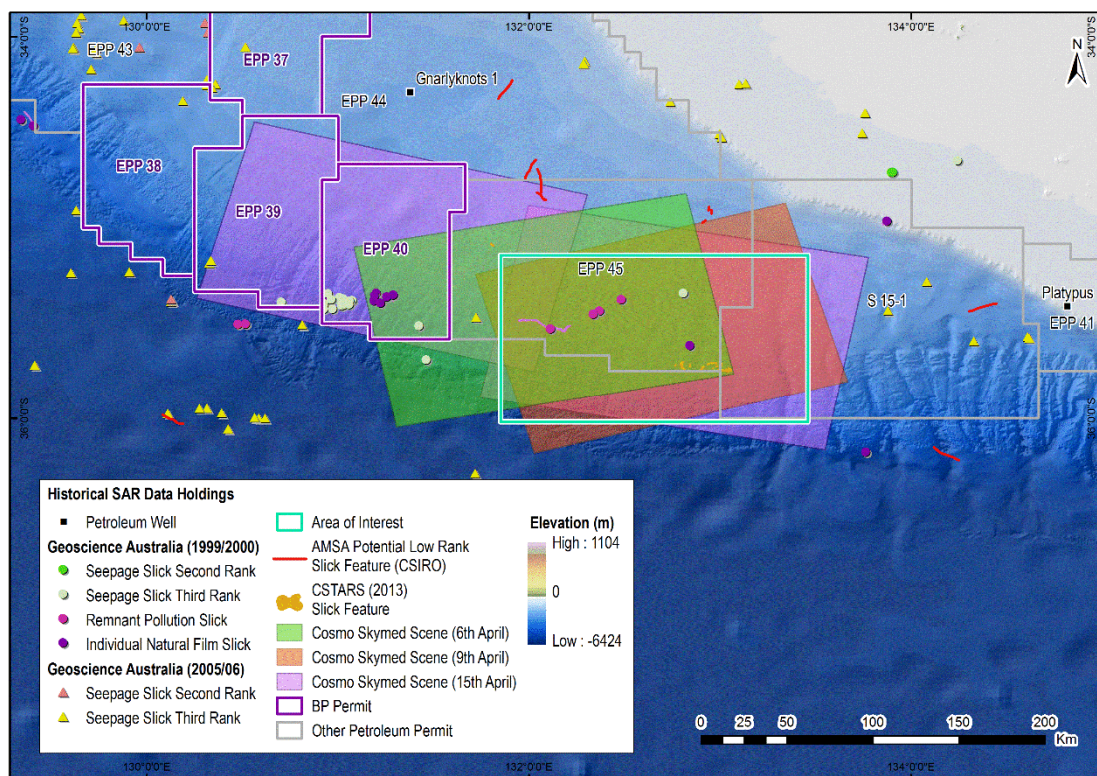


Figure 40 SAR scenes (4) having part of the scene coverage within the area of interest for the period April 6th to 15th 2013 from the various SAR satellite platforms.

Table 4 SAR acquisitions for the four scenes.

DATE	RADAR BAND	RESOLUTION	BEAM MODE	SATELLITE	WIND
6/04/2013 21:13	X	30m	Wide region	Cosmo skymed 1	5 - 7 m/s
9/04/2013 21:43	X	30M	Wide region	Cosmo skymed 4	12 m/s
15/04/2013 8:29	X	30M	Wide region	Cosmo skymed 4	1 m/s
15/04/2013 8:53	X	30M	Wide region	Cosmo skymed 1	1 m/s

Synthetic aperture radar capture program results and discussion

This study contributes a minor increase (1.7%) in the SAR data available to this project with 4 scenes collected augmenting the total of 231 publicly available scenes over the GAB.

As part of the analysis of SAR data it is important to understand prevailing meteorological conditions to understand if wind field conditions are optimal for slick observations. Of the four scenes three were deemed to have wind conditions that would make slick detection difficult and limit the opportunities for reporting. Only one scene was deemed to have predominantly good (2-12 m/s) wind characteristics required to be able to discriminate potential slicks from the surrounding waters (Table 5 and Figure 41).

Table 5 Predominant wind field across SAR scene obtained during the study.

TOTAL NUMBER OF CAPTURES (4)	
Limited < 1 m/s	2 (50%)
Moderate 1-2 m/s	0 (0%)
Good 2-7 m/s	1 (25%)
Good 7-12 m/s	0 (0%)
Moderate 12-15 m/s	1 (25%)
Limited >15 m/s	0 (0%)

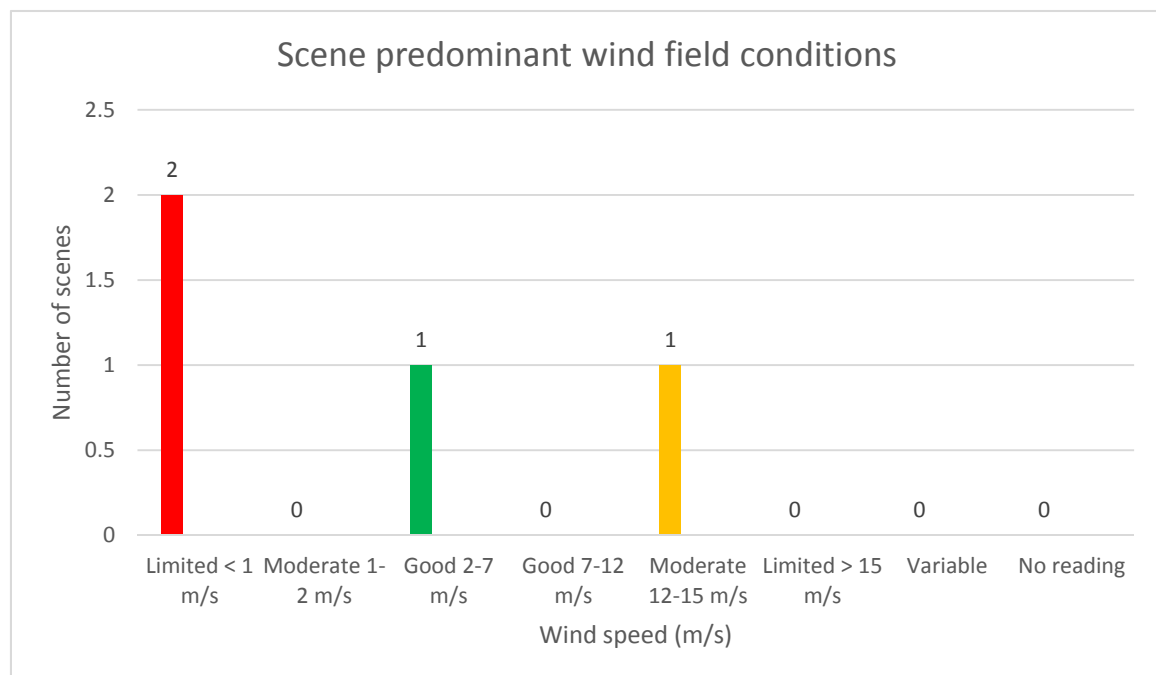


Figure 41 Predominant wind field across the 4 SAR scenes obtained during the study.

A combined total of 23 SAR anomalies were observed by CSTARS in the one scene with optimal observation conditions. Within this scene acquired on the April 6th 2013, the satellite service provider (CSTARS) for this study interpreted two areas of SAR anomalies in the 4 scenes acquired (Figure 40 and Figure 42). The first anomaly is of an elongated shape

in nature – about 2.5km in the northwest-southeast orientation and about 200m in the northeast-southwest orientation (see APPENDIX 5: TASK 2 SAR DATA). The morphology of the feature would be typical for slicks observed from seeps.

The other features were also observed within the same scene and comprised features with various orientations with a total of 22 anomalies identified. The majority were oriented west-east and were 500 m – 4.5 km in length and ~ 200m in wide (a minority were in a north south orientation with similar dimensions) and were all potentially attributable to slicks formed from a seep due to their irregular linear morphology and as such CSTARs attributed the anomalies to seeps. It should be noted that these anomalies occurred on the edge of the scene and therefore it cannot be established with complete certainty that these features are not attributable to other oceanographic features such as the surface current expressions.

When these anomalies are compared with the historical data these anomalies cluster with anomalies identified in the historical data (Figure 43).

The data provided by this task of the study permitted correlation of these anomalies with potential seafloor or geological features identified in bathymetry and seismic data. This permitted particular features to be ranked more highly when determining marine survey targets. This process is detailed in section 4.

.

CSK1 Apr 06, 2013 21:13 GMT

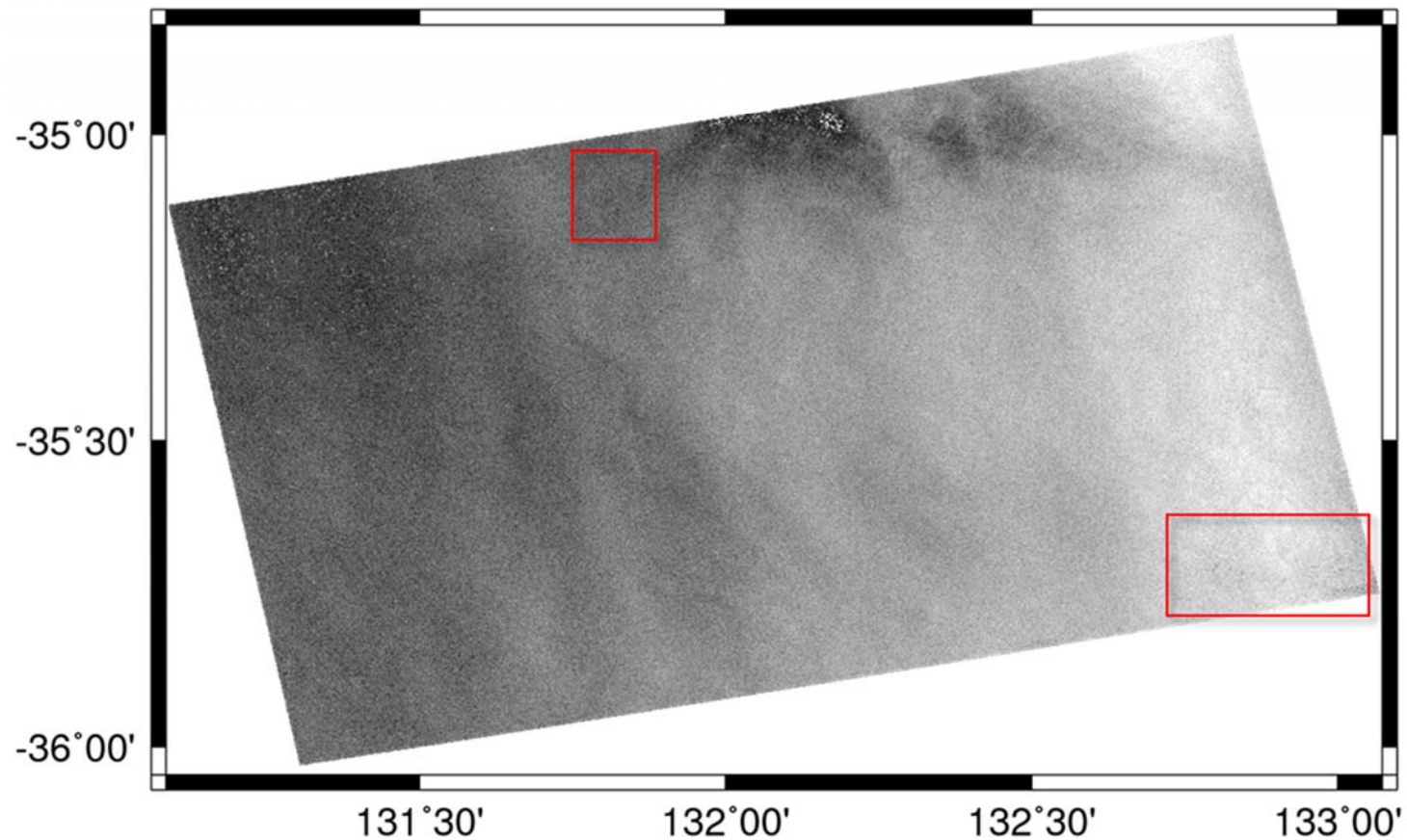


Figure 42 Cosmo-skymed 1 synthetic aperture radar scene for April 6th 2013 report for area of interest with slicks identified in the middle top of the scene (one slick) and the bottom right (cluster of slicks).

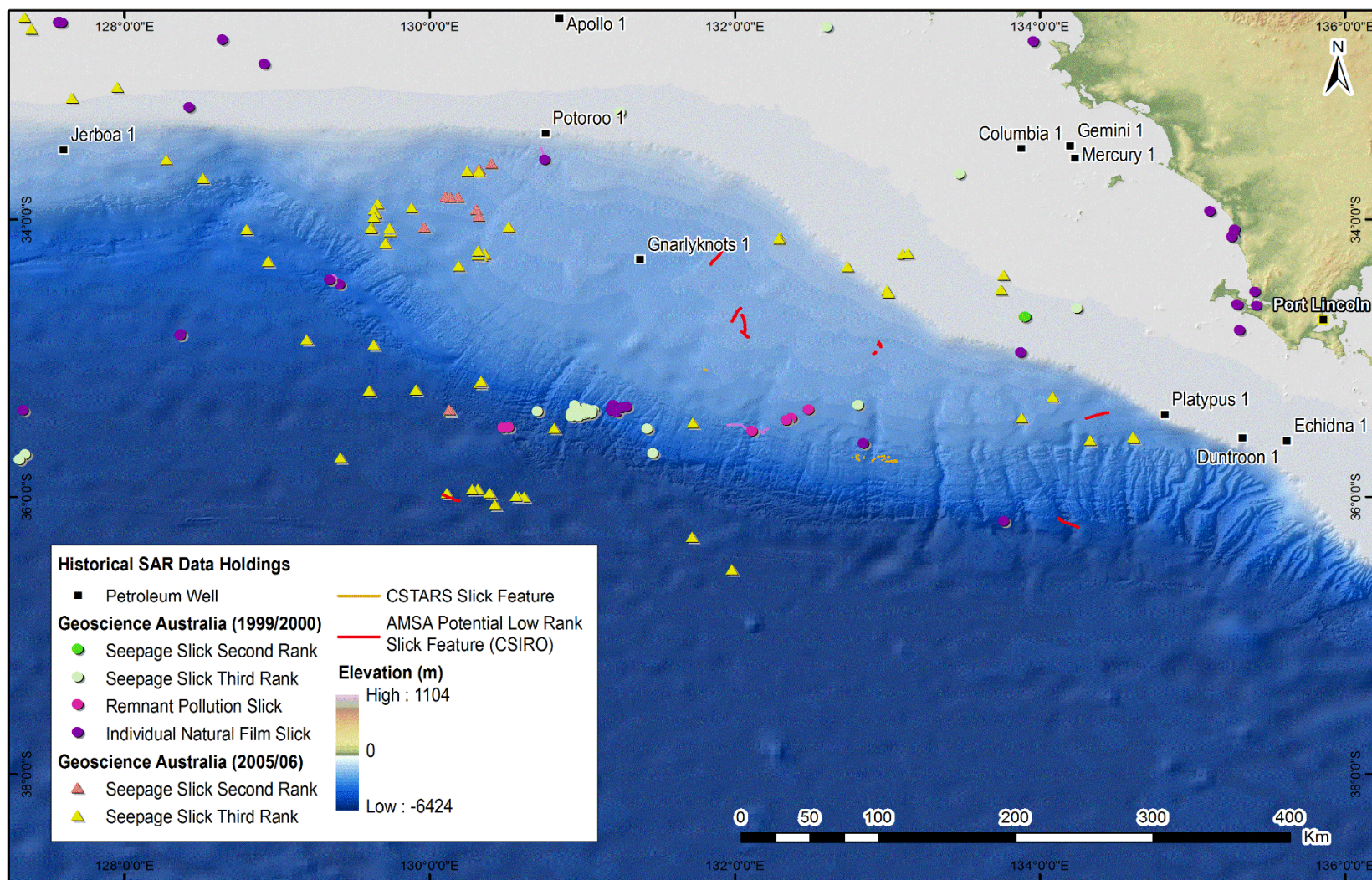


Figure 43 Combined historical and capture program (CSTARS Slick Features) sea surface synthetic aperture radar anomalies for the Great Australian Bight.

4. VOYAGE PLANNING AND PROJECT 5.1 OUTCOMES FOR THE GAB SS2013_CO2 AND IN2015_CO2 VOYAGES.

Reconnaissance survey through R/V Southern Surveyor research charter (SS2013_CO2)

This task was focussed on the development of a detailed reconnaissance voyage plan (SS2013_CO2) based on the outcomes of the prior tasks as they become available with areas possible seepage ranked based on prioritisation. As the reconnaissance survey was a joint voyage between Themes 5 and 3 (and to a minor extent theme 2) planning conducted in collaboration with these leaders. As the voyage was a shared mission, there was limited dedicated time available to pursue the search for hydrocarbon seeps in the GAB. Therefore the collection of samples at sites where baseline conditions were expected away from possible areas of seepage was prioritised. A subsequent seeps and benthic survey was planned however was not possible due to funding constraints. The development of the survey plans was highly iterative and comprised many pragmatic compromises on the scope of the program based on the operational and time constraints of the voyage. At all times the voyage/theme leaders attempted to balance the overall goals of the GAB Research Program and the individual theme objectives.

The scientific objectives of the voyage were the:

Study of benthic ecosystems and natural hydrocarbon seepage in deep (200-3,000 m) waters of the Great Australian Bight (GAB) are part of the focus of a research program (the GAB Science Plan). The Science Plan aims to describe key elements of marine ecosystems across the GAB, including in the deep central GAB area associated with oil and gas exploration activity. Characterising benthic ecosystem structure and function is important because there are virtually no existing benthic biological data beyond continental shelf depths (< 200 m) in the GAB. Conservation values attributed to Commonwealth Marine Reserves (CMR) spanning wide depth ranges are untested on the mid- and lower continental slope, while oil and gas lease areas extend across the GAB Marine Park (GAB MP). The benthic ecosystem description will be strengthened with context provided by an improved understanding of hydrocarbon seeps and migration pathways in the GAB.

Of particular importance for achieving Theme 5, project 5.1 objectives was the collection of a suite of diverse data and samples both in areas unlikely encounter seeps as well as selected prioritised areas of potential seepage based on the analysis of other data sets (e.g. SAR, existing prior survey data, and seismic data screening).

Seep target prioritisation process

Prioritisation of the survey areas of interest for the voyage combined both seismic and synthetic aperture radar to determine areas with coincident high ranked slicks and seismic anomalies. In the prioritisation of sites consideration of optimal voyage routes was key in the site selection due to the limited voyage time. Three sites were identified to the Southeast of the Ceduna basin (Figure

44) optimally situated along the vessel voyage track. These areas coincided with both potential slicks identified by Geoscience Australia in 1999/2000 (Figure 43) and potential slicks identified within CSTARs data collected during the course of this project (Figure 43) as well as the occurrence of seismic anomalies.

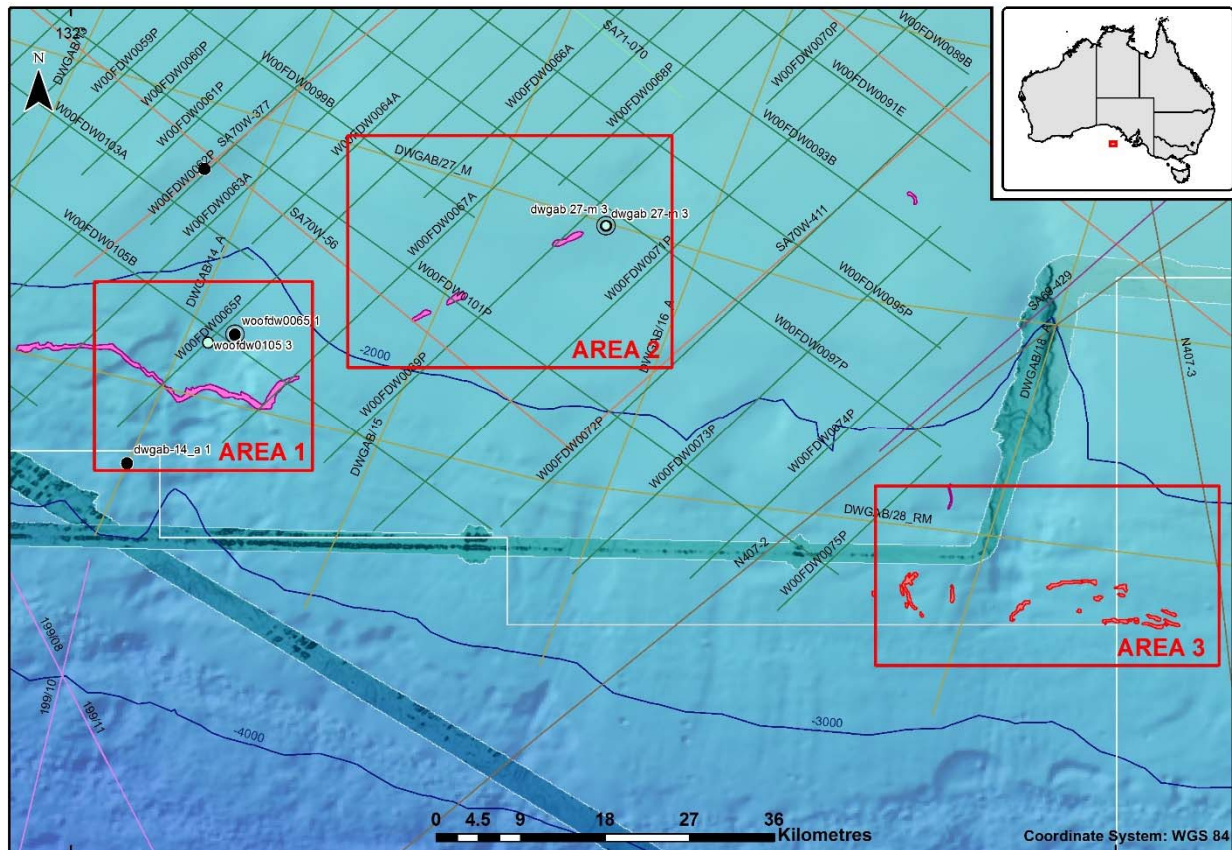


Figure 44 Showing target areas 1-3 interpreted as having indications of potential seepage. The labelled lines are the available public 2D seismic holdings. Black or light blue dots are seismic anomalies. The ringed seismic anomaly sites are shown below in Figure 45 and Figure 46. The purple outlined areas are slick extents from the GA/NPA 199/2000 SAR study whereas the red areas are potential slick extents from the CSTARs data collected during this study.

Area 1

Area 1 prior to the voyage the area was characterised by low quality bathymetric data. The area is also sparsely covered by 2D seismic lines from the DWG MSS survey (dwgab-14a and dwgab-28r) as well as Flinders deepwater 2D MSS seismic lines (W00FDW -0067A, -0065P, -0105B). A single GAB2 2D MSS seismic line also crosses the area but is unavailable from public holdings.

Seismic interpretation shows that the area is located on the upper part of the abyssal slope the areas overlies a potential subsurface anticline intersected by deep routed faults which penetrate the Hammerhead and possibly Tiger formations. These faults are associated with seabed scarps and footwall slide planes (Figure 45).

The area has a fractured/disrupted seafloor with small/shallow faults and fractures. In the shallow subsurface bright spots are present which could indicate shallow gas accumulations. These are associated with features interpreted as gas chimneys (Figure 45).

Additional evidence for potential seepage was provided the presence of a large slick feature identified by Nigel Press and Associates and Geoscience Australia in their 1999/2000 Radarsat study (Figure 44). The SAR slick feature was interpreted by NPA to be a remnant pollution slick, possibly due to its proximity to the main shipping lane that transects the GAB. The slick is extensive has and elongate morphology oriented from east to west (24 km long and 800m wide). It was not possible for CSIRO to review the actual SAR scene from which the object was interpreted to set the slick in context with the prevailing weather conditions at the time of capture, or ascertain if a vessel was present within the scene to warrant the interpretation of a remnant pollution slick.

The NPA/GA description concludes that the presence of this slick and the further three slicks identified within the same capture period within Area 2 which formed broken line over 50 km in all are probably the most distinct slicks of the whole study. The interpretation suggested that the linearity of these features were suspicious and thus the features were categorised as remnant pollution.

The slick morphology is however not inconsistent with those observed associated with seeps in other areas of the world. Whilst the slick is large, its association with rugose bathymetric features and interpreted seismic leakage indicators warranted further investigation to ascertain if the active seepage was occurring in this area.

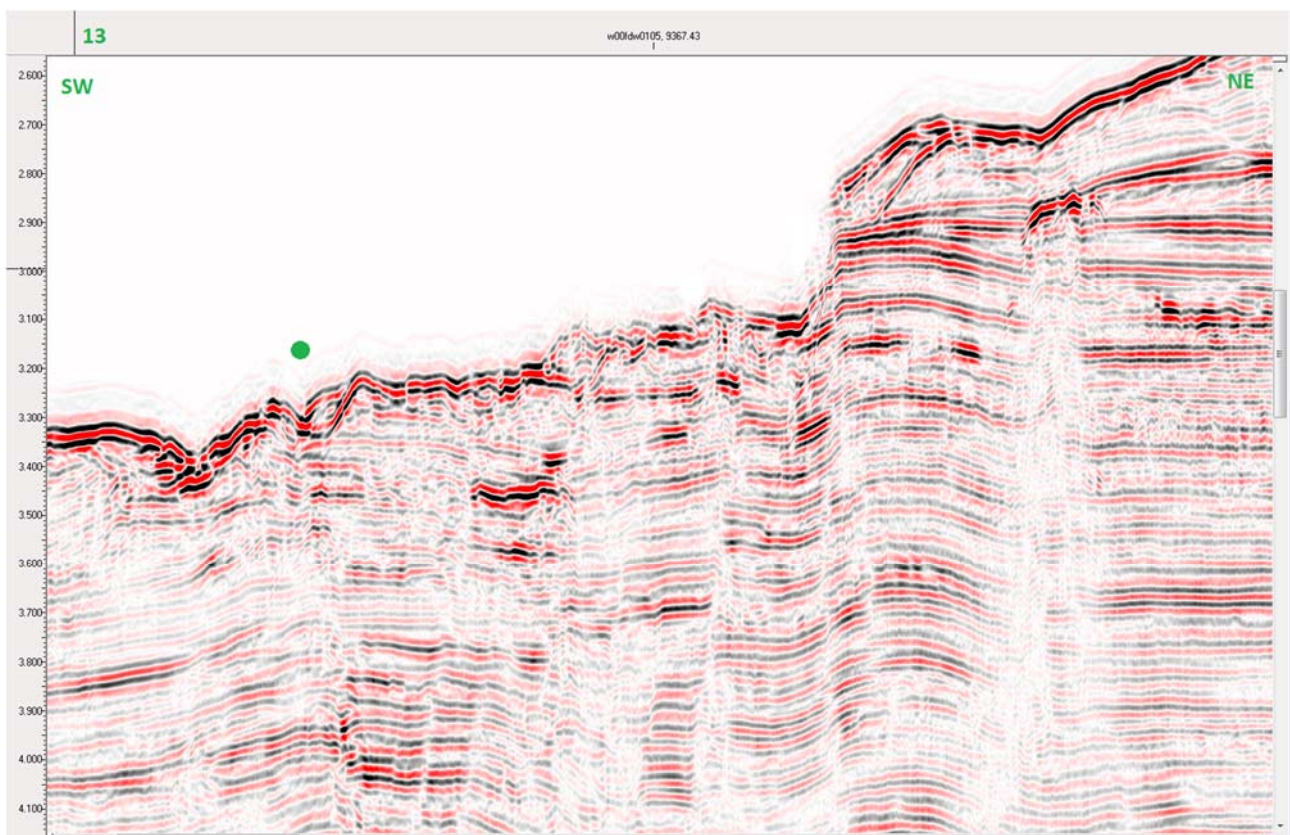


Figure 45 2D seismic line woofdw0065 seismic anomalies showing the seafloor scarp to the north east and fractured/disrupted seafloor with small/shallow faults and fractures. In the shallow subsurface bright spots and possible associated gas chimneys.

Area 2

This area is covered by sparsely spaced 2D seismic lines primarily from the Flinders Deepwater 2D MSS survey, GAB R5 Deepwater MSS, DWGAB, South Australian Shelf R4 MSS surveys (W00FDW-0097P, -0071P, -0069P, -0097A, -0101P, -0067A, DWGAB/27_M, -15, -AB/27_M, SA6-395, SA70W-56). Prior to the voyage no multibeam data was available over the area.

This area lies in water depths of approximately 1700m within the lower continental slope. Within this area the seismic data appears to show a smooth undulating seafloor. One anomaly is apparent within the seismic data (line dwgab 27-m, Figure 46) comprising a sharp fractured/disrupted sea floor incised furrow related to a deeper and chaotic faulting interpreted as a possible fluid conduit with occasional bright spots present.

Additional evidence for potential seepage was provided the presence of three slick features identified by Nigel Press and Associates and Geoscience Australia in their 1999/2000 Radarsat study (Figure 44). As discussed above NPA/GA description concludes that the presence of these slick and the further large slick identified within the same capture period within in Area 1 The interpretation suggested that the linearity of these features were suspicious and thus the features were categorised as remnant pollution.

Once again the slick morphologies are not inconsistent with those observed associated with seeps in other areas of the world. Their association with interpreted seismic leakage indicators warranted further investigation to ascertain if the active seepage was occurring in this area.

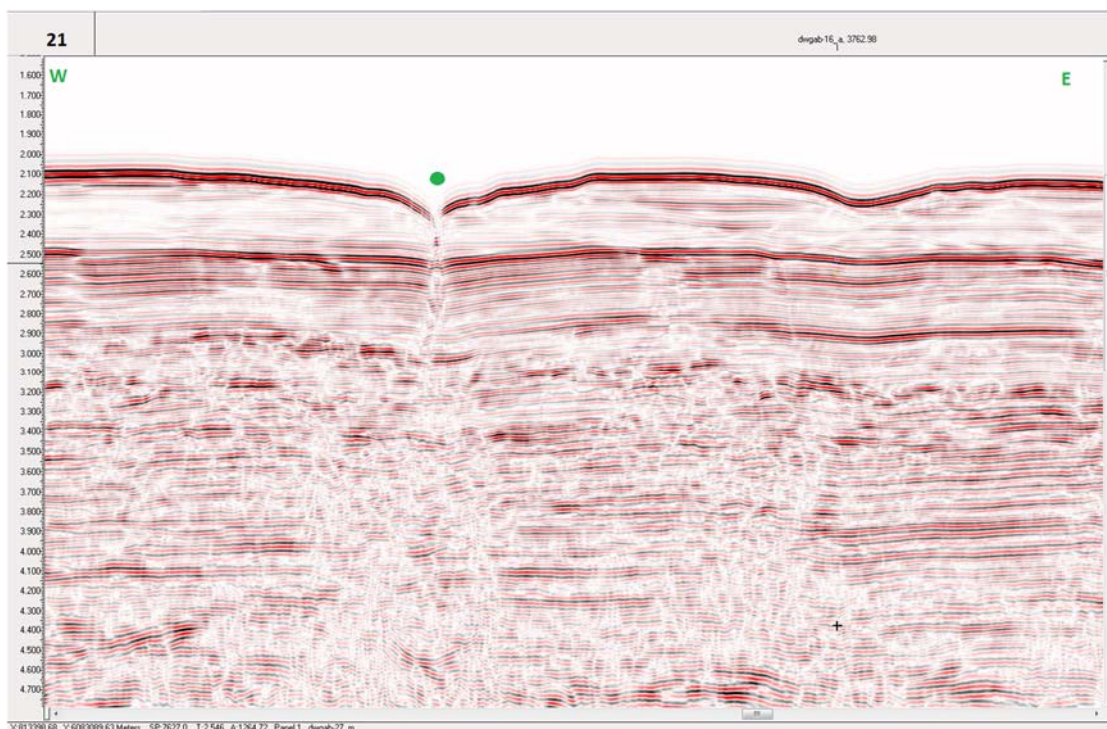


Figure 46 2D seismic line dwgab 27-m seismic anomaly showing a sharp fractured/disrupted sea floor incised furrow related to a deeper and chaotic faulting interpreted as a possible fluid conduit with occasional bright spots present.

Area 3

Prior to the voyage Area 3 was characterised by poor quality multibeam data coverage, Area 1 prior to the voyage the area was characterised by low quality bathymetric data. The area is also very sparsely covered by 4 2D seismic lines from the DWG MSS survey and GAB2 2D MSS of which only two DWG 2D seismic lines were available digitally (DWGAB/18_A, - 28_RM).

Seismic interpretation shows that the area is located on the upper part of the abyssal slope. However no clear evidence was observed for leakage indicators in this data.

The primary evidence potential seepage was provided the presence of a cluster of slick feature identified by CSTARTS as part of the SAR captures acquired during this project (Figure 40 and Figure 43). The slicks form two groups with one group oriented north south and a second group oriented predominantly east-west. The features have elongate and curved morphologies typical of those associated with slicks originating from seeps, and as such provided a strong rationale to investigate this area, especially as it was on the vessel voyage track to the other identified areas.

Baseline sampling areas

The baseline sampling areas for the project 5.1 of the program were married to seafloor sampling locations selected by the Themes 2 and 3 in order to provide comprehensive biological and geochemical characterisation of these sites. In the selection of the sites the theme leaders determined sampling station locations to reduce the likelihood of encountering seeps which would not be representative of the broad GAB ecosystem and benthic environment. 25 stations at 5 depth horizons (200, 400, 1000, 1500 and 2000 m) across 5 transects (5 meridians of longitude) were sampled (Figure 58). To achieve relatively high sampling density in the region of the GAB Marine Park (GAB MP) and active oil and gas leases, one transect (Transect 2) was located in the centre of the GAB Marine Park, and one located at 10 n.m. either side of the MP (Transects 1 and 3). Two others were located in the eastern GAB at 80 and 150 n.m. distance from the centre of the GAB MP (Transects 4 and 5 respectively) (Figure 58). The samples and data generated from these baseline sampling areas is discussed in section 5 below.

Sampling at preselected reference sites (away from areas of potential natural seepage) was designed to facilitate an understanding of pre-drill baseline conditions and will include water column water sampling, and sediment sampling (in conjunction with Benthic Biodiversity Theme), to establish baseline geochemical hydrocarbon conditions.

R/V Southern Surveyor research charter (SS2013_C02) voyage equipment

The voyage plan for the SS2013_C02 voyage comprised a large array of equipment used to address the overall objectives of the mission. These are discussed in detail within the voyage plan

(<http://mnf.csiro.au/~media/Files/Voyage-plans-and-summaries/Southern-Surveyor/Voyage%20plans-summaries/2013/VOYAGE%20PLAN%20c02-13.ashx>) and voyage summary (<http://mnf.csiro.au/~media/Files/Voyage-plans-and-summaries/Southern-Surveyor/Voyage%20plans-summaries/2013/VOYAGE%20SUMMARY%20c02-13.ashx>).

Particular equipment of relevance for theme 5 objectives was the following:

1. Instrumented coring platform (BOAGS). This CSIRO-developed platform integrates visual (HD video and stereo cameras), acoustic (echo sounder and acoustic Doppler current profiler, ADCP), hydrocarbon and other sensor data. Sediment were sampled using a multi-corer fitted to the BOAGS. Adequate to good cores were taken at all 25 stations, despite most being difficult to core; Smith-McIntyre grab samples replaced or supplemented core samples at a few shallow stations. Complete sets of sensor data were collected from most BOAGS casts; data were incomplete during a few early casts as the sensor system was fine-tuned. Dual frequency acoustic data at 120kHz and 38kHz were taken on each cast, and a full deep water calibration completed (Objective 11). Collectively, these samples and data will make significant contributions to progress against objectives in the Benthic, Pelagic and Petroleum Geochemistry Themes.
2. CTD Rosette: A full set of water samples was taken at all 25 stations. The set includes water collections and filtered samples for subsequent analysis; all analysis of dissolved oxygen, salinity and nutrients were completed during the voyage by the MNF hydrochemist. These samples and data will also make large contributions to progress against objectives in the Pelagic and Petroleum Geochemistry Themes.
3. Underway hydrocarbon sensors: Sensor data were taken during the great majority of the survey and integrated with GPS and UTC time stamp. Water samples were collected from the underway system at sensor response anomalies or on specific observations. These samples and data will make substantial contributions to progress against objectives in the Petroleum Geochemistry Theme. If observed, surface slicks will be sampled using a suite of techniques including Gore-sorbers, GO-nets and glass bottles.
4. Collaborative microbial study with Hazen laboratory (University of Tennessee): A full set of samples was collected from each of five stations in proximity to the BP leases and Geotechnical Survey area; these samples and data will contribute to the BP-Hazen laboratory multi-ocean study of microbial systems, and contribute to the collaboration with the Australian team (Benthic Theme).
5. Acoustic data: Single-beam multi-frequency (12, 38 and 120 kHz) water-column acoustic data (EK60), multibeam swath bathymetry (EM300) and sub-bottom profile (TOPAS) data were acquired at all times the vessel was underway. The acoustic systems provided good data with few problems. Approximately 3Gb of bathymetry data and 10 Gb of sub-bottom profiler data were acquired. Combining information from the three acoustic systems enabled characterisation of the relative hardness and sedimentary environment of the seafloor sediment for core targeting; data will support interpretation of other benthic biodiversity and petroleum geochemical analyses. 6 and 7.

All operational and sample data are in the CESRE ISS database, following a substantial error checking process. Data sets are archived and backed up in the ship onboard data management system, and will be archived, with metadata, in the CSIRO Data Warehouse following full

processing. All samples are acquitted, have Chain of Custody documentation, and are packed for immediate distribution to laboratories where analyses will take place.

IN2015_C02 planning

This voyage was undertaken without input into the voyage planning from theme 5 participants, as it was focused on pelagic and benthic theme objectives. The voyage plan for this voyage can be found on the Marine National Facility website at the following link.

http://mnf.csiro.au/~media/Files/Voyage-plans-and-summaries/Investigator/Voyage%20Plans%20summaries/2015/IN2015_C02%20FINAL%20Voyage%20Plan%20FINAL%2020151118.ashx

Whilst the voyage was not planned to address theme 5 objectives a suite of acoustic sensors were utilized which included a Kongsberg EK60 split beam 18kHz and 38kHz single beam echosounder, a Kongsberg/Simrad EM122, 12kHz multibeam echosounder and Kongsberg/Simrad EM710, 70kHz multibeam echo sounder (for shallow water). Both the single and multibeam echosounders were used to map acoustic water column backscatter whilst the multibeam echosounders were also used for the development of seafloor bathymetric maps.

The voyage summary for this voyage can be found on the Marine National Facility website at the following link. http://mnf.csiro.au/~media/Files/Voyage-plans-and-summaries/Investigator/Voyage%20Plans%20summaries/2015/IN2015_C02%20Voyage%20Summary-20160220-FINAL-optimised.ashx

SS2013_C01 Geological interpretation

Approximately 5,185 line km of the Great Australian Bight were surveyed during the SS2013_c02 voyage. The bathymetry characterized during the voyage ranged in depth from 200m to 2,800m comprising seafloor from the shelf break through to the abyssal slope (Figure 47).

When combined with other historical multibeam survey data, low resolution bathymetry sounding data and Ceduna 3D seismic survey data (Figure 47) several features are apparent. The morphology of the Ceduna sub-basin voyage survey area is dominated by a broad continental slope which within the center of the basin is up to 170 km wide. This shallow slope from ~600-2000m is cross cut from northeast to southwest by a series shallow channels. Which in the upper slope form feeder channels which coalesce in larger downslope channels. As evidenced within the 3D seismic first return data (bathymetry) the channel sides show evidence of slump and mass wastage features, whereas within the channels themselves rugose and furrowed morphologies are prevalent. Across much of the lower continental slope with increasing gradient, there is greater of evidence of slope failure, mass wastage and slumping which is predominantly focused down slope,

and independent to the channels. On the break in continental slope and start of the abyssal slope, coincident with the path of the channels, the seafloor is frequently cut by incised canyons. The heads of these canyons are characterized by vertical 50-100m high scarps below which the seafloor has a rugose and undulating terrains.

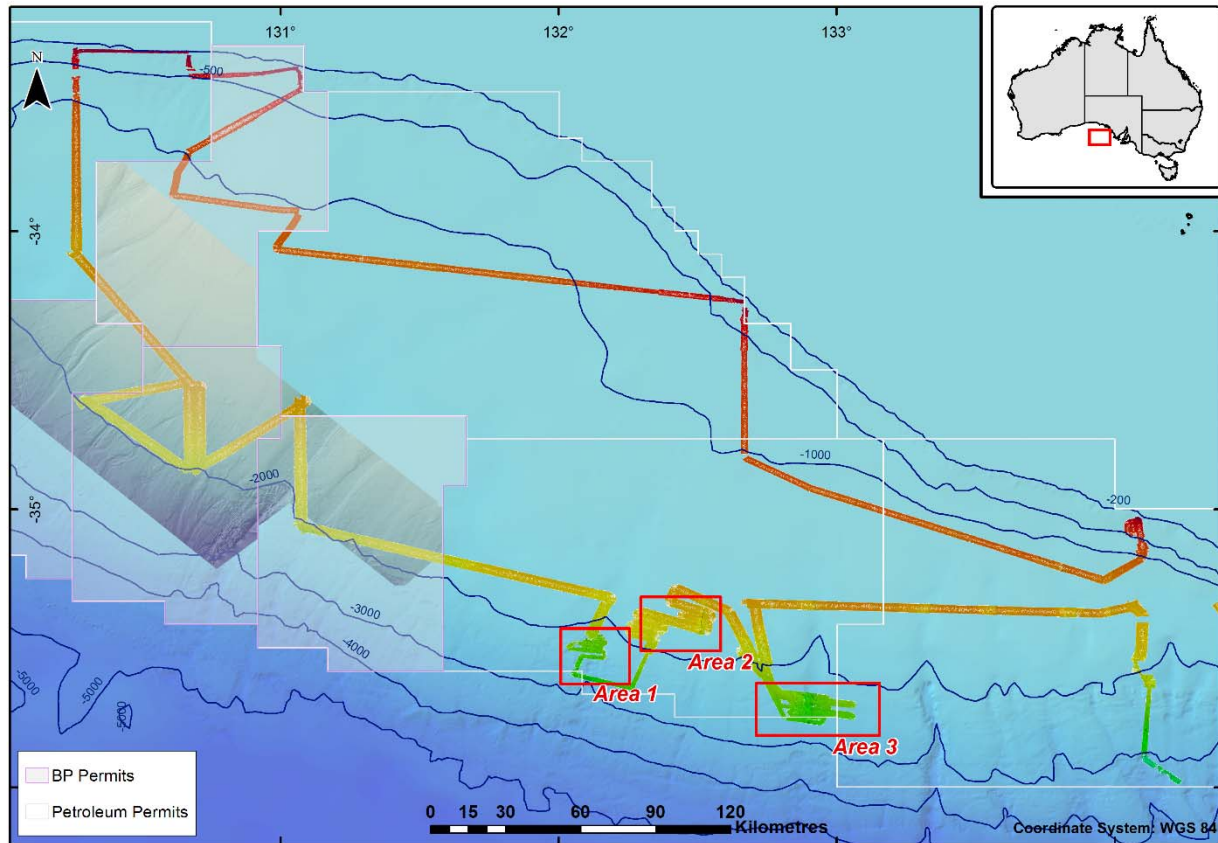


Figure 47 SS2013_C01 multibeam bathymetry data collected over voyage track and potential seep target areas.

The three potential seep target areas across the transition from continental to abyssal slope. Between 1500-m and 2800 m water depth. The multibeam bathymetry data is shown in greater detail in Figure 48.

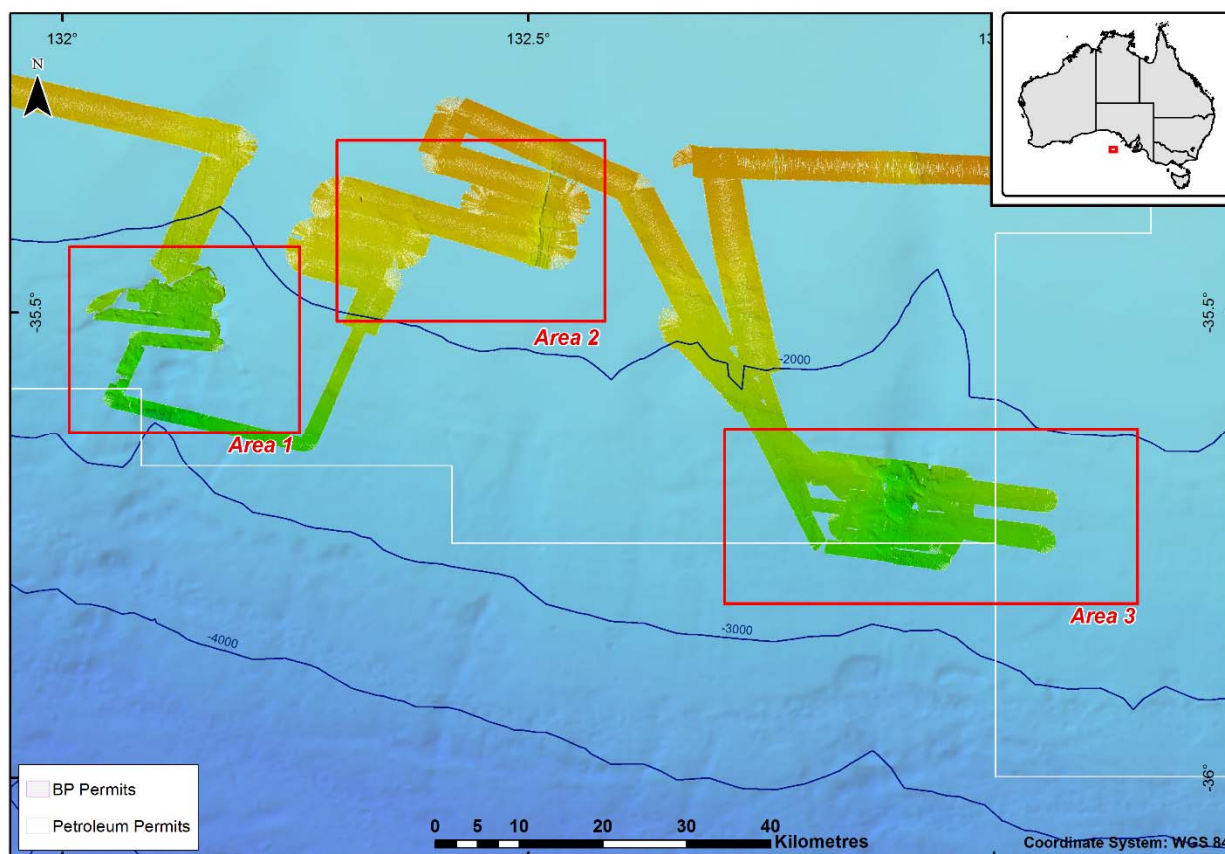


Figure 48. SS2013_C01 multibeam bathymetry data collected over potential seep target areas.

Area 1

Multibeam acoustic data acquired over area 1 during the SS2013_C01 voyage shows a complex seabed geomorphology. The area is characterised as the excavated head of a submarine canyon. The overlying Wobbegong and Dugong sequences found further upslope and to the east and west of the area have been removed by what appears to be slope failure within an existing channel as seabed gradients begin to increase from the broad continental slope of the Ceduna basin into the deep higher gradient abyssal slope between the Ceduna and Recherche sub-basins. Where slope failure has occurred there is a near sheer cliff (Figure 49).

To the north, shallower, section of the area the seabed is characterised by a series of parallel north northeast-south southwest aligned seabed furrows (Figure 49). Below the canyon head cliff the seabed morphology is characterised by a deformed mounded undulating topography with a series of scalloped, possibly erosional, features. When the area seabed multibeam morphology is considered as a whole it is suggestive that these features are the result of mass wastage of sediments from the continental slope, with classic morphologies associated with deep sea turbidite and debris flows (Pickering and Hiscott, 2015).

These morphologies and the slope mechanisms for slope failure may be associated with the underlying fault movement and potential fluid escape. On a smaller scale there are a number of possible pockmarks and localised mounds which could indicate fluid escape within the slope below

the seafloor scarp. However these features are small and occur across at the maximum effective resolution of the multibeam data and therefore could represent noise.

Sub-bottom profiler and water column acoustic backscatter data from the single beam EK60 did not identify features with properties consistent with seepage. It should be noted that these two techniques can only identify features directly below the vessel track and therefore the techniques may not have imaged the water column and shallow subsurface over any of the pock mark features. No anomalies were identified in underway hydrocarbon sensor data collected nor were surface slicks observed in the area.

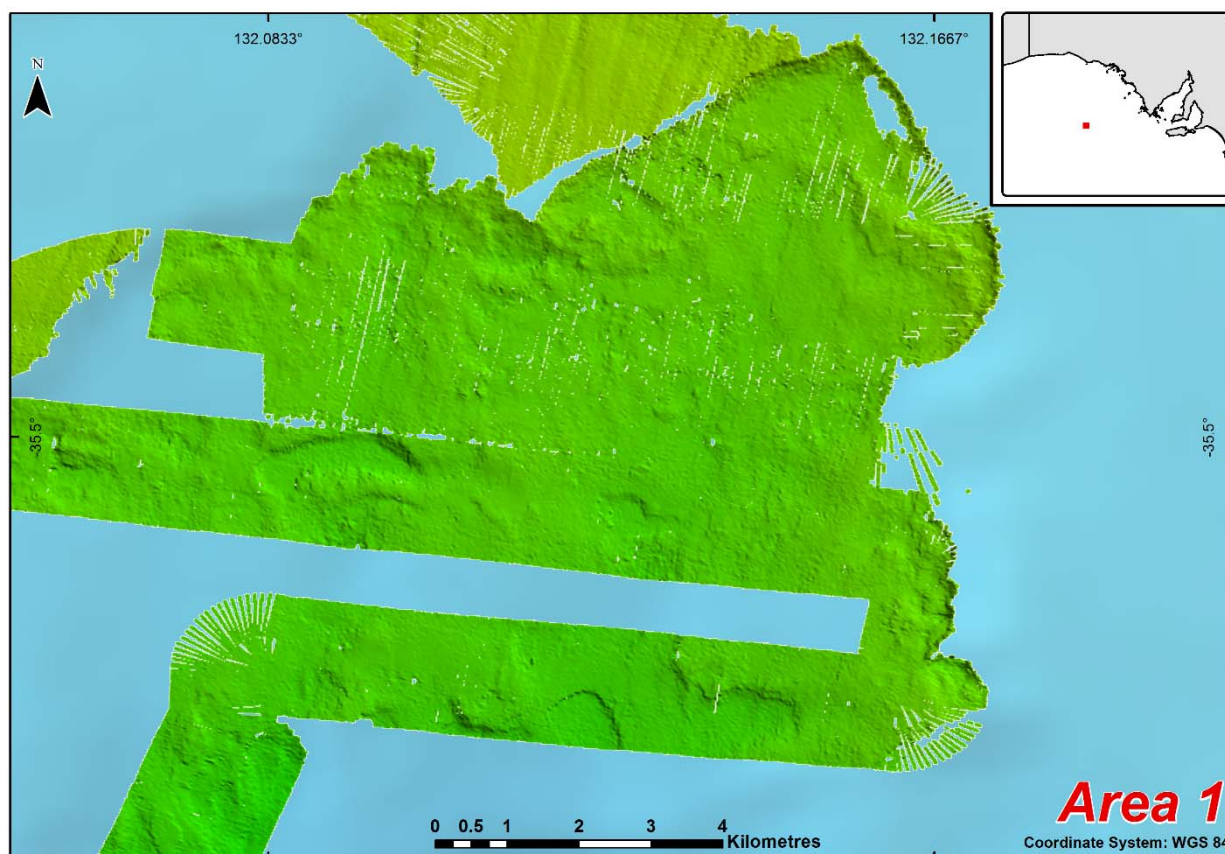


Figure 49. SS2013_C01 multibeam bathymetry of potential seepage Area 1.

Area 2

Multibeam acoustic data acquired over area 2 during the SS2013_C01 voyage shows a more uniform seafloor geomorphology within study Area 1 (Figure 48 and Figure 50). To the west of the area the seafloor is characterized by a uniform continental slope with occasional evidence of minor mass wastage of recent deposits across the broad slope. In addition there is the presence of N-S elongate 800 m long, 400 m wide and 80 m high mound on the seabed. This feature was studied as part of the IN2015_C01 voyage during which it was identified as a potential volcanic seamount.

To the east of the area the seafloor is characterized by a north-south oriented narrow incised channel. The channel appears to be furrowed and once again could be the product of deepwater turbidite flows. On the predominantly western flanks of the channel, potential pock mark features can be observed. As with Area 1 these features are small and occur across at the maximum effective resolution of the multibeam data and therefore could represent noise.

As with Area 1 sub-bottom profiler and water column acoustic backscatter data from the single beam EK60 did not identify features with properties consistent with seepage noting the prior caveats. No anomalies were identified in underway hydrocarbon sensor data collected nor were surface slicks observed in the area.

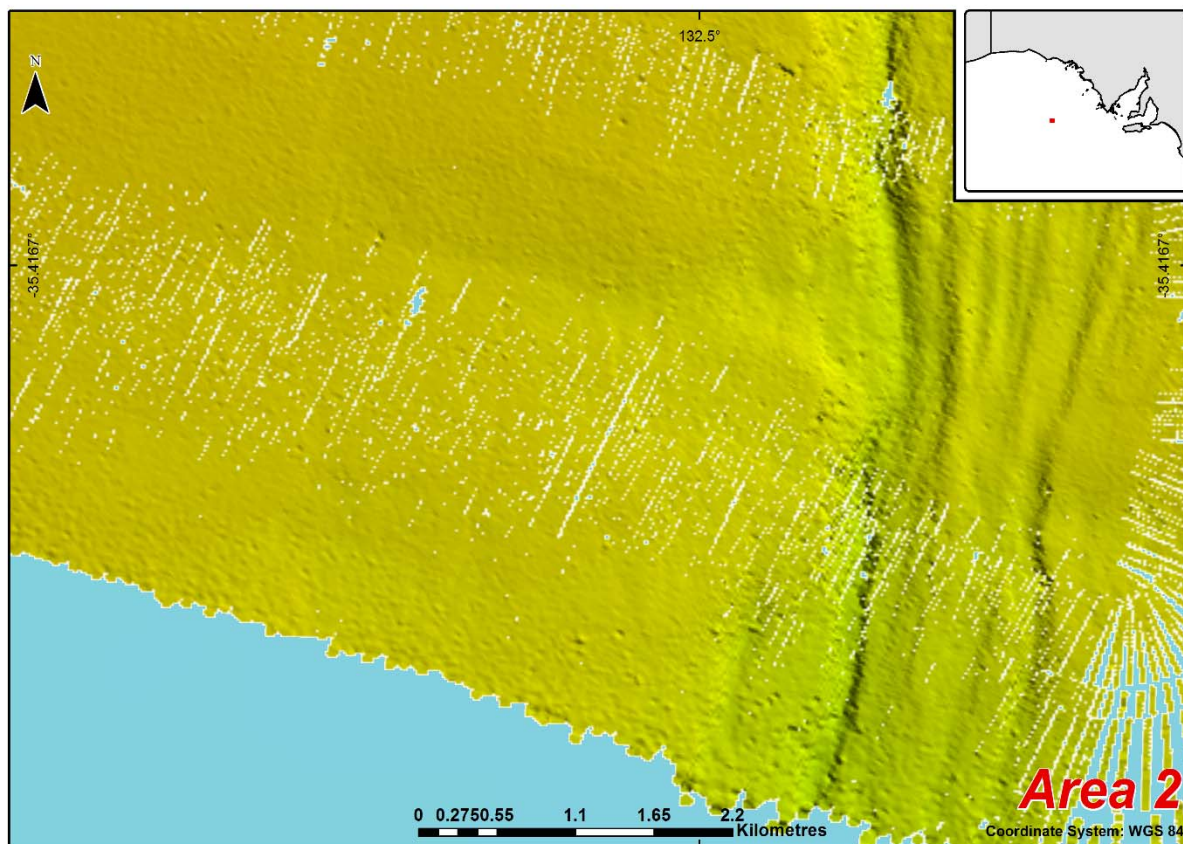


Figure 50. SS2013_C01 multibeam bathymetry of the eastern section of potential seepage Area 2.

Area 3

Multibeam acoustic data acquired over area 3 during the SS2013_C01 voyage shows a complex seafloor geomorphology (Figure 51). The seabed morphology is characterised a central, approximately 3km wide, channel surrounded by smooth seafloor terrains. The area occurs once again at the transition of the continental slope to the abyssal slope. Within the dominant channel feature cross-cutting the area from North to South the seabed morphology is characterised by a deformed mounded undulating topography with a series of scalloped, possibly erosional, features

and a series of seafloor scarps (Figure 51). To the south of the area this seabed morphology is replaced by a north-south oriented seafloor furrows. Once again these morphologies are consistent with those associated with deep sea turbidite and debrite flows (Pickering and Hiscott, 2015).

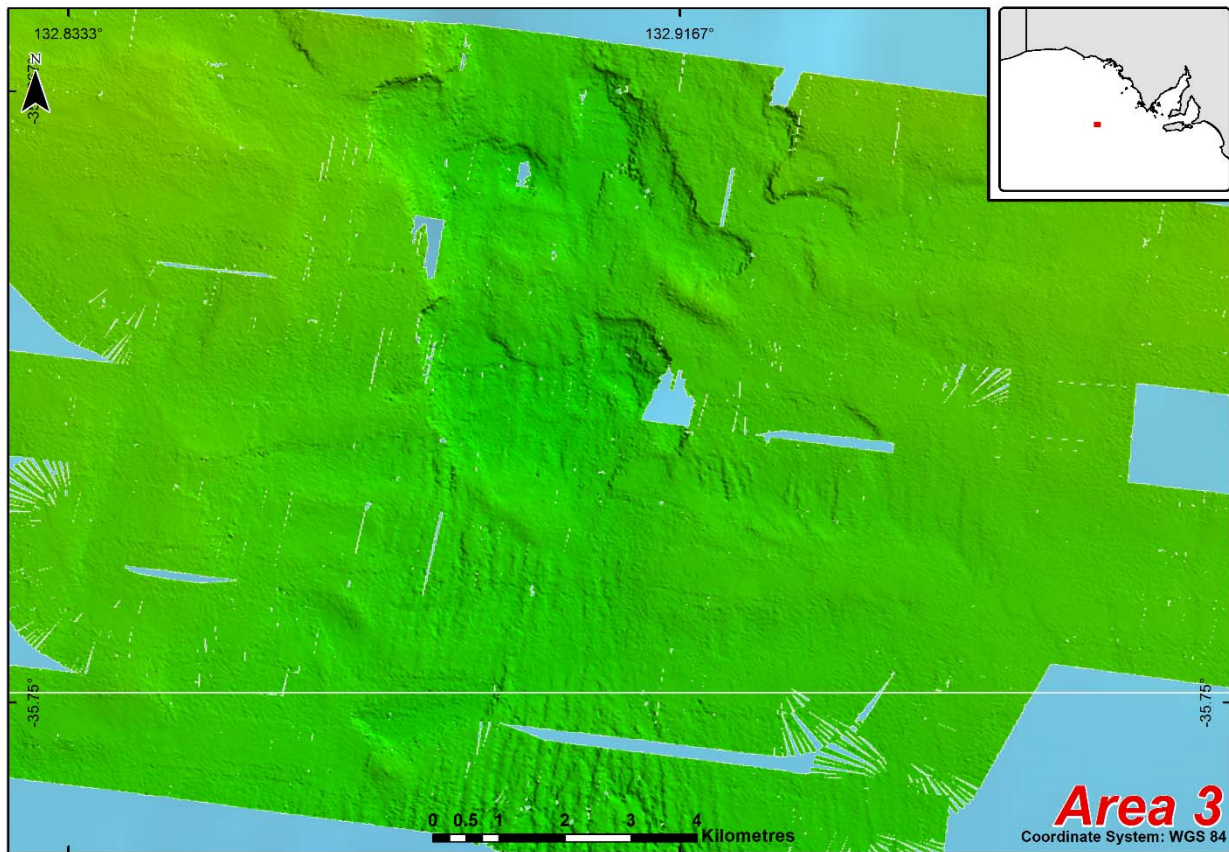


Figure 51. SS2013_C01 multibeam bathymetry of the eastern section of potential seepage Area 3.

As with the other areas studied there are low rank potential pockmarks and raised areas which occur in the undulating sediments of to the north of the area. These features may be associated with fluid escape however due to their proximity to seafloor scarps that have shed blocky materials, and their scale relative to the resolution of the multibeam data they are not considered definitive indicators of seepage.

As with Area 1 sub-bottom profiler and water column acoustic backscatter data from the single beam EK60 did not identify features with properties consistent with seepage noting the prior caveats. No anomalies were identified in underway hydrocarbon sensor data collected nor were surface slicks observed in the area.

Other indicators of seepage from the SS2013_C02 voyage

During the voyage several low intensity hydro-acoustic contacts were recorded (Figure 52) within singlebeam EK60 echo sounder data. These acoustic contacts have been subjected to rigorous quality control and cannot be unequivocally determined to be related to fluid escape from the seabed and as such are assigned a very low rank.

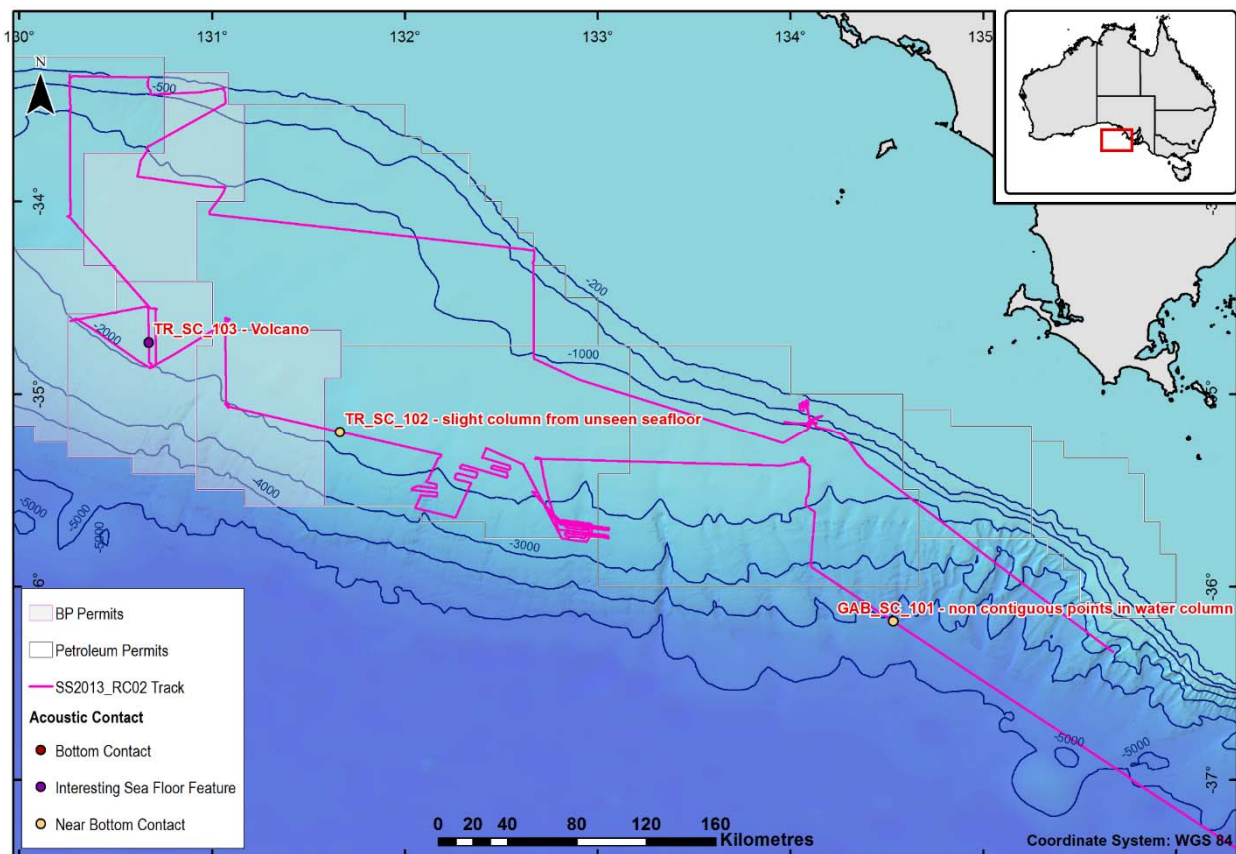


Figure 52. SS2013_C01 Acoustic contacts recorded during the voyage.

Prior reporting associated the TR_SC_102 acoustic anomaly with a sub-bottom profiler anomaly. On review of this data this has proven to have been an erroneously lodged image within the data system and no anomaly is observed at this location within the subbottom profiler data.

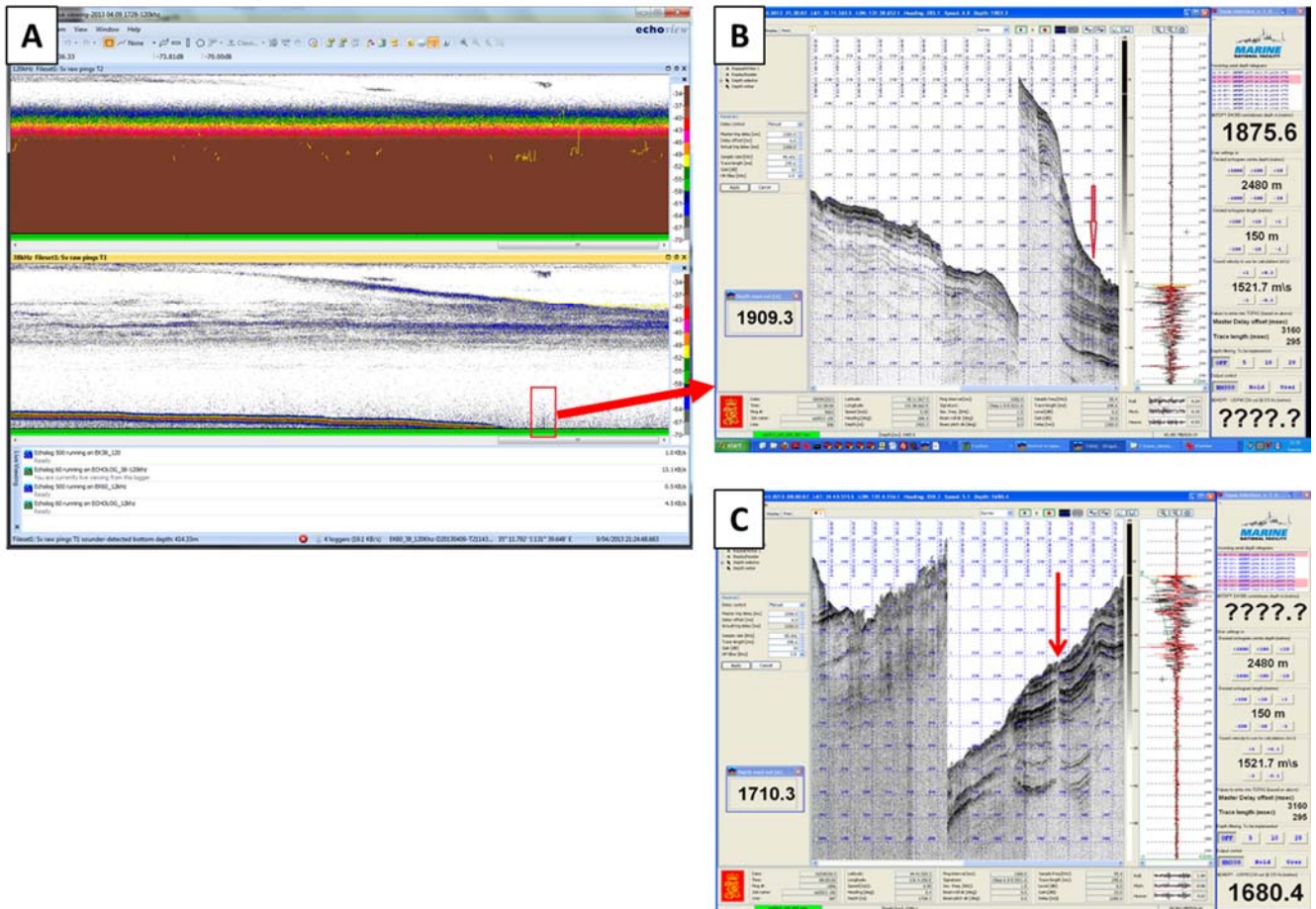


Figure 53. SS2013_C01 low rank TR_SC_102 acoustic water column anomaly (Inset A). With associated subbottom profiler data collected across the area (inset B). Inset C was previously erroneously associated with the .TR_SC_102 location.

Whilst underway sensor data was collected throughout and during deployment of the BOAG's coring system and the observation for slicks was undertaken from the bridge no further indications of seepage or fluid escape were observed. Samples collected from the voyage are detailed within section 5 below.

IN2015_C02 Geological data interpretation

As part of the data review process from the IN2015_C02 voyage, approximately 3,688 line km's of all water column acoustic backscatter data was reviewed (single and multibeam data) to identify potential hydro-acoustic flares within the water column indicative of release of gas from the seabed.

In addition the multibeam bathymetry (Figure 54) and multibeam backscatter (Figure 55) data was reviewed to determine seafloor morphologies and character in order to distinguish areas of potential natural seepage along the seafloor swath characterized during the voyage.

These processes used CSIRO standard workflows very similar to those employed for the SS2013_C02 voyage data in 2013.

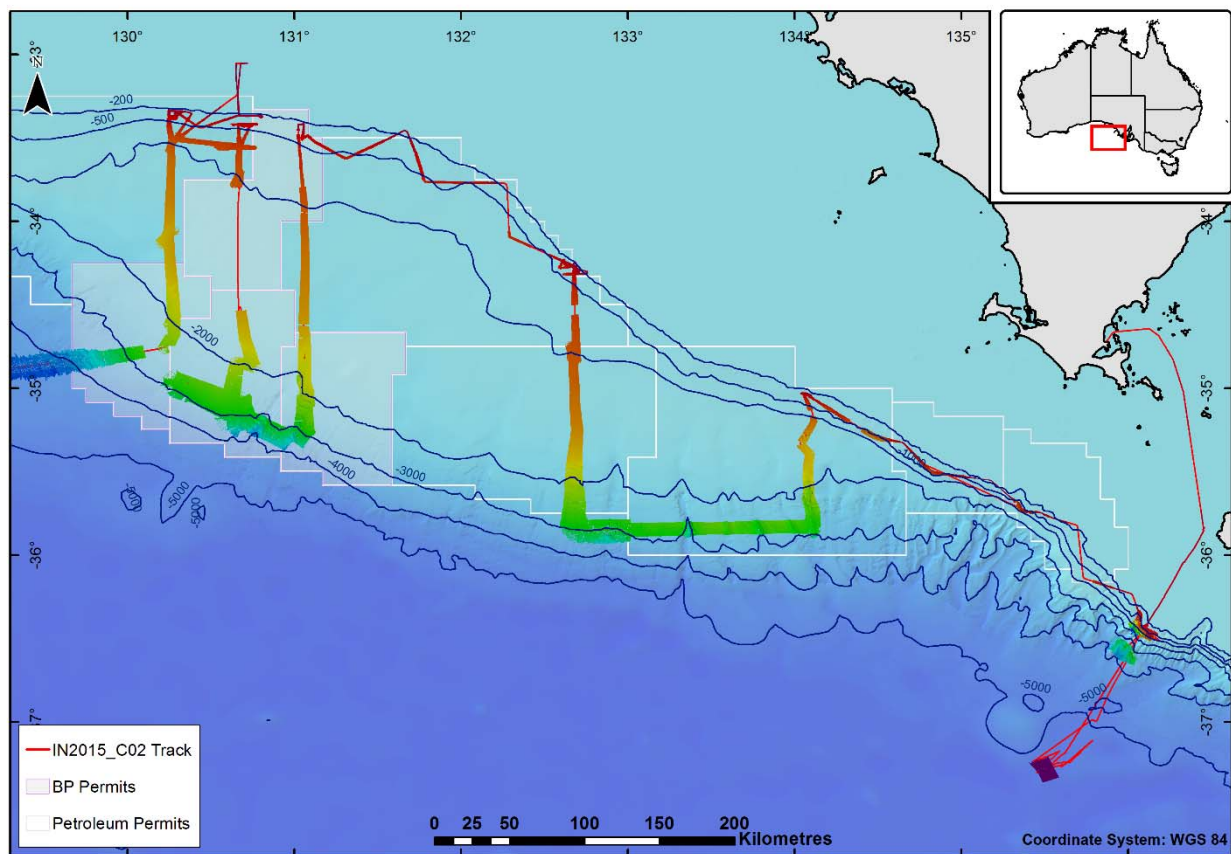


Figure 54. Multibeam bathymetry collected across the Ceduna and Duntroon sub basins of the Great Australian Bight during the IN2015_C02 voyage.

The rapid screening and review of the water column acoustic data failed to identify any hydro-acoustic anomalies that could be attributed to gas release from the seafloor throughout the whole of the survey area.

The seabed morphologies were consistent with those observed during the SS2013_C02 voyage and with first returns data from the Ceduna 3D seismic volume. The north-south transects across the Ceduna sub-basin describe the seafloor terrains from the shelf break to the abyssal slope, whilst the transits between transects characterized both the transition between the continental and abyssal slope and the shelf break (Figure 54). The data collected from the south southwest – north northeast oriented transect across the narrow continental shelf and Duntroon sub-basin from Kangaroo island to the lower abyssal slope were incomplete. Transits to this area characterized the Duntroon sub-basin shelf break.

The seafloor can be described as consisting of three predominant sedimentary domains. The first is that found on the shelf break where on the most part the seafloor is generally smooth and is frequently transected by channels, containing harder materials (multibeam backscatter data Figure 55) that cross cut the shelf break and likely transfer sediments from the shelf to the continental slope. The exceptions to this are the 132.5° East transect where the seafloor is rugose and there is evidence of a large scalloped features on the seafloor as well as areas of rugose and blocky

seafloor terrain. In this area there is little evidence for seepage on the 2D seismic lines which transect the area. The presence of these features is suggestive that this area represents an area of slope failure at the shelf break with sediments being chaotically distributed on the continental slope below. The shelf break along the Duntroon sub-basin transect, due to the very narrow continental slope has led to series of dramatic erosional channels and mass wastage features which are likely depositing sediments in to the many of the deeply incised canyons in this area.

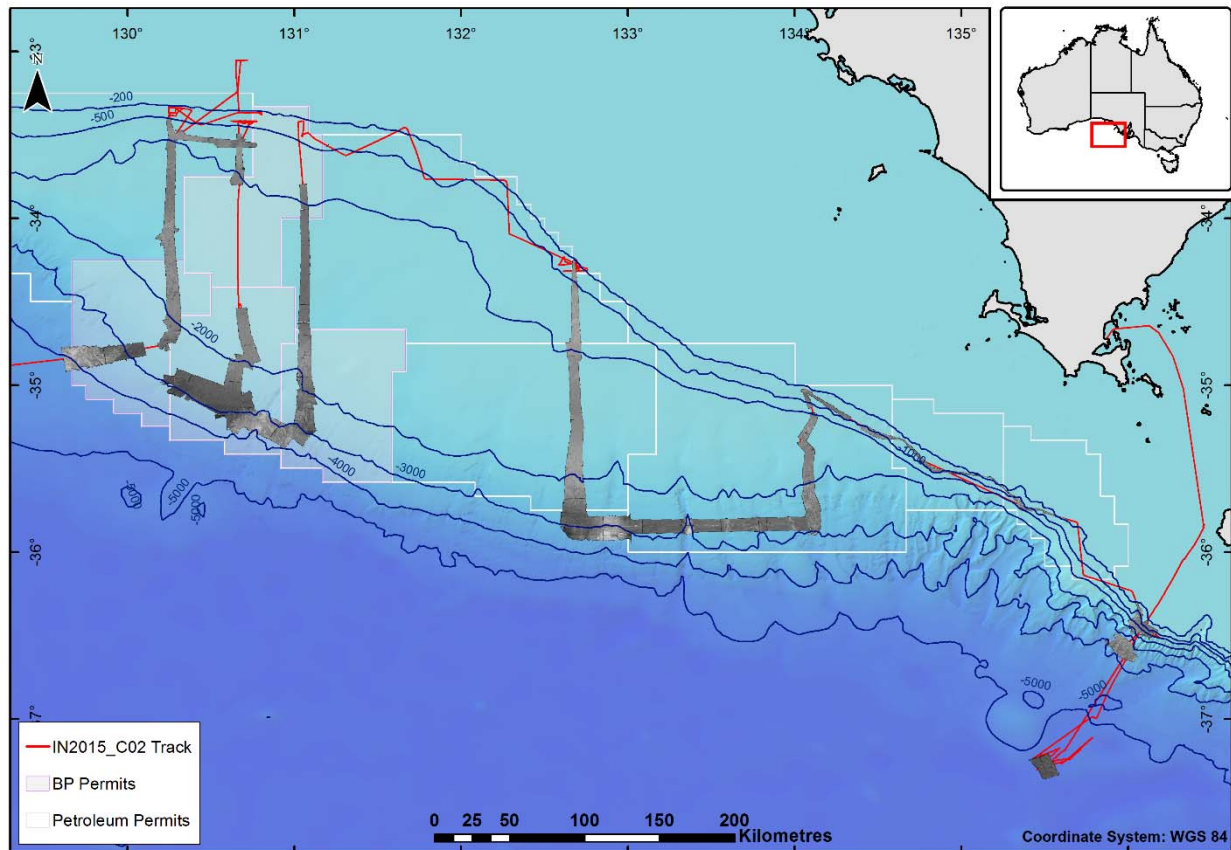


Figure 55. Normalised multibeam backscatter collected across the Ceduna and Duntroon sub basins of the Great Australian Bight during the IN2015_C02 voyage. The data was normalised to 65dB. Soft sediments are represented as dark grey whilst harder sediments are represented as light grey.

The second sedimentary domain is that of the continental slope present across the Ceduna sub-basin. The transects show very uniform gently sloping sediments occasionally cross cut by shallow mass wastage channels. The exception is for the transect to the east of the Ceduna sub-basin (transect 5) which traces the path of a broad north-south oriented scoured channel feature, which at the transition from the continental slope to the abyssal slope is characterized by the a large slope failure followed by further furrowed seafloor terrain further down the slope (Figure 56). The furrowed seafloor, slump deposits and slope failure scarps backscatter response represent harder materials than the surrounding seafloor materials suggesting that these sediments are more lithified (Figure 55). As discussed above these morphologies are typical of those associated with

deep sea turbidite and debrite flows (Pickering and Hiscott, 2015). The other areas abyssal slope areas during the IN2015_C02 voyage are crosscut by incised canyons and erosional debrite and turbidite deposits. No features indicative of seepage were observed in these data.

During the IN2015_C02 voyage beam trawl 141 across the abyssal slope of transect 5 in the eastern Ceduna sub-basin (Figure 56), collected both mussels and red muds, atypical for sediments and biota collected at these depths. The sparsely distributed publically available seismic lines were reviewed with only the DWGAB/22B being available within CSIRO holdings. Review of the DWGAB/22B line (Figure 57) determined that the evidence for any seepage was very weak from this data. Whilst the seismic data shows deep faulting this does not intersect the seabed, nor is there a visible conduit to the surface in this location. It should be noted however that whilst this was the logged location of the beam trawl the start and finish points were not logged and therefore the red muds and mussels may have been collected at some distance from the seismic line and therefore seepage cannot be unequivocally eliminated until further analysis is performed on the microbial assemblages associated with the collected mussels.

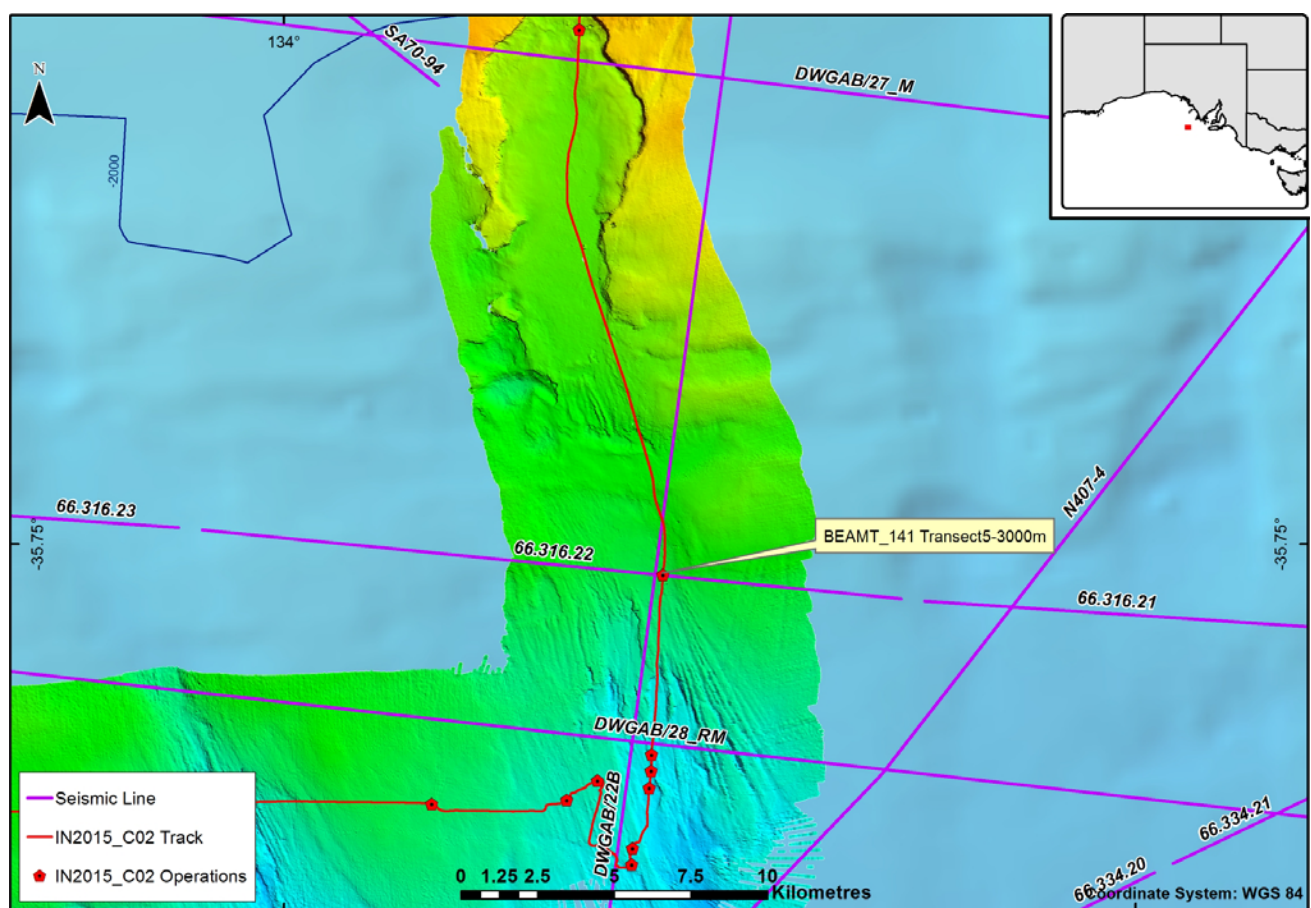


Figure 56. Location of beam trawl 141 (BEAMT_141) displayed on bathymetric map, showing historical seismic lines across the area.

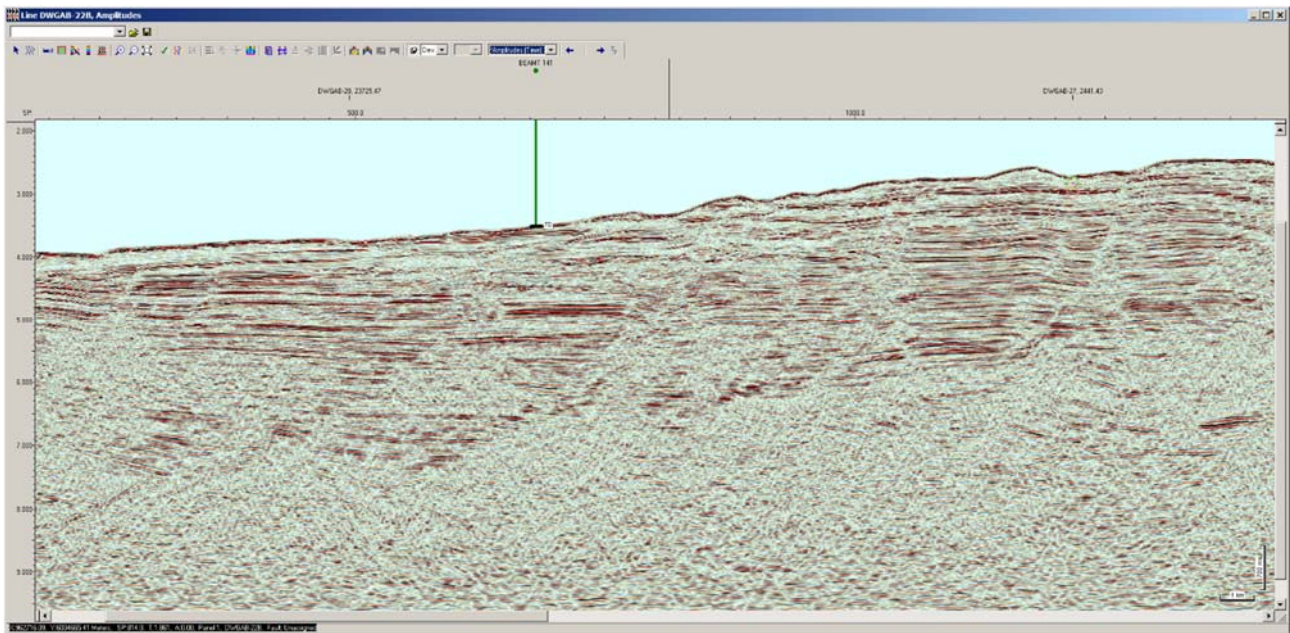


Figure 57. DWGAB/22B 2D seismic cross section scaled to the extent of Figure 56, with the location of beam trawl 141 marked.

Evidence of seepage from GABRP voyages

From the data collected during the SS2013_C02 and IN2015_C02 voyages there is only weak evidence for possible seepage from the data collected, which requires further investigation and qualification. This is in part due to the very limited time spent on the as part of the voyages for the specific purpose of identifying and characterizing potential seepage. This outcome is not a definitive indication of the absence of seepage in the basin, as the basin comprises a very large area and there continues to be a paucity of data collected to specifically identify areas of seepage.

5. SAMPLE ANALYSIS, DATA INTERPRETATION AND DEVELOPMENT OF UNDERSTANDING OF POTENTIAL LEAKAGE AND ACTIVE PETROLEUM SYSTEMS IN THE GAB

Introduction

Assessing the hydrocarbon content of the waters and sediments of the Great Australian Bight (GAB) is crucial in order to establish natural baseline conditions before commencing hydrocarbon exploration in the region. Understanding the nature and distribution of biogenic hydrocarbons may provide information on microbial activity in the water column and in seabed sediments, whilst an investigation of thermogenic hydrocarbons may assist in identifying areas of natural hydrocarbon seepage from the deep subsurface. These results may help to inform exploration strategies in the GAB region.

There is a paucity of water column and sediment chemical analysis data for the GAB, especially for hydrocarbon species, with fewer than 200 surface sediment samples having been analysed from the shelf slope and deep waters of the GAB region (Hughes, M. G., et al., 2009; Totterdell, J. M., et al., 2009). Previous studies which included organic geochemical analyses, failed to identify thermogenic hydrocarbons (Freary, D. A., et al., 2004; Hughes, M. G., et al., 2009; Totterdell, J. M., et al., 2009). As part of the GAB Research Program expanding this dataset has been identified as an important in order to develop a more comprehensive understanding of the geochemical baseline conditions.

A first step towards fulfilment of these GAB Research Program objectives was the planning and implementation of a reconnaissance/baseline survey, which was undertaken during April 2013 using the R/V Southern Surveyor. This survey was designed to sample the water column and seabed sediments along five depth stratified transects (shallow-deep water) across the GAB (Figure 58). Due to time constraints and the competing requirements of the survey, dedicated sampling of potential seeps was not one of the survey objectives. Thus samples acquired for hydrocarbon analysis during this survey were intended to provide a baseline geochemical dataset, against which future samples resulting from a dedicated seeps survey could be compared.

Concurrent with the CSIRO survey was a BP-commissioned geotechnical survey of the BP acreage in the GAB, using the Fugro vessel the M/V Southern Supporter. This additional survey afforded researchers the chance to acquire additional, opportunistic, sediment samples to complement those collected during the R/V Southern Surveyor survey.

This section of the report presents the results of organic geochemical analysis of a sub-set of surface waters, water column, and sediment samples collected as part of the April 2013 R/V Southern Surveyor (CSIRO) and M/V Southern Supporter (Fugro) Great Australian Bight Surveys.

The main objectives of this section of the report are to determine if thermogenic hydrocarbon signatures were present, both in the vicinity of BP permits and regionally within the GAB in order to:

- produce a data baseline of hydrocarbon levels in the region,
- establish if there were any signs of natural hydrocarbon contamination of sediments and
- identify potential areas of hydrocarbon seepage from the subsurface.

This report is presented in two parts:

Part A: Text, Tables and Figures

Part B: Raw data which forms APPENDIX 1: DATA MANAGEMENT.

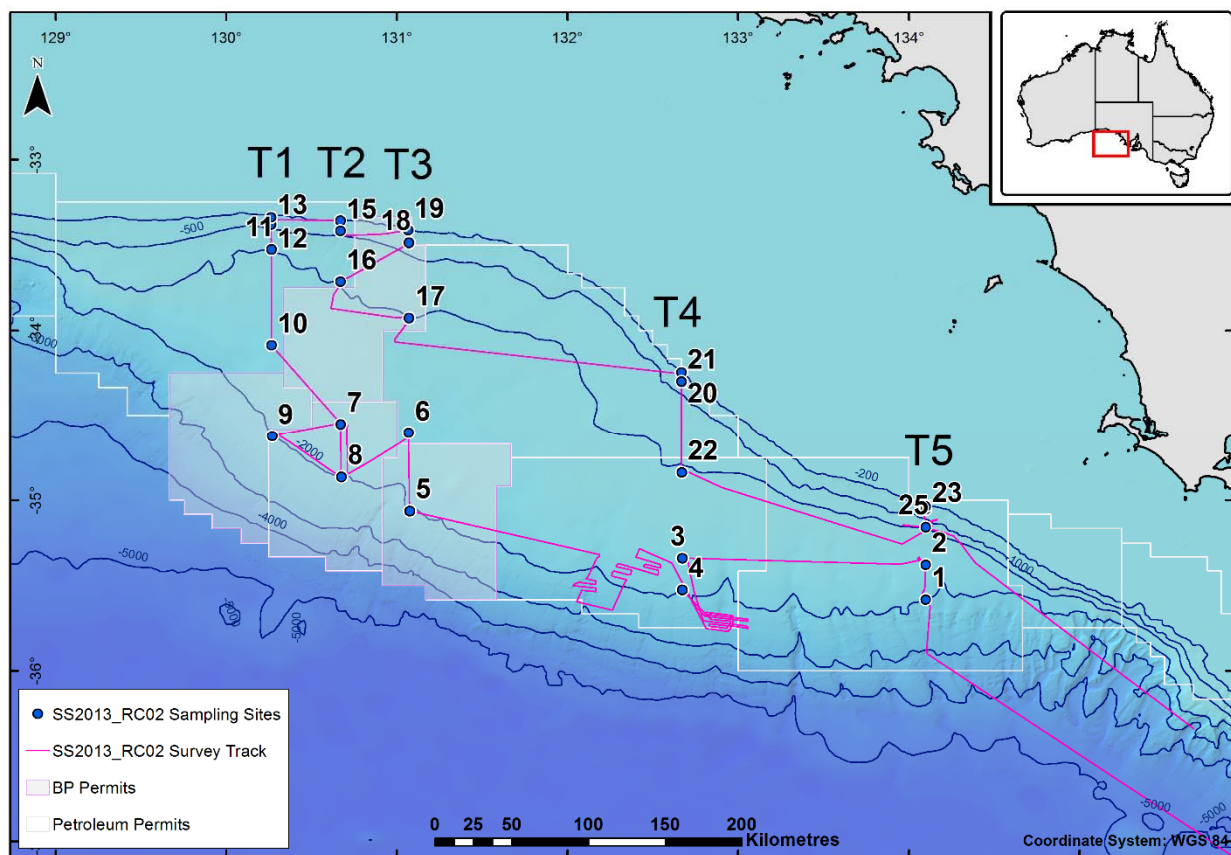


Figure 58 Map of the central and eastern GAB regions showing the 25 sampling stations (blue circles) on five transects (T1-5). Mapped features are: the former GAB Marine Park (blue outline, now part of the larger Great Australian Bight Commonwealth Marine Reserve); other Commonwealth Marine Reserves (grey outlines); BP lease areas in which exploratory activities will occur (green outlines). Isobaths: 200 m (green), 1000m (red), 2000m (blue) 3000 m (brown).

Samples

Sampling planning

Each of the surveys conducted in the GAB during 2013 had specific, and occasionally competing, requirements to fulfil. The primary focus of the BP-Fugro survey was to complete geotechnical investigations of 17 pre-selected sites. Any scientific sampling activities were required to cause minimal interruption to the geotechnical operations, whilst still resulting in the collection of useful samples. The CSIRO-led survey aboard the R/V Southern Surveyor involved collaboration between scientists from CSIRO, SARDI and the University of Tennessee. Twenty three different types of sample were collected for three Themes of the GAB Research Program. With such wide-ranging goals across the two surveys and with personnel from diverse backgrounds conducting the sampling, significant pre-survey planning was necessary to clearly define the sample sets. This careful planning meant that it was possible to collect a complementary suite of samples from each survey and, as such, augment the dataset generated across the region of the GAB investigated.

Five different sample types relevant to Project 5.1 were chosen for collection over the course of the marine surveys, targeting surface waters, the water column, the sediment-water interface and the seabed sediments themselves (Table 6). The sampling schemes drawn up for each survey can be found in APPENDIX 1: DATA MANAGEMENT.

Sample collection and handling

The collection of samples onboard the R/V Southern Surveyor was carried out by several members of the CSIRO science party who had received training in sampling methods and sample handling prior to the survey. Sampling onboard the M/V Southern Supporter was performed by a dedicated team of environmental scientists from Fugro, who were provided with protocols, equipment and training by CSIRO before the vessel sailed. The sample types collected during each cruise are detailed in Table 1, and the protocols stipulating the methods of collection and handling are provided in APPENDIX 1: DATA MANAGEMENT. Photographs showing the types of samples collected are shown in Figure 59.

Table 6 Descriptions of sample types collected during the CSIRO and BP-Fugro marine surveys of the Great Australian Bight, 2013.

Vessel (personnel)	Sample Type	Description
R/V Southern Surveyor(CSIRO)	GO net	Any surface expressions resembling potential slicks were collected. These potential slicks may be related to active natural hydrocarbon seepage, and may therefore offer information about the potential source rocks in the region. GO nets that were collected were solvent washed and subjected to the analyses described in Section 0.
	Niskin bottle waters	During CTD deployments, waters were collected using Niskin bottles at 3 depths throughout the water column – 60 m from the surface, 2/3 of the way through the water column and 50 m off the seabed. 1 litre waters samples were solvent extracted and the extracts subject to the analyses described in Section 0.
	Top water	The water immediately overlying the sediment-water interface which was retained in the multicore liner. This was collected as it was anticipated that

		waters immediately overlying the sediments would have a high abundance of dissolved hydrocarbons in areas of natural seepage. 1 litre water samples were subjected to the analyses described in Section 0.
	Headspace gas	Sediment was extruded from the bottom 3 cm of the collected multicorer core and transferred to an IsoPak bag. The bag was sealed and stored at -80°C to inhibit bacterial activity that may change the composition or isotopic ratios of the gases inside the bag. The gases were analysed according to the scheme described in Section 0. Core material was collected using a multicorer.
	Sediment	After collection of sediments for headspace gas analysis, the next lowermost 5 cm of core from multicores were extruded and transferred to a 250 ml wide-mouth glass jar, and stored at -20°C. Once at the destination laboratory, samples were analysed according to the details given in Section 0.
M/V Southern Supporter (Fugro)	Headspace gas	Sediment was extruded from the bottom 3 cm of the collected core and transferred to an IsoPak bag. The bag was sealed and stored at -80°C to inhibit bacterial activity that may change the composition or isotopic ratios of the gases inside the bag. The gases were analysed according to the scheme described in Section 0. Core material was collected using a piston core and a multicorer. Where a piston core was used, the bottom 3 cm of each 1 m section were retained for headspace gas analysis.
	Sediment	After collection of sediments for headspace gas analysis, the next lowermost 5 cm of core from multicores and piston cores were extruded and transferred to a pre-cleaned 1 litre tin, and stored at -20°C. Once at the destination laboratory, samples were analysed according to the details given in Section 0.



Figure 59 Photographs of sample types analysed as part of this report. Moving clockwise from far left: Multicorer liner containing sediment core exhibiting colour variations throughout sediments, which are overlain by seawater; decanting water from the sediment-water interface into 1 L amber glass bottle (top water samples); sectioning extruded sediment; sediment section wrapped in clean aluminium foil and sealed into IsoPak bag for headspace gas analysis; sediment section before being wrapped in clean aluminium foil.

Samples selected for analysis

Due to time and budgetary constraints, a sub-set of the collected sample suite was selected for analysis. All water samples received by CSIRO were subject to an initial round of analysis at the National Measurement Institute in Perth, Western Australia. Samples were solvent-extracted and analysed for their polycyclic aromatic hydrocarbon (PAH) contents by gas chromatography mass spectrometry (GC-MS). The purpose of this, preliminary stage of analysis was to identify samples that may have higher levels of hydrocarbons and therefore warrant more detailed analysis.

Wherever possible, samples that comprised a suite from any one location were analysed, in order to verify geochemical information arising from one particular type of sample. This approach is illustrated in Table 7 and Table 8 and in Figure 60. Samples were selected based on the following criteria:

If photographs and observations made by the people who took the samples provided an indication of discolouration in the sediments or waters (Table 7). This type of information flagged the sample as a possible contender for further investigation;

Where samples were returned from sampling stations that were proximal between the two surveys (Table 7 and Table 8 and in Figure 60);

If the sampling method returned enough material to constitute a reliable sample – too little material may throw any results into doubt.

Table 7 Selection criteria for sediment and water samples collected during the R/V Southern Surveyor cruise.

Station No.	Reason for Choosing Station	Core No. used for sample	Sediment Sample ID	Related Topwater Sample ID	Related Niskin Sample ID	Related Isopak Sample ID
1	Colouration of cores one and two, beige at surface with grey material at deepest point. Only one topwater sample from core 1.	1	W13/005093	W13/005073	W13/005098	W13/005092
2	Cores from this station have similar colouration to BOAGS 005.	2	W13/005172	W13/005152	W13/005175	No matching Isopak
3	Station is in the general vicinity of areas with previously identified SAR slicks.	3	W13/005300	W13/005280	W13/005279 (top water)	No matching Isopak
4	Station is in the general vicinity of areas with previously identified SAR slicks.	1	W13/005373	W13/005353	W13/005378	No matching Isopak
5	This station was in the area of the convergence lines, and GO net sample.	1	W13/005505	W13/005485	W13/005509	W13/005504
6	This station was in the area of the convergence lines, and GO net sample. Water & sediment collected from	2	W13/005587	W13/005567	W13/005590	No matching Isopak

	core 1 & 2. Close to M/V Southern Supporter site 3.					
7	General proximity to seafloor features (mud volcanoes) that were passed over during transit between stations 7 and 8. Close to M/V Southern Supporter site 2.	1	W13/005940	W13/005921	W13/005944	W13/005939
8	General proximity to seafloor features (mud volcanoes) that were passed over during transit between stations 7 & 8. Close to M/V Southern Supporter site 14.	3	W13/005884	W13/005864	W13/005888	W13/005883
9	Core 1 displayed interesting colouration, even though it was a short core. Water sampled from core 1 and 2, however there was only enough material for an isopak sample and no other sediment sample.	1	No Sample	W13/005743	W13/005767	W13/005762
10	Colouration of cores 1,2 and 3 highlighted in report.	1	W13/006021	W13/006001	W13/006025	W13/006020
11	Core 1 and 2 highlighted in report for having distinct beige-white-grey transitions in colour from top to bottom of core. Close up of sediment sample from core 2 indicated dark grey streaks in core.	2	W13/006107	W13/006087	none	No matching Isopak
13	Core 1 has been highlighted in report.	1	W13/006270	W13/006250	W13/006275	W13/006269
15	Close to M/V Southern Supporter site 15. Colouration of core 1 highlighted in report.	1	W13/006424	W13/006404	W13/006429	W13/006423
16	Cores 1 and 2 have been highlighted in the report.	1	W13/006648	W13/006629	No sample	No matching Isopak
19	Core 1 has been highlighted in the report. Sediment material is too coarse to remain in the core.	1	No Sample	No Sample	W13/006484	No Sample
22	Core 3 has been highlighted in the report.	2	W13/007019	W13/006999	W13/007023	W13/007028
24	Core 4 highlighted due to dark colouration, grey banding at base of core.	1	W13/007265	W13/007245	W13/007270	W13/007264
25	Core 2 highlighted due to colouration.	2	W13/007114	W13/007094	W13/007093 (top water)	W13/007121

Table 8 Selection criteria for sediment samples collected during the M/V Southern Supporter cruise.

Station Number	Station Information	1/2 Lower 5cm PC Sample ID	1/2 Top 5cm MC Sample ID	1/2 Lower 5cm MC Sample ID	Related Piston Core Isopak ID	Related Multicore Isopak ID
GEG13-02	High priority (3). Also coincides with Southern Surveyor sampling location 7	161A	021A	No sample	160A	019A
GEG13-03	Coincides with Southern Surveyor sampling location 6. However, quite low priority (13)	181A	111A	110A	180A	109A
GEG13-03a		181C	No sample	No sample	180C	No sample
GEG13-05	High priority (7)	169A	No sample	No sample	168A	No sample
GEG13-06	High priority (6)	167A	048A	047A	166A	046A
GEG13-07	High priority (9)	173A	075A	074A	172A	073A
GEG13-07a		173C	No sample	No sample	172C	No sample
GEG13-10	High priority (4)	163A	No sample	No sample	162A	No sample
GEG13-11	High priority (10)	175A	No sample	No sample	174A	No sample
GEG13-11a		175C	No sample	No sample	174C	No sample
GEG13-12	High priority (8)	171A	No sample	No sample	170A	No sample
GEG13-13a	High priority (5)	165A	No sample	No sample	164A	No sample
GEG13-13b		165C	No sample	No sample	164C	No sample
GEG13-14	Coincides with Southern Surveyor sampling location 8. However, quite low priority (12)	179A	No sample	No sample	178A	No sample
GEG13-17	High priority (1)	155A	003A	002A	154A	001A

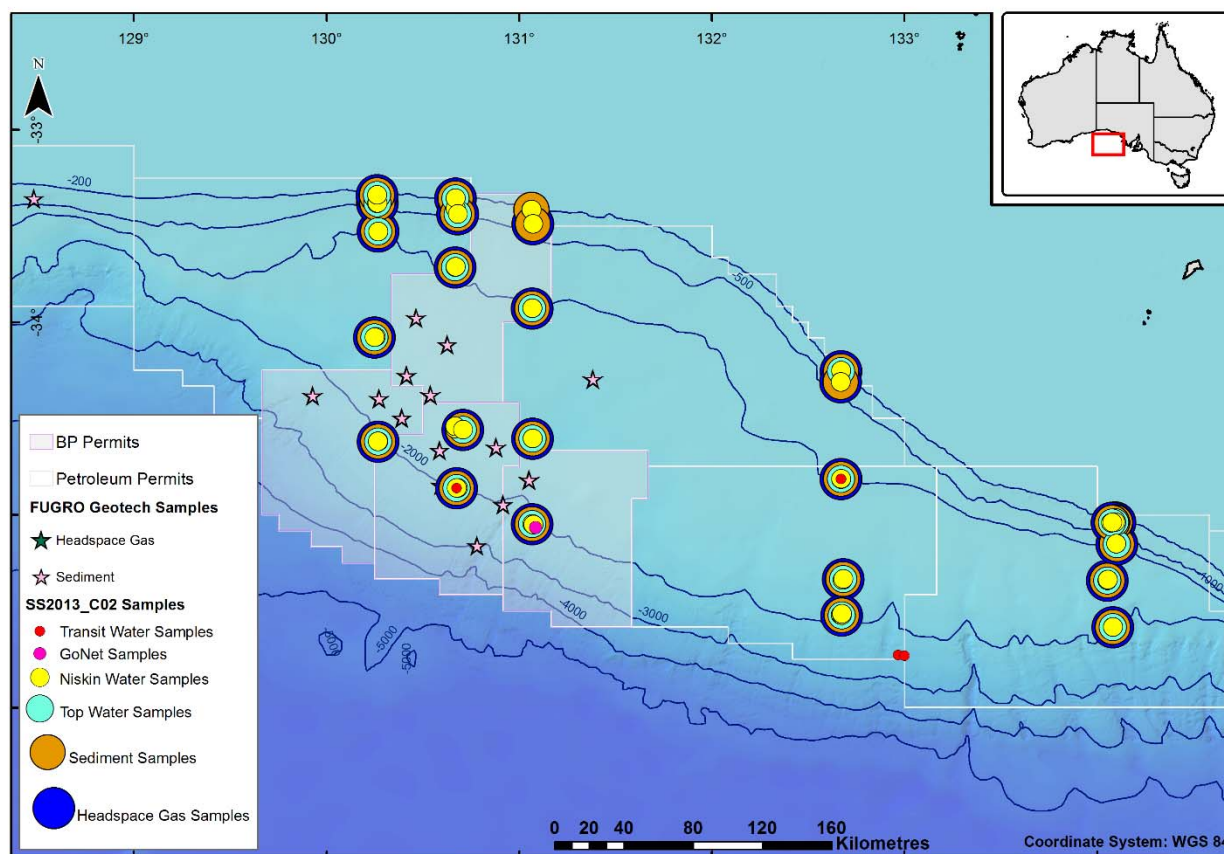


Figure 60 Map showing the distribution of samples selected for analysis from the CSIRO and BP-Fugro GAB marine surveys, 2013. Coloured dots overlying one another represent multiple samples collected from one location during the R/V Southern Surveyor cruise; stars overlying each other represent headspace gas and sediment sample collected during the M/V Southern Supporter marine survey.

Top and Niskin water, seabed sediment, surface water anomaly samples (e.g., GO net), headspace gases and other samples (i.e., pump water, Milli-Q blank, methanol blank, etc.) that were collected during the R/V Southern Surveyor (CSIRO) and M/V Southern Supporter (Fugro) GAB surveys and analysed in both NMIs and CSIRO's Organic and Isotope Geochemistry Laboratories are listed in Table 9, Table 10 and Table 11.

These lists also include some other samples such as system blanks, air blanks, BOC standards and solvent blanks that were analysed to assess the contributions of any background compounds to the results and thereby measure the relevance/ significance of compounds identified in the samples. Information on the type of analysis completed and list of appendices of mass chromatograms are also provided in these tables below.

Table 9 Water samples selected for analysis.

SI	SAMPLE ID	STATION ID	LATITUDE	LONGITUDE	DATE (UTC)	TIME (UTC)	WATER DEPTH (M)	SAMPLING DEPTH	ANALYSES	**RAW CHROMATOGRAMS
	Top Water*									
1	W13/005073	1	-35.58211300	134.08178100	07-Apr-13	1:30 AM	2004	Above sed-water interface	FS GC-MS of EOM	Appendix C
2	W13/005152	2	-35.34126700	134.05247100	07-Apr-13	9:37 AM	1524	Above sed-water interface	FS GC-MS of EOM	Appendix C
3	W13/005280	3	-35.33261800	132.68116700	08-Apr-13	12:22 AM	1494	Above sed-water interface	FS GC-MS of EOM	Appendix C
4	W13/005353	4	-35.52098900	132.67397800	08-Apr-13	1:22 PM	1924	Above sed-water interface	FS GC-MS of EOM	Appendix C
5	W13/005485	5	-35.04733400	131.06725500	10-Apr-13	2:41 AM	2006	Above sed-water interface	FS GC-MS of EOM	Appendix C
6	W13/005567	6	-34.60372600	131.06839000	10-Apr-13	10:21 AM	1479	Above sed-water interface	FS GC-MS of EOM	Appendix C
7	W13/005921	7	-34.55711300	130.70676800	12-Apr-13	5:11 AM	1482	Above sed-water interface	FS GC-MS of EOM	Appendix C
8	W13/005864	8	-34.86084200	130.67433800	11-Apr-13	8:48 PM	2010	Above sed-water interface	FS GC-MS of EOM	Appendix C
9	W13/005743	9	-34.61932300	130.26630600	11-Apr-13	9:45 AM	2014	Above sed-water interface	FS GC-MS of EOM	Appendix C
10	W13/006001	10	-34.07709400	130.24789900	12-Apr-13	1:00 PM	1544	Above sed-water interface	FS GC-MS of EOM	Appendix C
11	W13/006087	11	-33.52790900	130.26694300	12-Apr-13	8:17 PM	1015	Above sed-water interface	FS GC-MS of EOM	Appendix C
12	W13/006250	13	-33.33855300	130.26198300	13-Apr-13	4:06 AM	204	Above sed-water interface	FS GC-MS of EOM	Appendix C
13	W13/006404	15	-33.43841100	130.68118300	13-Apr-13	5:05 PM	477	Above sed-water interface	FS GC-MS of EOM	Appendix C
14	W13/006629	16	-33.71374100	130.66744700	14-Apr-13	10:50 AM	996	Above sed-water interface	FS GC-MS of EOM	Appendix C
15	W13/006999	22	-34.81236700	132.67045300	16-Apr-13	3:36 AM	1015	Above sed-water interface	FS GC-MS of EOM	Appendix C
16	W13/007245	24	-35.04043300	134.07694800	17-Apr-13	3:29 AM	375	Above sed-water interface	FS GC-MS of EOM	Appendix C

17	W13/007094	25	-35.15205700	134.10157900	16-Apr-13	6:48 PM	980	Above sed-water interface	FS GC-MS of EOM	Appendix C
	Niskin Water									
18	W13/005098	1	-35.58211300	134.08178100	07-Apr-13	1:30 AM	2004	1994	FS GC-MS of EOM	Appendix D
19	W13/005175	2	-35.34126700	134.05247100	07-Apr-13	9:37 AM	1524	1514	FS GC-MS of EOM	Appendix D
20	W13/005279	3	-35.33261800	132.68116700	08-Apr-13	12:22 AM	1494	1484	FS GC-MS of EOM	Appendix D
21	W13/005378	4	-35.52098900	132.67397800	08-Apr-13	1:22 PM	1924	1913	FS GC-MS of EOM	Appendix D
22	W13/005509	5	-35.04733400	131.06725500	10-Apr-13	2:41 AM	2006	1996	FS GC-MS of EOM	Appendix D
23	W13/005590	6	-34.60372600	131.06839000	10-Apr-13	10:21 AM	1479	1469	FS GC-MS of EOM	Appendix D
24	W13/005944	7	-34.55711300	130.70676800	12-Apr-13	5:11 AM	1482	1472	FS GC-MS of EOM	Appendix D
25	W13/005888	8	-34.86084200	130.67433800	11-Apr-13	8:48 PM	2010	2000	FS GC-MS of EOM	Appendix D
26	W13/005767	9	-34.61932300	130.26630600	11-Apr-13	9:45 AM	2014	2004	FS GC-MS of EOM	Appendix D
27	W13/006025	10	-34.07709400	130.24789900	12-Apr-13	1:00 PM	1544	1534	FS GC-MS of EOM	Appendix D
28	W13/006275	13	-33.33855300	130.26198300	13-Apr-13	4:06 AM	204	194	FS GC-MS of EOM	Appendix D
29	W13/006429	15	-33.43841100	130.68118300	13-Apr-13	5:05 PM	477	467	FS GC-MS of EOM	Appendix D
30	W13/006484	19	-33.41530200	131.06250100	13-Apr-13	8:46 PM	203	193	FS GC-MS of EOM	Appendix D
31	W13/007023	22	-34.81236700	132.67045300	16-Apr-13	3:36 AM	1015	1005	FS GC-MS of EOM	Appendix D
32	W13/007270	24	-35.04043300	134.07694800	17-Apr-13	3:29 AM	375	370	FS GC-MS of EOM	Appendix D
33	W13/007093	25	-35.15205700	134.10157900	16-Apr-13	6:48 PM	980	970	FS GC-MS of EOM	Appendix D
	GO Net									

34	W13/005510	Transit	-35.06542100	131.08632000	10-Apr-13	5:45 AM	Unknown	0	Extraction and FS GC-MS of EOM	Appendix E
	GO Net Blank									
35	W13/005511	Transit	N/A	N/A	10-Apr-13	5:45 AM	Unknown	0	Extraction and FS GC-MS of EOM	Appendix E
	Other Blanks									
36	W13/005386: Pump water blank	Transit	-35.72612100	132.96786100	08-Apr-13	6:30 AM	Unknown	0	FS GC-MS of EOM	Appendix E
37	W13/005387: Pump water blank	Transit	-35.72991900	132.99980200	08-Apr-13	6:40 AM	Unknown	0	FS GC-MS of EOM	Appendix E
38	W13/006027: Pump water blank	Transit	-34.86086900	130.67441700	12-Apr-13	1:18 AM	Unknown	5	FS GC-MS of EOM	Appendix E
39	W13/007024: Pump water blank	Transit	-34.81237800	132.67046400	16-Apr-13	5:27 AM	Unknown	5	FS GC-MS of EOM	Appendix E
40	W13/007025: Pump water blank	Transit	-34.81237800	132.67046400	16-Apr-13	5:27 AM	Unknown	5	FS GC-MS of EOM	Appendix E
41	W13/006854: Milli-Q blank	Transit	N/A	N/A	15-Apr-13	1:25 PM	N/A	N/A	FS GC-MS of EOM	Appendix E
42	W13/011709: Methanol blank	N/A	N/A	N/A	22-Apr-13	1:25 PM	N/A	N/A	FS GC-MS of EOM	Appendix E
43	NMI water extraction blank	N/A	N/A	N/A	Unknown	Unknown	N/A	N/A	FS GC-MS of EOM	Appendix F

*Top water – water sitting above the top surface of sediments recovered during retrieval of a core. The water is decanted from the core liner, taking care not to entrain core sediments. ** Peak definitions are provided in Appendix B together with all the raw chromatograms in Part B of the report. N/A = not applicable.

Table 10 Sediment samples selected for analysis.

SI	SAMPLE ID	STATION ID	LATITUDE	LONGITUDE	DATE (UTC)	TIME (UTC)	WATER DEPTH (M)	SAMPLING DEPTH	ANALYSES	RAW CHROMATOGRAMS
1	ASE BLK-1 (Associated system blank prepared during the extraction of sediments below)								Extraction of EOM, FS GC-MS of EOM	Appendix G
2	ASE BLK-2 (Associated system blank prepared during the extraction of sediments below)								As above	Appendix G
Multicore samples collected during the R/V Southern Surveyor (CSIRO) cruise										
3	W13/005093	1	-35.58211300	134.08178100	07-Apr-13	1:30 AM	2004	Lower 5 cm^	Cleaning, drying, extraction of EOM, FS GC-MS of EOM	Appendix G
4	W13/005172	2	-35.34126700	134.05247100	07-Apr-13	9:37 AM	1524	Lower 5 cm	As above	Appendix G
5	W13/005300	3	-35.33261800	132.68116700	08-Apr-13	12:22 AM	1494	Lower 5 cm	As above	Appendix G
6	W13/005373	4	-35.52098900	132.67397800	08-Apr-13	1:22 PM	1924	Lower 5 cm	As above	Appendix G
7	W13/005505	5	-35.04733400	131.06725500	10-Apr-13	2:41 AM	2006	Lower 5 cm	As above	Appendix G
8	W13/005587	6	-34.60372600	131.06839000	10-Apr-13	10:21 AM	1479	Lower 5 cm	As above	Appendix G
9	W13/005940	7	-34.55711300	130.70676800	12-Apr-13	5:11 AM	1482	Lower 5 cm	As above	Appendix G
10	W13/005884	8	-34.86084200	130.67433800	11-Apr-13	8:48 PM	2010	Lower 5 cm	As above	Appendix G
11	W13/006021	10	-34.07709400	130.24789900	12-Apr-13	1:00 PM	1544	Lower 5 cm	As above	Appendix G
12	W13/006107	11	-33.52790900	130.26694300	12-Apr-13	8:17 PM	1015	Lower 5 cm	As above	Appendix G
13	W13/006270	13	-33.33855300	130.26198300	13-Apr-13	4:06 AM	204	Lower 5 cm	As above	Appendix G
14	W13/006424	15	-33.43841100	130.68118300	13-Apr-13	5:05 PM	477	Lower 5 cm	As above	Appendix G
15	W13/006648	16	-33.71374100	130.66744700	14-Apr-13	10:50 AM	996	Lower 5 cm	As above	Appendix G
16	W13/007019	22	-34.81236700	132.67045300	16-Apr-13	3:36 AM	1015	Lower 5 cm	As above	Appendix G
17	W13/007265	24	-35.04043300	134.07694800	17-Apr-13	3:29 AM	375	Lower 5 cm	As above	Appendix G
18	W13/007114	25	-35.15205700	134.10157900	16-Apr-13	6:48 PM	980	Lower 5 cm	As above	Appendix G
19	ASE BLK-1 (Associated system blank prepared during the extraction of sediments below)									Appendix H
20	ASE BLK-2 (Associated system blank prepared during the extraction of sediments below)									Appendix H
Multicore samples collected during the M/V Southern Supporter (Fugro) cruise										
21	021A	GEG13-02	-34.52475367	130.7241706	Unknown	Unknown	1447	Top 5 cm	As above	Appendix H
22	111A	GEG13-03	-34.64875336	130.8796282	Unknown	Unknown	1529	Top 5 cm	As above	Appendix H
23	048A	GEG13-06	-34.37728165	130.5402318	Unknown	Unknown	1396	Top 5 cm	As above	Appendix H

24	075A	GEG13-07	-34.27649858	130.4151069	Unknown	Unknown	1437	Top 5 cm	As above	Appendix H
25	003A	GEG13-17	-33.35750406	128.4811621	Unknown	Unknown	373	Top 5 cm	As above	Appendix H
26	110A	GEG13-03	-34.64875336	130.8796282	Unknown	Unknown	1529	Lower 5 cm	As above	Appendix H
27	047A	GEG13-06	-34.37728165	130.5402318	Unknown	Unknown	1396	Lower 5 cm	As above	Appendix H
28	074A	GEG13-07	-34.27649858	130.4151069	Unknown	Unknown	1437	Lower 5 cm	As above	Appendix H
29	002A	GEG13-17	-33.35750406	128.4811621	Unknown	Unknown	373	Lower 5 cm	As above	Appendix H
Piston core samples collected during the M/V Southern Supporter (Fugro) cruise										
30	161A	GEG13-02	-34.52475367	130.7241706	Unknown	Unknown	1447	Lower 5 cm	As above	Appendix H
31	181A	GEG13-03	-34.64875336	130.8796282	Unknown	Unknown	1529	Lower 5 cm	As above	Appendix H
32	167A	GEG13-06	-34.37728165	130.5402318	Unknown	Unknown	1396	Lower 5 cm	As above	Appendix H
33	173A	GEG13-07	-34.27649858	130.4151069	Unknown	Unknown	1437	Lower 5 cm	As above	Appendix H
34	155A	GEG13-17	-33.35750406	128.4811621	Unknown	Unknown	373	Lower 5 cm	As above	Appendix H

^Lower 5 cm of core = bottom most 5 cm AFTER collection of lowest 3 cm for headspace gas. *Peak definitions are provided in Appendix B together with all the raw chromatograms in Part B of the report.

Table 11 Headspace gas samples selected for analysis.

SI	SAMPLE ID	STATION ID	LATITUDE	LONGITUDE	DATE (UTC)	TIME (UTC)	WATER DEPTH (M)	SAMPLING DEPTH	ANALYSES	**RAW CHROMATOGRAMS
Blanks and standards analysed together with the samples below										
1	Air (Blank)	N/A	N/A	N/A	N/A	N/A	N/A	N/A	Molecular composition, $\delta^{13}\text{C}$ of CH_4 and CO_2	Appendix I

2	Air (Blank)	N/A	N/A	N/A	N/A	N/A	N/A	N/A	As above	Appendix I
3	Air (Blank)	N/A	N/A	N/A	N/A	N/A	N/A	N/A	As above	Appendix I
4	BOC Standard	N/A	N/A	N/A	N/A	N/A	N/A	N/A	As above	Appendix I
5	BOC Standard	N/A	N/A	N/A	N/A	N/A	N/A	N/A	As above	Appendix I
Multicore samples collected during the R/V Southern Surveyor (CSIRO) cruise										
6	W13/005092	1	-35.58211300	134.08178100	07-Apr-13	1:30 AM	2004	Lowest 3 cm*	As above	Appendix I
7	W13/005504	5	-35.04733400	131.06725500	10-Apr-13	2:41 AM	2006	Lowest 3 cm	As above	Appendix I
8	W13/005762	9	-34.61932300	130.26630600	11-Apr-13	9:45 AM	2014	Lowest 3 cm	As above	Appendix I
9	W13/005883	8	-34.86084200	130.67433800	11-Apr-13	8:48 PM	2010	Lowest 3 cm	As above	Appendix I
10	W13/005939	7	-34.55711300	130.70676800	12-Apr-13	5:11 AM	1482	Lowest 3 cm	As above	Appendix I
11	W13/006020	10	-34.07709400	130.24789900	12-Apr-13	1:00 PM	1544	Lowest 3 cm	Not received / analysed	Appendix I
12	W13/006269	13	-33.33855300	130.26198300	13-Apr-13	4:06 AM	204	Lowest 3 cm	Molecular composition, $\delta^{13}\text{C}$ of CH_4 and CO_2	Appendix I
13	W13/006423	15	-33.43841100	130.68118300	13-Apr-13	5:05 PM	477	Lowest 3 cm	As above	Appendix I
14	W13/007028	22	-34.81236700	132.67045300	16-Apr-13	3:36 AM	1015	Lowest 3 cm	As above	Appendix I
15	W13/007121	25	-35.15205700	134.10157900	16-Apr-13	6:48 PM	980	Lowest 3 cm	As above	Appendix I
16	W13/007264	24	-35.04043300	134.07694800	17-Apr-13	3:29 AM	375	Lowest 3 cm	As above	Appendix I
Blanks and standards analysed together with the samples below										
17	Air (Blank)	N/A	N/A	N/A	N/A	N/A	N/A	N/A	As above	Appendix J
18	Air (Blank)	N/A	N/A	N/A	N/A	N/A	N/A	N/A	As above	Appendix J
19	Air (Blank)	N/A	N/A	N/A	N/A	N/A	N/A	N/A	As above	Appendix J
20	BOC Standard	N/A	N/A	N/A	N/A	N/A	N/A	N/A	As above	Appendix J
21	BOC Standard	N/A	N/A	N/A	N/A	N/A	N/A	N/A	As above	Appendix J
22	BOC Standard	N/A	N/A	N/A	N/A	N/A	N/A	N/A	As above	Appendix J
Multicore samples collected during the M/V Southern Supporter (Fugro) cruise										
23	001A	GEG13-17	-33.35750406	128.4811621	Unknown	Unknown	373	Lowest 3 cm	As above	Appendix J

24	019A	GEG13-02	-34.52475367	130.7241706	Unknown	Unknown	1447	Lowest 3 cm	As above	Appendix J
25	046A	GEG13-06	-34.37728165	130.5402318	Unknown	Unknown	1396	Lowest 3 cm	As above	Appendix J
26	073A	GEG13-07	-34.27649858	130.4151069	Unknown	Unknown	1437	Lowest 3 cm	As above	Appendix J
27	109A	GEG13-03	-34.64875336	130.8796282	Unknown	Unknown	1529	Lowest 3 cm	As above	Appendix J
Piston core samples collected during the M/V Southern Supporter (Fugro) cruise										
28	154A	GEG13-17	-33.35750406	128.4811621	Unknown	Unknown	373	Lowest 3 cm	As above	Appendix J
29	160A	GEG13-02	-34.52475367	130.7241706	Unknown	Unknown	1447	Lowest 3 cm	As above	Appendix J
30	166A	GEG13-06	-34.37728165	130.5402318	Unknown	Unknown	1396	Lowest 3 cm	Not received / analysed	Appendix J
31	172A	GEG13-07	-34.27649858	130.4151069	Unknown	Unknown	1437	Lowest 3 cm	As above	Appendix J
32	180A	GEG13-03	-34.64875336	130.8796282	Unknown	Unknown	1529	Lowest 3 cm	As above	Appendix J

*Lowest 3 cm of multicore/piston core – this was always the section collected for headspace gas analysis. **Raw gas analysis results are provided in Appendix K.

N/A = not applicable.

Geochemical Experimental procedures

Extraction of organic matter from water

The organic matter in water samples was extracted in the National Measurement Institute (NMI), Perth. In brief, 1 L of water sample was extracted three times with 30 mL of dichloromethane (DCM) and the combined extracts were concentrated to 0.5 mL. Then 8 μL of the composite internal standard solution (concentration 20 $\mu\text{g}/\text{mL}$ per deuterated compounds: naphthene-D8, acenaphthene-D10, phenanthrene-D10, chrysene-D12 and perylene-D12) was added to 400 μL of the sample extract. NMI did not preserve the associated system blanks prepared at the time of analysis, instead they provided a system blank extracted at a later date but using similar glassware and solvent (Appendix F, Part B of the Ahmed et al., 2014 report). The details of the extraction procedure are provided in “Appendix L: Protocol for the analysis of TPH/PAH in water” in Ahmed et al., 2014.

Quantitative analysis of PAH in the solvent extract of water

Concentrations of polycyclic aromatic hydrocarbons (PAHs) in the solvent extract of water samples were determined quantitatively in NMI by gas chromatography – mass spectrometry (GC-MS) using selected ion monitoring (SIM) data acquisitions. These procedures are also provided in “Appendix M: Standard Operating Procedure for the Determination of PAH” in Ahmed et al., 2014.

Extraction of GO net

The GO net sample was immersed in 200 mL of DCM in a 500 mL pre-cleaned glass beaker. The beaker was also baked at 400°C overnight prior to use to ensure complete removal of any pre-existing volatile hydrocarbons. Soluble organic matter in the GO net was extracted by ultrasonication for 10 min. The extract was transferred to a 250 mL round bottom flask (RBF) to which a solution of 30.13 μg benzene-D6, 33.69 μg toluene-D8, 30.52 μg naphthalene-D8 and 35.89 33.69 μg squalane in pentane was added. The extract was rotary evaporated to ≈ 1 mL and then cleaned by passing through a short silica column using DCM as the eluant to get it ready for subsequent gas chromatography – mass spectrometry (GC-MS) analyses. The GO net blank was extracted and prepared by following the same procedure.

Preparation of sediment samples

The jars containing the sediment samples were stored at -20 °C in a freezer. Prior to sub-sampling, the samples were thawed out. The semi-solid sediment was carefully placed on a piece of clean aluminium foil. A solvent cleaned stainless steel knife was used to cut out a rectangular shaped block of wet sediment (≈ 125 gm), which was then allowed to air dry overnight on a piece of clean aluminium foil in the fume cupboard. The sediment was then

crushed into a fine powder by gently grinding with mortar/pestle and preserved for extraction of organic matter.

Extraction of organic matter from sediment sample

The extractable organic matter (EOM) of sediment was extracted by using an Accelerated Solvent Extractor (Dionex ASE 300) at Macquarie University and DCM+Methanol (90:10) as the extraction solvent. A weighed amount of powdered sediment (≈ 40 g) was thoroughly mixed with a weighed amount of sand (≈ 60 g) (pre-cleaned thoroughly by baking at 400°C for 72 hours prior to use) in a glass bottle and then loaded into the stainless steel extraction cell. Both the top and bottom end of the cell were lined up with two pieces of circular-shaped pre-extracted filter paper before loading the sample. The cell ends were closed finger-tight and placed on the cell carousel. During analysis, the carousel rotated the sample cell into position for transfer to the oven chamber. The cell was then automatically sealed under pressure and subsequently filled with 30 mL of extraction solvent, heated and pressurized (preheat = 5 min, heat = 5 min). After the cell reached the set temperature (100°C), it was held in the oven at constant temperature and pressure (1500 psi), for 5 min static time. The analytes and solvent were filtered and collected in the vial, and the process was repeated twice. Once complete, the cell was returned to the carousel and the processes for the extraction of the next sample started. A system blank was run using the same procedure by using the same amount of sand but without any sediment. The extract was rotary evaporated to ≈ 1 mL in a RBF, and transferred to a 10 mL measuring cylinder. The RBF was rinsed and subsequent washings were added to the measuring cylinder. A $1/5^{\text{th}}$ aliquot of the extractable organic matter was blown to dryness to provide a gravimetric weight of the total EOM. Known amounts of deuterated standard mixture were added to the remaining $4/5^{\text{th}}$ which was then passed through a short column packed with silica, using DCM as the eluant to remove GC non-amenable prior to GC-MS analyses.

GC-MS analyses of extractable organic matter

Full scan GC-MS analyses of EOM from water, sediment and GO net samples plus relevant blanks were carried out using an Agilent 7890A gas chromatograph interfaced to a 5975 MSD (electron energy 70 eV). Chromatography was carried out on a DB-5MS fused silica column (60 m x 0.25 mm i.d. x 0.25 μm film thickness), using a splitless injection technique. The oven was programmed for an initial temperature 40°C for 2 min, followed by heating at $4^{\circ}\text{C min}^{-1}$ to 310°C .

Molecular composition of headspace gases

The samples for headspace gases were been prepared on board the vessel: sediment cores were placed into IsoPakTM bags, rolled to remove any excess air and sealed. The sealed bags were placed into a freezer at -80°C . Before analysis, the bags were kept in a fridge at 4°C overnight and then left on the bench for few hours to stabilize at room temperature. A gas

tight syringe was used to remove the headspace gas through the Isopak's integrated septum. The gas was then introduced into a sample loop (0.25 mL) at atmospheric pressure for GC analysis on an Agilent 6890N Natural Gas Analyser equipped with a thermal conductivity detector (TCD). Four packed columns with column switching were used to separate the gases, a 2 foot 12 % UCW982 on PAW 80/100 mesh (pre-column), a 15 foot 25% DC200 on Paw 80/100 mesh, a 10 foot HaysepQ 80/100 mesh and a 10 foot Molecular Sieve 13X 45/60 mesh column. The oven was isothermally maintained at 90°C throughout the 20 min run. The amounts of the separated gas components were determined against an external standard calibration. The molecular composition of gas samples was corrected to air-free values, assuming atmospheric ratios for the oxygen + argon / nitrogen peaks.

Isotopic composition of headspace gases

In order to avoid any possible isotopic fractionation once the septum on the IsoPak bags had been pierced, the gas samples were subject to carbon isotope analysis as soon as possible on the day that the septum was pierced. The carbon isotopic composition of gas was measured by GC-C-IRMS consisting of a GC unit (6890N, Agilent Technologies, USA) connected to a GC-C/TC III combustion device coupled via open split to a Delta V Plus mass spectrometer (ThermoFisher Scientific, Germany). The analytes of the GC effluent stream were oxidised to CO₂ in the combustion furnace held at 1000°C on a CuO/Ni/Pt catalyst. After on-line removal of water by a Nafion membrane, the CO₂ was transferred on-line to the mass spectrometer to determine carbon isotope ratios. For CH₄ and CO₂ 10 to 1000 µL of sample was injected into the split/splitless inlet system (Agilent Technologies, USA) working in split mode (20:1 ratio). The injector was held at a temperature of 200°C. The GC was held isothermally at 40°C and the gas components were separated on a fused silica capillary column (PoraPlot Q, 25 m x 0.32 mm ID, Varian). Helium was the carrier gas, set to a constant pressure of 14.5 psi.

Geochemical Results

Geochemistry of organic matter in water and related samples

The top and Niskin water samples included in this report (Table 12) were prepared, extracted (Ahmed et al., 2014 Part B: Appendix L) and then analysed for quantitative determination of PAHs in the NMI Laboratories using SIM data acquisition method (Ahmed et al., 2014: Appendix M). The EOM of these samples (Table 14) were also analysed in CSIRO Organic Geochemistry Laboratories using a full scan (m/z 50-550) data acquisition method to assess their overall qualitative composition and similarity/dissimilarity to natural petroleum hydrocarbons. Selected mass chromatograms showing the overall distribution of aliphatic and aromatic hydrocarbons in these EOMs are presented in Appendices C and D of Ahmed et al., 2014.

Quantitative analysis of PAHs in top and niskin waters

The quantitative data of PAHs in the solvent extracts of top and Niskin water samples are provided in Table 12 and Table 13, which show that the amounts of all PAHs, that were determined in this study, are below the levels of reporting (LOR = 0.01 µg/L) in almost all the samples except the methanol blank (W13/011079), and two recoveries (752WR01 and 743WR1). However, variable amounts of naphthalene (0.01-0.02 µg/L) could be detected in majority of the samples. Naphthalene, being a more volatile compound, is very likely to have been incorporated in these extracts cumulatively from solvents, glassware and/or from unknown source(s). However, the amounts of naphthalene in these extracts are very low (0.01 to 0.02 µg/L) with few exceptions and just above their LOR. It may be worthwhile to mention here that the level of detection (LOD) for this analysis method is 0.002 µg/L.

Qualitative investigation of extractable organic matter in top and niskin waters

Visual examination of the chromatograms (Appendices C and D) shows that most of the top and Niskin water samples (except Niskin water W13/005279 and top water W13/006087) do not contain any detectable amounts of petroleum hydrocarbons pointing to the absence of active hydrocarbon seepage in and around the sampling locations. Total ion chromatograms (TICs) of these samples are dominated by co-added internal standard compounds (i.e., 1,4-dichloromethane-D4, naphthalene-D8, acenaphthalene-D10, phenanthrene-D10, chrysene-D12 and perylene-D12) that were added to the extract by NMI, along with variable amounts of fatty acids which may be the remnants of microbial metabolism these water samples. High abundances of some <C₉ branched/cyclic compounds detected in most of these samples are very likely to be contaminants inherited from the system or solvents used during the isolation of these EOMs. Variable amounts of other contaminants such as phthalate and squalene could also be detected in some samples. It should be emphasized here that the relative amounts of these contaminants appear to be superficially high in the TICs due to scaling of the TIC. This fact can give the wrong impression regarding the relative abundances of contaminants compared to the other compounds detected. The majority of the EOM isolated from the top and Niskin water samples contains only trace amounts of C₂- and C₃-alkylbenzenes, naphthalene and methyl naphthalenes. However, all other aliphatic and aromatic hydrocarbons including *n*-alkanes, Pr and Ph are either very low or below detection limits suggesting that the trace amounts of alkylbenzenes and other compounds detected in these samples are possibly inherited cumulatively from solvents, glassware, etc. that were used for the extraction and preparation of these samples. The TIC of the EOM of Niskin water sample W13/005098 shown in Figure 61 demonstrate that petroleum hydrocarbons are either absent or present in very low abundances in waters from survey areas, suggesting the absence of any petroleum seepage in and around the sampling locations.

Table 12 Amount of hydrocarbons (µg compound/L water) detected in the top and Niskin water samples collected during Southern Surveyor Cruise 2013.

[illegible]

Table 13 Amount of hydrocarbons (µg compound/L water) detected in the top and Niskin water samples collected during Southern Surveyor Cruise 2013.

[illegible]

Note: W13/011079 is the methanol rinse received on 20/05/2013. 752WR01 and 743WR1 are recoveries

However, few samples, for example Niskin water W13/005279 (later identified as a top water) extract (Appendix D of Ahmed et al., 2014) and top water W13/006087 extract (Appendix C of Ahmed et al., 2014) show the presence of variable amounts of aliphatic and aromatic hydrocarbons (Figure 62). *n*-alkanes detected in the TICs (Figure 62) and other aliphatic and aromatic compounds in the relevant mass chromatograms indicate the presence of potential petroleum hydrocarbons in these two samples. In order to assess the geochemical characteristics of these petroleum hydrocarbons the relevant full scan GC-MS data were evaluated to gather maximum possible information from the preliminary analyses. For example, the *n*-alkane distributions of these two extracts are very similar (Figure 63 and Figure 64) and are characterised by nearly unimodal distribution of C₁₅ to C₃₆ *n*-alkanes with maxima at C₂₈. The overall distributions of aromatic hydrocarbons also indicate some similarity between the two samples (Figure 62). The aliphatic hydrocarbon parameters (Table 14) tentatively indicate their generation from fairly mature (CPI close to 1) source rocks deposited in anoxic to suboxic environments (Pr/Ph \approx 1 - 1.6, Table 14) (Didyk *et al.*, 1978; Tissot and Welte, 1984). Only a limited number of aromatic hydrocarbon parameters could be measured for Niskin water extract (W13/005279) due to very low amounts of oil present. However, the methylnaphthalene ratio (MNR) ratio (Table 15) of this sample indicate its generation at \approx 1.0 % VRE based on published calibration (Radke *et al.*, 1984). The top water extract (W13/006087) probably had more oil and therefore provided more aromatic hydrocarbon parameters (Table 15) which collectively indicate peak oil window maturity of \approx 0.8-1.0 % VRE for the source rocks based on published calibrations (Radke and Welte, 1983; Radke, 1988).

These preliminary analyses therefore tentatively indicate that these two water samples may contain some oil or oil-like substance that may have been generated from peak oil window mature source rocks deposited in anoxic to suboxic environment. The sharp decrease in the amounts of *n*-alkanes from C₂₈ to C₁₄ with decreasing carbon number and loss of low molecular weight hydrocarbons may have been caused by weathering (e.g. water washing and/or evaporative losses). However the distribution of hydrocarbons could also suggest a potential refined product.

The absolute amounts of oil present in these two waters are very low as indicated from their extremely low relative abundances compared to the amounts of standards and other compounds detected in the TICs (Figure 62). Due to the absence of any known oil seepage around the survey area, it is very likely that these trace amounts of hydrocarbons detected in the two waters are inherited from a contaminant oil of an unknown source.

TIC: 8 -78 min

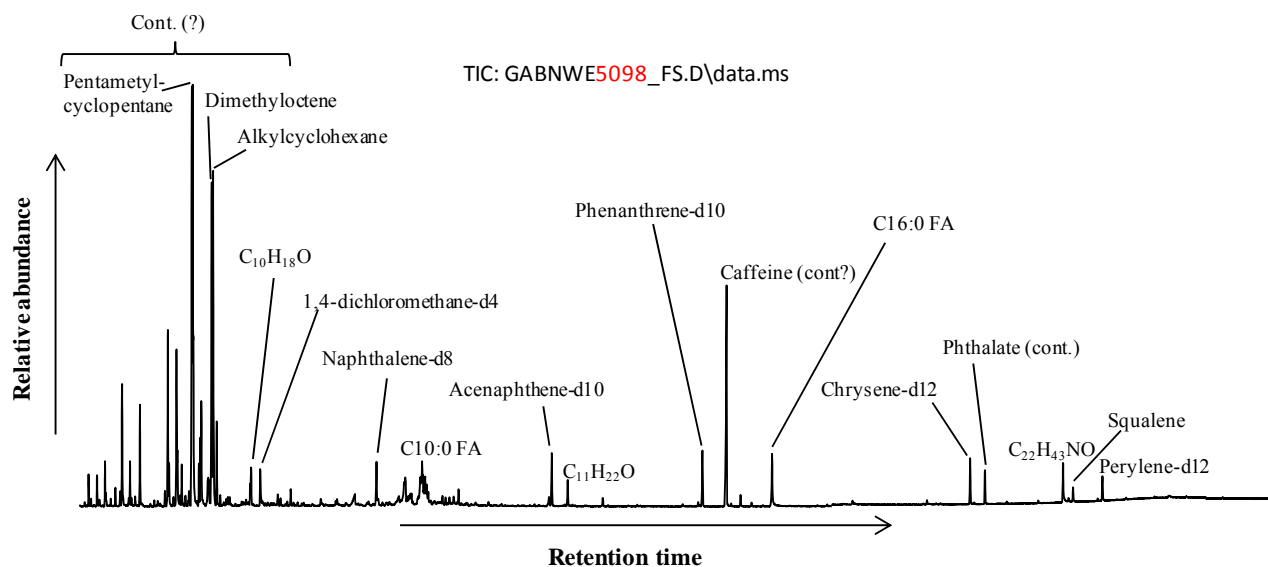


Figure 61 Total ion chromatogram showing the overall hydrocarbon distributions in the extractable organic matter of a Niskin water sample.

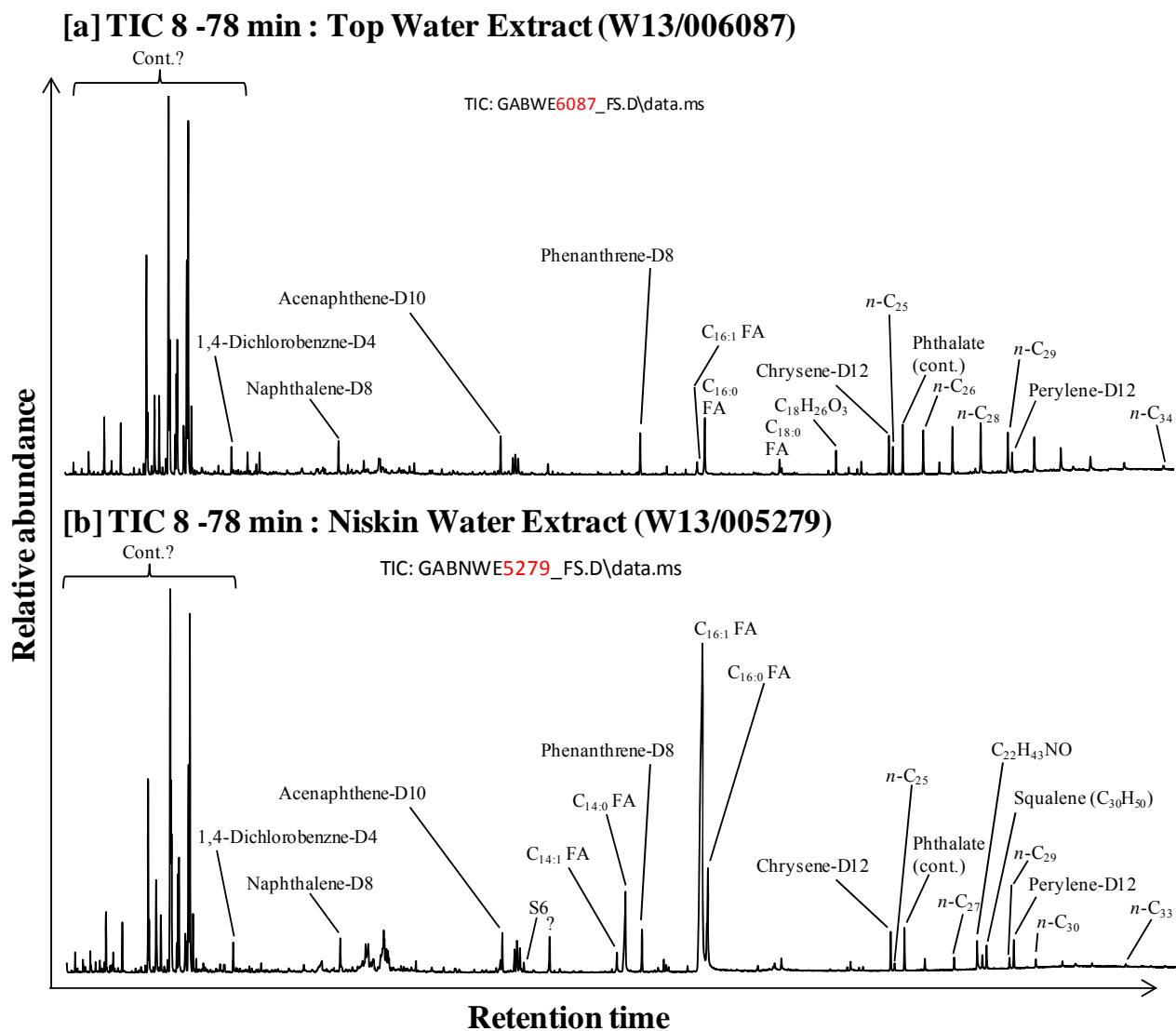


Figure 62 Total ion chromatograms showing the overall hydrocarbon distributions in the extractable organic matter of top and Niskin Water samples.

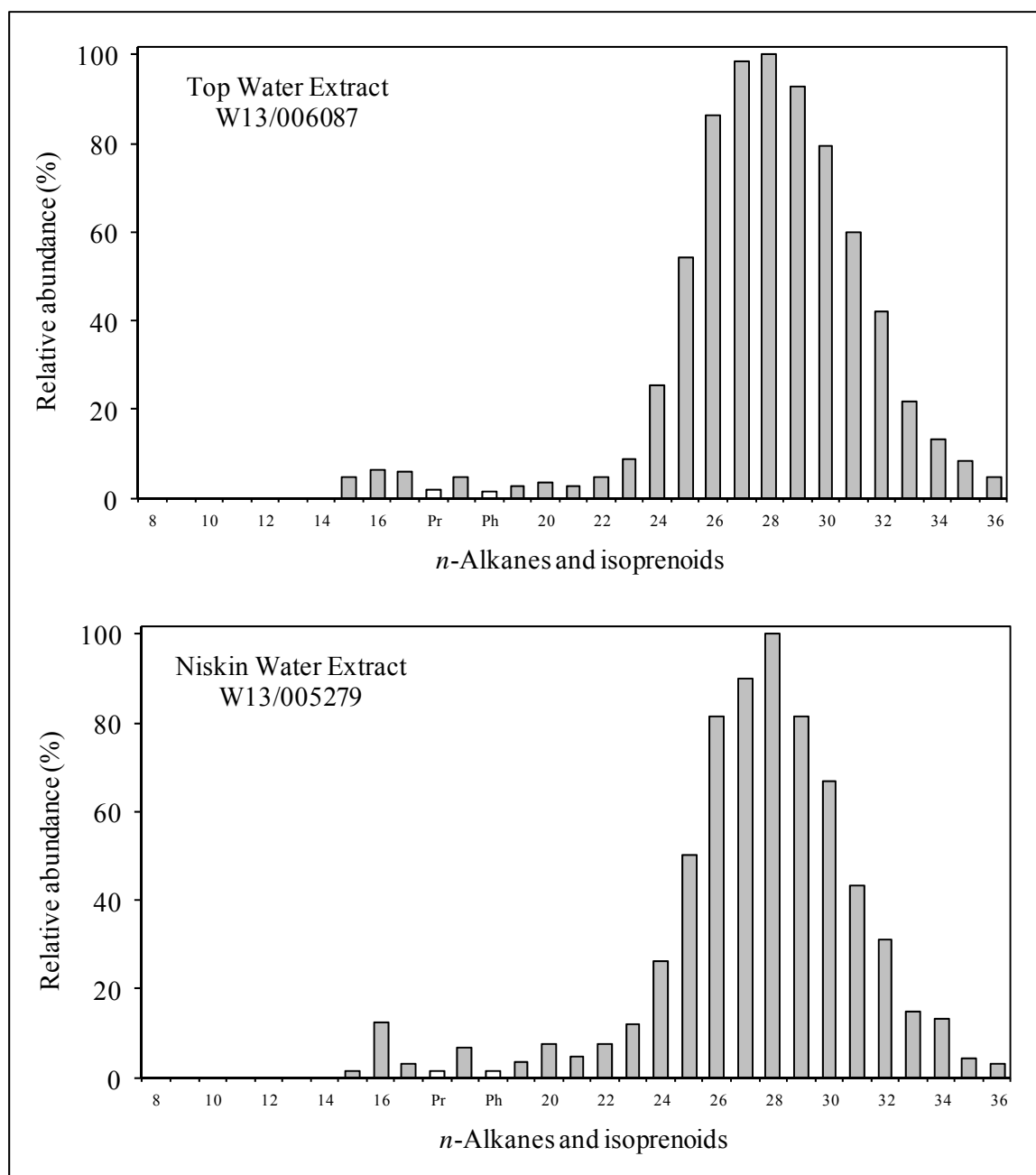


Figure 63 Histograms showing the distributions of *n*-alkanes and regular isoprenoids in the extractable organic matter of Top and Niskin water samples.

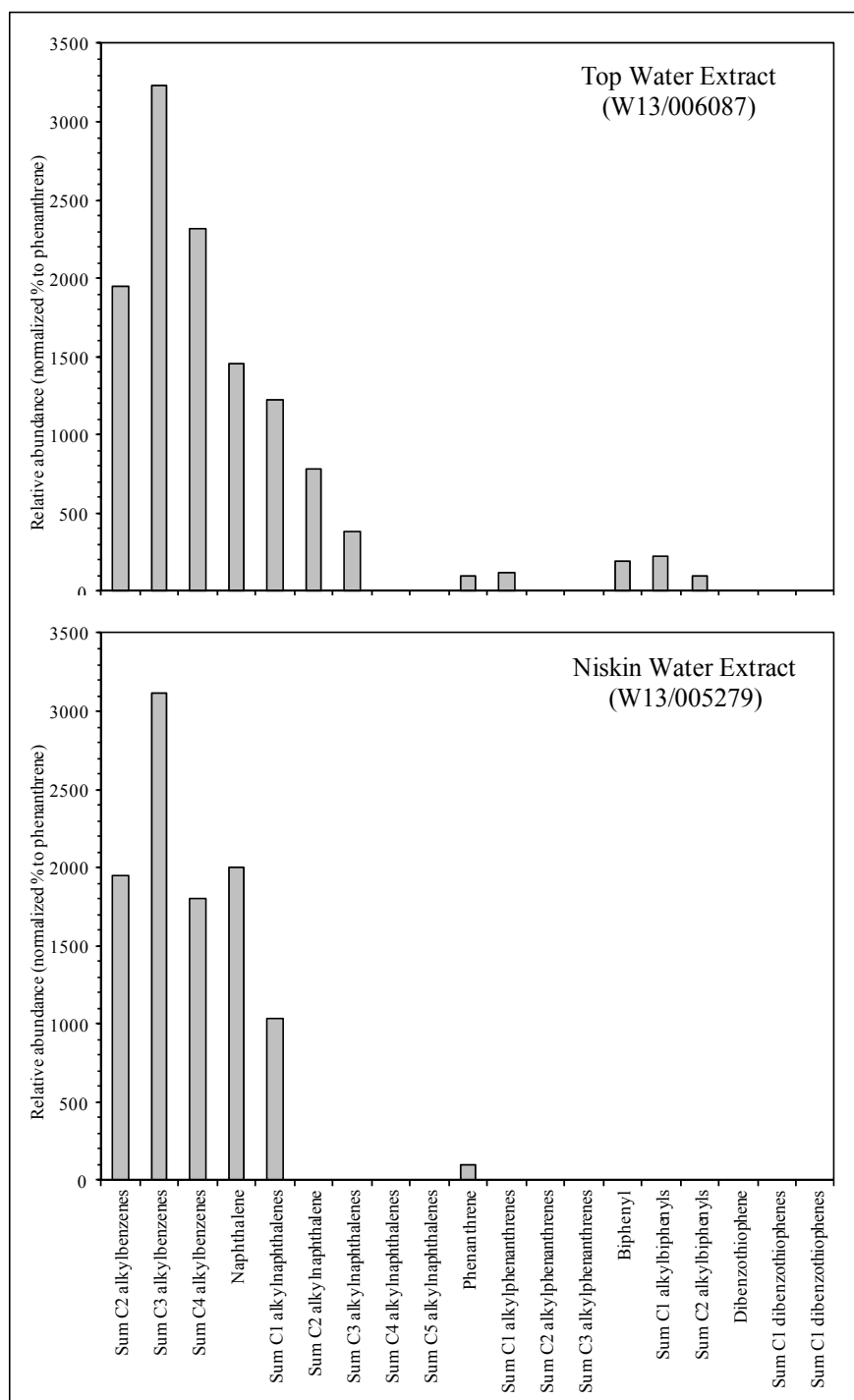


Figure 64 Distribution of alkylbenzenes, naphthalene, phenanthrene, biphenyl, dibenzothiophene and alkylated homologues in the extractable organic matter of top and Niskin water samples. Values calculated from the responses in the m/z 106, 120, 134, 128, 142, 156, 170, 184, 198, 178, 192, 206, 220, 154, 168, 182, 184, 198 and 212 mass chromatograms.

Table 14 Aliphatic hydrocarbon parameters of extractable organic matter isolated from the top and Niskin water samples collected during Southern Surveyor Cruise 2013.

Parameter	EOM of Top Water (W13/006087)	EOM of Niskin Water (W13/005279)
Pr/Ph	1.6	0.99
Pr/ <i>n</i> -C ₁₇	0.33	0.53
Ph/ <i>n</i> -C ₁₈	0.27	0.23
CPI ₂₂₋₃₂	1.00	0.94
CPI ₂₄₋₃₂	1.02	0.96
CPI ₂₆₋₃₂	1.03	0.96
CPI ₂₆₋₃₀	1.05	0.98
CPI ₂₆₋₂₈	1.06	0.99
CPI ₂₈₋₃₀	1.03	0.98
CPI ₂₀₋₂₂	0.66	0.62
<i>n</i> -C ₃₁ / <i>n</i> -C ₁₉	21	13
Wax index (<i>n</i> -C ₂₁₊₂₂ / <i>n</i> -C ₂₈₊₂₉)	0.04	0.07

Table 15 Aromatic hydrocarbon parameters of extractable organic matter isolated from the top and Niskin water samples collected during Southern Surveyor Cruise 2013.

Parameter	Top Water Extract (W 13/006087)	Niskin Water Extract (W 13/005279)
TMBI-1 (1,3,5-TMB/[1,3,5-TMB+1,2,3-TMB])	0.44	0.45
TMBI-2 (1,2,4-TMB/[1,2,4-TMB+1,2,3-TMB])	0.75	0.77
MEBI-1 (1M3EB+1M4EB)/(1M3EB+1M4EB+1M2EB)	0.75	0.75
TeMBI-x (1,2,3,5-TeMB/[1,2,3,5-TeMB+1,2,3,4-TeMB])	0.65	0.61
TeMBI-y (1,2,4,5-TeMB/[1,2,4,5-TeMB+1,2,3,4-TeMB])	0.54	0.55
Methylnaphthalene ratio (MNR: 2-MN/1-MN)	1.60	1.61
%Rc from MNR ((0.17*MNR)+0.82) from Radke et al. 1984	1.09	1.09
Naphthalene/ Σ Methylnaphthalenes	1.19	1.93
Ethylmethylphenanthrene ratio (ENR: 2-EN/1-EN)	2.6	n.d.
DNR-1 ([2,6-+2,7-DMN]/1,5-DMN)	3.2	n.d.
DNR-x ([2,6-+2,7-DMN]/1,6-DMN)	1.3	n.d.
DNR-y ([2,6-+2,7-DMN]/[2,6-+2,7-DMN+1,3+1,7-DMN])	0.48	n.d.
DNR-z (1,5-/[1,5-+1,2-DMN])	0.64	n.d.
TNR-1 (2,3,6-TMN/[1,4,6-+1,3,5-TMN])	0.65	n.d.
TNR-2 ([2,3,6-+1,3,7-TMN]/[1,4,6-+1,3,5-+1,3,6-TMN])	0.72	n.d.
TNRs ([1,3,7-+2,3,6-TMN]/1,3,6-TMN)	1.4	n.d.
TNR-x (1,2,5-TMN/[1,2,5-+1,2,4-+1,2,3-TMN])	0.56	n.d.
Log (1,2,5-TMN/1,3,6-TMN)	-0.35	n.d.
Log (1,2,7-TMN/1,3,7-TMN)	-0.50	n.d.
TMNr (1,3,7-TMN/[1,3,7-+1,2,5-TMN])	0.64	n.d.
1,3,6-TMN/1,3,7-TMN	1.3	n.d.
Methylphenanthrene index (MPI-1) =1.5*[3-MP+2-MP]/[P+9-MP+1-MP])	0.56	n.d.
Calculated vitrinite reflectance %Rc (MPI-1) =0.6*MPI-1+0.4 (for Ro <1.35), from Radke and Welte, 1984	0.74	n.d.
Methylphenanthrene distribution fraction (MPDF) =(3-MP+2-MP)/ Σ MPs)	0.42	n.d.
Log (1-MP/9-MP)	-0.18	n.d.
Methylphenanthrene ratio (MPR) = 2-MP/1-MP	0.85	n.d.
Calculated vitrinite reflectance %Rc (MPR) =0.99*log MPR+0.94, from Radke et al., 1984	0.87	n.d.
3-MBp/Bp	0.79	n.d.
3-MBp/4-MBp	3.0	n.d.

Extractable organic matter of Go net and Go net blank samples

Two GO nets, one containing a possible oil sample (although no oil was seen on the sea surface) and the other representing a blank (Table 9) were extracted with organic solvent in CSIRO Laboratories and the recovered extracts were then analysed by GC-MS using full scan data acquisition method. The EOM of the GO net sample exhibits hydrocarbon distributions very similar to those of a typical crude oil (Figure 65a). Hydrocarbon distribution patterns of the EOM isolated from the GO net blank (Figure 65b) are also largely similar to those of a crude oil, and exhibit significant similarities to those of the EOM of the GO net sample (Figure 65). However, the total hydrocarbon abundance in the GO net samples is much higher than that in the GO net blank which is evident from the recovery of 61 µg *n*-alkanes (C₁₂ to C₃₂) from the GO net sample compared to only 14 µg of those from the GO net blank (Table 16).

The aliphatic hydrocarbon parameters (Table 16) provide conflicting information, e.g., Pr/Ph ratio of the GO net sample is 0.79 indicating strongly anoxic depositional condition for the source rocks whereas this value is 1.7 for the GO net blank, which points to anoxic to suboxic palaeo-depositional conditions (Didyk, 1978). Similarly, there are some variations in CPI₂₀₋₂₂, wax index and fractionation index for these two samples which may have been caused by secondary alteration processes such as evaporation and/or weathering effects. This is supported by notable differences observed in the LMW *n*-alkane and aromatic hydrocarbon distributions of the GO net sample and GO net blank (Figure 66 and Figure 67 respectively). However, the majority of the other aliphatic hydrocarbon parameters (Table 16) and most of the aromatic hydrocarbon parameters (Table 17) of the GO net sample and GO net blank are almost identical, supporting the assertion that the hydrocarbons in the EOM from these two samples may have the same, or very similar, origins. The remarkable similarities in the distributions of aliphatic and aromatic hydrocarbons in the GO net and GO net blank provide unequivocal indication of their origin from the same or very similar source but not from any natural seepage.

The presence of hydrocarbons in both the blank illustrates some of the operational difficulties of working onboard vessels at sea where conditions are far from ideal to reliably collect samples. Due to the presence of contamination in the blank GO net and its close match to that of the GO net sample this GO net sample result is classed as unreliable.

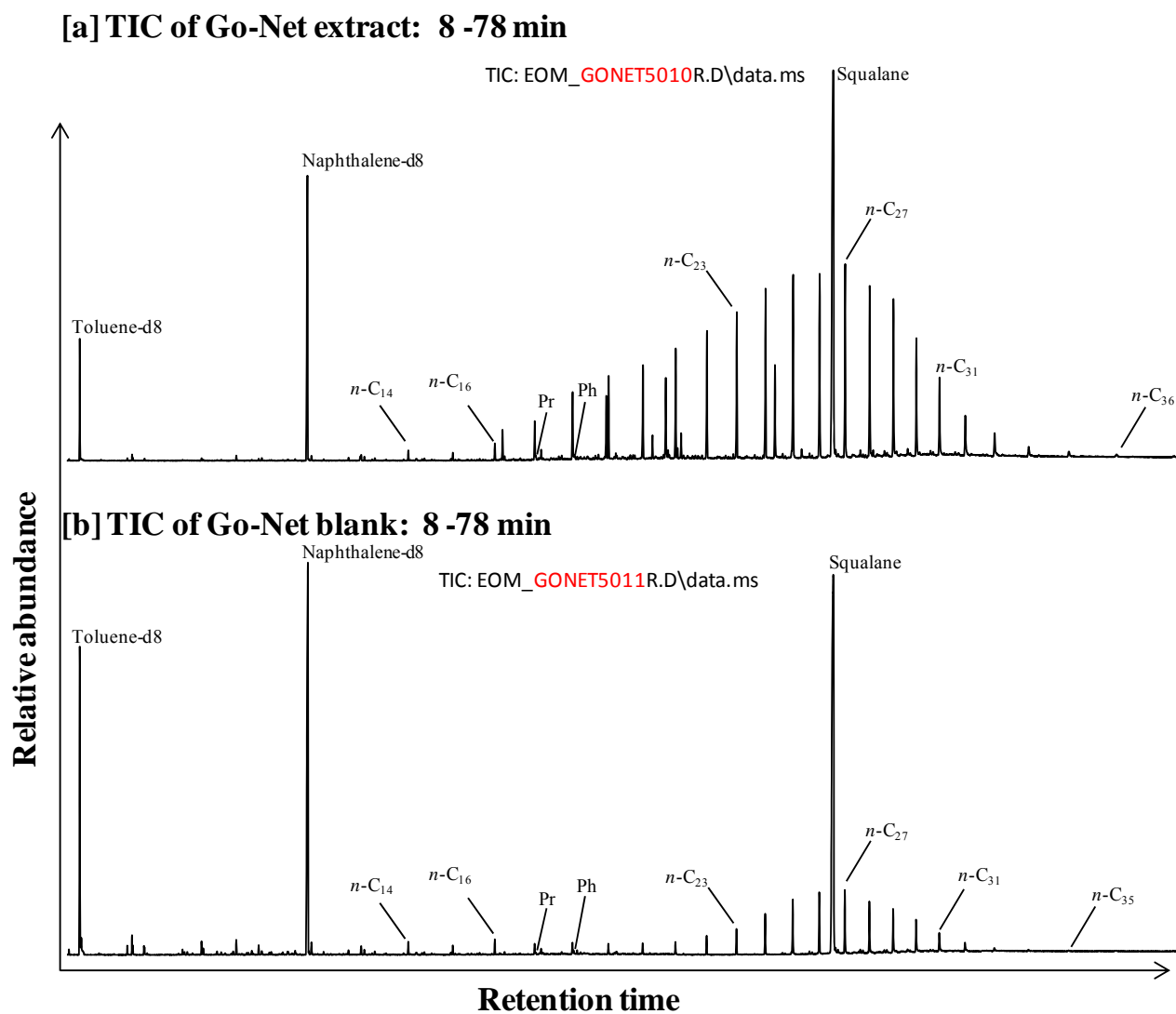


Figure 65 Total ion chromatograms showing overall hydrocarbon distributions in extractable organic matter of the GO net and GO net blank samples.

Table 16 Aliphatic hydrocarbon parameters of GO net and GO net blank samples.

Parameter	GO-NET Sample Extract	GO-NET Blank Extract
Pr/Ph	0.79	1.7
Pr/ <i>n</i> -C ₁₇	0.10	0.21
Ph/ <i>n</i> -C ₁₈	0.07	0.11
CPI ₂₂₋₃₂	1.07	1.04
CPI ₂₄₋₃₂	1.08	1.06
CPI ₂₆₋₃₂	1.09	1.04
CPI ₂₆₋₃₀	1.10	1.05
CPI 2 ₂₆₋₂₈	1.10	1.05
CPI 2 ₂₈₋₃₀	1.09	1.05
CPI 2 ₂₀₋₂₂	1.00	0.78
<i>n</i> -C ₃₁ / <i>n</i> -C ₁₉	0.96	2.3
Wax index (<i>n</i> -C ₂₁₊₂₂ / <i>n</i> -C ₂₈₊₂₉)	0.78	0.30
Fractionation index (<i>n</i> -C ₁₀ / <i>n</i> -C ₁₆₊₂₅)	0.004	0.071
Sum of C ₁₂ to C ₃₂ <i>n</i> -alkanes (µg)	61	14

Table 17 Aromatic hydrocarbon parameters of GO net and GO net blank samples.

Parameter	GO-NET Sample Extract	GO-NET Blank Extract
TMBI-1 (1,3,5-TMB/[1,3,5-TMB+1,2,3-TMB])	0.41	0.44
TMBI-2 (1,2,4-TMB/[1,2,4-TMB+1,2,3-TMB])	0.78	0.80
MEBI-1 (1M3EB+1M4EB)/(1M3EB+1M4EB+1M2EB)	0.82	0.82
TeMBI-x (1,2,3,5-TeMB/[1,2,3,5-TeMB+1,2,3,4-TeMB])	0.64	0.67
TeMBI-y (1,2,4,5-TeMB/[1,2,4,5-TeMB+1,2,3,4-TeMB])	0.60	0.64
Methylnaphthalene ratio (MNR: 2-MN/1-MN)	3.0	3.0
Naphthalene/ Σ Methylnaphthalenes	0.37	0.58
Ethylnaphthalene ratio (ENR: 2-EN/1-EN)	7.7	6.7
DNR-1 ([2,6-+2,7-DMN]/1,5-DMN)	14	16
DNR-x ([2,6-+2,7-DMN]/1,6-DMN)	1.7	1.8
DNR-y ([2,6-+2,7-DMN]/[2,6-+2,7-DMN+1,3+1,7-DMN])	0.65	0.67
DNR-z (1,5-/[1,5-+1,2-DMN])	0.47	0.46
TNR-1 (2,3,6-TMN/[1,4,6-+1,3,5-TMN])	1.9	1.9
TNR-2 ([2,3,6-+1,3,7-TMN]/[1,4,6-+1,3,5-+1,3,6-TMN])	1.1	1.2
TNRs ([1,3,7-+2,3,6-TMN]/1,3,6-TMN)	1.8	1.9
TNR-x (1,2,5-TMN/[1,2,5-+1,2,4-+1,2,3-TMN])	0.71	0.74
Log (1,2,5-TMN/1,3,6-TMN)	-0.50	-0.49
Log (1,2,7-TMN/1,3,7-TMN)	-0.37	-0.44
TeMNR-1 (2,3,6,7-TeMN/1,2,3,6-TeMN)	1.5	1.5
(1,2,5,6+1,2,3,5-TeMN)/1,2,3,6-TeMN	1.9	1.8
TMNr (1,3,7-TMN/[1,3,7-+1,2,5-TMN])	0.70	0.72
TeMNR (1,3,6,7-TeMN/[1,3,6,7+1,2,5,6-TeMN])	0.72	0.74
1,3,6-TMN/1,3,7-TMN	1.3	1.2
Methylphenanthrene index (MPI-1) = $1.5 \times [3\text{-MP} + 2\text{-MP}] / [P + 9\text{-MP} + 1\text{-MP}]$	0.74	0.87
Calculated vitrinite reflectance %Rc (MPI-1) = $0.6 \times \text{MPI-1} + 0.4$ (for Ro < 1.35), from Radke and Welte, 1988	0.85	0.92
Methylphenanthrene distribution fraction (MPDF) = $(3\text{-MP} + 2\text{-MP}) / \Sigma \text{MPs}$	0.69	0.69
Log (1-MP/9-MP)	0.01	-0.03
Methylphenanthrene ratio (MPR) = 2-MP/1-MP	2.5	2.7
Calculated vitrinite reflectance %Rc (MPR) = $0.99 \times \log \text{MPR} + 0.94$, from Radke et al., 1984	1.3	1.4
Dimethylphenanthrene ratio (DPR) = $(3,5\text{-} + 2,6\text{-DMP} + 2,7\text{-DMP}) / (1,3\text{-} + 3,9\text{-} + 2,10\text{-} + 3,10\text{-DMP} + 1,6\text{-DMP})$	0.70	0.76
Log (1,7-DMP/1,3-+3,9-+2,10-+3,10-DMP)	0.08	-0.37
DPR-x (1,7-DMP/1,7-+1,3-+3,9-+2,10-+3,10-DMP)	0.55	0.30
Fluoranthene/(fluoranthene + pyrene)	0.69	0.65
3-MBp/Bp	1.04	0.99
3-MBp/4-MBp	1.9	1.8
Dibenzothiophene/phenanthrene	0.04	0.04
Methyldibenzothiophene ratio (MDR) = 4-MDBT/1-MDBT	3.0	3.0
Calculated vitrinite reflectance %Rc (MDR) = $0.073 \times \text{MDR} + 0.51$, from Radke, 1988	0.73	0.73
Dimethyldibenzothiophene Ratio (DMDR) = $4,6\text{-DMDBT} / 3,6\text{-} + 2,6\text{-DMDBT}$	0.19	0.22
Dibenzothiophene/1,3,6,7-TeMN	0.82	0.63
Dibenzothiophene/1,2,5,6-+1,2,3,5-TeMN	2.1	1.8

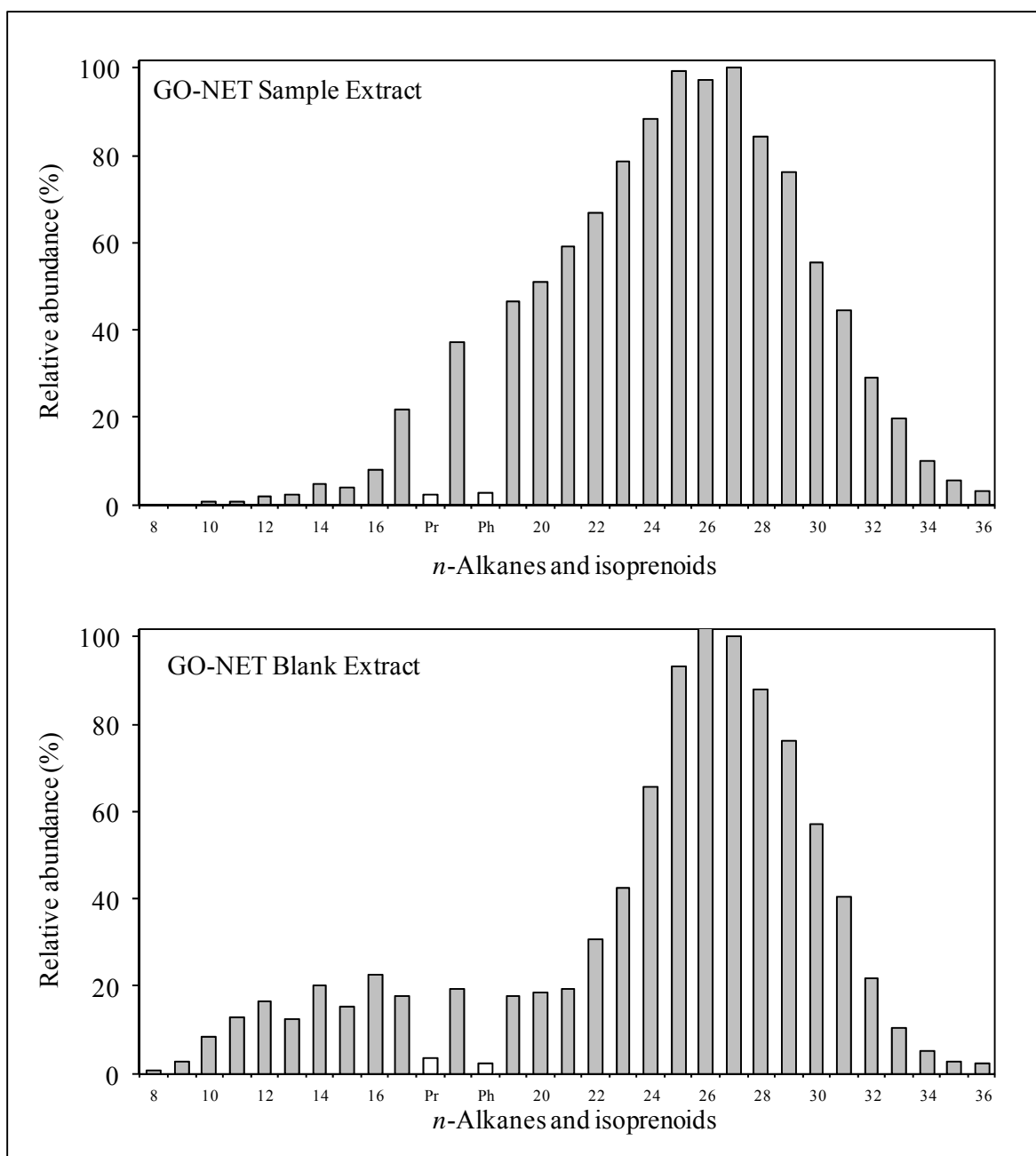


Figure 66 Histograms showing the distributions of *n*-alkanes and regular isoprenoids in the extractable organic matter of the GO net and GO net blank samples.

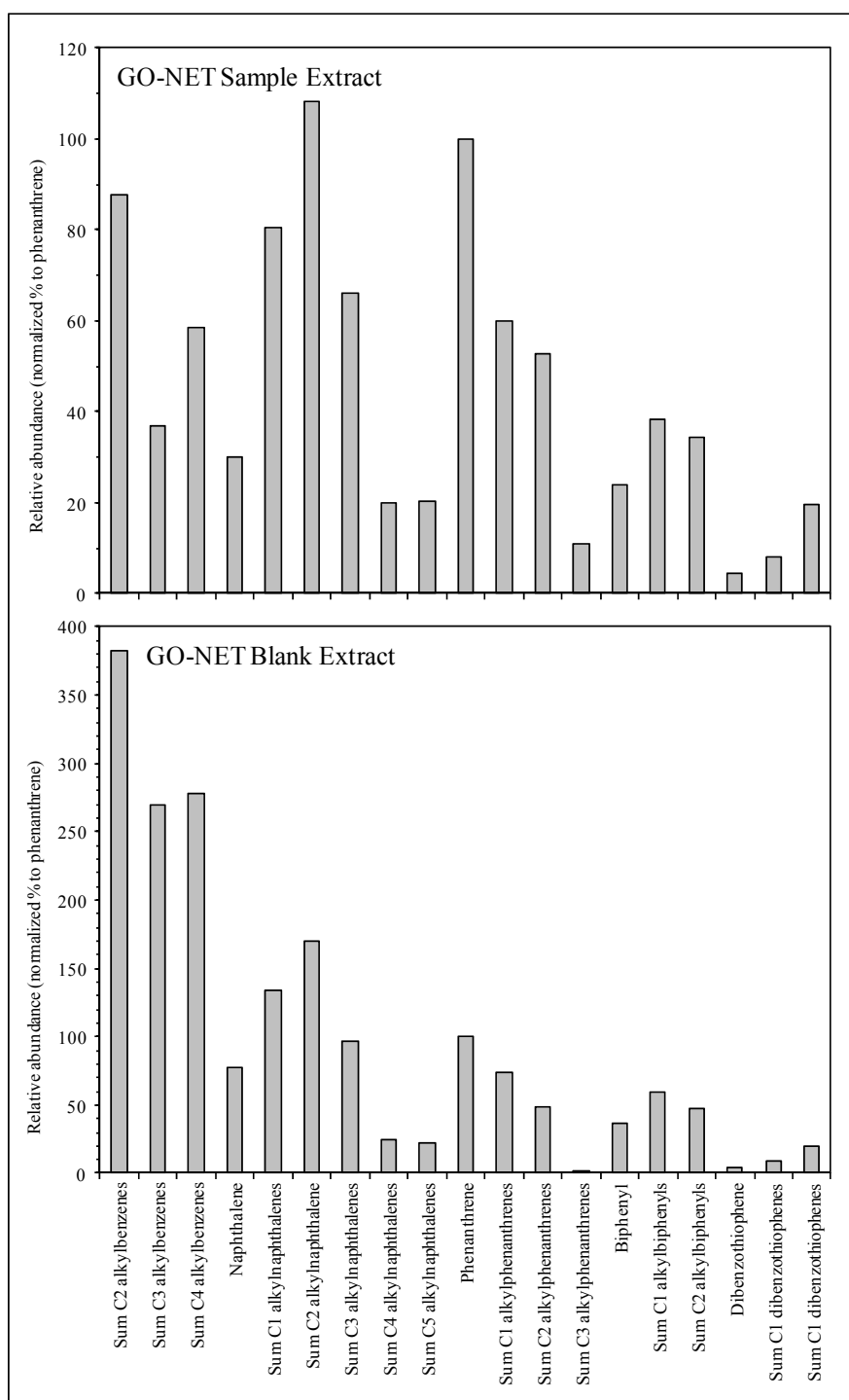


Figure 67 Distribution of alkylbenzenes, naphthalene, phenanthrene, biphenyl, dibenzothiophene and alkylated homologues in the GO net and GO net blank samples scaled to show all hydrocarbons. Values calculated from the responses in the *m/z* 106, 120, 134, 128, 142, 156, 170, 184, 198, 178, 192, 206, 220, 154, 168, 182, 184, 198 and 212 mass chromatograms.

Extractable organic matter of other samples

The EOM of transit waters collected from the pump, Milli-Q water blanks and a methanol blank (Table 9) have variable amounts of C₂-, C₃- and C₄-alkylbenzenes, naphthalene, methylnaphthalenes and in some cases also some C₂-alkylnaphthalenes and *n*-alkanes. These are probably cumulative contaminants from the solvent and materials that were used for the collection, extraction and/or preparation of the EOM. The methanol blank, however, appeared to be absent of contaminant compounds.

Geochemistry of organic matter in seabed sediments

The seabed sediment samples selected for organic geochemical analyses, and the associated systems blanks prepared during the extraction of EOM, are listed in Table 10. The samples were prepared at the CSIRO North Ryde Laboratories as demonstrated diagrammatically in Figure 68 and extracted by Dionex Accelerated Solvent Extractor (Dionex ASE 300) at Macquarie University, Sydney as described above. Solvent extraction data (Table 18) indicate that the sediment samples analysed in this report have widely variable extraction yields, i.e., from as low as ≈2 mg EOM/kg of sediment to as high as ≈3200 mg EOM/kg of sediment, with one sample not yielding any detectable amount of EOM. Despite the recovery of very high amounts of EOM for some of the sediment samples, TICs of the full scan GC-MS analyses of the total EOM of all the samples do not show the presence of any detectable amounts of geochemically significant aliphatic and aromatic hydrocarbons (see Figure 69). Few compounds (possibly contaminants) detected in these chromatograms are also present in the associated ASE system blanks prepared using the same glassware, solvent and other materials, but excluding the sediment sample. This indicates that the sediment samples analysed in this report, despite containing ≈0.100-129 mg of total EOM (Table 18), do not contain any detectable amount of geochemically significant petroleum hydrocarbons. It is very likely that the EOM of these samples is composed primarily of lipids and/or functionalised hydrocarbons produced by recent organic matter. However, one or two samples contain trace amounts of C₂₇ to C₃₀ *n*-alkanes (e.g., W13/005093, Figure 69) with odd over even predominance. The presence of these higher plant lipids (Tissot and Welte, 1984) supports the notion that the EOM of these sediments are mainly composed of lipids of recent organic matter. The lack of detectable quantities of petroleum hydrocarbons in seabed sediments around the GAB survey areas suggests the absence of active petroleum seepage in and around the sampling region.

Table 18 Extraction yields of selected sediment samples.

Sediment Sample ID	Wet sediment (gm)	Dry sediment (gm)	Water content (% of dry sediment, w/w)	Sediment extracted (gm)	Total EOM (mg)	Extract yield mg EOM /kg of sediment (ppm, w/w)
Samples collected during R/V Southern Surveyor (CSIRO) cruise						
W13/005093	141.81	90.16	57.29	39.82	10.00	251
W13/005172	117.72	72.90	61.48	39.60	17.15	433
W13/005300	128.65	75.82	69.68	38.50	26.35	684
W13/005373	157.51	93.92	67.71	41.80	32.55	779
W13/005505	124.94	77.64	60.92	37.10	72.50	1954
W13/005587	134.22	82.46	62.77	38.50	25.10	652
W13/005940	149.87	91.62	63.58	36.40	30.35	834
W13/005884	142.34	86.83	63.93	38.21	47.40	1241
W13/006021	143.47	88.32	62.44	40.64	23.50	578
W13/006107	143.15	89.63	59.71	39.90	19.75	495
W13/006270	121.70	80.08	51.97	39.80	18.45	464
W13/006424	140.29	91.11	53.98	38.57	51.45	1334
W13/006648	102.83	62.72	63.95	37.51	26.65	710
W13/007019	141.35	93.13	51.78	41.70	103.50	2482
W13/007265	119.67	74.53	60.57	37.87	71.45	1887
W13/007114	145.96	90.78	60.78	40.00	17.00	425
Samples collected during R/V Southern Supporter (Fugro) cruise						
021A	137.89	87.59	57.43	40.08	0.10	2
111A	163.14	111.43	46.41	40.35	0.20	5
048A	132.31	81.25	62.84	39.45	25.20	639
075A	118.15	73.75	60.20	40.04	6.40	160
003A	173.04	109.64	57.83	40.06	2.90	72
110A	171.64	123.16	39.36	39.91	nill	nill
047A	98.88	60.56	63.28	40.79	27.50	674
074A	95.21	58.17	63.68	40.01	32.00	800
002A	108.76	63.83	70.39	40.78	80.20	1967
161A	109.87	67.15	63.62	40.70	34.70	853
181A	112.72	69.43	62.35	42.05	72.70	1729
167A	101.78	67.48	50.83	40.02	0.40	10
173A	75.17	49.03	53.31	40.99	6.40	156
155A	77.62	49.68	56.24	40.75	128.90	3163

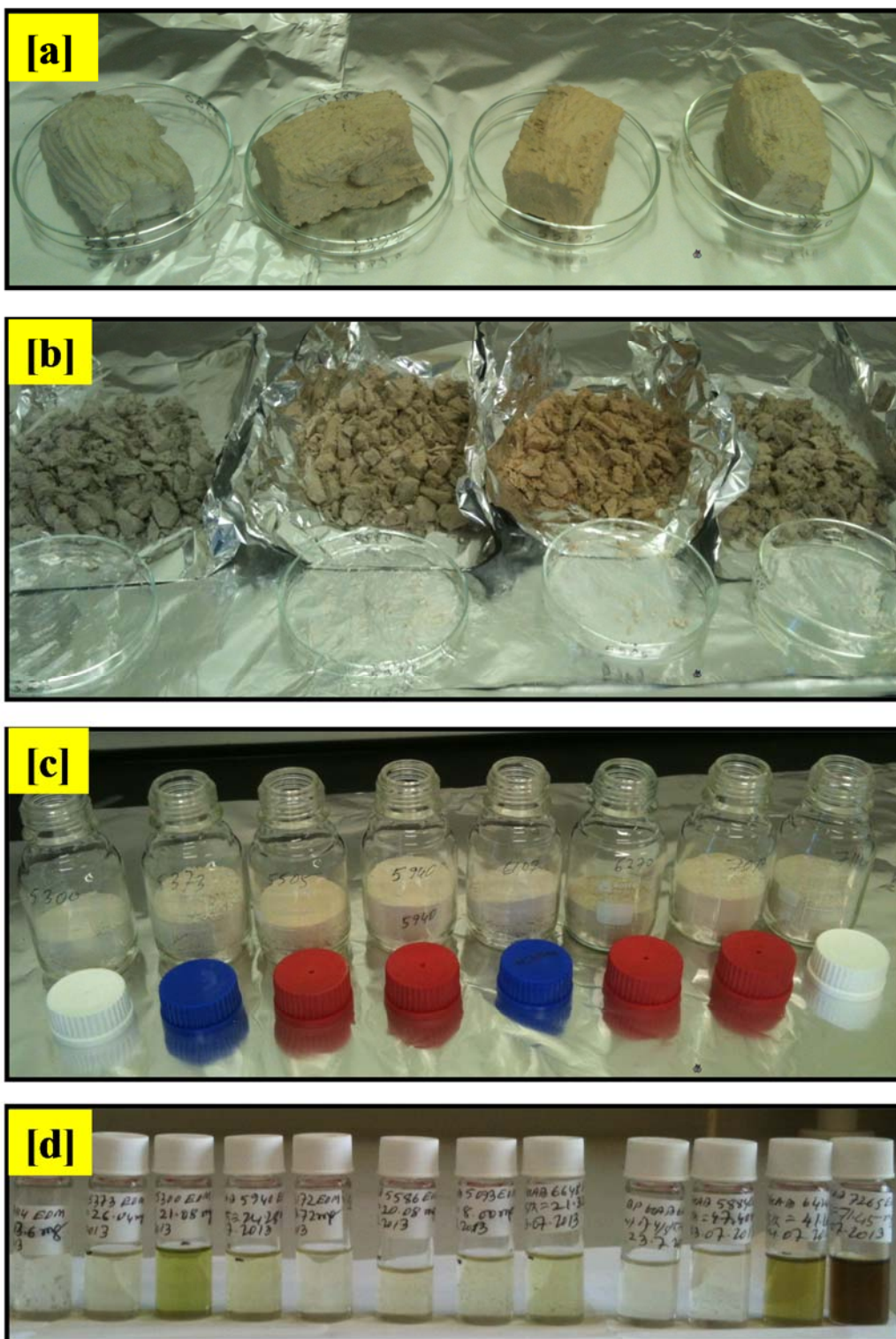


Figure 68 Stages of sediment sample preparation for solvent extraction of organic matter: (a) A rectangular shaped core was cut out and then placed onto clean glass Petri dishes, (b) core was cut into smaller pieces on a piece of clean aluminium foil, (c) air dried core was crushed into powder and preserved in Pyrex glass bottles and (d) solvent extracts ready for GC-MSD analyses.

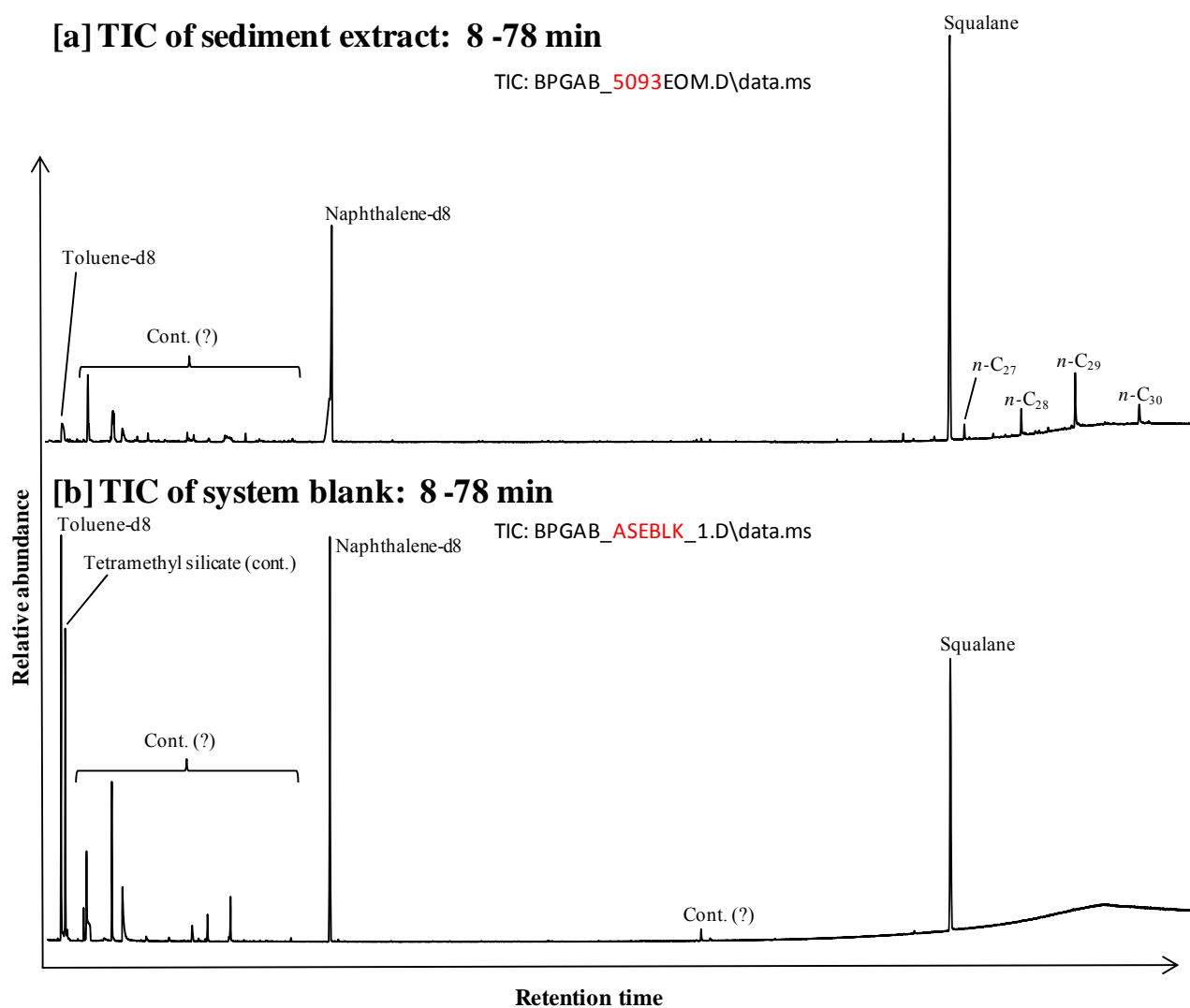


Figure 69 Total ion chromatograms of (a) extractable organic matter of a sediment sample collected during Southern Surveyor cruise and (b) associated Accelerated Solvent Extractor system blank showing overall hydrocarbon distributions.

Geochemistry of headspace gases

Selected headspace gas samples collected during the 2013 Surveys across the GAB have been analysed for molecular (Table 19) and carbon isotopic (Table 20) composition. A number of air blanks and BOC Standard gases (Table 19) were also analysed for comparison and calibration purposes. Raw gas chromatograms showing the molecular distributions are presented in Appendices I and J in Ahmed et al., 2014, whilst detailed results of molecular and isotopic compositions including those of blanks and standards are provided in Appendix K of Ahmed et al., 2014. Three sample bags, W13/006020, W13/006423, and 180, were found as flat indicating they did not contain any hydrocarbon or non-hydrocarbon gases and therefore were excluded from further analyses (Table 19). The other headspace gas samples were found to contain ≈ 1 to 50 % CO₂. Petroleum hydrocarbon gases, e.g., methane, ethane, etc. could not be detected in any of these samples, indicating hydrocarbons are either absent or below detection limits in these samples. The $\delta^{13}\text{C}$ values of CO₂ (duplicate measurements, Table 20) in two multicore headspace samples collected during the R/V Southern Surveyor (CSIRO) cruise range between -8.4 to -5.7 ‰ pointing to their possible origin from inorganic sources, i.e., igneous and/or mantle sources (Faiz *et al.*, 2007). CO₂ gases retrieved from two other multicore samples collected during the M/V Southern Supporter (Fugro) cruise are much lighter with $\delta^{13}\text{C}$ values ranging between -12.6 to -17.0 ‰; which are much lighter than the gases of magmatic origin (i.e., -5 to -10 ‰) and heavier than those generated by microbial oxidation of hydrocarbons and recent organic matter (i.e., -25 ± 5 ‰) (Faiz et al. (2007) suggesting that the CO₂ of these two headspace gases possibly originated from mixed magmatic and recent organic matter sources.

Table 19 Molecular composition of selected headspace gases expressed in normalized percent (based on air free calculation)

Sample ID	CO ₂	Methane	Ethane	Propane	iso-Butane	n-Butane	neo-Pentane	iso-Pentane	n-Pentane	C ₆₊	O ₂ + Ar	Nitrogen
Multicore samples collected during R/V Southern Surveyor (CSIRO) cruise												
W13/005092	6.39	0.0	0.0	0.0	0.0	0.0	0.0	0.0	0.0	0.0	0.0	93.61
W13/005504	1.07	0.0	0.0	0.0	0.0	0.0	0.0	0.0	0.0	0.0	0.0	98.93
W13/005762	1.96	0.0	0.0	0.0	0.0	0.0	0.0	0.0	0.0	0.0	0.0	98.04
W13/005883	12.34	0.0	0.0	0.0	0.0	0.0	0.0	0.0	0.0	0.0	0.0	87.66
W13/005939	50.13	0.0	0.0	0.0	0.0	0.0	0.0	0.0	0.0	0.0	0.0	49.87
W13/006020	Empty sample bag											
W13/006269	32.64	0.0	0.0	0.0	0.0	0.0	0.0	0.0	0.0	0.0	0.0	67.36
W13/006423	Empty sample bag											
W13/007028	0.62	0.0	0.0	0.0	0.0	0.0	0.0	0.0	0.0	0.0	0.0	99.38
W13/007121	0.61	0.0	0.0	0.0	0.0	0.0	0.0	0.0	0.0	0.0	0.0	99.39
W13/007264	1.07	0.0	0.0	0.0	0.0	0.0	0.0	0.0	0.0	0.0	0.0	98.93
Multicore samples collected during R/V Southern Supporter (Fugro) cruise												
001 A	4.10	0.0	0.0	0.0	0.0	0.0	0.0	0.0	0.0	0.0	0.0	95.90
019 A	11.27	0.0	0.0	0.0	0.0	0.0	0.0	0.0	0.0	0.0	0.0	88.73
046 A	5.04	0.0	0.0	0.0	0.0	0.0	0.0	0.0	0.0	0.0	0.0	94.96
073 A	1.65	0.0	0.0	0.0	0.0	0.0	0.0	0.0	0.0	0.0	0.0	98.35
109 A	19.35	0.0	0.0	0.0	0.0	0.0	0.0	0.0	0.0	0.0	0.0	80.65
Piston core samples collected during R/V Southern Supporter (Fugro) cruise												
154 A	3.45	0.0	0.0	0.0	0.0	0.0	0.0	0.0	0.0	0.0	0.0	96.55
160 A	3.51	0.0	0.0	0.0	0.0	0.0	0.0	0.0	0.0	0.0	0.0	96.49
166 A	3.55	0.0	0.0	0.0	0.0	0.0	0.0	0.0	0.0	0.0	0.0	96.45
172 A	1.83	0.0	0.0	0.0	0.0	0.0	0.0	0.0	0.0	0.0	0.0	98.17
180 A	Empty sample bag											

Table 20 Stable carbon isotopic composition of selected headspace gases.

Sample ID	$\delta^{13}\text{CO}_2$ (‰ VPDB)
Multicore samples: R/V Southern Surveyor (CSIRO) cruise	
W13/005883	-8.4
	-7.6
W13/005939	-5.7
	-5.7
Multicore samples: R/V Southern Supporter (Fugro) cruise	
019 A	-12.6
	-12.6
109 A	-17.0
	-16.9

Geochemical analysis conclusions

- The quantitative analysis of solvent extracts isolated from seawater samples indicate that polycyclic aromatic hydrocarbons (PAHs) are largely absent in/around the BP permits in the Great Australian Bight, Australia. Smaller amount of naphthalene, a highly volatile bicyclic aromatic hydrocarbon, detected in majority of the samples is probably a contaminant cumulatively inherited from solvents, glassware and/or unknown source(s).
- The qualitative organic geochemical analyses of extractable organic matter isolated from seawater, seabed sediment, and GO net samples, and headspace gases extracted from multicore/piston core samples collected from the Great Australian Bight region indicate that petroleum hydrocarbons are either absent or below the limits of detection pointing to an absence of active hydrocarbon seepage in and around the sampling region.
- Two top water samples contain low to moderate amounts of petroleum hydrocarbons. Preliminary geochemistry data provide tentative indication of their generation from peak oil window mature source rocks deposited in anoxic to suboxic environment. Due to the absence of any known oil seepage around the survey area sampling sites, it is very likely that these trace amount of hydrocarbons detected in the two waters are inherited from a contaminant oil of an unknown source.
- The seabed sediment samples contain variable amounts of extractable organic matter ranging from ≈ 2 to 3200 mg EOM/kg of sediment (with one sample containing no extractable organic matter) which do not comprise any detectable quantities of petroleum hydrocarbons. It is likely that this organic matter may be composed almost entirely of lipids and/or functionalised organic compounds from recent organic matter.
- The aliphatic and aromatic hydrocarbon distributions of extractable organic matter isolated from the GO net sample and GO net blank are very similar and resemble those of a typical crude oil. It is very likely that hydrocarbons of these two samples represent some contaminant oil, not any natural seepage. However, detailed biomarker analyses may provide more reliable information on the nature and origin of hydrocarbons in these two samples.
- The headspace gas samples analysed in this report do not contain any detectable amounts of petroleum hydrocarbons (i.e., methane, ethane, etc.). CO₂ gas detected in these samples ranged from low to very high amounts (≈ 1 -50 %), and had highly variable $\delta^{13}\text{C}_{\text{CO}_2}$ values. The isotopic data indicate an origin of Southern Surveyor CO₂ gas from magmatic sources and Southern Supporter CO₂ gas from mixed magmatic and recent organic matter sources.

6. CONCLUSION

Project 5.1 (Delineation and characterization of cold hydrocarbon seeps) forms a component in Theme 5 (petroleum systems) of the Great Australian Bight Research Program.

The overall intent of the project was to address the perceived risk of hydrocarbon generation in the Bight Basin, and the Ceduna Sub-basin through investigation of potential hydrocarbon seepage mechanisms and occurrence, and provide valuable pre-drill understandings of baseline hydrocarbon concentrations at preselected reference sites.

To identify potential sites of hydrocarbon seepage a multidisciplinary approach was taken which incorporated; the interpretation of seismic data, determination of fault leakage risk through a structural and geomechanical evaluation, identification of seabed features and morphologies indicative of seepage, delineation of water column acoustic contacts indicative of fluid and gas escape from the seabed, classification of sea surface slick anomalies and sampling of the seafloor in areas of possible seepage and far field locations to understand the distribution of hydrocarbons in sediments.

Whilst the project failed to identify active seepage in the Great Australian Bight the project did identify potential mechanisms for hydrocarbon seepage including possible indicators of seepage within the Paleocene section. A large number of moderate confidence leakage indicators were observed in 2D seismic data as were sea surface slick anomalies. Due to the time and budgetary constraints on the project it was only possible to investigate a limited number of these sites. The failure to identify seeps within the project is not an indication that hydrocarbon seepage is not occurring elsewhere in the GAB, rather that, the sites of any active seepage has, as yet, to be identified.

The baseline sampling in areas where seeps were not interpreted to be present has initiated the collection of geochemical data set describing the natural hydrocarbon loadings in the GAB which can be augmented with additional studies into the future.

7. REFERENCES

- Ahmed, M., Ross, A., Stalvies, C., Armand, S., Fuentes, D., Gong, S., Sestak, S. 2014. Organic geochemical study of seawater, seabed sediment and headspace gas samples to monitor baseline hydrocarbon levels around BP permits in the Great Australian Bight, Australia, Part B.
- Asquith, G., Krygowski, D., 2004. Basic well log analysis second edition, AAPG Methods in exploration series, no.16, American Association of Petroleum Geologists, Tulsa, Oklahoma.
- Backe, G., Swierczek, E., MacDonald, J., Bailey, A., Tassone, D., Abul Khair, H., Holford, S., King, R., 2012. Seismic attributes and structural interpretation - it takes two to tango. APPEA Journal, p. 437-454.
- Becker, E.L., Cordes, E.E., Macko, S.A., Fisher, C.R. 2009. Importance of seep primary production to *Lophelia pertusa* and associated fauna in the Gulf of Mexico. Deep-Sea Research I, 56, 786–800.
- Blevin, J.E., Cathro, D.L., 2008. Australian Southern Margin Synthesis, Project GA707. Geoscience Australia.
- Blevin, J.E., Totterdell, J.M., Logan, G.A., Kennard, J.M., Struckmeyer, H.I.M., Colwell, J.B., 2000. Hydrocarbon prospectivity of the Bight Basin—petroleum systems analysis in a frontier basin. In: 2nd Sprigg Symposium – Frontier Basins, Frontier Ideas, Adelaide, 29–30 June, 2000. Geological Society of Australia, Abstracts 60, 24–29.
- Bourget, J., Zaragosi, S., Mulder, T., Schneider, J.-L., Garlan, T., Van Toer, A., Mas, V., Ellouz-Zimmermann, N., 2010. Hyperpycnal-fed turbidite lobe architecture and recent sedimentary processes: a case study from the Al Batha turbidite system, Oman margin. Sedimentary Geology, 229 (2010), 144–159.
- Bourdet, J., Kempton, R., Ross, A., Pironon, J. 2016. Petroleum migration in the Bight Basin; a fluid inclusion approach to constraining composition and timing, Geofluids VII, 23-25 June 2016, China University of Geosciences, Wuhan, China.
- Bradshaw, B.E., Rollet, N., Totterdell, J.M., Borissova, I., 2003. A revised structural framework for frontier basins on the southern and southwestern Australian continental margin. Geoscience Australia Record 2003/03.
- Bretan, P., Yielding, G., Mathiassen, O.M., Thorsnes, T., 2011. Fault-seal analysis for CO₂ storage: an example from the Troll area, Norwegian Continental Shelf. Petroleum Geoscience 17, 2, 181-192.
- Brooks, J.M., Kennicutt, II, M.C., Fisher, S.A., Macko, K., Cole, J.J., Bidigare, R.R., and Vetter, R.D., 1987. Deep-sea hydrocarbon seep communities: Evidence for energy and nutritional carbon sources. Science, 238, 1138-1142.
- Çiftçi, N.B., Langhi L., Nadri, D. and Strand J., 2012a. Top seal bypass risk along the southern flank of the Gippsland Basin, South-eastern Australia. CSIRO Report, CSIRO Australia.

- Çiftçi, N.B., Giger, S.B. and Clennell, M.B., 2012b. Testing fault seal prediction algorithms using geomodels of experimentally produced fault zones. Fault and Top Seals Conference, 1-3 October, 2012, Montpellier, France.
- Clarke, J.D.A., Alley, N.F., 1993. Petrologic data on the evolution of the Great Australian Bight. In: R.H. Findlay, R. Unrug, M.R. Banks and J.J. Veevers (Editors), Assembly, evolution and dispersal; proceedings of the Gondwana eight symposium. International Gondwana Symposium, 8, pp. 585-596.
- Cordes, E.E., McGinley, M.P., Podowski, E.L., Becker, E.L., Lessard-Pilon, S., et al. 2008. Coral communities of the deep Gulf of Mexico. *Deep-Sea Res*, 55: 777–787.
- Currie, T.J., Alexander, R., & Kagi, R.I. (1992). Coastal bitumens from Western Australia — long distance transport by ocean currents. *Organic Geochemistry*, 18, 595-601.
- Davies, H.L., Clarke, J.D.A., Stagg, H.M.J., McGowran, B., Alley, N.F., Willcox, J.B., 1989. Maastrichtian and younger sediments from the Great Australian Bight. Bureau of Mineral Resources, Australia, Report 288.
- Deptuck, M. E., Piper, D. J. W., Savoye, B. and Gervais, A. (2008), Dimensions and architecture of late Pleistocene submarine lobes off the northern margin of East Corsica. *Sedimentology*, 55: 869–898.
- dGB, 2012. Fault Enhancement Filtering. <http://www.opendtect.org/index.php/support.html>
- Didyk, B.M., Simoneit, B.R.T., Brassell, S.C., Eglinton, G., (1978) Organic geochemical indicators of palaeoenvironmental conditions of organic sedimentation. *Nature*, 272, 216-222.
- Dockrill, B, Shipton, Z.K., 2010. Structural controls on leakage from a natural CO₂ geologic storage site: Central Utah, U.S.A. *Journal of Structural Geology*, 32, 1768-1782.
- Faiz, M., Saghafi, A., Sherwood, N., Wang, I., (2007) The Influence of Petrological Properties and Burial History on Coal Seam Methane Reservoir Characterisation, Sydney Basin, Australia. *International Journal of Coal Geology*, 70(1-3), 193-208.
- Feary, D.A., James, N.P., 1995. Cenozoic biogenic mounds and buried Miocene (?) Barrier reef on a predominantly cool-water carbonate continental margin—Eucla Basin, western Great Australian Bight.
- Feary, D.A., James, N.P., 1998, Seismic stratigraphy and geological evolution of the Cenozoic, cool-water Eucla Platform, Great Australian Bight: *American Association of Petroleum Geologists Bulletin*, v. 82, p. 792–816.
- Feary, D.A., et al., 2000. Proceedings of the Ocean Drilling Project, Initial reports, Volume 182: College Station, Texas, Ocean Drilling Program, p. 1–58.
- Fisher, Q.J., Knipe, R.J., 1998. Fault sealing processes in siliciclastic sediments. In: G. Jones, Q.J. Fisher and R.J. Knipe (Editors), *Faulting, Fault Sealing and Fluid Flow in Hydrocarbon Reservoirs*. Geol. Soc., London, Spec. Publ., 147: 117–134.

- Fraser, A.R., Tilbury, L.A., 1979. Structure and stratigraphy of the Ceduna Terrace region, Great Australian Bight Basin. *The APEA Journal*, 19, 53-65.
- Freeman, B., G. Yielding, D. T. Needham, M. E. Badley, (1998) Fault seal prediction: The gouge ratio method, in M. P. Coward, T. S. Daltaban, and H. Johnson, eds., *Structural geology in reservoir characterization: Geological Society London Special Publication 127*, p. 19–25.
- Fristad, T., Groth, A., Yielding, G., Freeman, B., 1997. Quantitative fault seal prediction: a case study from Oseberg Syd. In: P. Møller-Pedersen and A.G. Koestler (Editors), *Hydrocarbon Seals: Importance for Exploration and Production*. Norwegian Petroleum Society (NPF), Special Publication 7. Elsevier, Amsterdam, pp. 107–124.
- Gervais, A., Savoye, B., Mulder, T. and Gonthier, E. (2006) Sandy modern turbidite lobes: a new insight from high resolution seismic data. *Mar. Petrol. Geol.*, 23, 485–502.
- Gradstein, F.M., Ogg, J.G. and Smith, A.G., 2004. *A geologic time scale 2004*. Cambridge University Press, 589p.
- Giger, S. B., Clennell, B., Ciftci, B., Clark, P., Craig, H., Ricchetti, M., Delle Piane, C., Freij-Ayoub, R. and Middleton, B., 2010. *Dynamic fault seals (Year 3) final report*. CSIRO, Report No. 111873, 219 p.
- Griffiths, C. M., Dyt, C., 2001. Six Years of SedSim Exploration Applications, *AAPG Bull.*, 85 (2001), 13.
- Griffiths, C., Dyt, C., Paraschivoiu, E., Liu, K., 2001. SedSim in hydrocarbon exploration. In: Merriam, D. and Davis, J. (Eds.), *Geologic Modelling and Simulation*. Kluwer Academic, New York, 71–97.
- Griffiths, C. M., Paraschivoiu, E., 1998. Three-Dimensional Forward Stratigraphic Modelling Of Early Cretaceous Sedimentation On The Leveque And Yampi Shelves, Browse Basin. *APPEA Journal*, 38 (1), 147-158.
- Gupta, A., 2007. *Large rivers geomorphology and management*. Wiley. ISBN 978-0-470-84987-3.
- Hageman, S., Lukasik, J., McGowran, B., Bone, Y., 2003. Paleoenvironmental Significance of *Celleporaria* (Bryozoa) from Modern and Tertiary Cool-water Carbonates of Southern Australia. *PALAIOS*, 2003, V. 18, 510–527
- Hall, A.P., McKirdy, D.M., Grice, K., & Edwards, D.S. (2014). Australasian asphaltite strandings: Their origin reviewed in light of the effects of weathering and biodegradation on their biomarker and isotopic profiles. *Marine and Petroleum Geology*, 57, 572-593.
- Haq, B.U., Hardenbol, J., Vail, P.R., 1987. Chronology of fluctuating sea levels since the Triassic. *Science*, 235, March 1987, 1156-1167.
- Haq, B.U., Hardenbol, J., Vail, P.R., 1988. Mesozoic and Cenozoic chronostratigraphy and eustatic cycles. In: Wilgus, C.K., Hastings, B.S., Kendall, C.G.St.C., Posamentier, H.W., Ross, C.A. and Van Wagoner, J.C. (Eds), *Sea-level changes: an integrated approach*. Society of Economic Paleontologists and Mineralogists, Spec. Pub. 42, 71–108.

- Henriet, J.P., De Mol, B., Vanneste, M., Huvenne, V. & van Rooij, D. 2001. Carbonate mounds and slope failures in the Porcupine Basin: a development model involving past fluid venting. In: Shannon, P.M., Haughton, P.D.W. and Corcoran, D.V. (eds). *The Petroleum Exploration of Ireland's Offshore Basins*. Geol. Soc. London Spec. Publ., 188, 375-383.
- Hovland, M., Croker, P. F., Martin, M., 1994. Fault-associated seabed mounds (carbonate knolls?) off western Ireland and north-west Australia: *Marine and Petroleum Geology*, v. 11, no. 2, p. 232–246
- Hovland, M., Mortensen, P.B., Brattegard, T., Strass, P., Rokoengen, K., 1998. Ahermatypic coral banks off mid-Norway: evidence for a link with seepage of light hydrocarbons. *Palaios*, 13: 189-200.
- Hovland, M., Risk, M., 2003. Do Norwegian deep-water coral reefs rely on fluid seepage? *Marine Geology*, 198, 83-96.
- Hughes, M.G., Nichol, S., Przeslawski, R., Totterdell, J., Heap, A.D., Fellows, M. and Daniell, J., 2009. Ceduna Sub-basin: Environmental Summary. *Geoscience Australia Record* 2009/09. 96pp.
- James, N.P., Feary, D.A., Betzler, C., Bone, Y., Holbourn, A.E., Li, Q., Machiyama, H., Toni Simo, J.A., Surlyk, F., 2004, Origin of late Pleistocene bryozoan reef mounds; Great Australian Bight: *Journal of Sedimentary Research*, v. 74, p. 20–48, doi: 10.1306/062303740020.
- Jollivet, D., Faugeres, J.-C., Griboulard, R., Desbruyers, D., Blanc, G., 1990. Composition and spatial organization of a cold seep community on the South Barbados accretionary prism: Tectonic, geochemical and sedimentary context. *Progress in Oceanography*, 24 (1-4), pp. 25-45.
- Jones, A.T., Logan, G.A., Kennard, J.M., Rollet, N. 2005. Reassessing potential origins of Synthetic Aperture Radar (SAR) slicks from the Timor Sea Region of the North West Shelf on the basis of field and ancillary data. *APPEA Journal*, 2005, 311-332.
- Kempton, R., Bourdet, J., Gong, S., Ross, A., 2016, Petroleum migration in the Bight Basin: a fluid inclusion approach to constraining source, composition and timing. *Australian Earth Sciences Convention*, 26-30 June 2016, Adelaide Convention Centre, Adelaide, South Australia.
- Kennicutt, II, M.C., Brooks, J.M., Bidigare, R.R., Fay, R.R., Wade, T.L. and Macdonald, T.J., 1985. Vent-type taxa in a hydrocarbon seep region on the Louisiana slope. *Nature*, London, 317, 351-352.
- Killick, M. F., 1998. Phanerozoic denudation of the Western Shield of Western Australia. *Geological Society of Australia Abstracts* 49, 248.
- King, S.J., Mee, B.C., 2004. The seismic stratigraphy and petroleum potential of the Late Cretaceous Ceduna Delta, Ceduna Sub-basin, Great Australian Bight. In: Boulton, P.J., Johns, D.R. and Lang, S.C. (Eds), *Eastern Australasian Basins Symposium II*. Petroleum Exploration Society of Australia, Special Publication, 63–73.
- Kohn, B. P., O'Sullivan, P. B., Gleadow, A. J. W., 2000. Phanerozoic denudation history of southwest Australian crystalline terranes inferred from apatite fission track thermochronology. In: Noble W. P., O'Sullivan P. B. & Brown R. W. eds. *9th International Conference on Fission*

- Track Dating and Thermochronology, Lorne, 2000, pp. 213–215. Geological Society of Australia Abstracts 58.
- Kohn, B.P., Gleadow, A.J.W., Brown, R.W., Gallagher, K., O'Sullivan, P.B., Foster, D.A., 2002. Shaping the Australian crust over the last 300 million years: Insights from fission track thermotectonic imaging and denudation studies of key terranes, *Australian Journal of Earth Sciences*, 49:4, 697-717.
- Koltermann, C. E., Gorelick, S. M., 1992. Palaeoclimatic Signature in Terrestrial Flood Deposits. *Science*, 256, 1775-1782.
- Krassay, A.A., Totterdell, J.M., 2003. Seismic stratigraphy of a large, Cretaceous shelf-margin delta complex, offshore southern Australia. *AAPG Bulletin*, 87(6), 935–963.
- Lane, H., Müller, D.R., Totterdell, J.M., Whittaker, J.M., 2012. Developing a consistent sequence stratigraphy for the Wilkes Land and Great Australian Bight margins. *Eastern Australasian Basins Symposium IV*.
- Langhi, L., Zhang, Y., Gartrell, A., Underschultz, J.R., Dewhurst, D.N., 2010. Evaluating hydrocarbon trap integrity during fault reactivation using geomechanical 3D modelling: An example from the Timor Sea, Australia. *AAPG Bulletin* 94, 567-591.
- Langhi, L., Ross, A., Crooke, E., Jones, A., Nicholson, C., Stalvies, C., 2014. Integrated hydroacoustic flares and geomechanical characterization reveal potential hydrocarbon leakage pathways in the Perth Basin, Australia. *Marine and Petroleum Geology*, 51, 63-69.
- Larionov, V.V., 1969. Borehole Radiometry. Moscow, U.S.S.R., Nedra.
- Lavering, I., Jones, A., 2001. Carbonate Shoals and Hydrocarbons in the Western Timor Sea. *PESA News* 55, 40–42.
- Li, F., Dyt, C., Griffiths, C.M., Jenkins, C., Rutherford, M., Chittleborough, J., 2005. Seabed sediment transport and offshore pipeline risks in the Australian Southeast. *APPEA Journal* 45, 523-534.
- Ligtenberg, J.H., 2005. Detection of fluid migration pathways in seismic data: Implications for fault seal analysis. *Basin Research* 17, 141–153.
- Lisk, M., Hall, D., Ostby, J., & Brincat, M.P. (2001). Addressing the oil migration risks in the Great Australian Bight. *PESA Eastern Australasian Basins Symposium*, 25-28 November 2001, Melbourne, Australia, 553-562.
- Logan, G.A., Jones, A.T., Kennard, J.M., Ryan, G.J., Rollet, N., 2010. Australian offshore natural hydrocarbon seepage studies, a review and re-evaluation. *Marine and Petroleum Geology*, 27, 26–45.
- Manzocchi, T., Childs, J. J. Walsh., 2010. Faults and fault properties in hydrocarbon flow models in *Geofluids*, 2010, 10, 94–113.
- Martinez, P., Harbaugh, J. W., 1993. *Simulating Nearshore Environments*. Pergamon Press, New York.

- McKirdy, D.M., Cox, R.E., Volkman, J.K., & Howell, V.J., 1986. Botryococcane in a new class of Australian non-marine crude oils. *Nature*, 320, 57-59.
- McKirdy, D.M., Summons, R.E., Padley, D., Serafini, K.M., Boreham, C.J., & Struckmeyer, H.I.M., 1994. Molecular fossils in coastal bitumens from southern Australia: signatures of precursor biota and source rock environments. *Organic Geochemistry*, 21, 265-286.
- Meyer, M., Harff, J., Dyt, C., 2011. Modelling Coastline Change of the Darss-Zingst Peninsula with Sedsim. (in J. Harff et al. (eds.)), *The Baltic Sea Basin, Central and Eastern European Development Studies*, (CEEDES) 2011, Part 5, 281-298, DOI: 10.1007/978-3-642-17220-5_14
- Moscardelli, L., Wood, L., Mann, P., 2006. Mass-transport complexes and associated processes in the offshore area of Trinidad and Venezuela. *AAPG Bulletin*, v. 90, no. 7 (July 2006), 1059–1088
- O'Brien, G.W., Woods, E. P., 1995., Hydrocarbon-related diagenetic zones (HRDZs) in the Vulcan Subbasin, Timor Sea; recognition and exploration implications: *Australian Petroleum Exploration Association Journal*, v. 35, no. 1, p. 220–252.
- O'Brien, G.W., Glenn, K., Lawrence, G., Williams, A., Webster, M., Cowley, R., Burns, S., 2002. Influence of hydrocarbon migration and seepage on benthic communities in the Timor Sea, Australia. *The APPEA Journal* 42, 225–240.
- Reading, H.G., 1996. *Sedimentary Environments: Processes, Facies and Stratigraphy*. Blackwell Science, p. 704.
- Roberts, H.H., Aharon, P., 1994. Hydrocarbon-derived carbonate buildups of the northern Gulf of Mexico continental slope: a review of submersible investigations. *Geo-Marine Letters* 14 (2–3), 135–148.
- Padley, D., McKirdy, D.M., Murray, A.P., Summons, R.E., 1993. Oil Strandings on the beaches of Southern Australia: Origins from natural seepage and shipping. In: Øygard, K (Ed.), *Poster Sessions from the 16th International meeting on Organic Geochemistry*, 20-24 September 1993, Stavanger, Norway, 660-663.
- Padley, D., 1995. Petroleum geochemistry of the Otway Basin and the significance of coastal bitumen strandings on adjacent southern Australian beaches, Ph.D. Thesis, Department of Geology and Geophysics, The University of Adelaide (Unpublished).
- Pickering, K.T., Hiscott, R.N. 2015. *Deep marine systems: Processes Deposits, Environments, Tectonics and Sedimentation*. Wiley, p. 672.
- Pierre, C., Fouquet, Y., 2007. Authigenic carbonates from methane seeps of the Congo deep-sea fan. *Geo-Mar Lett* (2007) 27: 249–257.
- Radke, M., Welte, D.H., (1983) The methylphenanthrene index (MPI): a maturity parameter based on aromatic hydrocarbons. In: M. Bjorøy (Ed.), *Advances in Organic Geochemistry*. Wiley, Chichester, pp. 504-512.
- Radke, M., Leythaeuser, D., Teichmüller, M., (1984) Relationship between rank and composition of aromatic hydrocarbons from coals of different origins. *Organic Geochemistry*, 6, 423-430.
- Radke, M., (1988) Application of aromatic compounds as maturity indicators in source rocks and crude oils. *Marine and Petroleum Geology*, 5, 224-236.
- Roberts, H. H., Hardage, B. A., Shedd, W. W., Hunt Jr., J., Herron, D., 2006. Seafloor reflectivity; an important seismic property for interpreting fluid/gas expulsion geology and the presence of gas hydrate: *The Leading Edge*, v. 25, no. 5, 620–628.

- Ruble, T.E., Logan, G.A., Blevin, J.E., Struckmeyer, H.I.M., Liu, K., Ahmed, M., Eadington, P.J., & Quezada, R.A. (2001). Geochemistry and charge history of a palaeo-oil column: Jerboa-1, Eyre Sub-basin, Great Australian Bight. In: Hill, K.C. and Bernecker, T. (Eds), Eastern Australasian Basins Symposium: a refocused energy perspective for the future. Petroleum Exploration Society of Australia, Special Publication, 521–530.
- Salles, T., Marches, E., Dyt, C., Griffiths, C., Hanquiez, V., Mulder, T., 2009. Simulation of the interactions between gravity processes and contour currents on the Algarve Margin (South Portugal) using the stratigraphic forward model Sedsim. *Sedimentary Geology*, 229, 3, 95–109.
- Salles, T. B., Griffiths, C. M., Dyt, C.P., Li, F., 2011a. Australian shelf sediment transport responses to climate change-driven ocean perturbations. *Marine Geology* 282, 268–274.
- Salles, T. B., Griffiths, C. M., Dyt, C.P., 2011b. Aeolian sediment transport integration in general stratigraphic forward modelling. *Journal of Geological Research*, vol. 2011, Article ID 186062, 12 pages.
- Sayers, J., Symonds, P., Direen, N.G., Bernardel, G., 2001. Nature of the continent–ocean transition on the nonvolcanic rifted margin of the central Great Australian Bight. *In*: Wilson, R.C.L., Whitmarsh, R.B., Taylor, B. and Froitzheim, N. (Eds), Non-volcanic rifting of continental margins: a comparison of evidence from land and sea. Geological Society of London, Special Publications 187, 51–77.
- Schofield, A., Totterdell, J.M., 2008. Distribution, timing and origin of magmatism in the Bight and Eucla basins. *Geoscience Australia Record* 2008/24.
- Shanmugam, G. and Moiola, R. J., 1991. Types of submarine fan lobes; models and implications AAPG Bulletin, January 1991, v. 75, 156-179.
- Shanmugam, G. and Moiola, R. J., 1988. Submarine fans: characteristic,s, models, classification and reservoir potential. *Earth Science Reviews*, 24, 383-428.
- Sharples, A.G.W.D., Huuse, M., Hollis, C., Totterdell, J.M., Taylor, P.D., 2014. Giant middle Eocene bryozoan reef mounds in the Great Australian Bight. *Geology*, 42/8; p. 683–686.
- Somerville, R., 2001. The Ceduna Sub-basin – a snapshot of prospectivity. *The APPEA Journal*, v. 41, 321–346.
- Sperrevik, S., Gillespie, P.A., Fisher, Q.J., Halvorsen, T., Knipe, R.J. 2002. Empirical estimation of fault rock properties. In: Koestler, A.G., Hunsdale, R. (eds) *Hydrocarbon Seal Quantification*. Norwegian Petroleum Society (NPF) Special Publication, Elsevier, Amsterdam, 11, 109–125.
- Struckmeyer, H.I.M., Totterdell, J.M., Blevin, J.E., Logan, G.A., Boreham, C.J., Deighton, I., Krassay, A.A., Bradshaw, M.T., 2001. Character, maturity and distribution of potential Cretaceous oil source rocks in the Ceduna Sub-basin, Bight Basin, Great Australian Bight. In: Hill, K.C. and Bernecker, T. (Eds), Eastern Australasian Basin Symposium, a refocused energy perspective for the future. Petroleum Exploration Society of Australia, Special Publication, 543–552.

- Talukder, A.R. 2012. Review of submarine cold seep plumbing systems: leakage to seepage and venting. *Terra Nova* 24, 255-272.
- Talukder, A.R., Ross, A., Crooke, E., Stalvies, C., Trefry, C., Qi, X., Fuentes, D., Armand, S., Revill, A., Shipboard Scientific Party, 2013. Natural seepage on the continental slope to the east of Mississippi Canyon in the northern Gulf of Mexico. *Geochem. Geophys. Geosyst.* 14.
- Tapley, D., Mee, B.C., King, S.J., Davis, R.C., Leischner, K.R., 2005. Petroleum potential of the Ceduna Sub-basin: impact of Gnarlyknots-1A. *The APPEA Journal*, 45(1), 365–380.
- Taylor, D., 1975, Palaeontological report–Potoroo 1, Well completion report: Adelaide, Shell Development (Australia), 96–104.
- Teasdale, J., 2004. Southern Australian Margin SEEBASE® Compilation, April 2004. Geoscience Australia, Canberra.
- Tikku, A.A., Cande, S.C., 1999. The oldest magnetic anomalies in the Australian-Antarctic Basin: are they isochrons. *Journal of Geophysical Research*, 104, 661-677.
- Tissot, B.P., Welte, D.H., (1984) Petroleum formation and occurrence, pp. 699. Springer, Berlin.
- Tetzlaff, D. M., Harbaugh, J. W., 1989. Simulating Clastic Sedimentation; Computer Methods In The Geosciences, Van Nostrand Reinhold, New York, 202.
- Totterdell, J.M., Blevin, J.E., Struckmeyer, H.I.M., Bradshaw, B.E., Colwell, J.B., Kennard, J.M., 2000. A new sequence framework for the Great Australian Bight: starting with a new slate. *The APPEA Journal*, 40, 95–117.
- Totterdell, J.M., Bradshaw, B.E., 2004. The structural framework and tectonic evolution of the Bight Basin. In: Boulton, P.J., Johns, D.R. & Lang, S.C. (Eds), *Eastern Australasian Basins Symposium II*. Petroleum Exploration Society of Australia, Special Publication, 41–61.
- Totterdell, J.M., Krassay, A.A., 2003. Sequence stratigraphic correlation of onshore and offshore Bight Basin successions. *Geoscience Australia Record* 2003/02.
- Totterdell, J., Mitchell, C. (Editors), 2009. Bight Basin geological sampling and seepage survey: RV Southern Surveyor SS01/2007. *Geoscience Australia Record* 2009/24.
- Totterdell, J.M., Struckmeyer, H.I.M., Boreham, C.J., Mitchell, C.H., Monteil, E., & Bradshaw, B.E. (2008). Mid–Late Cretaceous organic-rich rocks from the eastern Bight Basin: implications for prospectivity. In: Blevin, J.E., Bradshaw, B.E. and Uruski, C. (eds), *Eastern Australasian Basins Symposium III*, Petroleum Exploration Society of Australia, Special Publication, 137–158.
- Underschultz, J. 2007. Hydrodynamics and membrane seal capacity. *Geofluids*, 7, 1–11.
- Woodside Australian Energy, 2004. Well completion report Gnarlyknots-1A interpretive data (EPP-29, Ceduna Sub-basin).
- Wu, S., Qin, Z., Wang, D., Peng, X., Wang, Z., Yao, G., 2011. Analysis on seismic characteristics and triggering mechanisms of mass transport deposits on the northern slope of the South China Sea. *Chinese Journal of Geophysics* Vol.54, No.6, 2011, 1056-1068.

- Yielding, G., Freeman, B. & Needham, D.T. 1997. Quantitative fault seal prediction. American Association of Petroleum Geologists Bulletin, 81, 897-917.
- Yielding, G., 2002. Shale Gouge Ratio - calibration by geohistory. In: Koestler, A.G. & Hunsdale, R. (eds) Hydrocarbon Seal Quantification. Norwegian Petroleum Society (NPF) Special Publication, Elsevier, Amsterdam, 11, 1–15.
- Zhang, Y., Gartrell, A., Underschultz, J.R. and Dewhurst, D.N., 2009, Numerical modelling of strain localisation and fluid flow during extensional fault reactivation: implications for hydrocarbon preservation. Journal of Structural Geology 3

APPENDIX 1: DATA MANAGEMENT

Raw Datasets Created:

MBES and single beam acoustic files were collected throughout the SS2013_C02 survey.

SBP SEGY files were collected throughout the SS2013_C02 survey.


SAR image data was collected via programmed satellite captures.

Survey Database

A survey database was used to collect various data records throughout the SS2013_C02 survey. Database tables were:

GPS and Hydrocarbon Sensor data

- Project_ID
- Cruise_ID
- Trip_ID
- ReadingDate
- ReadingTime
- LocalDateTime
- Latitude
- Longitude
- Latitude2
- Longitude2
- Temperature
- Flowrate
- COG
- SOG
- Status
- Comment
- ReliabilityFlag
- TrackChecked
- UTCDate
- UTCTime
- PCDate
- PCTime
- DistanceToSite
- Sensor1
- Sensor1_Conc1
- Sensor1_CalibType1
- Sensor1_Conc2
- Sensor1_CalibType2
- Sensor1_Conc3
- Sensor1_CalibType3



Set of fields for each of the four sensors used for the survey

Cast Data (from BOAGS)

- Project_ID
- Cast_ID
- LatY_DD
- LngX_DD
- TimeElapsedSeconds
- Depth
- Temperature
- Conductivity
- Pressure
- Salinity
- Diss_Oxygen
- Methane
- PH
- Flourescence
- Turbidity
- SoundVelocityCM
- Sensor1
- Sensor2
- Sensor3
- Sensor4
- Sensor5
- Sensor6
- Sensor7
- Sensor8
- Flag

Cast Results

Depth binned results from the CTD casts

- Project_ID
- Cast_ID
- UTCDate
- UTCTime
- Sample_ID
- Bottle_ID
- Depth
- Temperature
- Conductivity
- Pressure
- Salinity
- Diss_Oxygen
- Nitrate
- Phosphate
- Silicate
- Ammonia

- Nitrite
- Methane
- Sensor1
- Sensor2
- Sensor3
- Sensor4
- Sensor5
- Sensor6
- Sensor7
- Sensor8
- Flag

Activity Log

- Project_ID
- Cruise_Num
- Trip_ID
- UTCDateFrom
- UTCTimeFrom
- UTCDateTo
- UTCTimeTo
- LocalDateTime
- LatY_DD
- LngX_DD
- Activity
- DistanceToSite

Photographs

- Project_ID
- Cruise_Num
- Trip_ID
- UTCDate
- UTCTime
- LocalDateTime
- LatY_DD
- LngX_DD
- Description
- LinkedImageName
- txtLinkedImageName
- ForLabel
- DistanceToSite

Oiling Observations

- Project_ID

- Cruise_Num
- Trip_ID
- StartDateTime
- UTCStartDate
- UTCStartTime
- StartLatY_DD
- StartLngX_DD
- EndingDateTime
- UTCEndingDate
- UTCEndingTime
- EndLatY_DD
- EndLngX_DD
- Type1
- PrimaryTypeDesc
- Type1_Obs_Class
- Type2
- SecondaryTypeDesc
- Type2_Obs_Class
- Type3
- TertiaryTypeDesc
- Type3_Obs_Class
- Comments
- DistanceToSite

Samples

- Project_ID
- Cruise_Num
- Trip_ID
- SampleID
- Sampledby
- UTCDate
- SamplingStartTimeUTC
- LocalDateTime
- LatY_DD
- LngX_DD
- SampleDepth
- SamplePurpose
- SampleMethod
- SampleLocation
- StationNum
- SampleType
- SamplerType
- VialSize
- NumContainers

- StorageTemperature
- SamplePreservative
- SampleVolume
- SampleShipped
- ForLabName
- ForAnalysis
- CoCnumber
- CustomSampleID
- Sensor1
- Sensor2
- Sensor3
- Sensor4
- Core_RosettePos_number
- Comments
- DistanceToSite
- ExtractionDate
- FinalMedia
- StandardsUsed

Sonar Contacts

- Project_ID
- Cruise_Num
- Trip_ID
- ContactLocation
- ContactID
- Contact_Source
- Contact_TYPE
- Contact_Shape
- Contact_BaseDepth
- Contact_Height
- UTCDate
- UTCTime
- LocalDateTime
- LatY_DD
- LngX_DD
- Btm_LatY_DD
- Btm_LngX_DD
- WaterColumnDepth
- LinkedImageName
- txtLinkedImageName
- LinkedImageName2
- txtLinkedImageName2
- LinkedImageName3
- txtLinkedImageName3

- DistanceToSite
- PermitBlock
- Comment

Cast Details

- Project_ID
- Cruise_Num
- Trip_ID
- CastLocation
- StationNum
- Cast_ID
- MaxCastDepth
- WaterColumnDepth
- DistanceOffBottom
- Cast_Type
- UTCDate
- UTCTime
- LocalDateTime
- LngX_DD
- LatY_DD
- UTCTime_Btm
- LngX_DD_Btm
- LatY_DD_Btm
- UTCTime_End
- LngX_DD_End
- LatY_DD_End
- LinkedImage
- txtLinkedImage
- LinkedImage2
- txtLinkedImage2
- LinkedImage3
- txtLinkedImage3
- comments
- DistanceToSite

Data Processing and Derived Datasets:

Geotiffs were created from the raw multibeam acoustic data using CARIS.

SBP screen captures were regularly taken by the vessel personnel.

Geochemistry data sets created:

Quantitative analysis of PAH in the solvent extract of water

Gas chromatography mass spectrometry Selected Ion Monitoring for the following polycyclic aromatic hydrocarbons of interest:

- Acenaphthene
- Acenaphthylene
- Anthracene
- Benzo(a)anthracene
- Benzo(a)pyrene
- Benzo(b)fluoranthene
- Benzo(g,h,i)perylene
- Chrysene
- Dibenzo(a,h)anthracene
- Fluoranthene
- Fluorene
- Indeno(1,2,3-c,d)pyrene
- 1-Methylnaphthalene
- 2-Methylnaphthalene
- Naphthalene
- Phenanthrene
- Pyrene
- Dibenzothiophene
- Biphenyl

Selected Ion Monitoring GC-MS analyses of extractable organic matter in sediment samples

Partial mass chromatograms and peak identifications using M/Z Ions 106, 120, 128, 134, 142, 154, 156, 166, 168, 170, 178, 180, 182, 184, 192, 197, 198, 202, 206, 212, 216, 220, 234,

Molecular composition of headspace gases in sediments

Compositions of:

- CO₂
- Methane
- Ethane
- Propane
- iso -Butane
- n -Butane
- neo- Pentane
- iso- Pentane
- n- Pentane
- C₆+ O₂ + Ar
- Nitrogen

Isotopic composition of headspace gases in sediments

- $\delta_{13}\text{C}_{\text{CH}_4}$ (‰)
- $\delta^{13}\text{C}_{\text{CO}_2}$ (‰)

SAR images were interpreted and any potential slicks identified were exported as shapefiles.

SedSim and TrapTester models were developed for the project, and outputs used for this report.

Data Curation and Archive:

Data files (raw data, derived datasets, working files, reports) relating to the project are stored on CSIRO's network servers in secure locations only accessible to personnel listed in the GAB Research Program - Project Plan 5.1. All SS2013_CO2 voyage data is available through CSIRO Data Trawler <http://www.cmar.csiro.au/data/trawler/>.

A metadata record will be created for each dataset these metadata records will be uploaded to the AODN catalogue.

All data, apart from the geological models, is amenable to upload and archival through the CSIRO data trawler, National Offshore Petroleum Information Management System (NOPIMS) and Australian Oceanographic Data Network (AODN).

Any data not uploaded to publically available databases will be provided to BP.

Data Access, Use Agreements and Licensing:

None

Publication of Datasets:

Not published

APPENDIX 2: STUDENT PROJECTS

Not applicable no students included within the project.

APPENDIX 3: PROJECT PUBLICATIONS

Reports

L. Langhi, J. Strand (2014) The structural controls on potential hydrocarbon leakage conduits in the Great Australian Bight., CSIRO Confidential report number EP148116. pp52.

M. Ahmed, A. Ross, C. Stalvies, S. Armand, D. Fuentes, S. Gong and S. Sestak (2014) Organic geochemical study of seawater, seabed sediment and headspace gas samples to

monitor baseline hydrocarbon levels around BP permits in the Great Australian Bight, Australia. Part A : Text, Tables and Figures. CSIRO Report Number: to be determined. pp54

M. Ahmed, A. Ross, C. Stalvies, S. Armand, D. Fuentes, S. Gong and S. Sestak (2014) Organic geochemical study of seawater, seabed sediment and headspace gas samples to monitor baseline hydrocarbon levels around BP permits in the Great Australian Bight, Australia. Part B : Sampling Tables, Protocols and Raw Data. CSIRO Report Number: to be determined. Pp810-

Presentations and Conference abstracts

Strand, J., Langhi, L., Ross, A., (Accepted) Predictive stratigraphic forward modelling of the Ceduna Sub-basin; application to fault sealing. AAPG ICE, 13-16 September 2015, Melbourne, Australia.

Langhi, L., Strand, J., Ross, A., (Accepted) Biogenic mounds in the central Ceduna Sub-basin; implications for hydrocarbon migration. AAPG ICE, 13-16 September 2015, Melbourne, Australia.

Papers

Langhi, L., Strand, J., Ross, A., (Submitted to management committee) Fault-related biogenic mounds in the Ceduna Sub-basin; implications for hydrocarbon migration, Marine and Petroleum Geology.

Patents: None

Media Releases: None

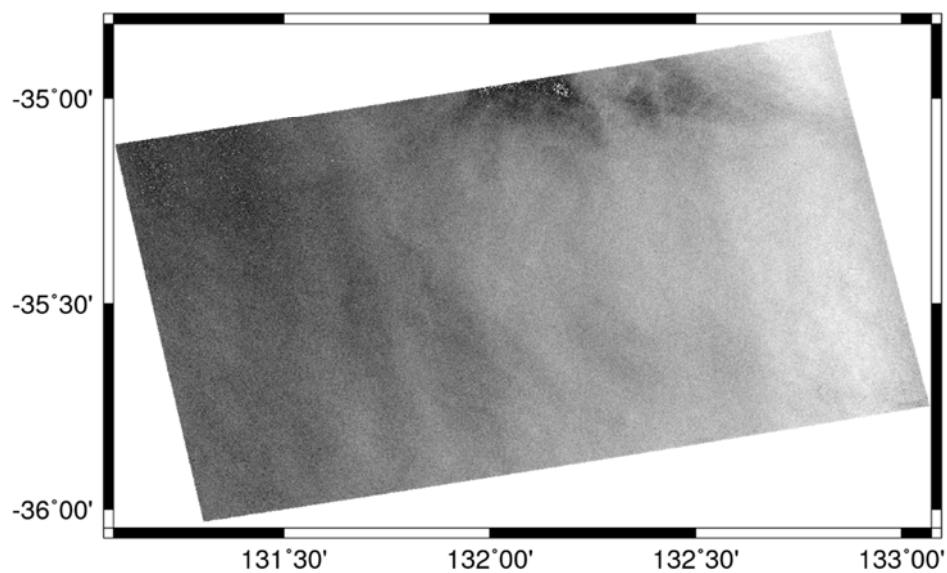
APPENDIX 4: INTELLECTUAL PROPERTY

Unique discoveries: None

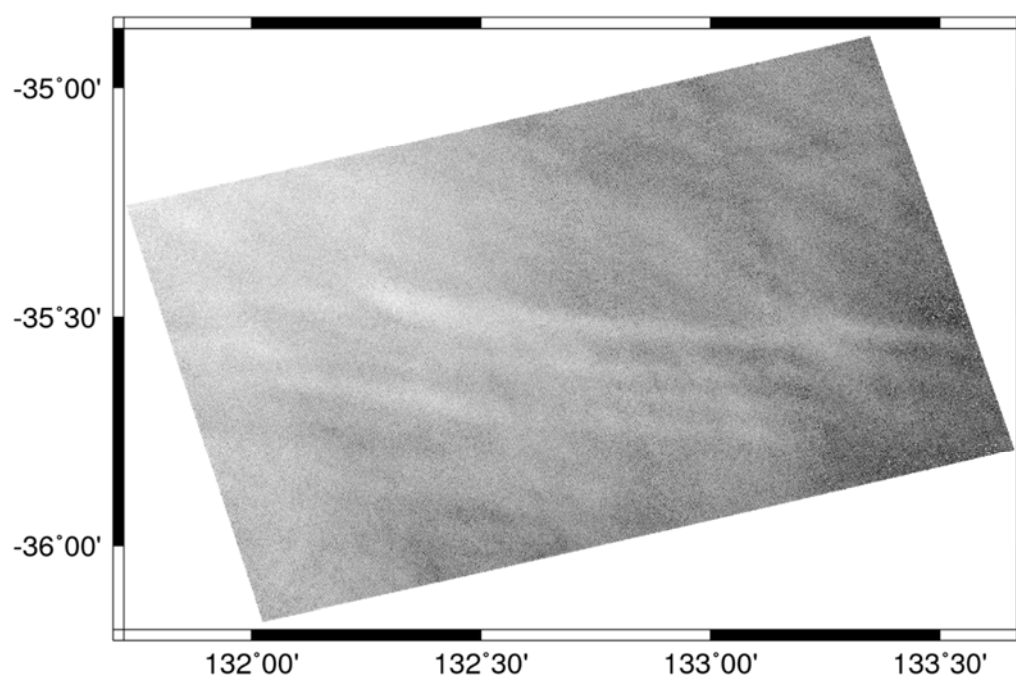
Action plan: Not applicable

APPENDIX 5: TASK 2 SAR DATA

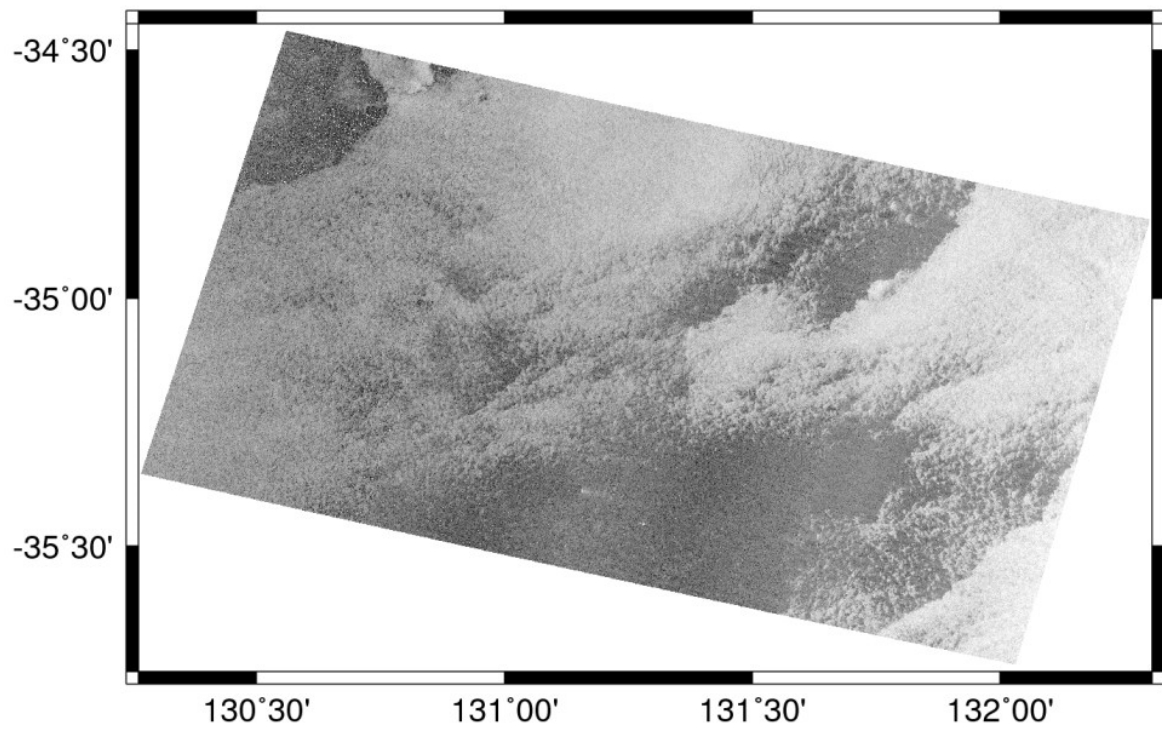
CSK1 Apr 06, 2013 21:13 GMT



CSK4 Apr 09, 2013 21:43 GMT



CSK4 Apr 15, 2013 08:29 GMT





THE UNIVERSITY
of ADELAIDE



Flinders
UNIVERSITY